(1)

DESIGN OF A ROBUST CONTROLLER FOR AN UNSTABLE NONMINIMUM PHASE GUIDED MISSILE

THESIS

Randall L. Riddle
Captain, USAF

AFIT/GAE/ENY/89D-29

DEPARTMENT OF THE AIR FORCE
AIR UNIVERSITY
AIR FORCE INSTITUTE OF TECHNOLOGY

Wright-Patterson Air Force Base, Ohio

AFIT/GAE/ENY/89D-29

DESIGN OF A ROBUST CONTROLLER FOR AN UNSTABLE NONMINIMUM PHASE GUIDED MISSILE

THESIS

Randall L. Riddle
Captain, USAF

AFIT/GAE/ENY/89D-29

AFIT/GAE/ENY/89D-29

DESIGN OF A ROBUST CONTROLLER FOR AN UNSTABLE NONMINIMUM PHASE GUIDED MISSILE

THESIS

Presented to the Faculty of the School of Engineering
of the Air Force Institute of Technology
Air University
In Partial Fulfillment of the
Requirements for the Degree of
Master of Science in Aeronautical Engineering

Randall L. Riddle, B.S.
Captain, USAF

December 1989

Preface

The purpose of study was to investigate the application of theories for the design of robust control systems for multiple input multiple output systems, and to apply these techniques to a realistic control system. The techniques investigated are known as the H_2 and H_∞ design techniques, and involve the minimization of the 2- and ∞-norms of the system transfer function matrices. Considerable system modification is required to apply these techniques, and a methodology for accomplishing this modification is developed. Evaluation of the controllers developed requires simulating the system performance, and a digital simulation is developed for this purpose.

I received considerable help in developing the controllers and simulation contained herein, and for this help I am deeply grateful. I am indebted to my advisor, Capt. D. Brett Ridgely, for the many hours he spent tutoring me in H_2 and H_∞ control theory, as this material is not supplied in any class offered at AFIT at this time. I am grateful to my thesis committee members, Capt. Curtis P. Mracek, Capt. Randy N. Paschall, and Dr. Brad Liebst, for their invaluable help in keeping my thesis comprehensible and complete. I wish to thank Jim Coburn of Sverdrup Technology, Inc. for supplying the generic missile model and data from which the model herein was derived. For getting me started in the right direction and for their unfailing years of support, I thank my parents,

Janet and Leon Riddle. Most of all, I wish to thank my wife Sherry for her unbelievable understanding and tolerance on those many nights when I was glued to the computer, and for always providing a warm and loving port in the storm.

Randall L. Riddle

Table of Contents

List of Figures

List of Tables

List of Symbols

A, B, C, D	state space matrices
A_n	missile normal acceleration
A_{ref}	missile reference area
a	speed of sound
$C_{m_{(\cdot)}}$	stability derivative
$C_{n_{(\cdot)}}$	stability derivative
cg	center of gravity
H_2	Hardy space with finite 2-norm
H_∞	Hardy space with finite ∞-norm
h	altitude
I	moment of inertia; identity matrix
j	$\sqrt{-1}$
$K_{(\cdot)}$	gain
LOS	line-of-sight
L_{ref}	missile reference length
M	Mach number
$M_{(\cdot)}$	dimensional stability derivative
m	missile mass
$N_{(\cdot)}$	dimensional stability derivative
q	dynamic pressure
R_T	range to target
r	vector of command signals
S_u, S_y	Cholesky matrix
s	Laplace variable

T	matrix of transfer functions
u	control signal
V	missile velocity
v	output vector
$W_{(\cdot)}$	weighting filter
w	external disturbances
X_2	Riccati solution
X_∞	Riccati solution
x	state vector
Y_2	Riccati solution
Y_∞	Riccati solution
y	output vector; error vector
α	angle of incidence
γ	missile bearing angle
Δ	normally distributed random variable
δ	fin deflection
η	sensor noises
θ_m	missile heading angle
θ_s	antenna angle relative to missile
ξ	plant disturbances
ρ	air density; weighting matrix
$\bar{\rho}$	spectral radius
σ	singular value
τ	time constant
ϕ	boresight error signal
ϕ_e	true boresight error
ϕ_T	bearing to target

ω	antenna servomotor input; frequency
$\dot{(\cdot)}$	first derivative
$\ddot{(\cdot)}$	second derivative
$\tilde{(\cdot)}$	scaled or normalized value
$(\cdot)_{com}$	commanded value
$\lvert\cdot\rvert$	magnitude
$\lVert\cdot\rVert_2$	2-norm
$\lVert\cdot\rVert_\infty$	∞-norm

Abstract

H_2 and H_∞ design techniques are applied to a state space representation of a surface-to-air missile system with unstable nonminimum phase airframe response characteristics. A method for converting the tracking and command following problems to the "standard problem" is given. Artificial frequency-dependent filtering of external inputs is required for proper closed loop system performance, and a method for deriving the filters is developed. Areas requiring further study are identified.

DESIGN OF A ROBUST CONTROLLER FOR AN UNSTABLE NONMINIMUM PHASE GUIDED MISSILE

I. INTRODUCTION

The purpose of this thesis is to investigate and apply new H_2 and H_∞ robust control system design techniques to a surface-to-air missile control system, and compare the performance of the resultant systems to the performance of a system with a controller derived from conventional control system synthesis techniques.

A surface-to-air missile example was chosen for comparison because it will test the robust controller design methodologies' capability tc handle extreme cases. The transfer functions of the chosen missile have right half-plane poles and zeros (open-loop unstable and nonminimum phase). The missile is unstable due to the location of the center of gravity, which is aft of the aerodynamic center, and is nonminimum phase due to the use of tail-mounted control surfaces. The objective is to design a controller which stabilizes the system and makes it responsive to commands so that guidance commands successfully steer the missile to the target.

Three design methodologies will be compared. The first is a classical approach, using root locus and time response analyses to derive a control system with good performance in

the nominal case. The second is the H_2 approach which provides robustness for systems exposed to well-defined stochastic disturbances and parameter variations. The third is the H_∞ methodology which minimizes system response to unknown but deterministic disturbances and provides robustness with respect to unstructured uncertainties. The relative performance of these methods will be compared by implementing each controller in a two degree-of-freedom digital simulation. To provide a baseline for performance, each controller will first be implemented in a nominal model which is not subject to disturbances. Each will then be implemented in a more realistic model which provides: (a) both time-varying and constant parameter variations in the system components and equations of motion, (b) stochastic disturbances via target glint, sensor noise and turbulence, and (c) deterministic disturbances via loss of target data. The measure of merit used for these simulation runs will be miss distance, as well as detailed examination of missile transient responses.

II. Overview

The scope of this report is broad, as a large number of tasks must be completed prior to comparing the performance of the different controllers. These include development of the system description, conversion to state space format, derivation of the different controllers, and simulation of the missile engagement scenarios. This chapter details how these tasks are organized and presented in this report, so it will be easier for the reader to follow the development.

Missile System Description

In Chapter III, the missile system is described in detail. The equations of motion for the missile body are developed and the system transfer functions are given for both the missile body and the target tracking system. Flight conditions are described for both: (1) a nominal situation where the environment and missile system are not subject to changes or variations, and (2) a more realistic situation where the environment changes, the missile system components are subject to variation, and disturbances enter the system.

State Space Representation

In Chapter IV, the missile system description given in Chapter III is converted to a state space representation, which is necessary to apply the robust control methods. Both

the nominal model and the model with variations are described in detail.

Classical Control System Design

In Chapter V, a controller for the missile system is derived using standard classical design techniques, including root locus, time response, and frequency domain analysis. Acceptable performance is obtained with a simple proportional feedback controller. The author realizes that better performance could probably be obtained with lead/lag, integrator, and derivative controllers. Due to scope limitations, however, these options were not pursued in favor of focusing on robust controller design.

H_2 Controller Design

In Chapter VI, the theory for H_2 controller design is reviewed and applied to the missile system. This involves some manipulation of the original state space representation and addition of many artificial weighting filters to the plant inputs and outputs to get the problem into the form solvable by existing theory. Producing these manipulations and artificial filters constituted the bulk of the design effort, and the methods for selecting these are described in detail.

H_∞ Controller Design

In Chapter VII, the theory for H_∞ controller design is applied to the missile system. The plant manipulations and artificial filtering of inputs and outputs needed for this

design effort are similar to those needed for the H_2 design. For this system, no additional problem formulation effort is required, so this chapter is devoted solely to a review of the H_∞ problem requirements and derivation of the controller.

Performance Comparisons

In Chapter VIII, the performance of each of the controllers developed is compared. Comparison is based on missile flyout simulation results, with miss distance being the primary figure of merit. Development of the flyout simulation is briefly discussed. Comparison of flyout time histories allows some qualitative comparisons in addition to the quantitative results yielded by miss distance comparison.

Results and Conclusions

In Chapter IX, the author makes remarks about the advantages and disadvantages of the robust controller designs and methodologies. Areas of further study are identified.

Filters

The artificial filters developed for the H_2 and H_∞ controller designs are described in detail in Appendix A.

Flyout Time Histories

Appendix B contains missile system output time histories, missile and target position plots, and tabulated state histories for a representative sample of the flyout runs.

Controllers

The controllers obtained for the H_2 and H_∞ designs are composed of 24 states each. Reduced-order controllers were obtained for use in the simulation. Both the full-order and reduced-order controllers are described in detail in Appendix C.

III. Surface-to-Air Missile System Description

The surface-to-air missile system description used herein is provided by Sverdrup Technology, Inc. [12]. The system description is derived from a digital model generated by Jim Coburn of Sverdrup as a generic model of a tail-control missile to be used for training and experimentation purposes.

The model is composed of: (1) a system-specific data base, and (2) a simulation execution program. The simulation execution program is generic in its routines, and depends upon specific data provided by the data base for simulation of a particular missile system. The data base for a generic tail-control missile created by Coburn, with some slight modifications, was used. These modifications include simplification of the antenna servomechanism for ease of computation, omission of lowpass filters associated with the servo op-amp, moving the center of gravity aft to cause the system to be statically unstable, and simplification to two dimensions.

Missile velocity and altitude time histories are postulated to provide some realistic parameter variations. Any inaccuracy in this representation of the model is solely the fault of the author.

The model developed herein describes motion in a single plane only, and does not simulate missile axial forces (drag) or the effects of gravity.

Equations of Motion

The following equations of motion [2] model the airframe dynamics. They are used to derive the transfer functions and state space models associated with the airframe.

$$A_n(s) = N_\alpha \alpha(s) + N_\delta \delta(s) \tag{3.1}$$

$$\ddot{\theta}_m(s) = -M_\alpha \alpha(s) + M_\delta \delta(s) \tag{3.2}$$

$$\dot{\alpha}(s) = \dot{\theta}_m(s) - \dot{\gamma}(s) \tag{3.3}$$

$$\dot{\gamma}(s) = \frac{A_n(s)}{|V|} = \frac{N_\alpha \alpha(s) + N_\delta \delta(s)}{|V|} \tag{3.4}$$

with the above defined as

A_n = component of acceleration normal to airframe

θ_m = missile heading angle

α = angle of attack

γ = bearing of missile velocity vector

δ = control surface deflection

$|V|$ = magnitude of missile velocity

The dimensional stability derivatives [9:412-445] are given by

$$N_\alpha = C_{n_\alpha} q A_{ref}/m \tag{3.5}$$

$$N_\delta = C_{n_\delta} q A_{ref}/m \tag{3.6}$$

$$M_\alpha = C_{m_\alpha} q A_{ref} L_{ref}/I \tag{3.7}$$

$$M_\delta = C_{n_\delta} q A_{ref} L_{ref}/I \tag{3.8}$$

where the stability derivatives (C_{n_α}, etc.) are tabulated in [12] as a function of Mach number, and the other parameters

are defined as

q = dynamic pressure ($=\rho V^2/2$) (N/m^2)

A_{ref} = missile reference area ($= 0.031 m^2$ [12])

m = missile mass (kg)

I = missile moment of Inertia ($kg\text{-}m^2$)

L_{ref} = Missile reference length ($= 0.2m$ [12])

The sign conventions used for the missile airframe parameters are as shown in Figure 3.1.

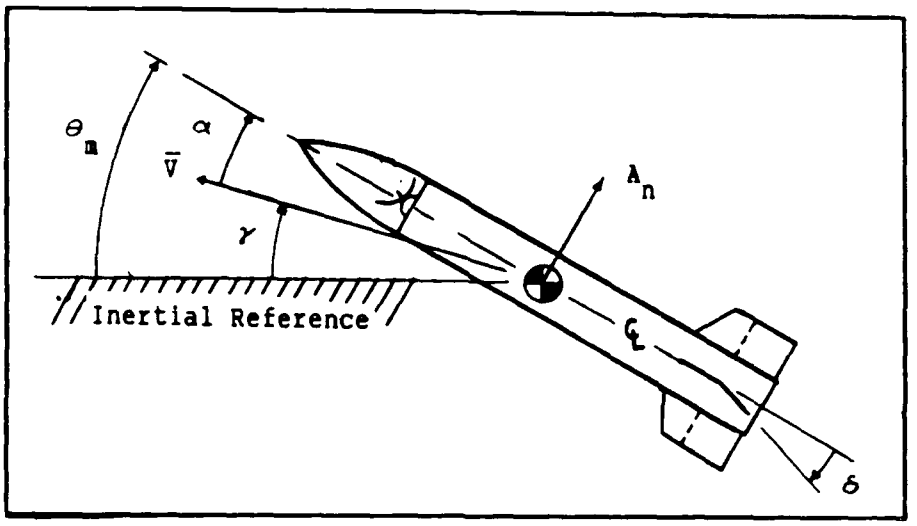

Fig 3.1. Missile Sign Conventions

The target tracking antenna and servomechanism are attached to the front end of the missile. The tracker data is given in transfer function form in [12] and will be listed in the next section.

Nominal Flight Condition

This section lists the values used in the nominal model. For this time-invariant description, all flight conditions are

held constant, and no noise or disturbances enter the system. The nominal flight conditions (fixed based on data from [12] and with atmospheric data from [1]) are listed in Table 3.1. A computer simulation of the missile flyout will be constructed using these constant values for the nominal flight condition. This model will be used as a baseline for determining noise and disturbance effects.

Table 3.1. Nominal Flight Conditions

Center of Gravity	2.63 m
Mass	127 kg
Inertia	271.3 kg-m^2
Altitude	20 kft
Mach	3.5
Velocity	1100 m/s
Speed of sound	315 m/s
Dynamic pressure	$4x10^5$ N/m^2
Air density	0.65 kg/m^3

Nominal Airframe. The airframe stability derivatives for this nominal flight condition were extracted from the tabulated data in [12] and are given in Table 3.2.

Table 3.2. Stability Derivatives

C_{n_α}	11.5
C_{n_δ}	5.7
C_{m_α}	-0.1
C_{m_δ}	-0.3

The values in Tables 3.1 and 3.2 were then applied to

equations 3.5-3.8 to yield the dimensional stability derivatives listed in Table 3.3.

Table 3.3. Dimensional Stability Derivatives

N_α	2.0 (g's/deg)
N_δ	1.0 (g's/deg)
M_α	-0.91 (deg/sec^2/deg)
M_δ	-2.74 (deg/sec^2/deg)

These coefficients yield the following transfer functions, using the equations of motion listed above and adding the servomechanism dynamics

$$\frac{\delta(s)}{\delta_{com}(s)} = \frac{77}{s+77} \quad [12] \tag{3.9}$$

$$\frac{\dot{\theta}_m(s)}{\delta_{com}(s)} = \frac{-211(s+1.1894)}{(s+77)(s+1.5917)(s-0.5717)} \tag{3.10}$$

$$\frac{\theta_m(s)}{\delta_{com}(s)} = \frac{-211(s+1.1894)}{s(s+77)(s+1.5917)(s-0.5717)} \tag{3.11}$$

$$\frac{\alpha(s)}{\delta_{com}(s)} = \frac{-39.3(s+5.3725)}{(s+77)(s+1.5917)(s-0.5717)} \tag{3.12}$$

$$\frac{A_n(s)}{\delta_{com}(s)} = \frac{77(s+2.5278)(s-2.5278)}{(s+77)(s+1.5917)(s-0.5717)} \tag{3.13}$$

Target Tracking System. The target tracking system will be synthesized from two components; a simplified boresight error resolver and an antenna mounted on a servomechanism. The boresight error resolver returns an error signal, ϕ, in response to the boresight error input ϕ_e (angular position of target relative to antenna boresight position), with a transfer function

$$\frac{\dot{\phi}(s)}{\phi_e(s)} = \frac{20.7}{s+5.26} \quad [12] \qquad (3.14)$$

The sign convention for ϕ_e is as shown in Figure 3.2, where θ_s is the angular displacement of the antenna relative to the missile centerline and ϕ_T is the bearing to target.

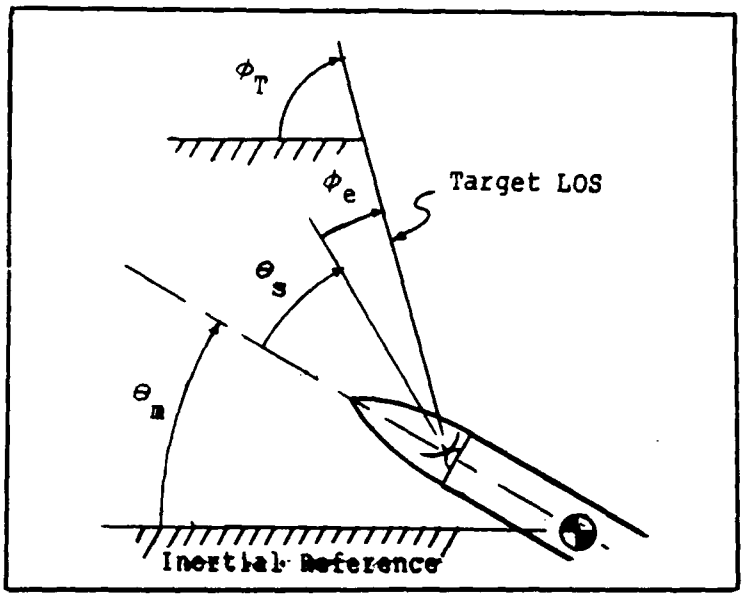

Figure 3.2. Tracking System Sign Conventions

The antenna servomechanism is attached to the antenna pedestal such that it generates an angular displacement rate of the antenna boresight $\dot{\theta}_s$ in response to an input signal ω. The transfer function for the servomechanism is

$$\frac{\dot{\theta}_s(s)}{\omega(s)} = \frac{94}{s+104} \quad [12] \qquad (3.15)$$

This combined servomotor/resolver system can be represented as shown in Figure 3.3.

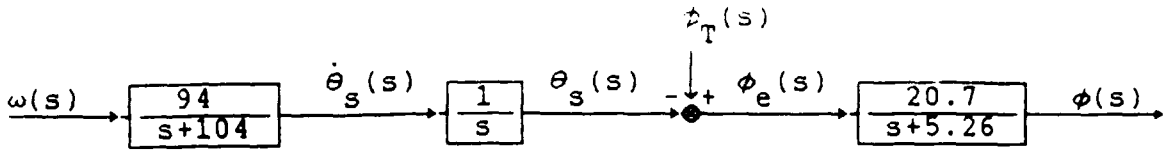

Figure 3.3. Target Tracking System

Coupled System. When the antenna is coupled to the airframe the total integrated system looks as in Figure 3.4.

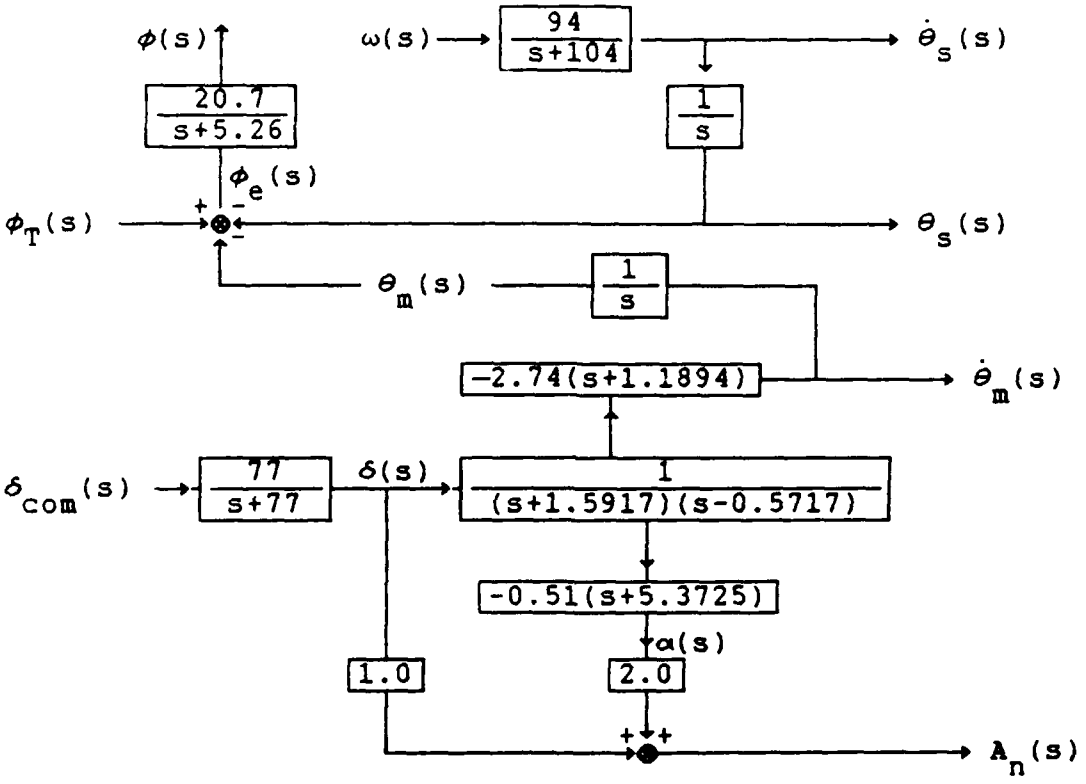

Figure 3.4. Coupled System Block Diagram

Note that the output of the error resolver has not yet been fed into the antenna servomechanism. This will be done during the design process.

Derivation of the additional transfer functions associated with the coupled system yields

$$\frac{p(s)}{\delta_{com}(s)} = \frac{4368(s+1.1834)}{s(s+77)(s+1.5917)(s-0.5717)(s+5.26)} \quad (3.16)$$

$$\frac{\phi(s)}{\phi_T(s)} = \frac{20.7}{(s+5.26)} \quad (3.17)$$

$$\frac{\phi(s)}{\omega(s)} = \frac{-1945.8}{s(s+104)(s+5.26)} \quad (3.18)$$

Time Varying System with Disturbance Inputs

This section lists all the time-varying parameters, parameter variations, and disturbance inputs to the system. These effects are simulated in the time-varying model.

Missile. In reality, the missile does not operate in a constant deterministic environment and many of the physical parameters of the system are not known accurately due to component variation from missile to missile. A realistic simulation of the missile must include the effects of these variations. To this end, time functions will be used to model parameters which vary over the time of guided operation (8 seconds), some of the component properties will be perturbed, and disturbances will be added.

Time Varying Parameters. In order to realistically vary flight conditions with time, the assumption is made that the missile has finished boosting, initiated the sustained propulsion phase, and starts guidance at a 15kft altitude, climbing at a constant rate of 1000 feet per second. This flight path is assumed based on a typical surface-to-air missile launch, and the target altitude induced by this

profile is dependant upon actual time to intercept. The time function for the missile altitude is then

$$h(t) = 15{,}000 + 1000t \quad \text{(feet)} \tag{3.19}$$

Given standard atmospheric conditions, this causes the air density and local speed of sound to vary as [1:70]

$$\rho(t) = 0.7626 - 0.0214t \quad (kg/m^3) \tag{3.20}$$

$$a(t) = 322.27 - 1.26t \quad (m/s) \tag{3.21}$$

Missile velocity normally varies slightly as the propellant is burned during the sustained phase, so the following velocity time function is assumed based on propulsion data from [12]

$$V(t) = 1000 + 80t - 8t^2 \quad (m/s) \tag{3.22}$$

Since the reference data tabulates aerodynamic coefficients as a function of local Mach number, it is necessary to express this value as

$$M(t) = V(t)/a(t) = \frac{1000 + 80t - 8t^2}{322.27 - 1.26t} \tag{3.23}$$

For ease of calculation, it is desired to express this function as a simple polynomial in time only. This can be accomplished by using a Taylor series expansion (which for the case of ratios of polynomials is equivalent to carrying out the division). The Taylor series expansion yields an infinite order polynomial, which is normally truncated at the point where the desired accuracy is reached for the interval of interest. An interval of eight seconds and an accuracy of 2% are used for all of the Taylor series expansions developed in

this section (that is, when the highest order term contributes less than 2% to the value at eight seconds, it and all following terms are ignored). Taylor series expansion yields the Mach number time function

$$M(t) = 3.103 + 0.26t - 0.0238t^2 \text{ (dimensionless)} \quad (3.24)$$

Based on the above values for density and velocity, dynamic pressure can be expressed as

$$q(t) = \rho(t)\, V(t)^2/2$$
$$= (0.7626 - 0.0214t)(1000 + 80t - 8t^2)^2/2 \quad (3.25)$$

Inertia, mass, and stability derivatives were derived from the tabulated data [12], where they are listed as function of Mach number and time. Using equation 3.24, these were all converted to time functions, yielding

$$m(t) = 127 - 2t \quad (kg) \quad (3.26)$$

$$\Delta cg(t) = 0.84 - 0.0008t \quad (m) \quad (3.27)$$

$$I(t) = 279.6 - 1.58t + 0.0027t^2 (kg\text{-}m^2) \quad (3.28)$$

$$C_{n_\alpha}(t) = 11.30 - 0.0447t + 0.0409t^2 \quad (3.29)$$

$$C_{n_\delta}(t) = 6.130 - 0.0447t + 0.0409t^2 \quad (3.30)$$

$$C_{m_\alpha}(t) = 0.0017 - 0.037t + 0.0038t^2 \quad (3.31)$$

$$C_{m_\delta}(t) = -0.329 + 0.0181t - 0.0017t^2 \quad (3.32)$$

Using equations 3.5-3.8 for dimensional stability derivatives, equations 3.25-3.32 are used to generate the following equations for dimensionsal stability derivatives as functions

of time

$$N_\alpha(t) = 1.871 + 0.202t - 0.0262t^2 + 0.0008t^3 \quad (3.33)$$

$$N_\delta(t) = 1.016 + 0.076t - 0.0161t^2 - 0.0004t^3 \quad (3.34)$$

$$M_\alpha(t) = +0.0144 - 0.3109t - 0.0111t^2 + 0.0085t^3 \quad (3.35)$$

$$M_\delta(t) = -2.78 - 0.230t + 0.044t^2 - 0.001t^3 \quad (3.36)$$

Component Variations. Many other parameters of the system vary from missile to missile, but not with time. In composing these variations, the author's best estimate was used.

The time constant (τ_f) of the fin servomechanism can vary. The perturbed servomechanism transfer function can be written as

$$\frac{\delta(s)}{\delta_{com}(s)} = \frac{1/\tau_f}{s + 1/\tau_f} = \frac{77+\Delta}{s + (77+\Delta)} \quad (3.37)$$

where Δ is normally distributed with zero mean and a variance σ^2 determined by manufacturing quality control. A variance value of 4 was assumed. Standard statistical notation denotes this as $\Delta = N(0,4)$. Similarly, it was assumed that the body rate sensor suffers from a variance of 1% in gain, so it sees a variation of N(0,.01) from its normal gain of 1. Also, it was assumed the normal acceleration sensor sees a variation of N(0,.01) from its normal gain of 1.

Disturbances. There are disturbances in the form of turbulence and power supply noise entering the missile airframe system. Reference [9] presents data describing turbulence disturbances, and from this reference atmospheric

turbulence can be modeled as random wind gusts of velocity w_g, where $w_g = N(0,3)$ (m/sec). Also from [9], it can be seen that wind gusts can be modeled as affecting the airframe as a change in angle of incidence. Specifically, the wind gust can be modeled as an additional component to α, namely α_g, with the transfer function

$$\frac{\alpha_g(s)}{w_g(s)} = \frac{1}{|V|(s + 1/\tau_m)} \tag{3.38}$$

where τ_m is a time constant dependant on the airframe. It is assumed for this missile that τ_m is very large, such that the above transfer function can be approximated as

$$\frac{\alpha_g(s)}{w_g(s)} = \frac{1}{|V|s} \tag{3.39}$$

or

$$\dot{\alpha}_g(s) = \frac{w_g(s)}{|V|} \tag{3.40}$$

Using the nominal velocity as an approximation, the turbulence disturbance is modeled as $\dot{\alpha}_g = N(0,0.003)$.

Another disturbance entering the missile system is power supply noise (ξ). This disturbance appears as a random input to the fin servomotor, entering at the same point as δ_{com}. Such noises can be characterized as having zero mean with some variance σ^2 dependent on the magnitude of the noise in the system. This noise also has distinct frequency characteristics, and can be represented as a random signal $\beta = N(0,\sigma^2)$ being passed thru a filter with the same frequency

characteristics as the noise. For instance, if the noise lies within the frequency range $[\omega_1 \ \omega_2]$, it can be represented as

$$\xi(s) = \frac{K_f \beta}{s(s + \omega_1)(s + \omega_2)} \tag{3.41}$$

where K_f is set to achieve unity gain over the frequency range of interest. For the power supply noise, the following values are assumed

$$\beta = N(0,0.05) \tag{3.42}$$

$$\omega_1 = \omega_2 = 400 \ \text{sec}^{-1} \tag{3.43}$$

Target Tracking System. The target tracking system, being composed of electronic parts and not particularly dependent upon the flight conditions for its operating parameters, does not suffer any of the time-varying parameter changes that the missile does. It does see component variations and disturbances similar to the missile, however, and these must be addressed.

Component Variations. The resolver can be modeled as consisting of a time constant τ_r and a gain K_r,

$$\frac{\phi(s)}{\phi_e(s)} = \frac{K_r}{s + 1/\tau_r} \tag{3.44}$$

and is subject to variations in both of these values. K_r is assumed to vary as N(0,2) and $1/\tau_r$ as N(0,0.5). The servomotor can be modeled in this fashion also. For the servomotor, it is assumed that K_s varies as N(0,4) and $1/\tau_s$ as N(0,4) (independently). In addition, it was assumed that the

sensors which detect the rate and position of the antenna suffer variances of 1% in accuracy, so each of these sees a variation of N(0,0.01) from its normal gain of 1.

Disturbances. The electrical components of the target tracking system are subjected to the same power supply noise as the fin servomotor described above. Thus, this same noise will be injected into the angle error resolver and the antenna servomotor.

Finally, target data is corrupted by target glint. Glint enters the system as a random pulse-to-pulse variation in target position. The glint was assumed to be distributed as N(0,25) (meters). This can be converted to an angular noise input ξ dependent on target range (R_T) by using the small angle approximation and converting radians to degrees to get

$$\xi = N(0,1500/R_T) \tag{3.45}$$

All of the above noise and disturbance inputs are modeled in the simulation. To do this, it is necessary to model how these inputs enter the system in state space form. This is done in Chapter IV.

IV. State Space Description

The state space representation of the airframe is derived from the equations of motion. The standard state space nomenclature [6:2]

$$\dot{x} = A\,x + B\,u \tag{4.1}$$

$$y = C\,x + D\,u \tag{4.2}$$

will be used as a base for building the state space representations used herein. The systems described will grow too large to maintain this simple notation and preserve clarity, so subscripts and additional vectors will be added as needed. The development of this representation will parallel the Laplace domain development in Chapter III as much as possible.

Missile Airframe

Using the standard nomenclature above, the missile airframe is represented by

$$x = \begin{bmatrix} \delta \\ \dot{\theta}_m \\ \theta_m \\ \alpha \end{bmatrix} \begin{matrix} \text{(fin deflection, deg)} \\ \text{(body rate, deg/sec)} \\ \text{(heading angle, deg} \\ \text{(angle of attack, deg)} \end{matrix} \tag{4.3}$$

$$u = \delta_{com} \quad \text{(fin deflection command, deg)} \tag{4.4}$$

$$y = \begin{bmatrix} A_n \\ \dot{\theta}_m \end{bmatrix} \text{(normal acceleration, g's)} \tag{4.5}$$

Using these state, input, and output vectors, the corresponding A, B, C, and D matrices from the transfer functions in Chapter III are

$$A = \begin{bmatrix} -77 & 0 & 0 & 0 \\ -2.74 & 0 & 0 & 0.91 \\ 0 & 1 & 0 & 0 \\ -0.51 & 1 & 0 & -1.02 \end{bmatrix} \tag{4.6}$$

$$B = \begin{bmatrix} 77 \\ 0 \\ 0 \\ 0 \end{bmatrix} \tag{4.7}$$

$$C = \begin{bmatrix} 1 & 0 & 0 & 2 \\ 0 & 1 & 0 & 0 \end{bmatrix} \tag{4.8}$$

$$D = \begin{bmatrix} 0 \\ 0 \end{bmatrix} \tag{4.9}$$

This system is controllable [6:53], but the θ_m state is not observable [6:66].

Target Tracking System

For the target tracking system, the vectors are

$$x = \begin{bmatrix} \phi \\ \dot{\theta}_s \\ \theta_s \end{bmatrix} \begin{matrix} \text{(boresight error signal, deg)} \\ \text{(antenna rate, deg/sec)} \\ \text{(antenna angle measured from missile centerline, deg)} \end{matrix} \tag{4.10}$$

$$u = \begin{bmatrix} \phi_T \\ \omega \end{bmatrix} \begin{matrix} \text{(bearing to target, deg)} \\ \text{(antenna servo input, deg/sec)} \end{matrix} \tag{4.11}$$

$$y = \begin{bmatrix} \phi \\ \dot{\theta}_s \\ \theta_s \end{bmatrix} \tag{4.12}$$

This yields

$$A = \begin{bmatrix} -5.26 & 0 & -20.7 \\ 0 & -104 & 0 \\ 0 & 1 & 0 \end{bmatrix} \tag{4.13}$$

$$B = \begin{bmatrix} 20.7 & 0 \\ 0 & 94 \\ 0 & 0 \end{bmatrix} \tag{4.14}$$

$$C = \begin{bmatrix} 1 & 0 & 0 \\ 0 & 1 & 0 \\ 0 & 0 & 1 \end{bmatrix} \tag{4.15}$$

$$D = \begin{bmatrix} 0 & 0 \\ 0 & 0 \\ 0 & 0 \end{bmatrix} \tag{4.16}$$

Coupled System

Combining the tracker with the airframe, and making the substitution $\phi_e = \phi_T - \theta_m - \theta_s$ (See Figure 3.4) yields the following state-space representation of the combined system, hereafter referred to as the plant. At this time, it is convenient to split the input vector into two separate vectors, one of which contains those inputs which can be manipulated by the designer, δ_{com} and ω, the other containing the input which is an external signal, ϕ_T. These input vectors will hereafter be designated u and w, respectively. Note the additional subscripts: p to denote the plant, 11 to denote those matrices corresponding to the input u_p, and 12 to denote those matrices

corresponding to the input w_p. Thus, the plant is represented by

$$\dot{x}_p = A_p x_p + B_{p11} u_p + B_{p12} w_p \tag{4.17}$$

$$y_p = C_p x_p + D_{p11} u_p + D_{p12} w_p \tag{4.18}$$

where

$$x_p = \begin{bmatrix} \delta \\ \dot{\theta}_m \\ \theta_m \\ \alpha \\ \phi \\ \dot{\theta}_s \\ \theta_s \end{bmatrix} \tag{4.19}$$

$$u_p = \begin{bmatrix} \delta_{com} \\ \omega \end{bmatrix} \tag{4.20}$$

$$w_p = [\ \phi_T\ ] \tag{4.21}$$

$$y_p = \begin{bmatrix} \dot{\theta}_m \\ A_n \\ \phi \\ \dot{\theta}_s \\ \theta_s \end{bmatrix} \tag{4.22}$$

$$A_p = \begin{bmatrix} -77 & 0 & 0 & 0 & 0 & 0 & 0 \\ -2.74 & 0 & 0 & 0.91 & 0 & 0 & 0 \\ 0 & 1 & 0 & 0 & 0 & 0 & 0 \\ -0.51 & 1 & 0 & -1.02 & 0 & 0 & 0 \\ 0 & 0 & -20.7 & 0 & -5.26 & 0 & -20.7 \\ 0 & 0 & 0 & 0 & 0 & -104 & 0 \\ 0 & 0 & 0 & 0 & 0 & 1 & 0 \end{bmatrix} \tag{4.23}$$

$$B_{p11} = \begin{bmatrix} 77 & 0 \\ 0 & 0 \\ 0 & 0 \\ 0 & 0 \\ 0 & 0 \\ 0 & 94 \\ 0 & 0 \end{bmatrix} \tag{4.24}$$

$$B_{p12} = \begin{bmatrix} 0 \\ 0 \\ 0 \\ 0 \\ 20.7 \\ 0 \\ 0 \end{bmatrix} \tag{4.25}$$

$$C_p = \begin{bmatrix} 0 & 1 & 0 & 0 & 0 & 0 & 0 \\ 1 & 0 & 0 & 2 & 0 & 0 & 0 \\ 0 & 0 & 0 & 0 & 1 & 0 & 0 \\ 0 & 0 & 0 & 0 & 0 & 1 & 0 \\ 0 & 0 & 0 & 0 & 0 & 0 & 1 \end{bmatrix} \tag{4.26}$$

$$D_{p11} = \begin{bmatrix} 0 & 0 \\ 0 & 0 \\ 0 & 0 \\ 0 & 0 \\ 0 & 0 \end{bmatrix} \tag{4.27}$$

$$D_{p12} = \begin{bmatrix} 0 \\ 0 \\ 0 \\ 0 \\ 0 \end{bmatrix} \tag{4.28}$$

This is the 'clean' version of the missile model and will be used for the classical design approach.

Time Varying System with Disturbance Inputs

In addition to the above system representation, the realistic system is subject to time-variant changes in environmental conditions, component variations, and noise

inputs as described in Chapter III.

Disturbances. The noise inputs are appended to the clean state space representation such that

$$\dot{x}_p = A_p x_p + B_{p11} u_p + B_{p12} w_p + B_{p2} \xi \tag{4.29}$$

$$y_p = C_p x_p + D_{p11} u_p + D_{p12} w_p + D_{p2} \xi + \eta \tag{4.30}$$

where equations 4.17-4.22 still apply and

$$B_{p2} = \begin{bmatrix} 0 & 0 & 1 \\ 1 & 0 & 0 \\ 0 & 0 & 0 \\ 1 & 0 & 0 \\ 0 & 1 & 0 \\ 0 & 0 & 1 \\ 0 & 0 & 0 \end{bmatrix} \tag{4.31}$$

$$D_{p2} = \begin{bmatrix} 0 & 0 & 0 \\ 0 & 0 & 0 \\ 0 & 0 & 0 \\ 0 & 0 & 0 \\ 0 & 0 & 0 \end{bmatrix} \tag{4.32}$$

$$\xi = \begin{bmatrix} N(0,0.003) \\ N(0,1500/R_T) \\ N(0,0.05) \end{bmatrix} \begin{matrix} \text{(turbulence)} \\ \text{(target glint)} \\ \text{(power supply noise)} \end{matrix} \tag{4.33}$$

$$\eta = \begin{bmatrix} N(0,0.1) \\ N(0,0.05) \\ 0 \\ N(0,.1) \\ N(0,.05) \end{bmatrix} \begin{matrix} \text{(body rate gyro noise)} \\ \text{(accelerometer noise)} \\ \text{(no measurement noise)} \\ \text{(rate gyro noise)} \\ \text{(potentiometer noise)} \end{matrix} \tag{4.34}$$

Two items in the above deserve note. First, notice that target glint has a variance that is a function of range. This indicates that this signal is non-stationary, which creates special problems. This is another time-varying parameter. Secondly, notice that η's third element is zero. This is because ϕ is an electrical signal directly

available for measurement, and has no measurement noise corruption associated with it.

In addition to these random noise inputs, the real system is also subjected to a discrete deterministic (but unknown) disturbance, specifically loss of target data due to ECM. While qualitative statements can usually be made about factors such as this, it cannot be treated as a known quantity which can be compensated for.

Time-varying parameters and Component Variations. Next, parameter variations must be considered. These will enter into the real system as variations in missile velocity, mass, inertia, atmospheric conditions, center of gravity location, servomechanism time constants, component gains, and high-frequency unmodeled dynamics. These effects will all be simulated, except the high-frequency unmodeled dynamics. This exception is due solely to the desire to limit the scope of this investigation. This variation of parameters, both time-varying and invariant, will be modeled by making the A, B, and C matrices functions of time and adding the component variations as follows

$$A_p = \begin{bmatrix} -77+\Delta_1 & 0 & 0 & 0 & 0 & 0 & 0 \\ M_\delta & 0 & 0 & -M_\alpha & 0 & 0 & 0 \\ 0 & 1 & 0 & 0 & 0 & 0 & 0 \\ -N_\delta/V & 1 & 0 & -N_\alpha/V & 0 & 0 & 0 \\ 0 & 0 & -20.7+\Delta_2 & 0 & -5.26+\Delta_3 & 0 & -20.7+\Delta_2 \\ 0 & 0 & 0 & 0 & 0 & -104+\Delta_5 & 0 \\ 0 & 0 & 0 & 0 & 0 & 1 & 0 \end{bmatrix} \quad (4.35)$$

$$B_{11} = \begin{bmatrix} 77+\Delta_1 & 0 \\ 0 & 0 \\ 0 & 0 \\ 0 & 0 \\ 0 & 0 \\ 0 & 94+\Delta_4 \\ 0 & 0 \end{bmatrix} \tag{4.36}$$

$$B_{p12} = \begin{bmatrix} 0 \\ 0 \\ 0 \\ 0 \\ 20.7+\Delta_2 \\ 0 \\ 0 \end{bmatrix} \tag{4.37}$$

$$C_p = \begin{bmatrix} 0 & 1+\Delta_7 & 0 & 0 & 0 & 0 & 0 \\ N_\delta(1+\Delta_6) & 0 & 0 & N_\alpha(1+\Delta_6) & 0 & 0 & 0 \\ 0 & 0 & 0 & 0 & 1 & 0 & 0 \\ 0 & 0 & 0 & 0 & 0 & 1+\Delta_8 & 0 \\ 0 & 0 & 0 & 0 & 0 & 0 & 1+\Delta_9 \end{bmatrix} \tag{4.38}$$

where N_α, N_δ, M_α, M_δ, and V vary as defined in Chapter III and the Δ's are defined as

$$\Delta = \begin{bmatrix} N(0,4) \\ N(0,2) \\ N(0,0.5) \\ N(0,4) \\ N(0,4) \\ N(0,0.01) \\ N(0,0.01) \\ N(0,0.01) \\ N(0,0.01) \end{bmatrix} \tag{4.39}$$

Note that the Δ's are preset and do not vary with time.

With the problem now in the proper form, the design effort is initiated in Chapter V.

V. Classical Control System Design

In this section, the objective is to derive a missile control system based on classical design principles. Using the root locus, bode plot, and step response analysis tools, a controller is designed which stabilizes the missile, provides good tracking loop performance for the target tracker, and guides the missile to the target location using standard proportional navigation techniques.

The standard methodology for this type of design follows the algorithm: (1) design an autopilot which stabilizes the missile airframe and makes it responsive to command inputs, (2) design a feedback controller which provides for accurate tracking of the target line-of-sight, both stand-alone and in the presence of missile maneuvers, and (3) develop a guidance law which guides the missile to the target in the desired manner. These three tasks are traditionally taken as separate problems, and will be treated as such in this design.

Autopilot Design

The design objective for the autopilot is to obtain a stabilized body rate command system. This design goal is driven primarily by the guidance scheme used for proportional navigation described later in this section. Autopilot design for this airframe is complicated by two factors. First, the missile is open-loop statically unstable. This in itself is not a particularly difficult problem, which can usually be

surmounted by simple body rate and normal acceleration feedback. It is complicated in this design by nonminimum phase dynamic response of the missile normal acceleration, caused by tail-mounting the fins. Initially, a positive fin deflection, as defined in Chapter III, will induce normal acceleration in the positive direction. However, the positive fin deflection causes a negative angle-of-incidence rate, which generates a negative normal force stronger than the positive normal force due to fin deflection, and a negative normal force is the final result, after some time lag dependent upon the specific airframe dynamics.

To meet the design goal it is necessary to design feedback loops using sensor outputs. The airframe dynamics and sensors are described in Chapter III. The two outputs available for stabilizing the airframe are body rate and normal acceleration. The design will be accomplished using sequential loop closures. First, the body rate loop will be examined and closed, followed by the normal acceleration loop. Figure 5.1 depicts the scheme used to accomplish the design goal.

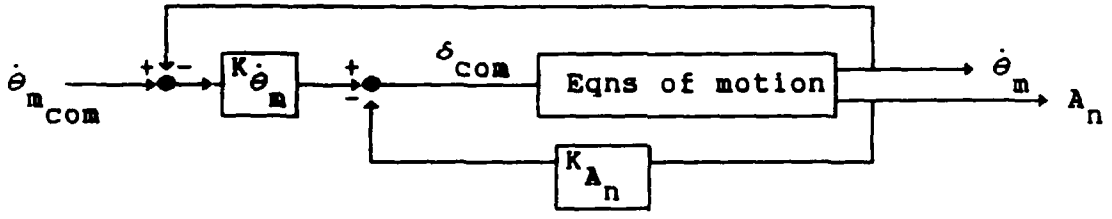

Figure 5.1. Body Rate and Normal Acceleration Feedback

The transfer functions for these two loops (derived from the equations of motion in Chapter III) are

$$\frac{A_n(s)}{\delta_{com}(s)} = \frac{77(s+2.5278)(s-2.5278)}{(s+77)(s+1.5917)(s-0.5717)} \qquad (3.13)$$

$$\frac{\dot{\theta}_m(s)}{\delta_{com}(s)} = \frac{-211(s+1.1894)}{(s+77)(s+1.5917)(s-0.5717)} \qquad (3.10)$$

The root loci for these functions are shown in Figures 5.2 and 5.3, respectively. Note that the scale of these figures precludes inclusion of the locus for the pole at s = -77. This was done to focus on the action of the critical poles near the origin. Note also that these loci are for negative values of the K's as defined in Figure 5.1.

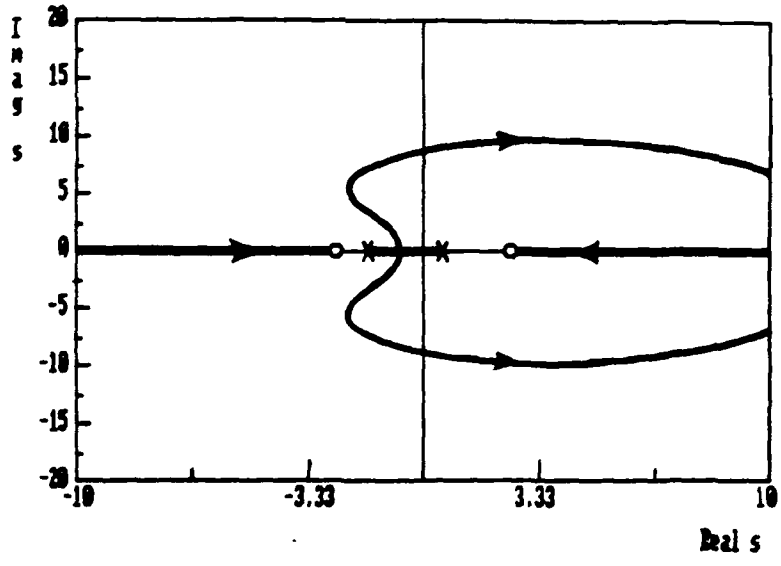

Figure 5.2. Root locus for Normal Acceleration Feedback (Negative Gain)

To stabilize the missile, feedback must be used to move the system poles as far as possible into the left half-plane

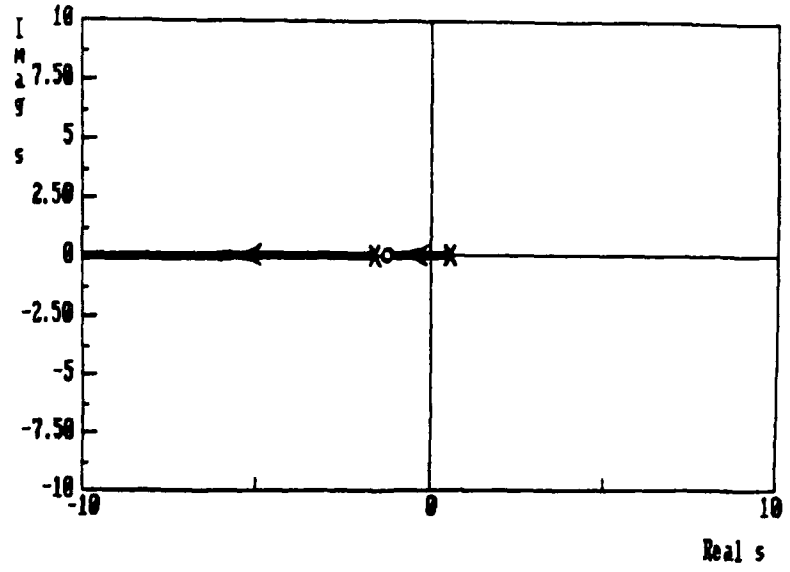

Figure 5.3. Root Locus for Body Rate Feedback (Negative Gain)

while maintaining good damping. To make the autopilot a body rate command system, $K_{\dot{\theta}_m}$ must be driven as high as possible (this is known as increasing the loop gain). It is evident from inspection of the root loci that first the gain of the body rate loop must be increased to move the unstable pole into the left-half plane. Also, it is desirable to move the pole at -1.5917 until it is left of the A_n zero at -2.5278 in order to modify the shape of the A_n root locus. A negative gain of magnitude 1 or greater will accomplish this. A body rate gain of -2 changes the normal acceleration loop transfer function to

$$\frac{A_n(s)}{\delta_{com}(s)} = \frac{77(s+2.5278)(s-2.5278)}{(s+71)(s+5.92)(s+1.03)} \qquad (5.1)$$

With the poles so placed, the root locus for the normal acceleration feedback loop now looks as in Figure 5.4.

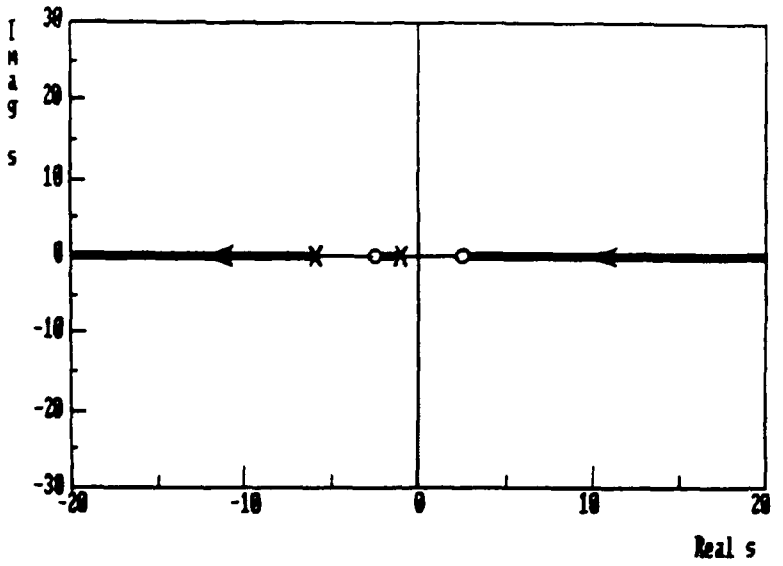

Figure 5.4. Root Locus for Normal Acceleration Feedback, with $K_{\dot{\theta}_m} = -2$. (Negative Gain)

This locus is much better than the previous one from a design viewpoint. Evaluation reveals that a negative gain in this loop is desired to decrease response time. The leftmost pole shown in Figure 5.4 joins rapidly with the servomotor pole at s = -71 and this pair then moves toward the right half-plane zero as the gain is increased. Thus, to preserve good damping, a maximum gain of -0.7 can be allowed. It is desired to keep the missile as stable as possible, so a value of -0.14 will be used. This is primarily to keep the gain and phase margins [7:430-433] high, which provides some robustness to modeling uncertainties. The body rate open-loop transfer function is given by

$$\frac{\dot{\theta}_m(s)}{\dot{\theta}_{m_{com}}(s)} = \frac{422(s+1.1894)}{s^3+67.24s^2+77.63s-1.1863} \qquad (5.2)$$

The Bode phase and magnitude plots for this transfer function are shown in Figure 5.5, from which it can be seen that these gains for the airframe control loop yield a gain margin of greater than 40 dB and a phase margin of 84 degrees.

Further examination reveals that increasing the body rate gain buys very little movement of the rightmost pole, while bringing the other two closer together, so that a lower acceleration gain is allowed to maintain damping and preserve good gain and phase margins. Therefore, a body rate gain of -2 and an acceleration gain of -0.14 provide about the best performance possible.

The step response due to a body rate command is shown in Figure 5.6. This figure shows that the design objective of a body rate command system is met very well.

Target Tracker

The design goals for the tracker system are: (1) minimize target track error, (2) minimize response time, and (3) minimize transient behavior. For this design effort, the tracker will be considered detached from the missile. Once again, successive loop closures will be used to consider feeding back both antenna rate and position. The antenna rate loop will be closed first, followed by the position loop. The scheme used to accomplish this design goal is depicted in Figure 5.7.

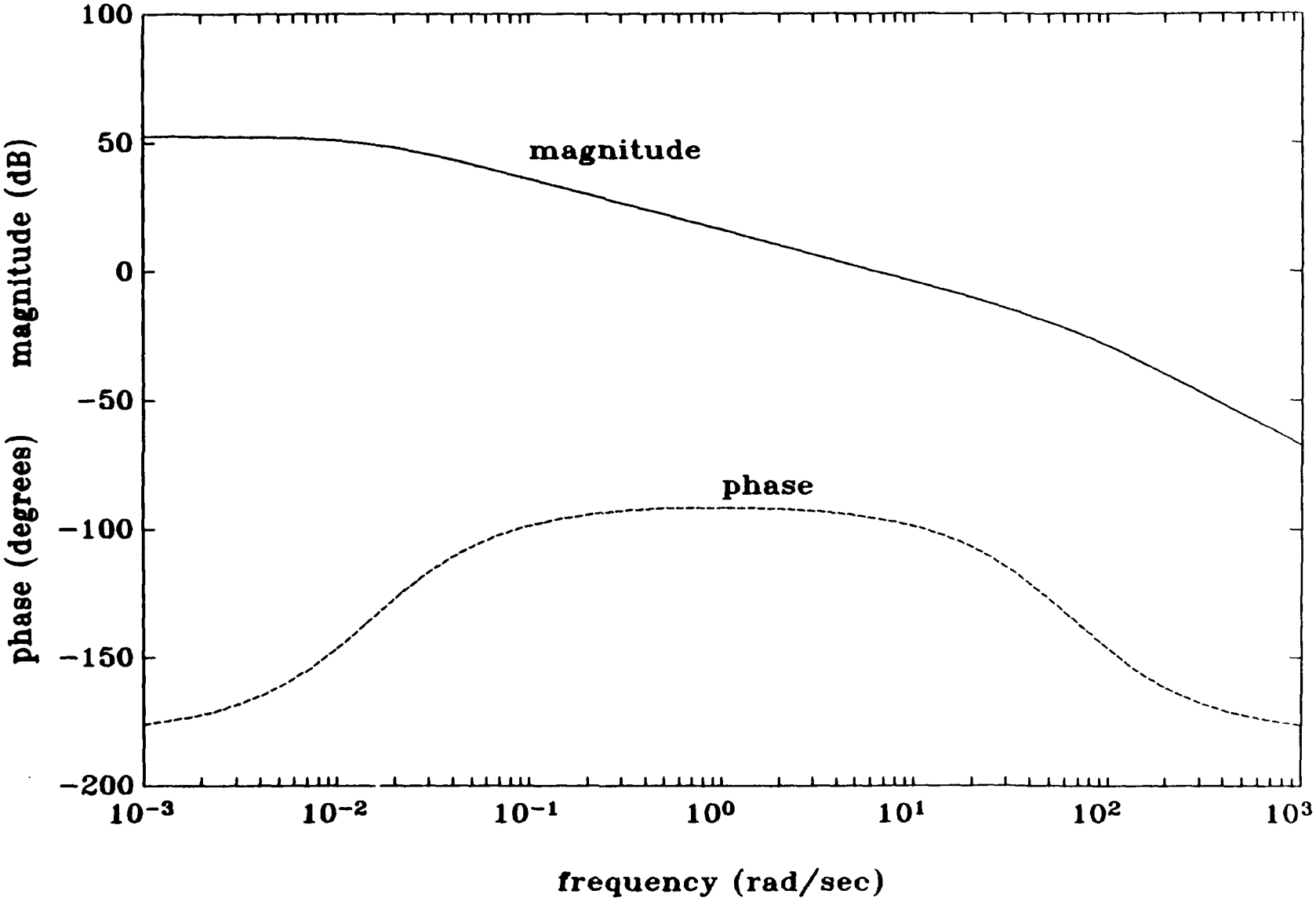

Figure 5.5. $\dot{\theta}_{\blacksquare}$ Open-Loop Transfer Function Bode Plots

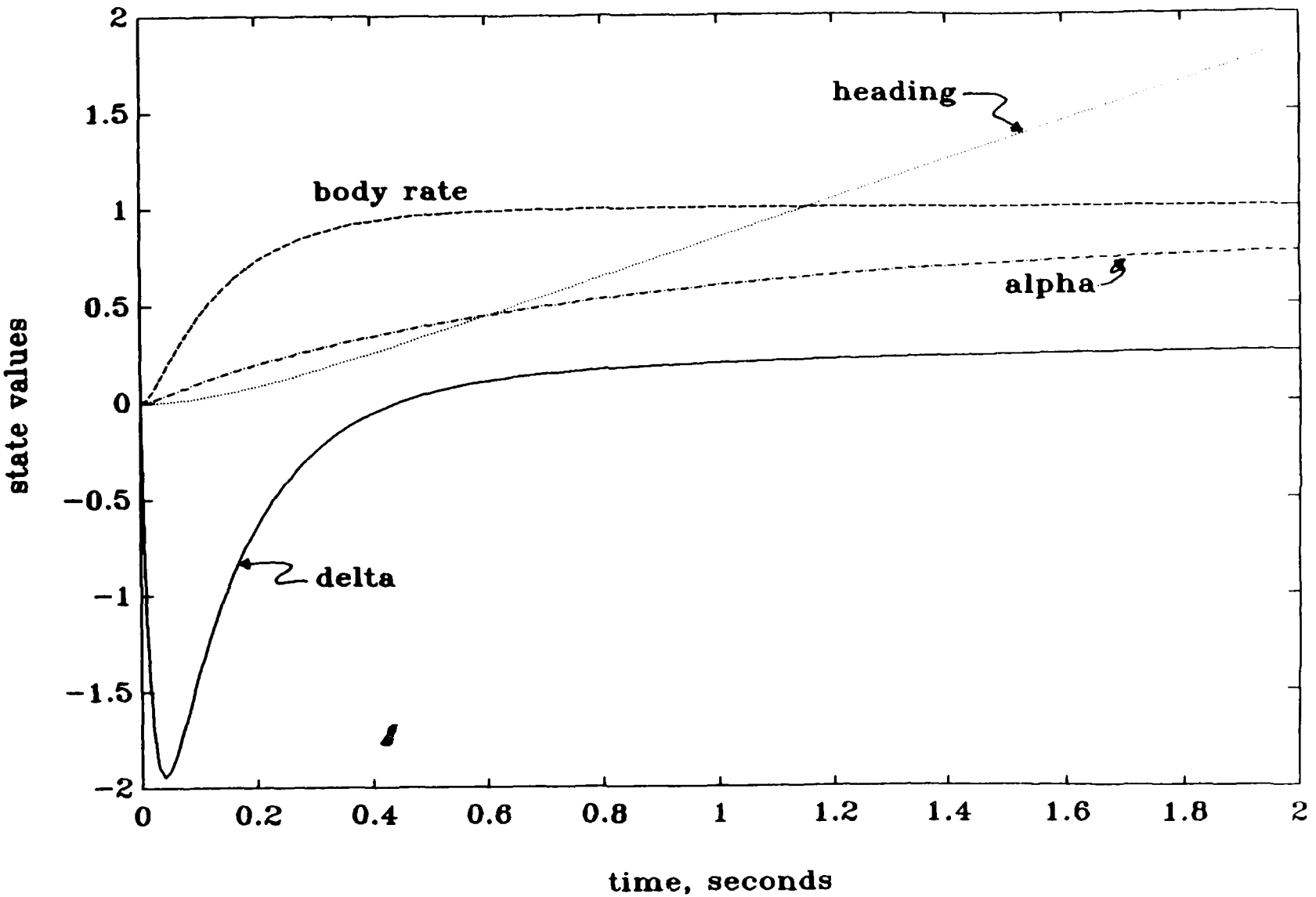

Figure 5.6. Airframe Response to Step Body Rate Command

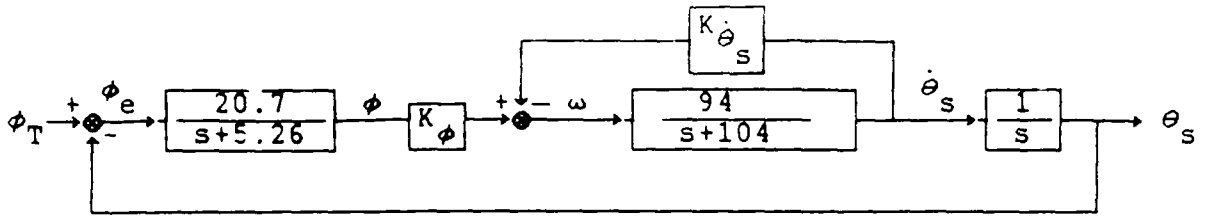

Figure 5.7. Tracker Feedback Loops

The step response of the 'unmodified' tracker (with K_ϕ=1 simply to close the loop and $K_{\dot{\theta}_s}$=0) is shown in Figure 5.8. This response shows the tracker to be slightly overdamped, but otherwise a fairly good design to begin with. As described in Chapter III, all three states of this component are directly available for measurement. However, only the ϕ and $\dot{\theta}_s$ measurements are needed to facilitate the design, since the boresight error resolver forms a natural unity feedback of θ_s, as is apparent in Figure 5.7. The transfer functions for the loops of interest are (with $K_{\dot{\theta}_s} = 0$ and $K_\phi = 1$)

$$\frac{\theta_s(s)}{\phi_T(s)} = \frac{-1945.8}{s(s+104)(s+5.26)} \tag{5.3}$$

$$\frac{\dot{\theta}_s(s)}{\omega(s)} = \frac{94}{(s+104)} \tag{5.4}$$

The root loci for these transfer functions are shown in Figures 5.9 and 5.10, respectively. Looking at these root loci, the best course of action is not obvious. It is desirable to make K_ϕ as high as possible, to increase the loop gain, but obviously this will drive the poles unstable in

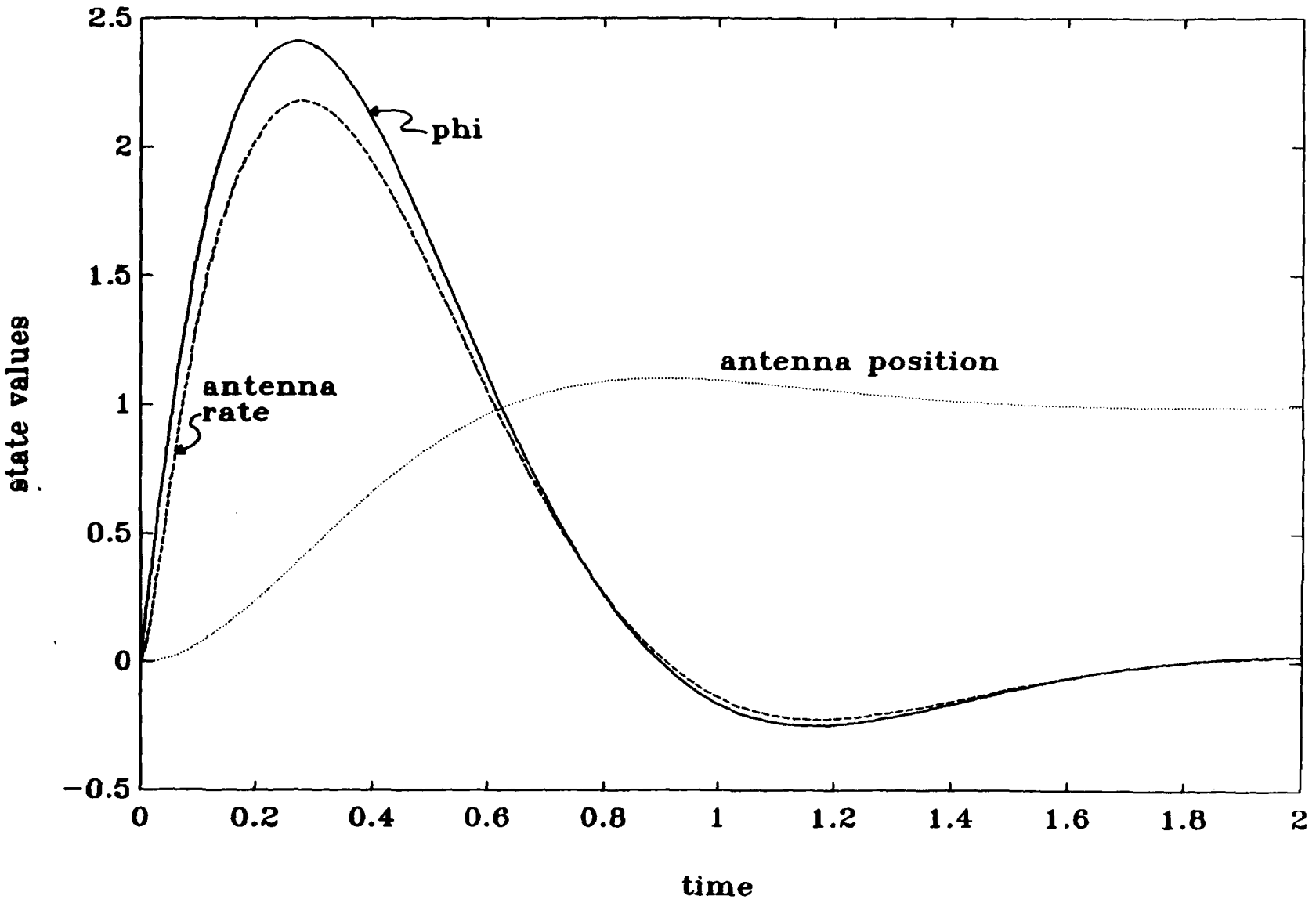

Figure 5.8. Unmodified Tracker Response to Step ϕ_T Command

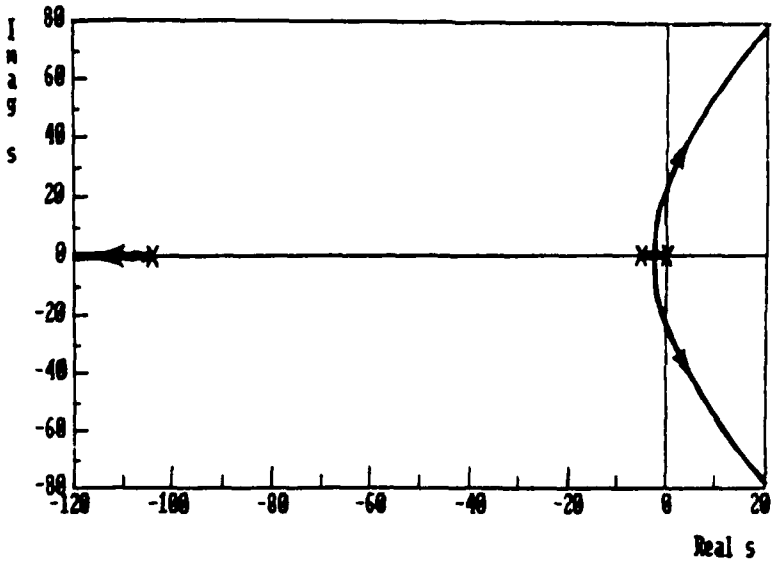

Figure 5.9. Root Locus for K_{ϕ} Gain(θ_s Feedback)

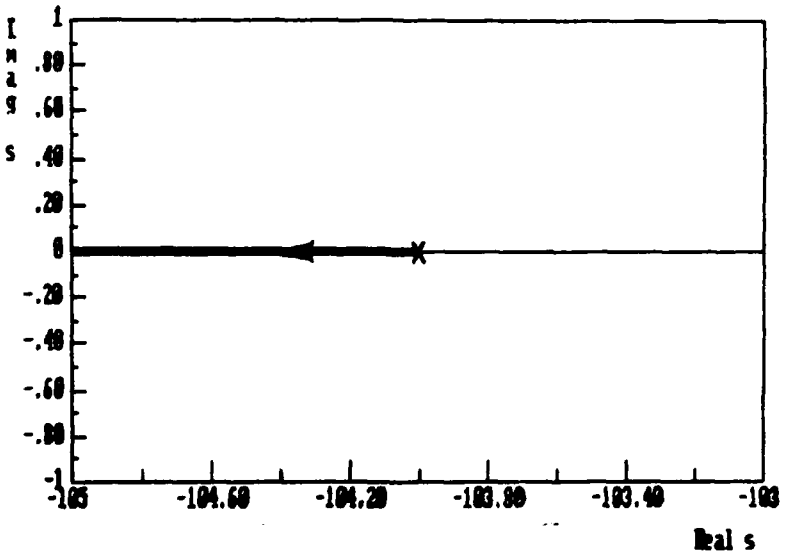

Figure 5.10. Root Locus for $\dot{\theta}_s$ Feedback

short order. However, increasing the gain on $K_{\dot{\theta}_s}$ will move the 'center of gravity' of the loci, with favorable results. This can be seen in the root locus for K_{ϕ} with $K_{\dot{\theta}_s}$=10. This gain moves the servomotor pole to -1044, and the new K_{ϕ} root

locus, shown in Figure 5.11, is much more tractable from a design point of view.

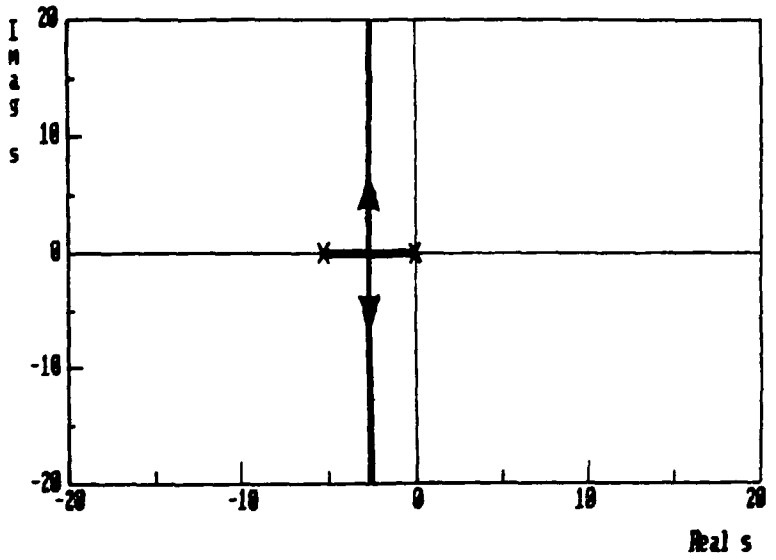

Figure 5.11. Root Locus for K_{ϕ} with $K_{\dot{\theta}_s} = 10$.

Now K_{ϕ} can be increased to a value of 15, which provides high loop gain and yet maintains good damping. The new step response of the system, shown in Figure 5.12, displays this behavior. Examination of the Bode plot for the open-loop transfer function

$$\frac{\theta_s(s)}{\phi_T(s)} = \frac{29187}{s(s+2.56)(s+1044)} \qquad (5.5)$$

as shown in Figure 5.13, reveals that the gain margin for this design is 39 dB, and the phase margin is 27 degrees. Increasing $K_{\dot{\theta}_s}$ further would enhance the time response, but would degrade the stability margins, so no further modification will be made. The resultant closed-loop system is shown in Figure 5.14.

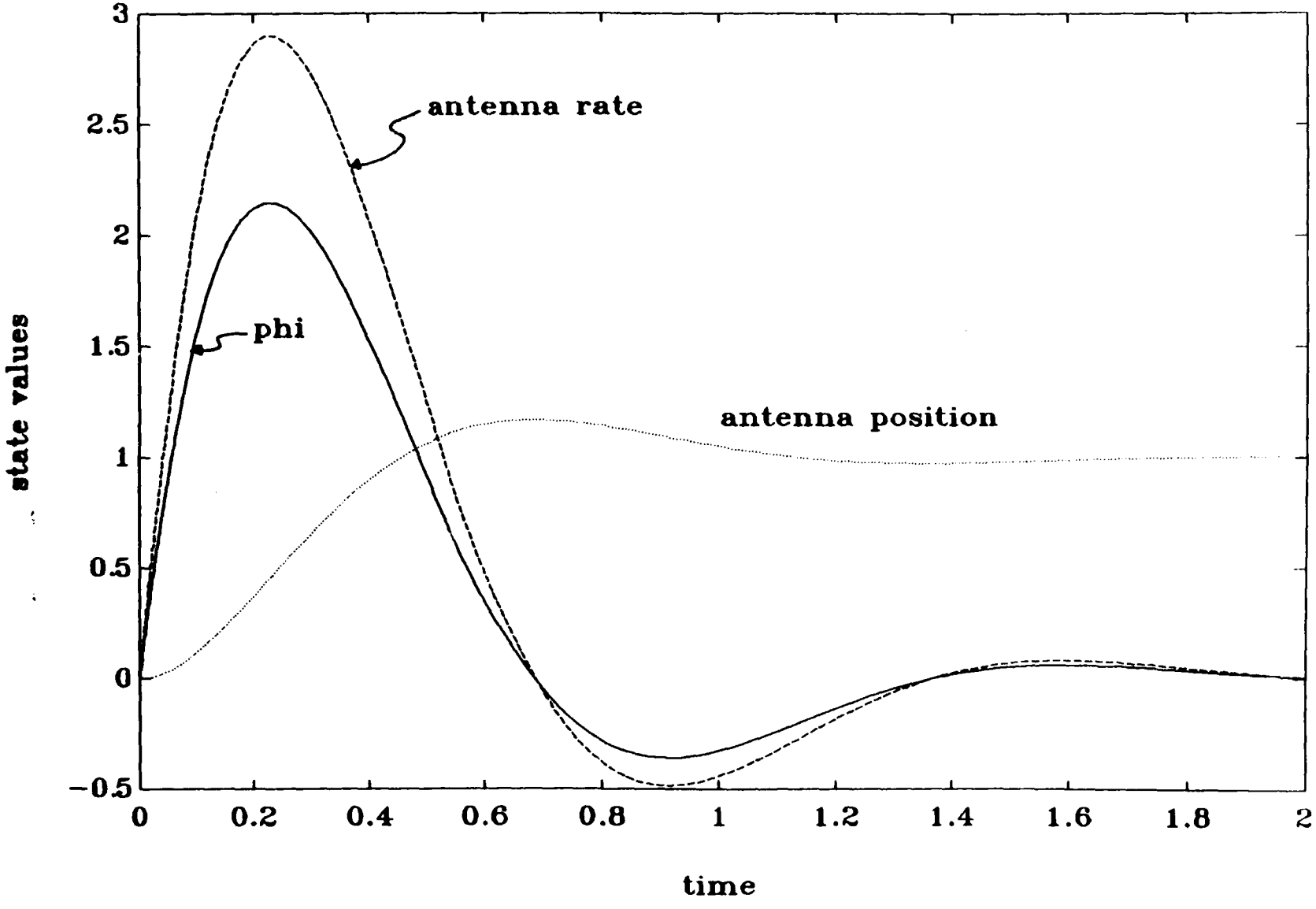

Figure 5.12. Response of Tracker to Target Position Step Command

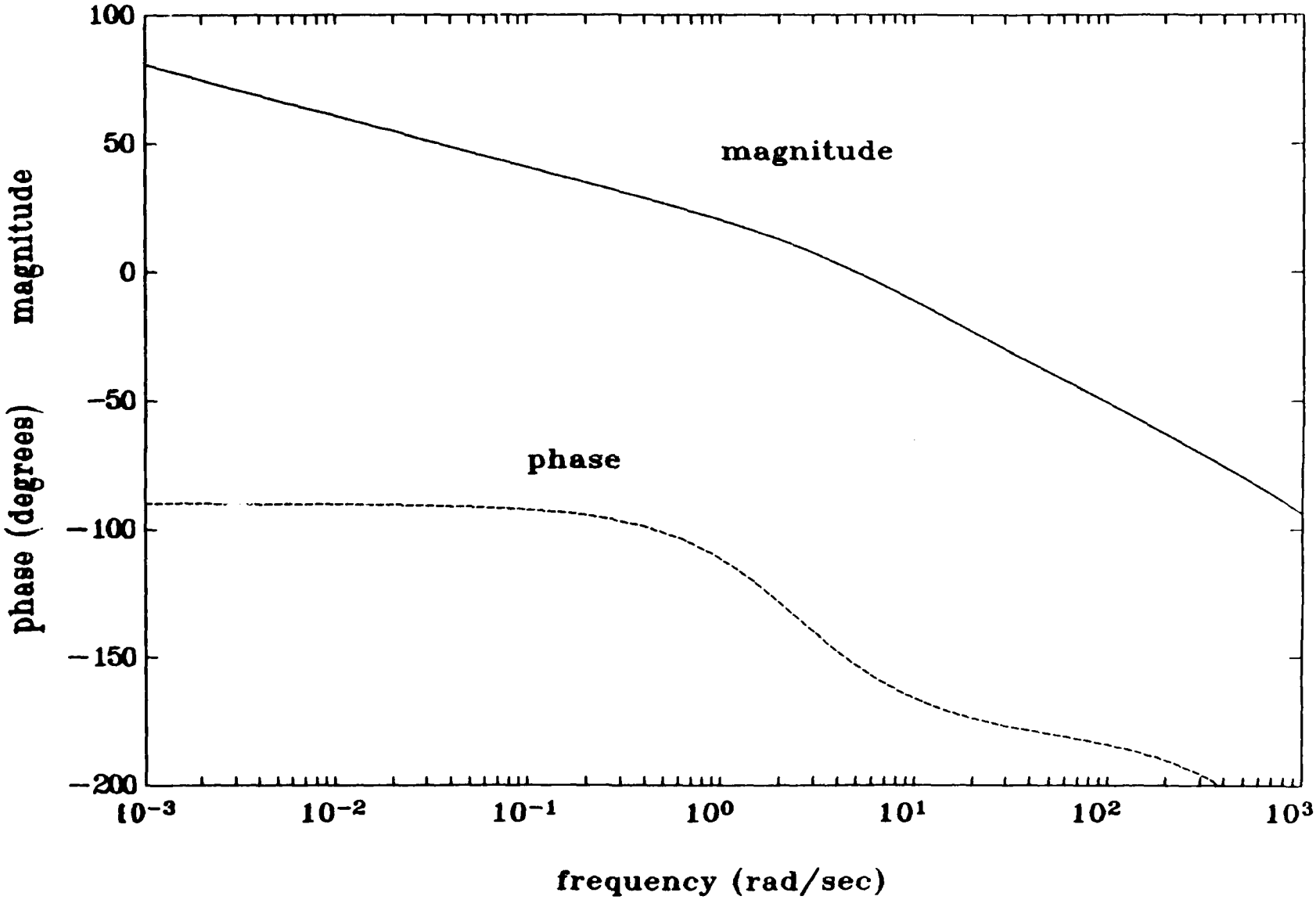

Figure 5.13. θ_s Open-Loop Transfer Function Bode Plots

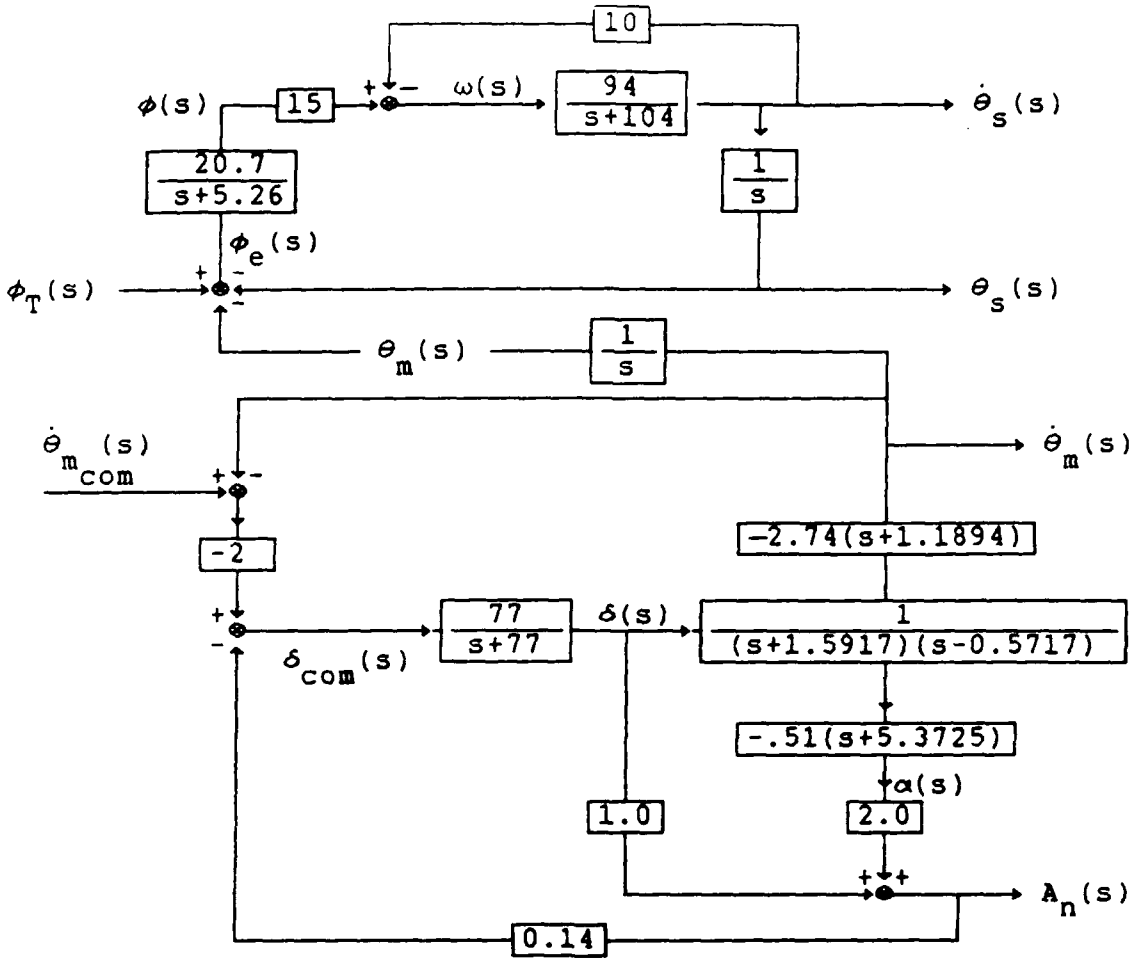

Figure 5.14. Closed-Loop System Block Diagram

At this point, the design would normally be finished. Unfortunately, the step response of the coupled system (Figure 5.15) to a body rate step command shows that missile maneuvers are adversely affecting the tracking accuracy. This is most obvious in the magnitude of ϕ, the filtered boresight error. Also notice the difference between $\dot{\theta}_s$ and $\dot{\theta}_m$, which ideally should be exactly opposite for perfect tracking, since the target is not moving. This effect may be minimized by feeding the airframe body rate to the antenna rate command signal, ω.

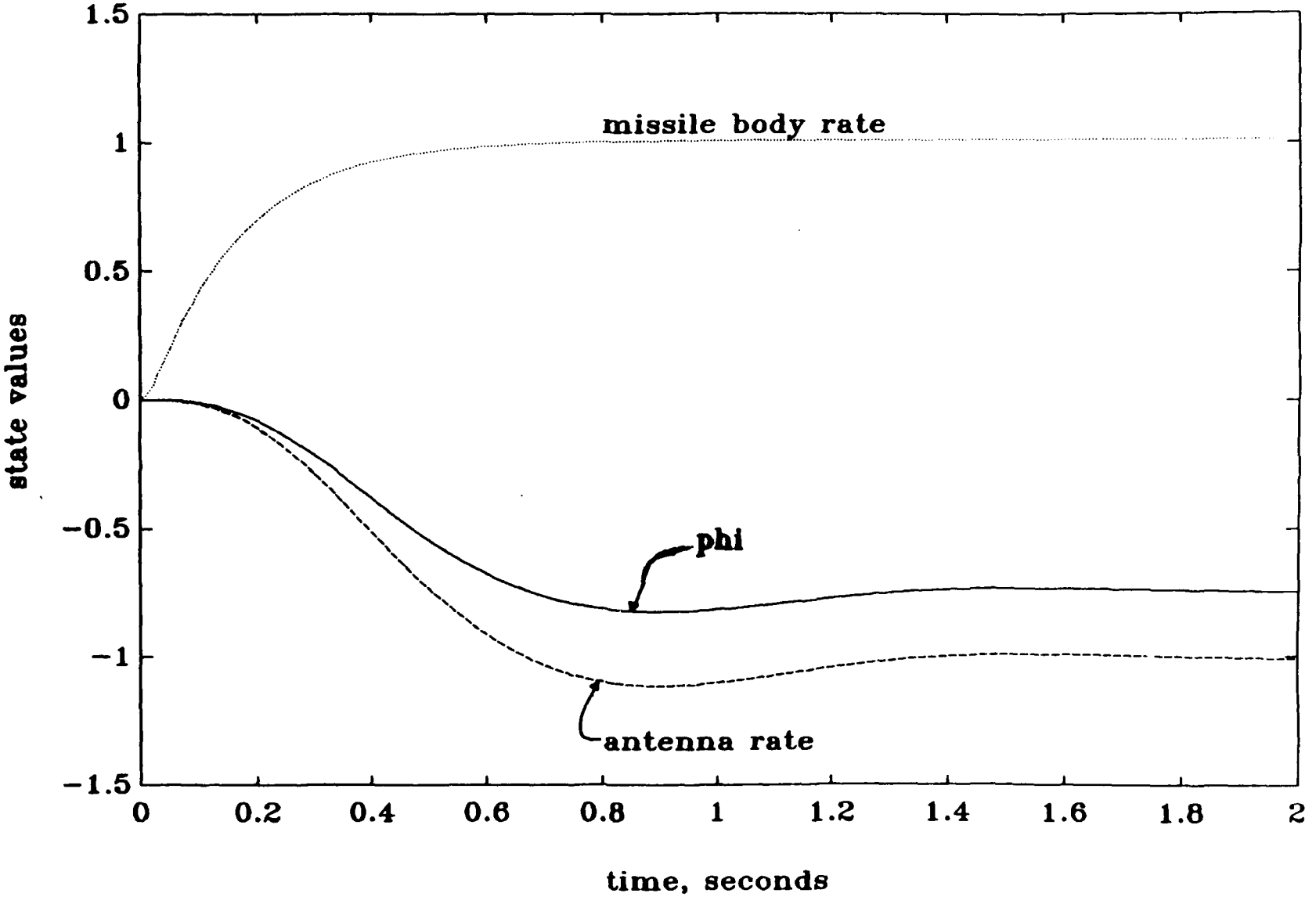

Figure 5.15. System Response to Body Rate Step Command

The corresponding block diagram for this scheme is shown in Figure 5.16, where K_ω is the gain for the body rate feedback to ω, which is to be determined.

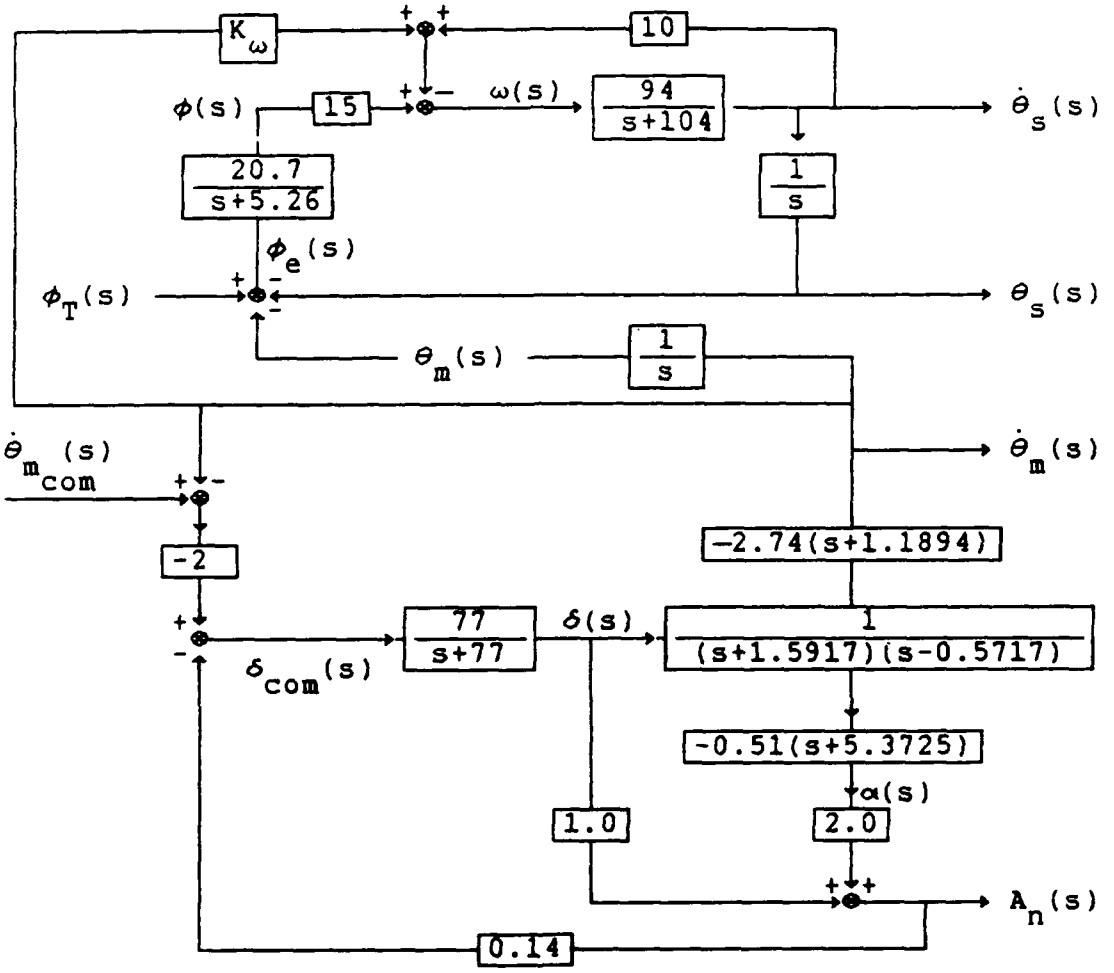

Figure 5.16. Closed Loop System Block Diagram

Repeated step response evaluation reveals that a gain of 10 for K_ω largely cancels out the transient effect, as shown in Figure 5.17.

Guidance Law Computation

Traditional guidance techniques for achieving

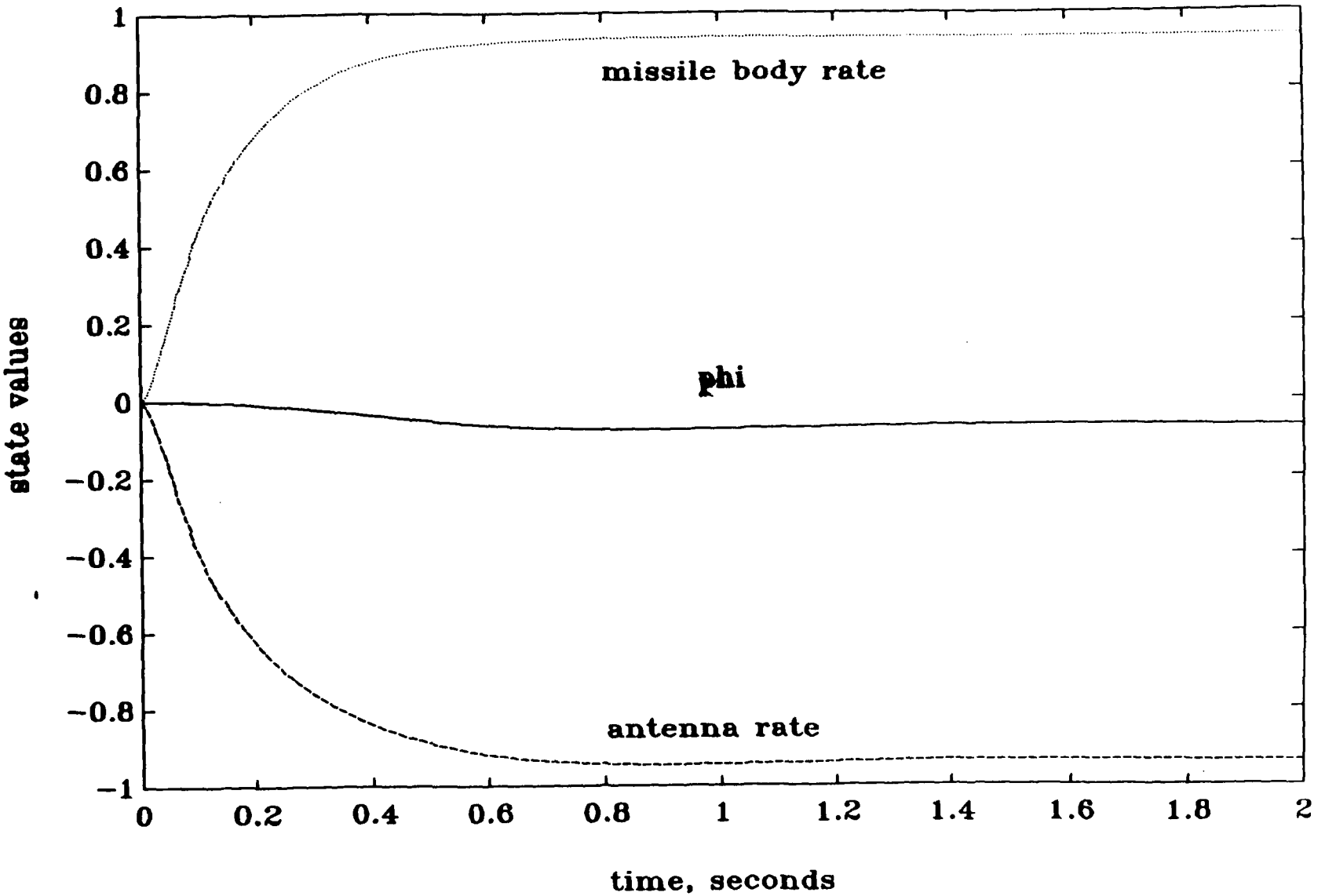

Figure 5.17. System Response to Body Rate Step Command

proportional navigation [2:2-14] indicate that the guidance computer must command a normal acceleration of the airframe proportional to the LOS rate of the target relative to the missile. The guidance law is then of the form

$$A_{n_{com}} = (K_g)(\text{LOS Rate}) \tag{5.6}$$

However, A_n is related to the missile bearing angle γ by

$$A_n = \dot{\gamma} \, |V| \tag{5.7}$$

and $\dot{\gamma}$ is given by

$$\dot{\gamma} = \dot{\theta} - \dot{\alpha} \tag{5.8}$$

If $\dot{\alpha}$ is assumed small, then the guidance law becomes

$$\dot{\theta}_{m_{com}} = (K_g)(\text{LOS Rate})/|V| \tag{5.9}$$

Thus, the origin of the design goals for the airframe and tracker are made obvious. The constant of proportionality K_g for this guidance should also be a function of closing rate, so the above relation takes the form

$$\dot{\theta}_{m_{com}} = (K_g)|\dot{R}_T|(\text{LOS Rate})/|V| \tag{5.10}$$

This results in a non-linear problem, if both LOS rate and closing rate vary, as they do in a realistic encounter. Selection of the constant of proportionality is highly dependent upon expected engagement conditions. A lower guidance gain constant results in pursuit of faster targets, and a high one makes the missile more responsive to target maneuvers. Effectively, the guidance constant determines how

long it will take the missile to correct its course to the new predicted intercept heading. For this missile, a value of $K_g = 2.75$ was chosen based on several flyout scenarios against viable targets. A smaller value makes the missile fly a pursuit guidance on moderately fast (400 m/s) targets, a larger one causes it to react too violently to nominal (6g) target maneuvers. The nominal value of $|V| = 1100$ m/s was used in the above guidance law derivation. Also, assuming that the tracker is accurately tracking the target, the LOS rate is given by

$$\text{LOS rate} = \dot{\theta}_s + \dot{\theta}_m \tag{5.11}$$

Thus, the guidance law becomes

$$\dot{\theta}_{m_{com}} = 2.75|\dot{R}_T|(\dot{\theta}_s + \dot{\theta}_m)/1100$$

$$= 0.0025|\dot{R}_T|(\dot{\theta}_s + \dot{\theta}_m) \tag{5.12}$$

During the flyout runs, the above guidance law was found to generate very large initial accelerations, due to the assumption of small $\dot{\alpha}$. Therefore, an additional factor of $.3\dot{\alpha}$ was added to the guidance law, to limit the large normal accelerations. From Chapter III,

$$\dot{\alpha}(s) = \dot{\theta}_m(s) - \dot{\gamma}(s) \tag{3.3}$$

which (using proper unit conversions) converts to

$$\dot{\alpha}(s) = \dot{\theta}_m(s) - \frac{A_n(s)}{2} \tag{5.13}$$

yielding the guidance law

$$\dot{\theta}_{m_{com}}(s) = 0.0025|\dot{R}_T|\left\{ \dot{\theta}_s(s) + \dot{\theta}_m(s) \right\}$$
$$- (0.3)\dot{\theta}_m(s) - (0.5)A_n(s) \qquad (5.14)$$

Since the guidance problem is highly non-linear, the author has decided to exclude this portion of the problem from the optimal design requirements, and will instead use the same guidance law on each design. The above derived gains, feedbacks, and guidance law computations can be represented by a single feedback matrix K to be used in the control law

$$u_p = K\, y_p \qquad (5.15)$$

such that the closed-loop missile system system can be represented as

$$\dot{x}_p = A_{cl}\, x_p + B_{cl}\, w \qquad (5.16)$$

$$y_p = C_{cl}\, x_p + D_{cl}\, w \qquad (5.17)$$

where

$$A_{cl} = A_p - B_{p11}KC_p \qquad (5.18)$$

$$B_{cl} = B_{p12} \qquad (5.19)$$

$$C_{cl} = C_p \qquad (5.20)$$

$$D_{cl} = D_{p12} \qquad (5.21)$$

where A_p, B_{p11}, B_{p12}, C_p, D_{p11}, D_{p12}, x_p, u_p, and y_p are as given in Chapter IV (Equations 4.13-4.22), and K is given by

$$K = \begin{bmatrix} -1.7+0.0025*\dot{R}_T & -0.29 & 0 & 0.0025*\dot{R}_T & 0 \\ 0 & 10 & -15 & 10 & 0 \end{bmatrix} \qquad (5.22)$$

This representation facilitates implementation in the digital

simulation, which is designed to handle the state-space representation of the missile system.

VI. H_2 Controller Synthesis

The H_2 design objective is to find the feedback control law

$$u(s) = K(s)\, y(s) \tag{6.1}$$

such that the 2-norm of the closed loop transfer function matrix z(s)/w(s) is minimized, where w(s) are the system inputs (including commands, disturbances, and noise) and z(s) is an error signal. Simply stated, it is desired to minimize system error response to all signals entering the system.

The methodology for solving this problem is well-established in control theory literature, so a brief overview will be presented here. For a more extensive treatment, see Doyle et. al. [3].

Theory for State Space Solution of the H_2 Design Problem

The development presented in this section was taken from Doyle et. al. [3]. The standard block diagram representation of the small gain problem is shown in Figure 6.1.

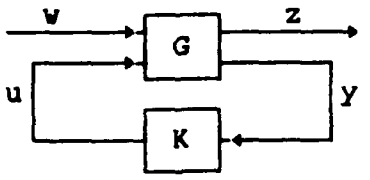

Figure 6.1. Standard Block Diagram

In Figure 6.1, w is the vector containing all system inputs, z is the vector containing error signals to be controlled, u is the control input vector, and y is the vector of measured

system errors. G is the open-loop plant and K is the controller to be designed. The resultant closed-loop matrix of transfer functions from w to z is denoted T_{zw}.

2-norm Definition. The objective of H_2 design is to find K such that T_{zw} is internally stabilized and the 2-norm of T_{zw}, denoted $\|T_{zw}\|_2$, is minimized. The 2-norm of T_{zw} is defined as

$$\|T_{zw}\|_2 := \left[\frac{1}{2\pi} \int_{-\infty}^{+\infty} \text{trace} \left[T_{zw}(j\omega)^* \, T_{zw}(j\omega) \right] d\omega \right]^{\frac{1}{2}} \qquad (6.2)$$

where the superscript * denotes the complex conjugate transpose.

This concept can be visualized easily in the single-input single-output (SISO) case, where the 2-norm is proportional to the area under the Bode plot of the closed-loop transfer function.

Visualization in the multi-input multi-output (MIMO) case is more difficult, but the principle is the same. In the MIMO case, the 2-norm is proportional to the sum of the areas under all of the singular value plots. Singular values are used to extend the concept of bode magnitude plots to the MIMO case. For an extensive treatment of the properties of the singular value plot, see AFWAL TR-85-3102 [8].

Problem Requirements and Scaling. In state space form, G can be represented as

$$\dot{x} = A\,x + B_1\,w + B_2\,u \qquad (6.3)$$

$$z = C_1\,x + D_{11}\,w + D_{12}\,u \qquad (6.4)$$

$$y = C_2 x + D_{21} w + D_{22} u \qquad (6.5)$$

To solve the H_2 problem via existing theory [3], the following conditions must be satisfied;

$$1)\ D_{11} = 0 \qquad (6.6)$$

$$2)\ D_{22} = 0 \qquad (6.7)$$

$$3)\ (a)\ D_{12}^T D_{12} = I \qquad (6.8)$$

$$(b)\ D_{21} D_{21}^T = I \qquad (6.9)$$

4) (A,B_1) stabilizable & (C_1,A) detectable

5) (A,B_2) stabilizable & (C_2,A) detectable

Condition 1 requires that the vector of error signals z receives no direct feedforward from the disturbances w. If this requirement is violated, $\|T_{zw}\|_2$ is equal to ∞ for any K(s) developed.

Condition 2 requires that the vector of measured errors receive no direct feedforward of the control inputs u. This condition can actually be relaxed if required [5] & [11], but this is not necessary for this problem.

Condition 3a requires that z receives direct feedforward of each element of u, and Condition 3b requires that each element of y receives direct feedforward of some element of w.

In summary, each measured output must be directly contaminated by some disturbance but not by any control inputs (as will be the case in any well-modeled system) and the error signal z must be affected by each control input directly (every control input must be controlled) but not directly by

any of the disturbance inputs (penalizing the disturbance inputs directly would yield an infinite 2-norm since they can't be affected).

Conditions 3a and 3b also require that the input u and the output y be scaled. This scaling is accomplished via a Cholesky decomposition [3], which yields unique upper triangular matrices that satisfy

$$S_u^T S_u = D_{12}^T D_{12} \tag{6.10}$$

$$S_y^{-1} S_y^{-T} = D_{21} D_{21}^T \tag{6.11}$$

where the superscript -1 indicates inverse and the superscript -T indicates transpose of the inverse. The scaling is appended to the original plant G as shown in Figure 6.2, where the superscript ~ denotes scaled values.

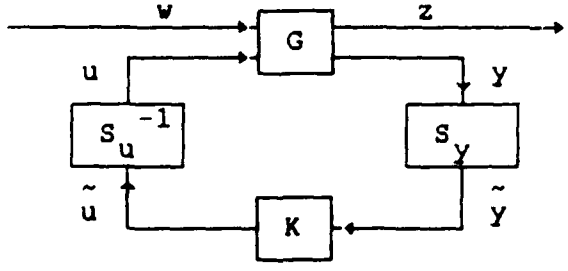

Figure 6.2. Block Diagram of Plant with Scaling

The scaling will be considered part of the plant in determining the controller, but will be considered part of the controller after the solution is obtained. Appending the scaling to the plant G results in a modification to the original plant representation. These modifications can be represented as follows, where the superscript ~ denotes the

scaled matrices, which are given by

$$\tilde{B}_2 = B_2 S_u^{-1} \tag{6.12}$$

$$\tilde{C}_2 = S_y C_2 \tag{6.13}$$

$$\tilde{D}_{12} = D_{12} S_u^{-1} \tag{6.14}$$

$$\tilde{D}_{21} = S_y D_{21} \tag{6.15}$$

The problem is now in the form required for application of the existing methods for derivation of the controller, as described in Doyle et. al. [3].

Solution. This method requires obtaining the real, unique, symmetric solutions X_2 and Y_2 to the two uncoupled Riccati equations

$$F_1^T X_2 + X_2 F_1 - X_2 G_1 X_2 + H_1 = 0 \tag{6.16}$$

$$F_2^T Y_2 + Y_2 F_2 - Y_2 G_2 Y_2 + H_2 = 0 \tag{6.17}$$

where

$$F_1 = A - \tilde{B}_2 \tilde{D}_{12}^T C_1 \tag{6.18}$$

$$G_1 = \tilde{B}_2 \tilde{B}_2^T \tag{6.19}$$

$$H_1 = \hat{C}_1^T \hat{C}_1 \tag{6.20}$$

$$\hat{C}_1 = (I - \tilde{D}_{12} \tilde{D}_{12}^T) C_1 \tag{6.21}$$

$$F_2 = A - B_1 \tilde{D}_{21}^T \tilde{C}_2 \tag{6.22}$$

$$G_2 = \tilde{C}_2^T \tilde{C}_2 \tag{6.23}$$

$$H_2 = \hat{B}_1 \hat{B}_1^T \tag{6.24}$$

$$\hat{B}_1 = B_1 (I - \tilde{D}_{21}^T \tilde{D}_{21}) \tag{6.25}$$

The optimal controller (denoted by the subscript cp) is then

given by

$$A_{cp} = A - K_f \tilde{C}_2 - \tilde{B}_2 K_c \tag{6.26}$$

$$B_{cp} = K_f \tag{6.27}$$

$$C_{cp} = -K_c \tag{6.28}$$

$$D_{cp} = 0 \tag{6.29}$$

where

$$K_c = \tilde{B}_2^T X_2 + \tilde{D}_{12}^T C_1 \tag{6.30}$$

$$K_f = Y_2 \tilde{C}_2^T + B_1 \tilde{D}_{21}^T \tag{6.31}$$

Problem Set-up

The problem now standing in the way of deriving a controller is the conversion of the missile model into one conforming to the standard problem.

The design objective is to derive a controller such that the antenna will track the target and the missile can be steered. This is a tracking problem and Francis [4] presents a methodology to convert the tracking problem to the small gain problem. That methodology will be employed here.

The Tracking Problem. To convert the tracking problem to the small gain problem, it is necessary to convert the desire to accurately track the target and guide the missile into a requirement to minimize some set of values. It is desired to minimize: (1) error between commanded and actual missile body rate, (2) transients in normal forces, (3) error between antenna boresight and target line-of-sight, (4) transients in antenna rates, and (5) control inputs. Expressing these

desires in terms of the tracking problem presented in [4] yields

$$z = \begin{bmatrix} r-v \\ \rho u \end{bmatrix} \tag{6.32}$$

$$y = [r-v] \tag{6.33}$$

where

ρ = diagonal matrix of control weighting factors
r = reference signal desired to track
v = controlled variables, which track reference signal
u = control inputs

For the missile system these become

$$v = \begin{bmatrix} \dot{\theta}_m \\ A_n \\ \phi \\ \dot{\theta}_s \\ \theta_s \end{bmatrix} \begin{matrix} \text{(missile body rate)} \\ \text{(normal acceleration)} \\ \text{(boresight error)} \\ \text{(antenna rate)} \\ \text{(antenna position)} \end{matrix} \tag{6.34}$$

$$r = \begin{bmatrix} \dot{\theta}_{m_c} \\ 0 \\ 0 \\ 0 \\ \theta_{s_c} \end{bmatrix} \begin{matrix} \text{(missile body rate command)} \\ \text{(desire no acceleration transient)} \\ \text{(desire no boresight error transient)} \\ \text{(desire no antenna rate transient)} \\ \text{(antenna position command)} \end{matrix} \tag{6.35}$$

$$u = \begin{bmatrix} \delta_{com} \\ \omega \end{bmatrix} \begin{matrix} \text{(fin deflection command)} \\ \text{(tracker command)} \end{matrix} \tag{6.36}$$

In block diagram form, the system looks as shown in Figure 6.3.

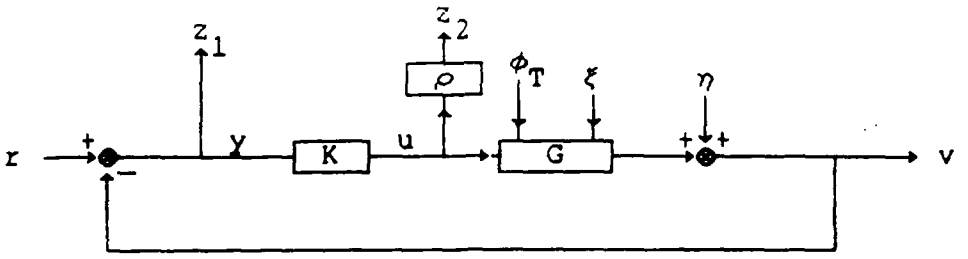

Figure 6.3. Converted System Block Diagram

Conversion to Small Gain Problem. It is desired to express the above system in the form

$$\dot{x} = A\,x + B1\,w + B2\,u \tag{6.3}$$

$$z = C1\,x + D11\,w + D12\,u \tag{6.4}$$

$$y = C2\,x + D21\,w + D22\,u \tag{6.5}$$

where K is considered 'open' and w is a vector containing all external inputs. The external inputs will be arranged as

$$w = \begin{bmatrix} r \\ \phi_T \\ \xi \\ \eta \end{bmatrix} \tag{6.37}$$

This yields, in terms of the system representation given in Chapter IV,

$$A = A_p \tag{6.38}$$

$$B1 = [\ 0\ B_{p12}\ B_{p2}\ 0\ ] \tag{6.39}$$

$$B2 = B_{p11} \tag{6.40}$$

$$C1 = \begin{bmatrix} -C_p \\ 0 \end{bmatrix} \tag{6.41}$$

$$C2 = \begin{bmatrix} -C_p \end{bmatrix} \tag{6.42}$$

$$D11 = \begin{bmatrix} I & -D_{p12} & -D_{p2} & -I \\ 0 & 0 & 0 & 0 \end{bmatrix} \tag{6.43}$$

$$D12 = \begin{bmatrix} -D_{p11} \\ \rho \end{bmatrix} \tag{6.44}$$

$$D21 = \begin{bmatrix} I & -D_{p12} & -D_{p2} & -I \end{bmatrix} \tag{6.45}$$

$$D22 = \begin{bmatrix} -D_{p11} \end{bmatrix} \tag{6.47}$$

However, this set of matrices does not meet Condition 1 above. Specifically, D11 is clearly not equal to a zero matrix. D22 actually is zero as D_{p11} is a zero matrix.

Addition of Weighting Functions. This problem can be solved by adding weighting filters to the system disturbances and to the variable z. The resultant system is of the form shown in Figure 6.4.

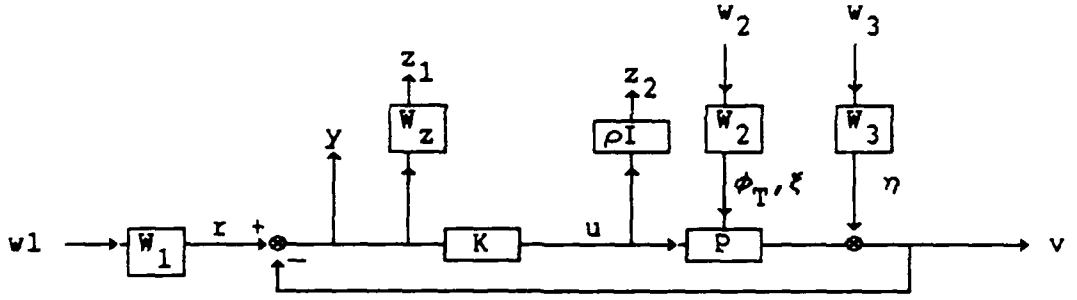

Figure 6.4. System with Weights

In this system, each of the weighting functions is frequency dependent. When expressed in state space form, each weighting function generates additional states, one for each pole present in the transfer function describing it. Therefore, each weighting function has its own A, B, C, and D matrices. Denoting the respective weighting function matrices with the subscripts associated with the W's in Figure 6.4 yields the new set of matrices describing the total system

(with K open as before)

$$A = \begin{bmatrix} A_p & 0 & [B_{p12}\ B_{p2}]C_3 & 0 & 0 \\ 0 & A_1 & 0 & 0 & 0 \\ 0 & 0 & A_2 & 0 & 0 \\ 0 & 0 & 0 & A_3 & 0 \\ -B_zC_p & B_zC_1 & -B_z[D_{p12}\ D_{p2}]C_3 & -B_zC_2 & A_z \end{bmatrix} \quad (6.48)$$

$$B1 = \begin{bmatrix} 0 & [B_{p12}\ B_{p2}]D_3 & 0 \\ B_1 & 0 & 0 \\ 0 & B_2 & 0 \\ 0 & 0 & B_3 \\ B_zD_1 & -B_z[D_{p12}\ D_{p2}]D_3 & -B_zD_2 \end{bmatrix} \quad (6.49)$$

$$B2 = \begin{bmatrix} B_{p1} \\ 0 \\ 0 \\ 0 \\ -B_zD_{p11} \end{bmatrix} \quad (6.50)$$

$$C1 = \begin{bmatrix} -D_zC_p & D_zC_1 & -D_zC_2 & -D_z[D_{p12}\ D_{p2}]C_3 & C_z \\ 0 & 0 & 0 & 0 & 0 \end{bmatrix} \quad (6.51)$$

$$C2 = \begin{bmatrix} -C_p & C_1 & -C_2 & -[D_{p12}\ D_{p2}]C_3 & 0 \end{bmatrix} \quad (6.52)$$

$$D11 = \begin{bmatrix} D_zD_1 & -D_zD_2 & -D_z[D_{p12}\ D_{p2}]D_3 \\ 0 & 0 & 0 \end{bmatrix} \quad (6.53)$$

$$D12 = \begin{bmatrix} -D_zD_{p11} \\ \rho \end{bmatrix} \quad (6.54)$$

$$D21 = \begin{bmatrix} D_1 & -D_2 & -[D_{p12}\ D_{p2}]D_3 \end{bmatrix} \quad (6.55)$$

$$D22 = \begin{bmatrix} 0 \\ D_{p11} \end{bmatrix} \tag{6.56}$$

Now, Condition 1 translates to $D_z=0$. Condition 3a is met (using scaling) as long as all the control input weights are non-zero, and 3b is met as long as care is taken that D_1 and D_2 are chosen such that each signal in y receives some direct feed-forward from at least one of the disturbances (ϕ_T, ξ, or η).

In addition to satisfying Condition 1, the weighting functions are a powerful design tool. They enable the designer to shape the system response. This is accomplished by: (1) designing the filter on the incoming disturbances such that the Bode plot of the filter looks like the Fourier Transform of the incoming signal; and (2) designing the filter on the error signal z_1 such that the desired portion of the spectrum of the error is penalized.

Filtering the Disturbance Input. The purpose of designing the disturbance input filters is to properly reflect the frequency content of the incoming signals. The automated state space solutions to the H_2 problem are constructed to minimize the 2-norm of T_{zw}. At this point, it is necessary to remember that the transfer function of a system is equivalent to the impulse response of the system. Therefore, minimizing the 2-norm of T_{zw} is equivalent to minimizing the error response to an impulse input. In reality, the system will not see impulse inputs, so minimizing the 2-norm of T_{zw} as is puts an unwanted requirement on the design. To express the true

design goals , it is necessary to convert T_{zw} to the true system response desired.

As an example, consider the case of a command w which enters the system as a step input. The Fourier Transform of a step function is $1/j\omega$. Plotted as magnitude (in dB) versus frequency, the transform looks as shown in Figure 6.5. Obviously, a step function has very low magnitude at high frequency and large magnitude at low frequency. Now consider a SISO plant P to which this command is applied as shown in Figure 6.6, where y is the response and z is the error to be minimized.

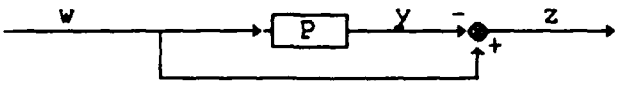

Figure 6.6. SISO Plant Block Diagram

Two cases will be examined, for comparison purposes. Representing these as P1 and P2, let

$$P1(j\omega) = \frac{1}{j\omega+1} \tag{6.57}$$

$$P2(j\omega) = \frac{10}{j\omega+10} \tag{6.58}$$

which yield the time responses shown in Figures 6.7 and 6.8, respectively. These systems have time constants of 1 and 10, respectively, and both have zero steady-state error. Accordingly, the quality of these systems should be reflected in the size of the 2-norm of T_{zw}. For plant P1,

$$T_{zw}(j\omega) = \frac{z(j\omega)}{w(jw)} = 1-P1(j\omega) = \frac{j\omega}{j\omega+1} \tag{6.59}$$

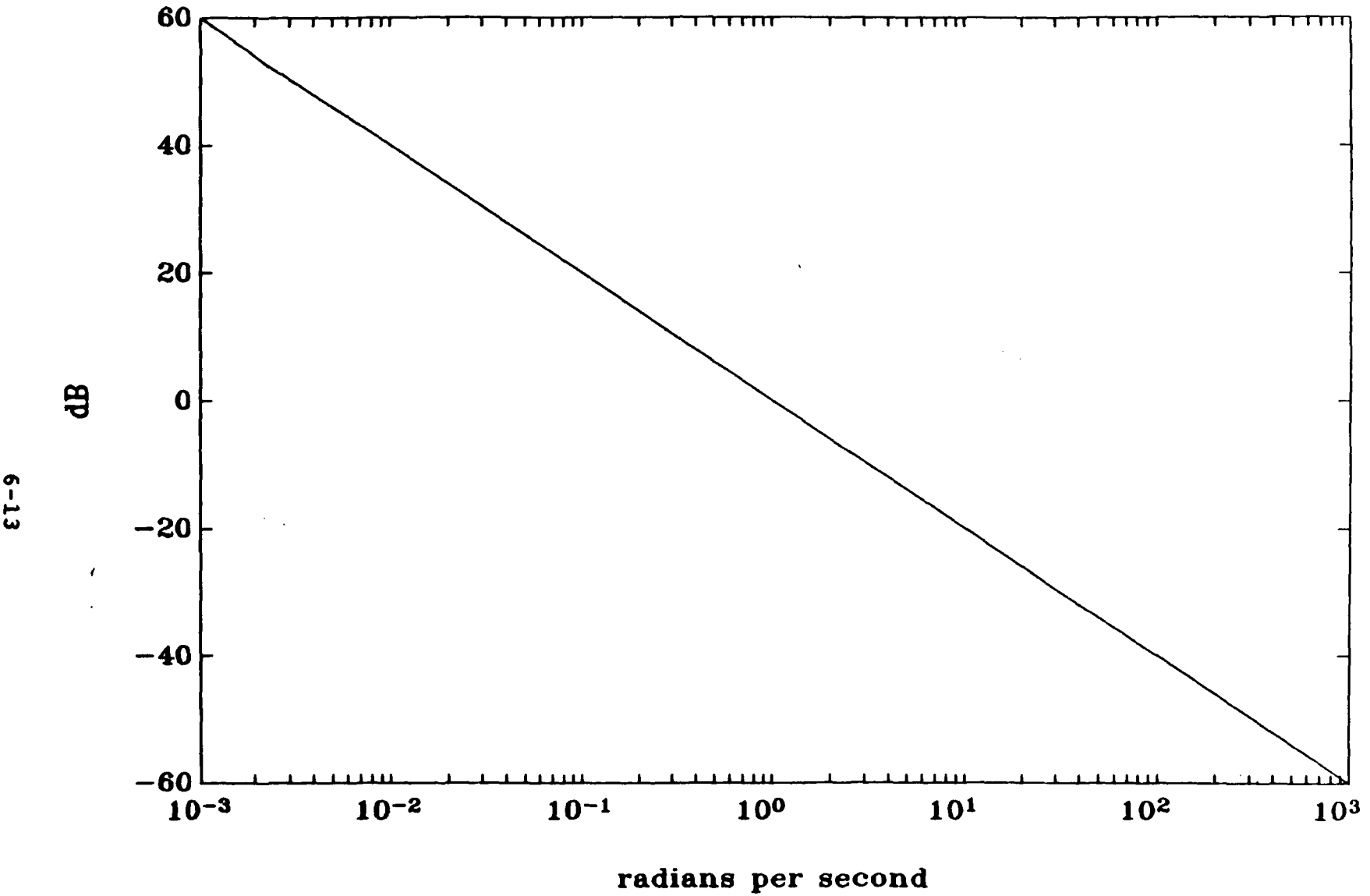

Figure 6.5. Fourier Transform of a Step Function

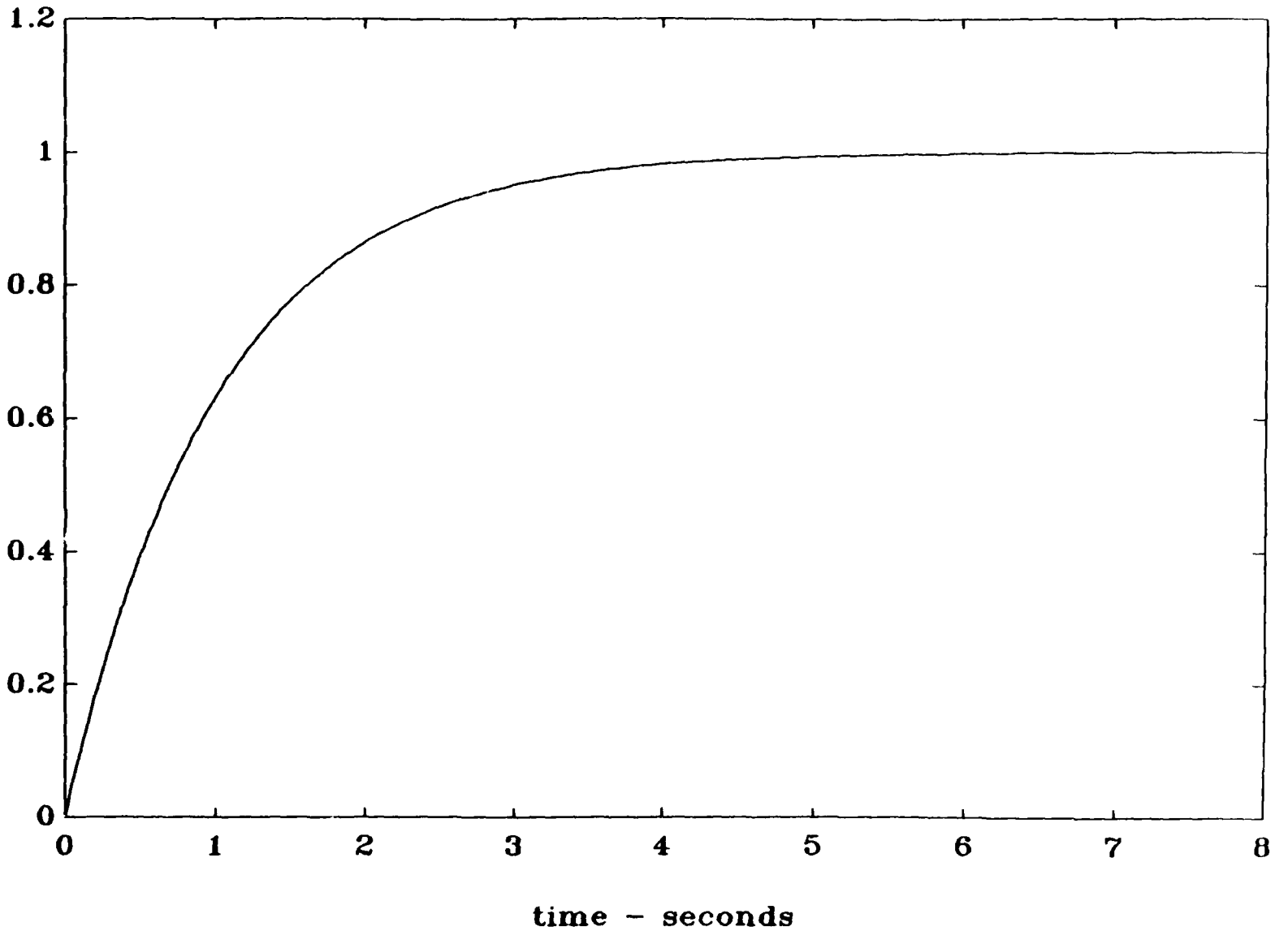

Figure 6.7. Step Response of P1

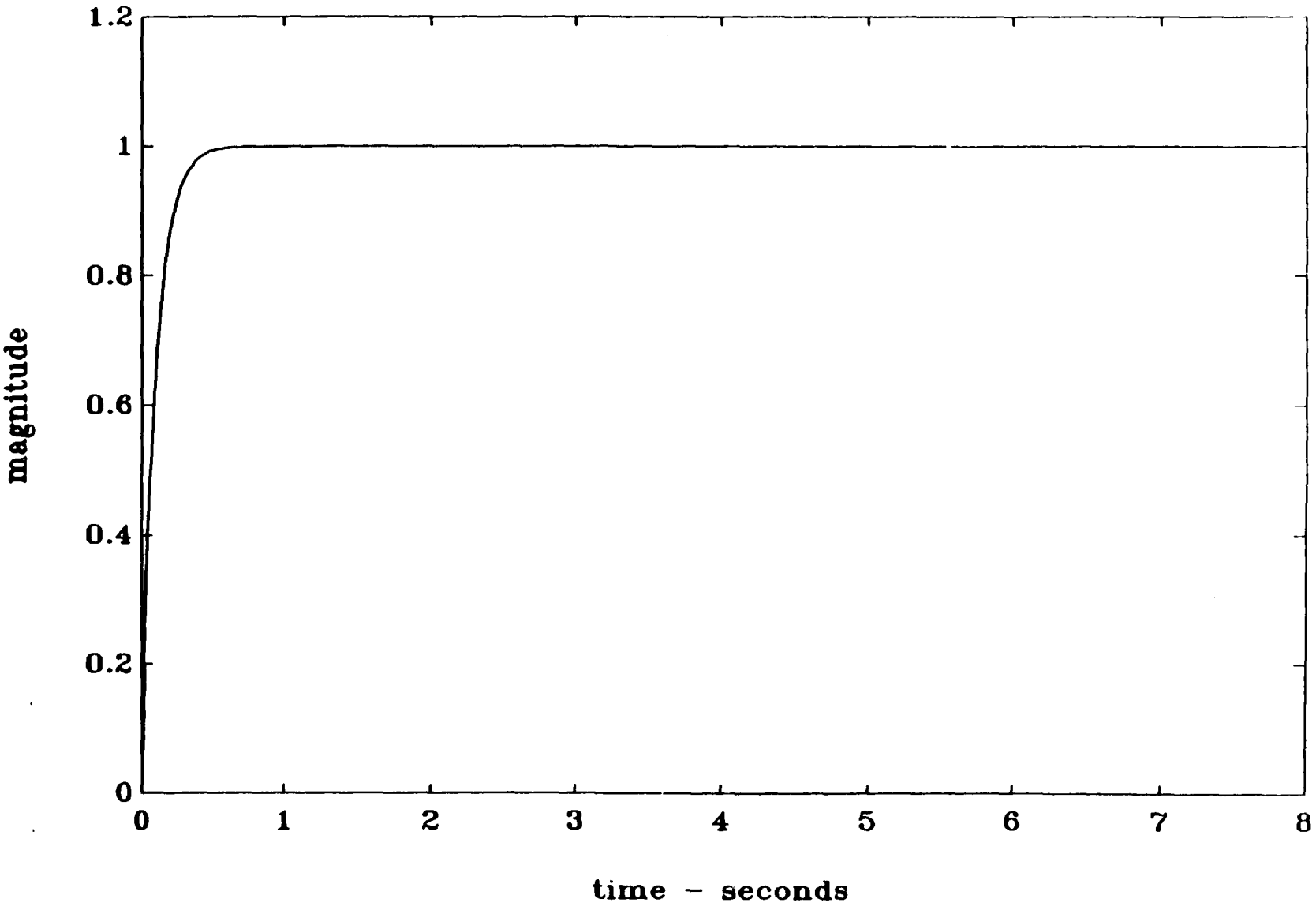

Figure 6.8. Step Response of P2

Taking the 2-norm,

$$\|T_{zw}\|_2 = \left[\frac{1}{2\pi} \int_{-\infty}^{+\infty} \text{trace} \left[\frac{j\omega}{j\omega+1}^{*} \frac{j\omega}{j\omega+1} \right] d\omega \right]^{\frac{1}{2}}$$

$$= \left[\frac{1}{2\pi} \int_{-\infty}^{+\infty} \text{trace} \left[\frac{\omega^2}{1+\omega^2} \right] d\omega \right]^{\frac{1}{2}}$$

$$= \left[\frac{1}{2\pi} \left[\omega - \tan^{-1}(\omega) \right] \Big|_{-\infty}^{\infty} \right]^{\frac{1}{2}}$$

$$= \infty \qquad (6.60)$$

Similarly, for P2,

$$T_{zw}(j\omega) = \frac{z(j\omega)}{w(jw)} = 1\text{-}P2(j\omega) = \frac{j\omega}{j\omega+10} \qquad (6.61)$$

Taking the 2-norm,

$$\|T_{zw}\|_2 = \left[\frac{1}{2\pi} \int_{-\infty}^{+\infty} \text{trace} \left[\frac{j\omega}{j\omega+10}^{*} \frac{j\omega}{j\omega+10} \right] d\omega \right]^{\frac{1}{2}}$$

$$= \left[\frac{1}{2\pi} \int_{-\infty}^{+\infty} \text{trace} \left[\frac{\omega^2}{100+\omega^2} \right] d\omega \right]^{\frac{1}{2}}$$

$$= \left[\frac{1}{2\pi} \left[\omega - 10 \tan^{-1}(\omega / 10) \right] \Big|_{-\infty}^{\infty} \right]^{\frac{1}{2}}$$

$$= \infty \qquad (6.62)$$

Clearly, this computation does not yield a very good measure of actual system performance for comparison purposes. Again, this is because the T_{zw} examined here is the error response to an impulse input. The effect of adding a filter with frequency characteristics matching that of a step function

will now be examined.

The Fourier Transform of a step function is $1/j\omega$. Adding a filter with this frequency characteristic yields a new system as shown in Figure 6.9.

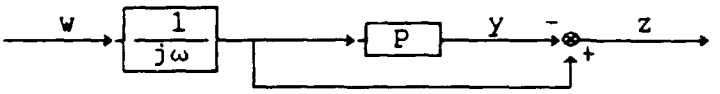

Figure 6.9. SISO Plant with Filter

Now T_{zw} for P1 looks like

$$T_{zw}(j\omega) = \frac{1}{j\omega}\,\frac{j\omega}{1+j\omega} = \frac{1}{1+j\omega} = \frac{1-j\omega}{1+\omega^2} \qquad (6.63)$$

Computing the 2-norm as before,

$$\|T_{zw}\|_2 = \left[\frac{1}{2\pi} \int_{-\infty}^{+\infty} \text{trace} \left[\frac{1-j\omega}{1+\omega^2} * \frac{1-j\omega}{1+\omega^2} \right] d\omega \right]^{\frac{1}{2}}$$

$$= \left[\frac{1}{2\pi} \int_{-\infty}^{+\infty} \text{trace} \left[\frac{1}{1+\omega^2} \right] d\omega \right]^{\frac{1}{2}}$$

$$= \left[\frac{1}{2\pi} \left[\tan^{-1}(\omega) \right] \Big|_{-\infty}^{\infty} \right]^{\frac{1}{2}}$$

$$= \left[\frac{1}{2\pi}\,\pi \right]^{\frac{1}{2}}$$

$$= \frac{\sqrt{2}}{2} \qquad (6.64)$$

For P2,

$$T_{zw}(j\omega) = \frac{1}{j\omega}\,\frac{j\omega}{10+j\omega} = \frac{1}{10+j\omega} = \frac{10-j\omega}{100+\omega^2} \qquad (6.65)$$

Computing the 2-norm,

$$\|T_{zw}\|_2 = \left[\frac{1}{2\pi} \int_{-\infty}^{+\infty} \text{trace}\left[\frac{10-j\omega}{100+\omega^2}^{*} \frac{10-j\omega}{100+\omega^2} \right] d\omega \right]^{\frac{1}{2}}$$

$$= \left[\frac{1}{2\pi} \int_{-\infty}^{+\infty} \text{trace} \left[\frac{1}{100+\omega^2} \right] d\omega \right]^{\frac{1}{2}}$$

$$= \left[\frac{1}{2\pi} \left[\frac{1}{10} \tan^{-1}(\omega / 10) \right] \Big|_{-\infty}^{\infty} \right]^{\frac{1}{2}}$$

$$= \left[\frac{1}{2\pi} \pi / 10 \right]^{\frac{1}{2}}$$

$$= \frac{\sqrt{5}}{10} \qquad (6.66)$$

Clearly, this is a much better reflection of the true performance of the systems in response to a step input. The key is to tailor the disturbance filter to look like the expected disturbance (or command) input. To get an even better idea of how close the system is responding to the desired, it is necessary to examine filtering of the error signal.

Filtering of the Error Signal. Suppose, using the plants above, that it is desired to penalize only the steady state error of the system. Since the above system has no steady state error, proper filtering of the error should reflect this. If it is desired to penalize steady state error only, then the gain of the filter should be high on the low frequency end and low on the high frequency end. A filter

which reflects this desire is simply $1/(j\omega+1)$. Appending this filter to the error output z yields the system shown in Figure 6.10.

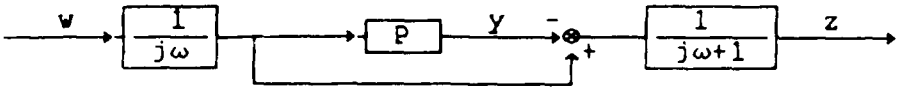

Figure 6.10. SISO Plant with Filters On Input and Output

The transfer function T_{zw} for P1 is then given by

$$T_{zw}(j\omega) = \frac{1}{j\omega}\,\frac{j\omega}{1+j\omega}\,\frac{1}{j\omega+1} = \frac{(1-\omega^2)-2j\omega}{(1+\omega^2)^2} \qquad (6.67)$$

and the 2-norm of T_{zw} becomes

$$\|T_{zw}\|_2 = \left[\frac{1}{2\pi}\int_{-\infty}^{+\infty} \text{trace}\left[\frac{(1-\omega^2)-2j\omega}{(1+\omega^2)^2}^{*}\,\frac{(1-\omega^2)-2j\omega}{(1+\omega^2)^2}\right]d\omega\right]^{\frac{1}{2}}$$

$$= \left[\frac{1}{2\pi}\int_{-\infty}^{+\infty}\left[\frac{1}{(1+\omega^2)^2}\right]d\omega\right]^{\frac{1}{2}}$$

$$= \left[\frac{1}{2\pi}\left[\frac{\omega}{2(\omega^2+1)} + \frac{1}{2}\tan^{-1}(\omega)\right]\Bigg|_{-\infty}^{\infty}\right]^{\frac{1}{2}}$$

$$= \left[\frac{1}{2\pi}\left[\left(0+\frac{\pi}{4}\right)-\left(0-\frac{\pi}{4}\right)\right]\right]^{\frac{1}{2}}$$

$$= \frac{1}{2} \qquad (6.68)$$

For P2, the transfer function becomes

$$T_{zw}(j\omega) = \frac{1}{j\omega}\,\frac{j\omega}{10+j\omega}\,\frac{1}{j\omega+1} = \frac{(10-\omega^2)-11j\omega}{(100+\omega^2)(1+\omega^2)} \qquad (6.69)$$

and the 2-norm becomes

$$\|T_{zw}\|_2 = \left(\frac{1}{2\pi} \int_{-\infty}^{+\infty} \left[\frac{1}{(100+\omega^2)(1+\omega^2)} \, d\omega \right] \right)^{\frac{1}{2}}$$

$$= \left(\frac{1}{2\pi} \left[\frac{1}{99} \left(\frac{-1}{10} \tan(\omega/10) + \tan^{-1}(\omega) \right) \right] \Bigg|_{-\infty}^{\infty} \right)^{\frac{1}{2}}$$

$$= \left(\frac{1}{2\pi} \left[\frac{1}{99} \left(\frac{-1}{10} \pi + \pi \right) \right] \right)^{\frac{1}{2}}$$

$$= \left(\frac{1}{220} \right)^{\frac{1}{2}} = 0.067 \qquad (6.70)$$

Now the true nature of this process is revealed, as the norm of P2 is very much smaller than that of P1, due to the fact that the error resultant from P2 has much less low frequency content (faster response) than that for P1. The principles of behavior demonstrated in this SISO example extend directly to the MIMO problem, with the added concept of relative weights between error signals.

Relative Weighting of Components of the Error Signal. In composing the problem, the ability to modifv the relative importance between the elements of the error signal z allows the designer to tune the response to his desires when some of the signals compete with each other. The most obvious competition takes place between the control signal u and the error signal z, as decreasing the penalty on u allows more control to be used to decrease z.

In a MIMO system, the same competition can occur between elements of the error signal itself. An obvious case of this

occurs if the desire is to penalize some tracking error and at the same time penalize the rate of the subject response. It is not possible to maintain a zero rate and still respond to the command. The determination of the relative penalties is almost always an iterative process. If the response is too slow, the position error is penalized more heavily. Likewise, if the response is too lightly damped, the rate is penalized more heavily.

In this context, the flexibility of the weighting filters shows its true potential. With the addition of the frequency dependent weights, not only can the designer set the relative penalties on the different errors overall, he can also set relative penalties between errors that vary over the entire spectrum. In the case of the position versus rate errors, this flexibility allows the designer to penalize the position more at low to intermediate frequency, so that the steady state error and rise time are reduced, and simultaneously penalize the rate in some frequency range where the system is exhibiting poor damping. This was the approach used in developing the weights on the missile system.

The weighting function W_z can be represented as

$$W_z = \rho_z \tilde{W}_z \tag{6.71}$$

where ρ_z is a diagonal matrix containing the relative weights between the components of the error signal and $\tilde{W}_z$ is a normalized frequency dependent weighting function which achieves unity gain at its maximum value. This is done to separate the magnitude of the filtered signal from the shape

of the filter, facilitating ease of design. By making such a separation, it is possible to automate the calculation of W_z whenever the weighting factors ρ or the shaping filters $\tilde{W}_z$ are modified.

All of the concepts needed to begin the design have been developed. It quickly becomes evident, however, that with the many design variables available (shape of input and output weighting filters, relative weights between error signals and control inputs, etc.) that the design must be carried out in some systematic fashion, or else the designer can be overwhelmed by the many options available. An algorithm was therefore developed to simplify this process.

Design Procedure. The first step in the design process is to break the tasking into manageable objectives. The design task was therefore broken into three portions: (1) target tracking, (2) missile command following, and (3) disturbance filtering.

Target Tracking. First, all input weighting filters were set to identity. Next, all weights on the body rate and normal acceleration error were set to zero, to focus on tracking the target only, and the weighting on δ was reduced to a small magnitude.

At this point, it was found to be necessary to raise the penalty on fin deflection, δ, to the same magnitude as the weight on the tracker command signal, ω, because the missile was attempting to maneuver the whole missile body in order to align the antenna with the target due to the low penalty on δ. This is shown in Figure 6.11, where the input is a ramp of one

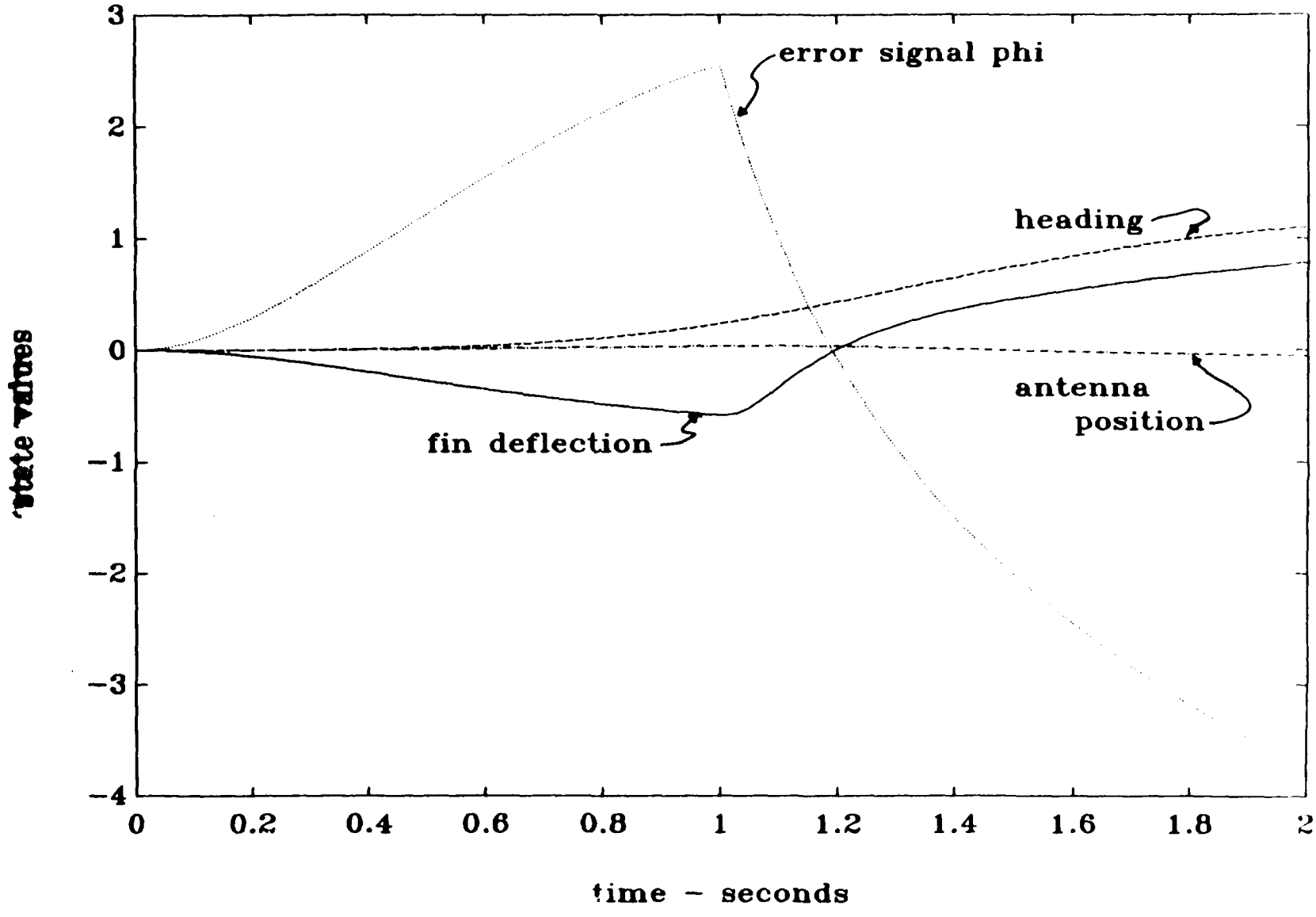

Figure 6.11. System Response to Ramp and Step Target Input

degree per second in the target position input.

Successive iterations revealed that the weighting mix that achieves the best target tracking available with this configuration was

$$\rho_z = \begin{bmatrix} 0 & 0 & 0 & 0 & 0 \\ 0 & 0 & 0 & 0 & 0 \\ 0 & 0 & 0.1 & 0 & 0 \\ 0 & 0 & 0 & 0.1 & 0 \\ 0 & 0 & 0 & 0 & 10000 \end{bmatrix} \tag{6.72}$$

$$\rho = \begin{bmatrix} 0.1 & 0 \\ 0 & 0.1 \end{bmatrix} \tag{6.73}$$

This yields the response shown in Figure 6.12 for a unit ramp antenna position command input followed by a negative unity step. From this figure, it can be seen that the transient response of the tracker is underdamped, and a steady state error of 25% is present on the ramp input. To overcome this error and transient, it is necessary to introduce the frequency-dependent weighting on both the input command w_1 and the output z.

To reflect the nature of the expected input commands to antenna position, the filter W_1 is modified (from the flat spectrum unity gain used at the start) such that the weighting on antenna position commands looks as shown in Figure 6.13, simulating a step command over the frequency range of interest. Also, the weighting on the antenna position error signal is modified to make it a low pass filter with a bandwidth of 40 radians per second, as shown in Figure 6.14. The weighting filter on the antenna rate was modified to look like a bandpass filter, as shown in Figure 6.15. In addition,

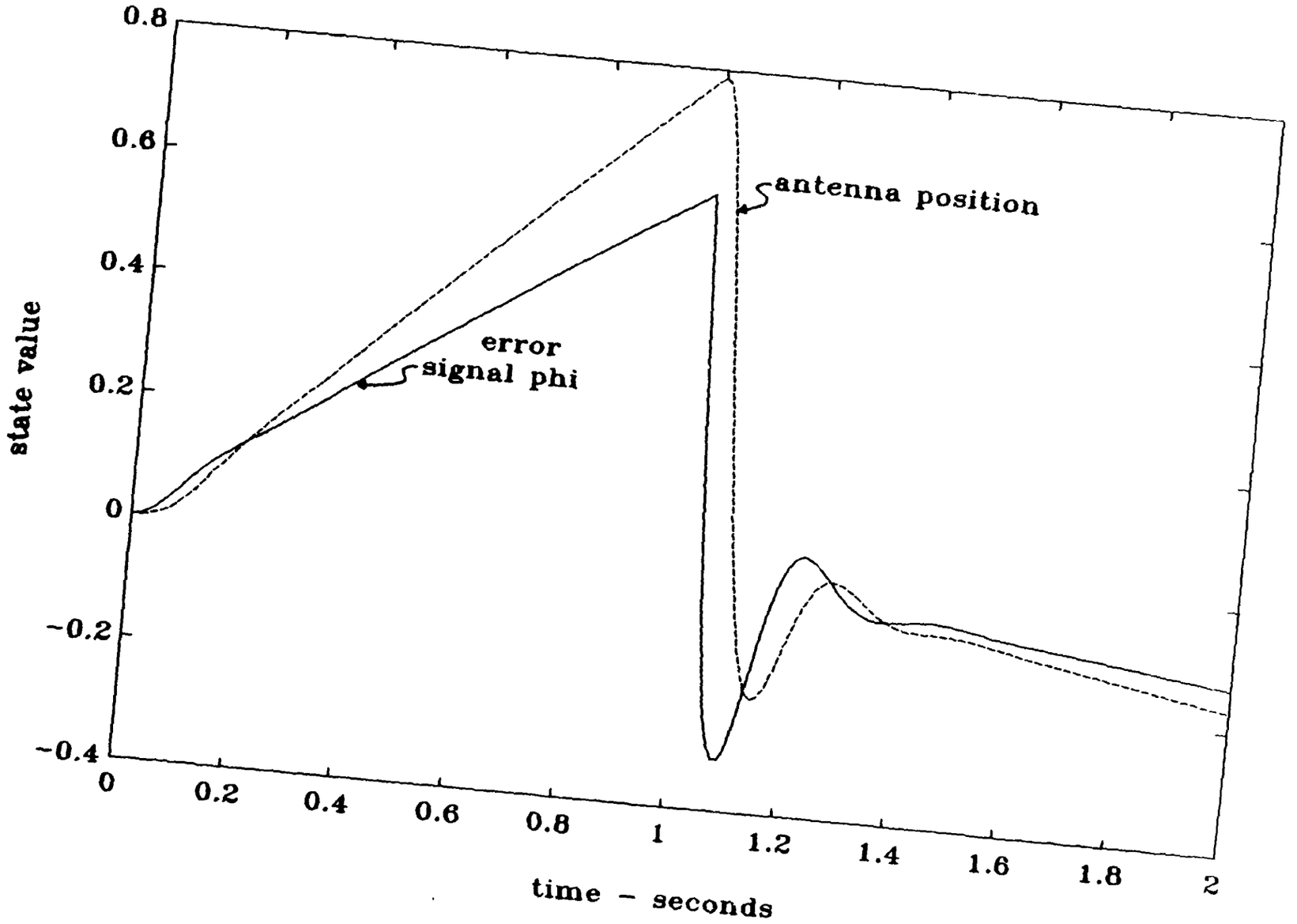

Figure 6.12. Tracker Response to Ramp and Step Target Input

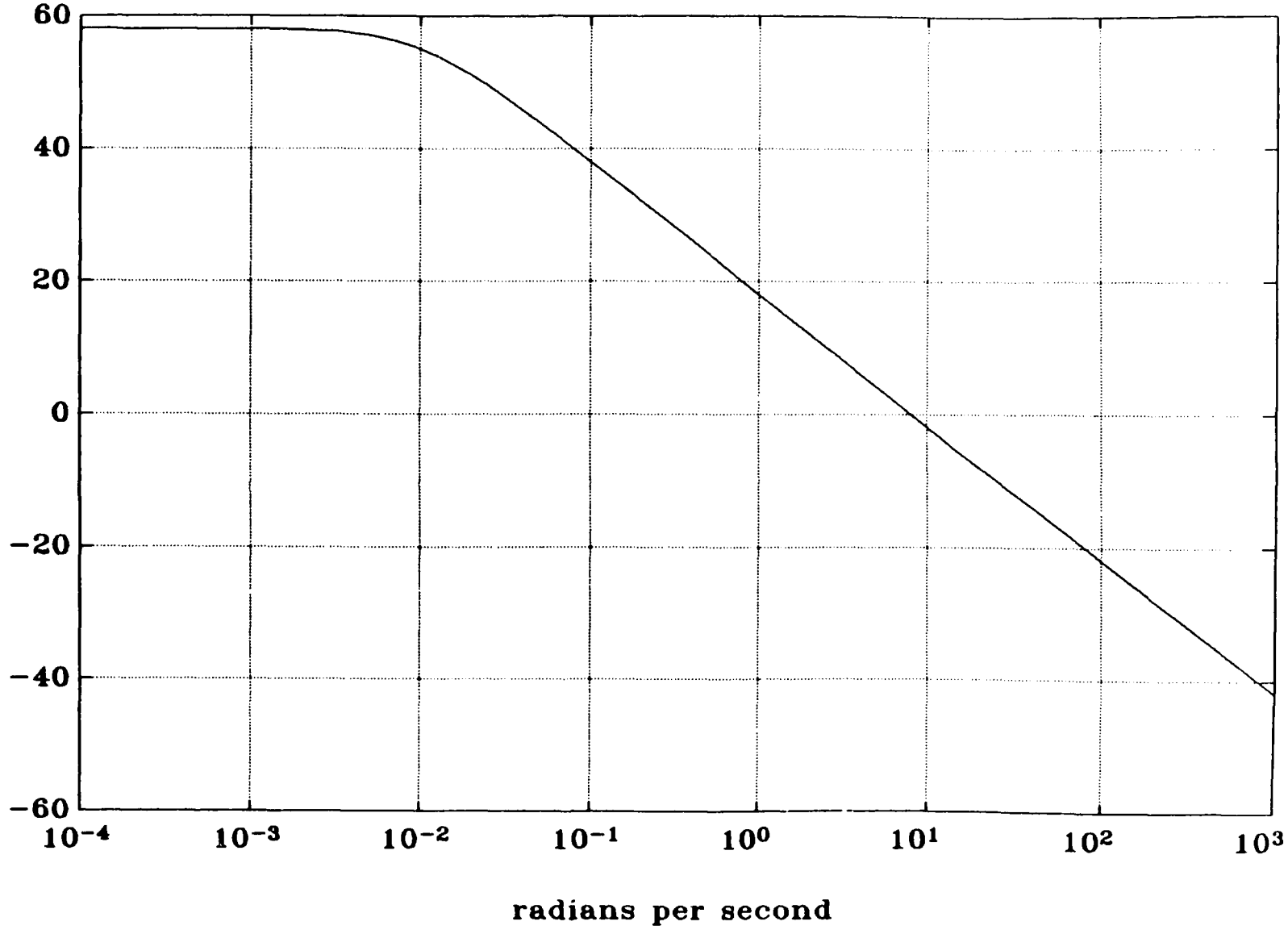

Figure 6.13. Antenna Position Command Input Filter

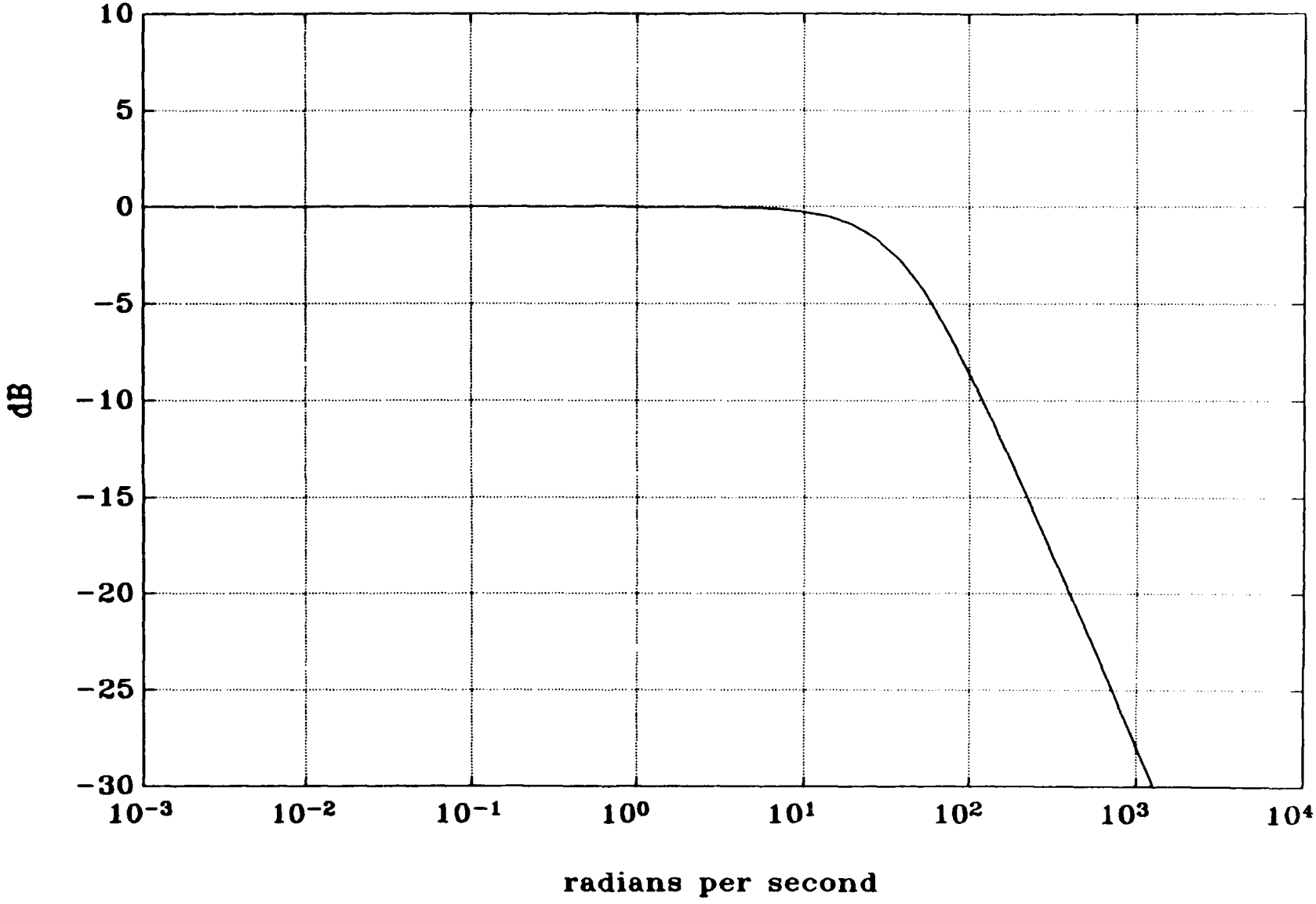

Figure 6.14. Antenna Position Error Weighting Filter

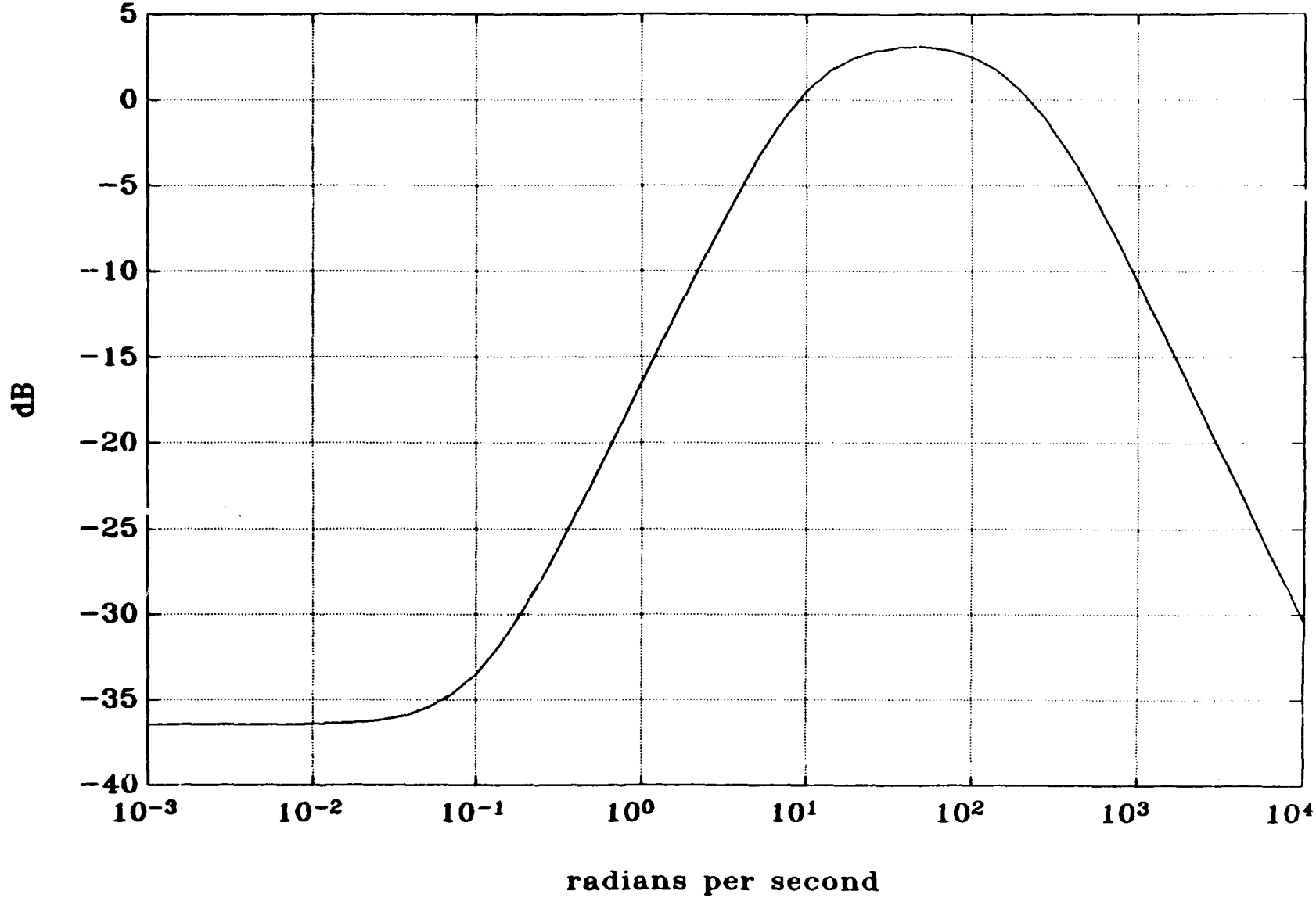

Figure 6.15. Antenna Rate Error Weighting Filter

the weighting matrix on the error signals was modified to

$$\rho_z = \begin{bmatrix} 0 & 0 & 0 & 0 & 0 \\ 0 & 0 & 0 & 0 & 0 \\ 0 & 0 & 0.1 & 0 & 0 \\ 0 & 0 & 0 & 10 & 0 \\ 0 & 0 & 0 & 0 & 1000 \end{bmatrix} \tag{6.74}$$

The response of the resultant controller is shown in Figure 6.16. This response is satisfactory. With the tracker designed, the missile control system is the next subject of interest.

Missile Control System. The above process was applied to the missile command signals and errors. This process required modifying the body rate command filter to look like a step function over the frequency range of interest, as shown in Figure 6.17. The body rate error filter was modified to look like a lowpass filter to penalize steady-state error more heavily than high-frequency error, as shown in Figure 6.18. In the same manner that antenna rate error was bandpassed to reduce the antenna transient, the normal acceleration error filter was converted to a bandpass to achieve the same effect, as shown in Figure 6.19. The weighting matrix on the error signals was modified to

$$\rho_z = \begin{bmatrix} 5 & 0 & 0 & 0 & 0 \\ 0 & 0.1 & 0 & 0 & 0 \\ 0 & 0 & 0.1 & 0 & 0 \\ 0 & 0 & 0 & 10 & 0 \\ 0 & 0 & 0 & 0 & 1000 \end{bmatrix} \tag{6.75}$$

These modifications yielded the response shown in Figure 6.20 for a missile body rate command of 1 degree per second. This response is acceptable. Now that the design responds correctly, it only remains to shape the disturbance inputs.

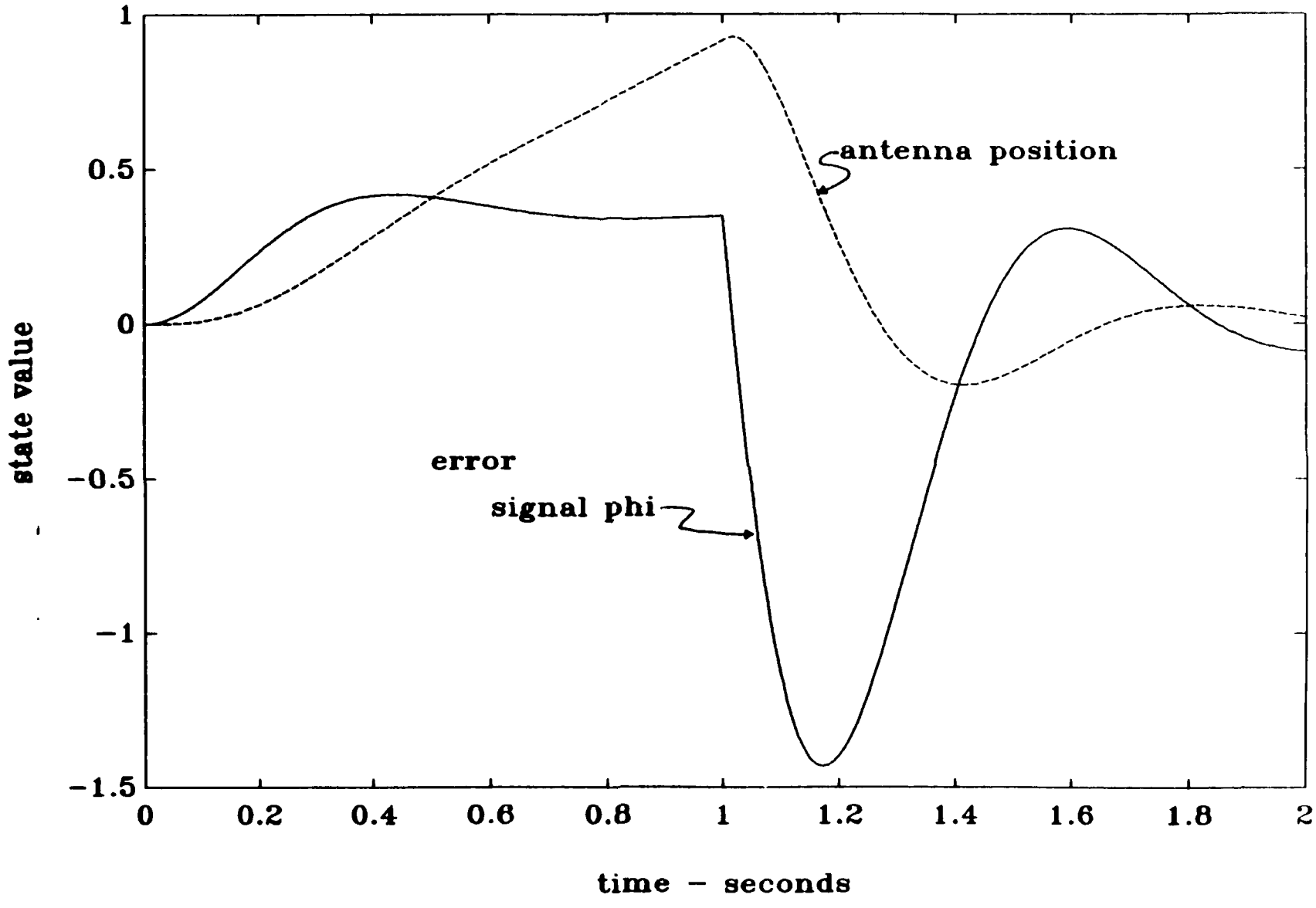

Figure 6.16. Tracker Response to Ramp and Step Target Inputs

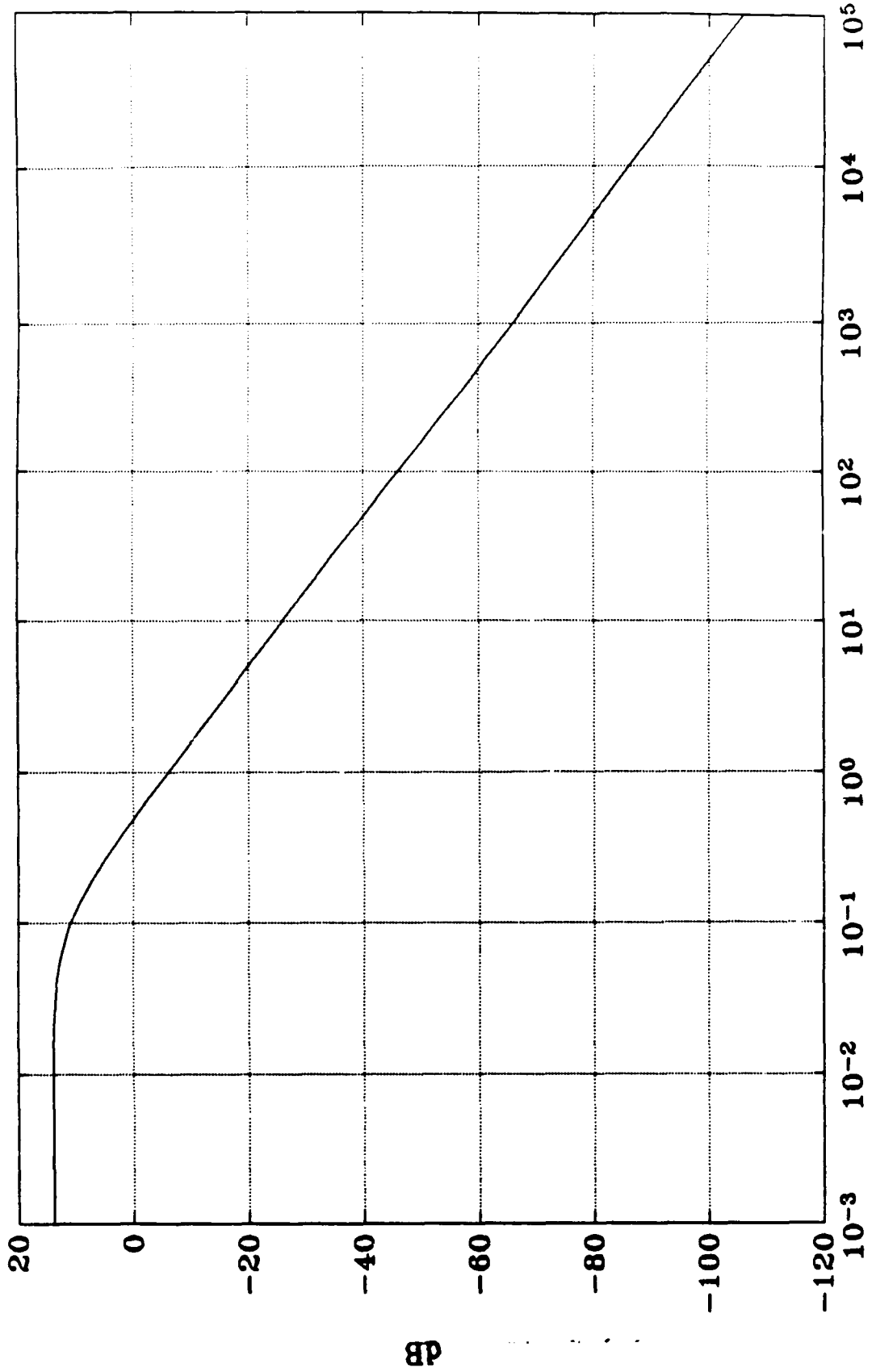

Figure 6.17. Body Rate Command Input Weighting Filter

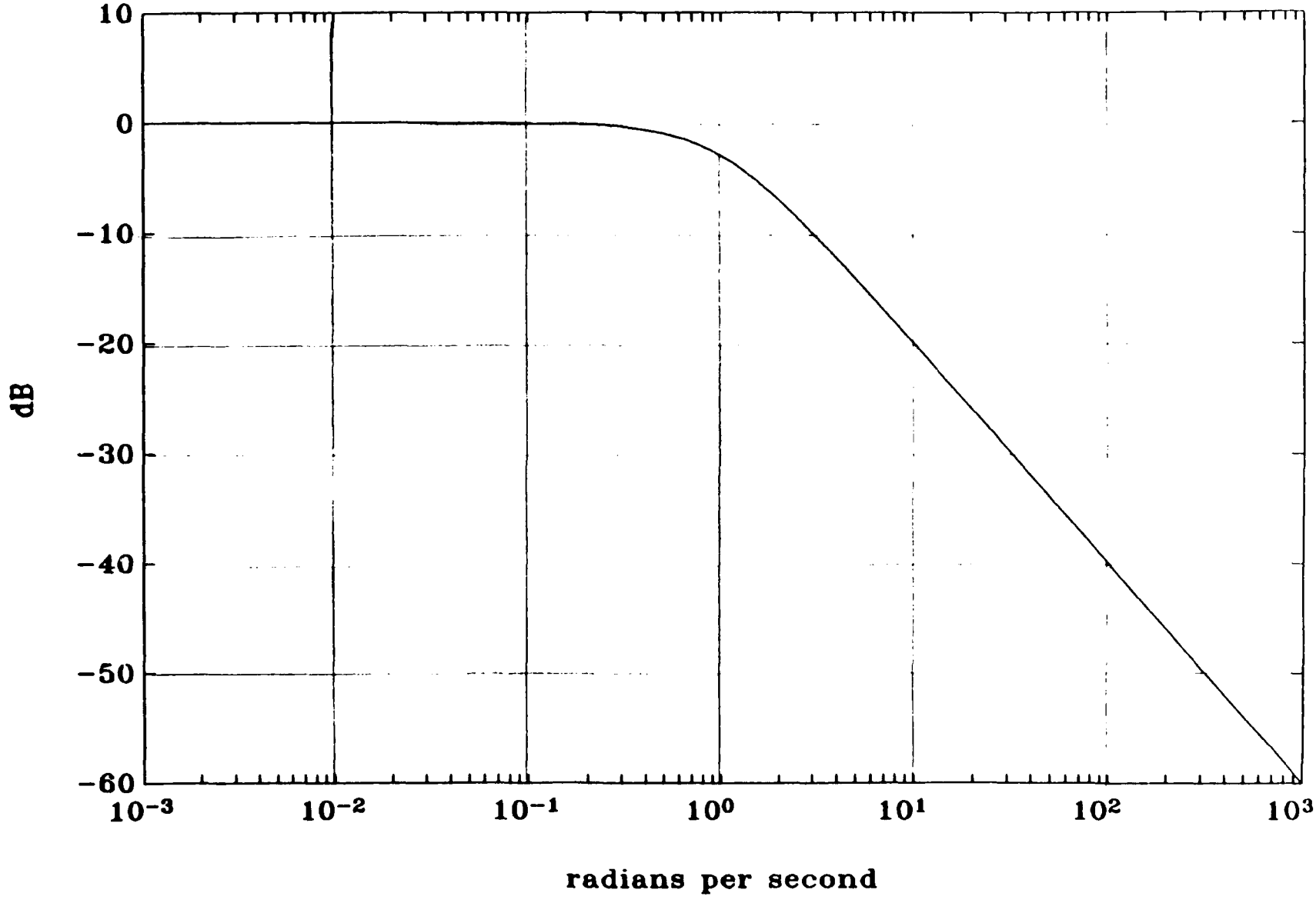

Figure 6.18. Body Rate Error Weighting Filter

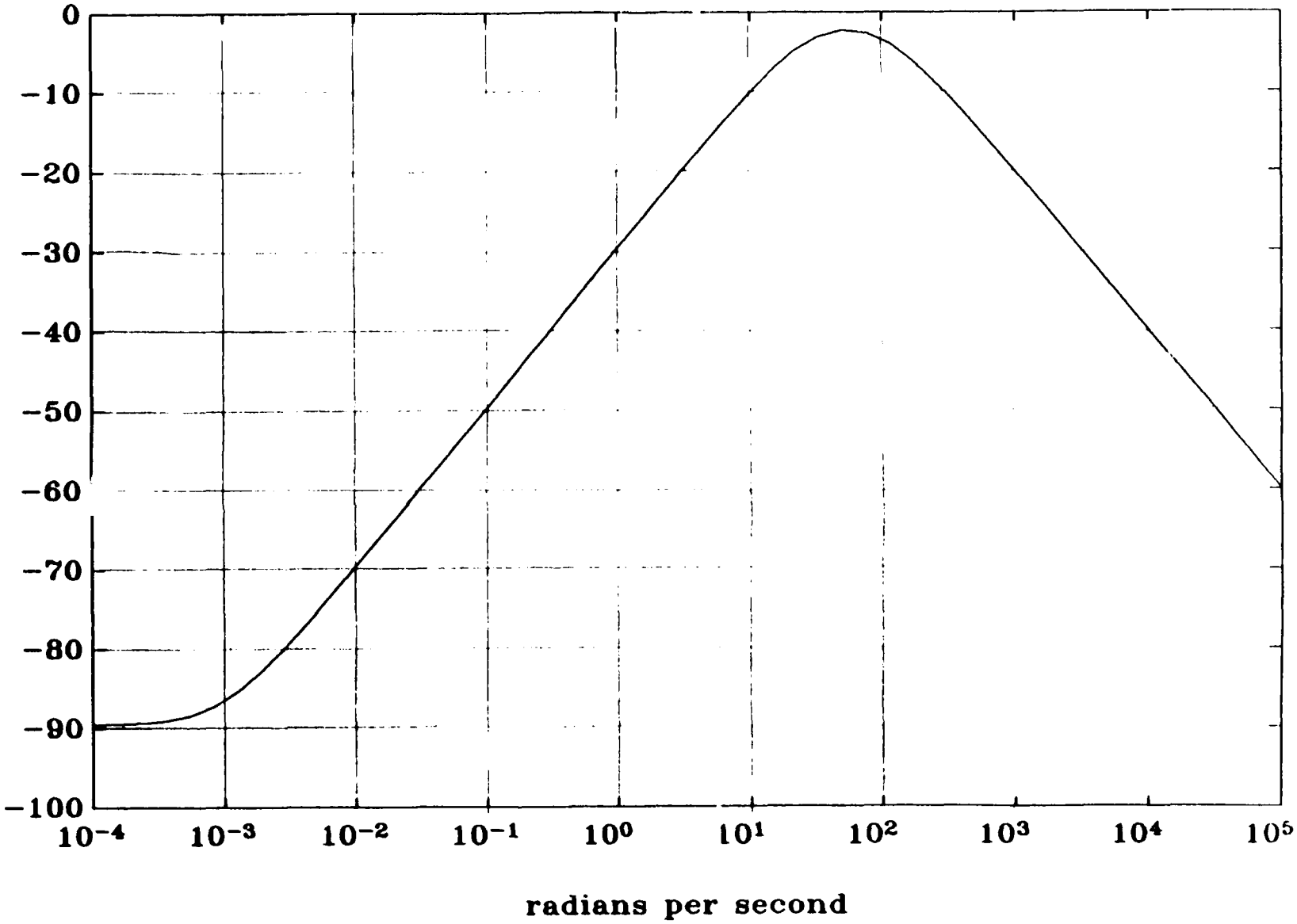

Figure 6.19. Normal Acceleration Error Weighting Filter

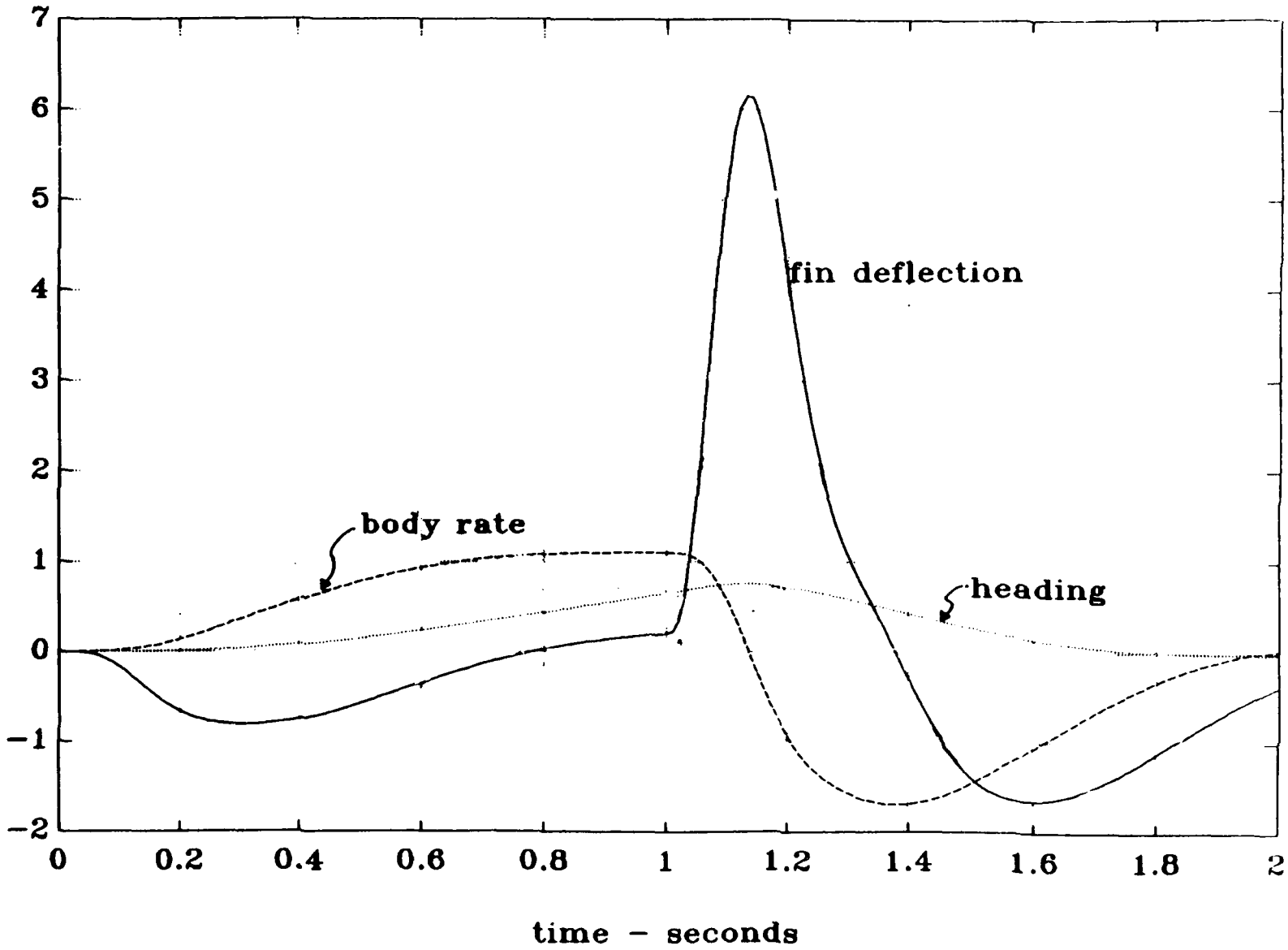

Figure 6.20. Airframe Response to Ramp and Step Target Inputs

Weighting Functions for the Missile System. The disturbance weighting filters developed for the missile system are described in Table 6.3.

Table 6.3. Disturbance Input Weighting Filters

Disturbance Filter	Description
Body Rate Command	-20 dB/decade above 0.1 rad/sec, low frequency gain 20 dB, to simulate a step command at high frequency.
Normal Acceleration Command	Flat at 0 dB over entire spectrum. Normal acceleration is used for damping only, no command.
Boresight Error Command	Same as Normal Acceleration Command.
Antenna Rate Command	Same as Normal Acceleration Command.
Antenna Position Command	-20 dB/decade above 0.01 rad/sec. Low frequency gain 58 dB,simulate step command.
Accelerometer Noise	High pass above 20 rad/sec, -40 dB at low frequency.
Rate Gyro Noise	High pass above 10 rad/sec, -40 dB at low frequency.
Potentiometer Noise	High pass above 40 rad/sec, -40 dB at low frequency.
Turbulence	High pass above 1 rad/sec, -40 dB at low frequency.
Glint	High pass above 50 rad/sec, -40 dB at low frequency.
Power Supply Noise	High pass above 400 rad/sec, -40 dB at low frequency.

See Appendix A for the respective transfer functions, Bode

plots, and state space representations. Inclusion of these weighting filters required further modification to the command and error filters. These modifications are reflected in Table 6.4.

Table 6.4. Error Signal Weighting Filters

Error Signal	Filter Description
Body Rate	Lowpass below 1 rad/sec, dropping off at -20 dB/decade thereafter.
Normal Acceleration	0 dB over the range 30 to 100 rad/sec.
Boresight Error	Lowpass below 0.01 rad/sec, -20 dB/decade thereafter
Antenna Rate Error	0 dB over the range 10 to 200 rad/sec.
Antenna Position Error	0 dB out to 40 rad/sec dropping off at -20 dB/decade thereafter.

Again, see Appendix A for a detailed description of the filters described in Table 6.4.

The set of weights used in the final design is given by

$$\rho_z = \begin{bmatrix} 400 & 0 & 0 & 0 & 0 \\ 0 & 0.1 & 0 & 0 & 0 \\ 0 & 0 & 0.1 & 0 & 0 \\ 0 & 0 & 0 & 10 & 0 \\ 0 & 0 & 0 & 0 & 1000 \end{bmatrix} \qquad (6.76)$$

This set of weights and filters yielded a compensator which responds as shown in Figure 6.21.

Closed-Loop System Representation.

Once the controller is obtained, it can be placed into

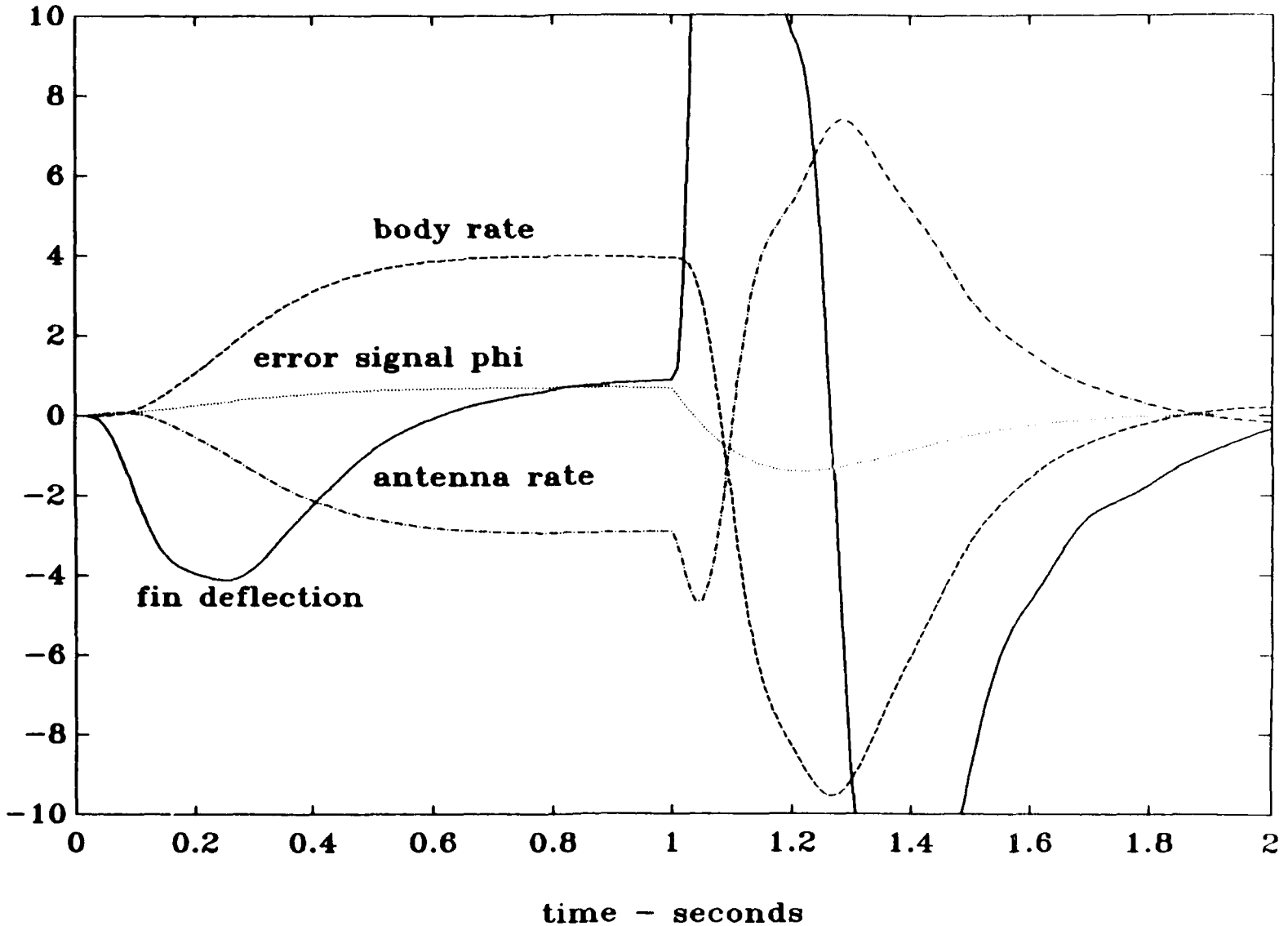

Figure 6.21. System Response to Ramp and Step Target Input

the original system, so that the closed-loop system can be represented as shown in Figure 6.22, where $[A_{cp}\ B_{cp}\ C_{cp}]$ correspond to the designed compensator and $[A_p\ B_p\ C_p]$ correspond to the original system. Note that the D matrices for the plant and the compensator have been omitted for clarity, since they are all identically zero. T_1 is the matrix which derives the error signals from the sensor values. Creation of T_1 requires implementing the proportional navigation laws described in Chapter V.

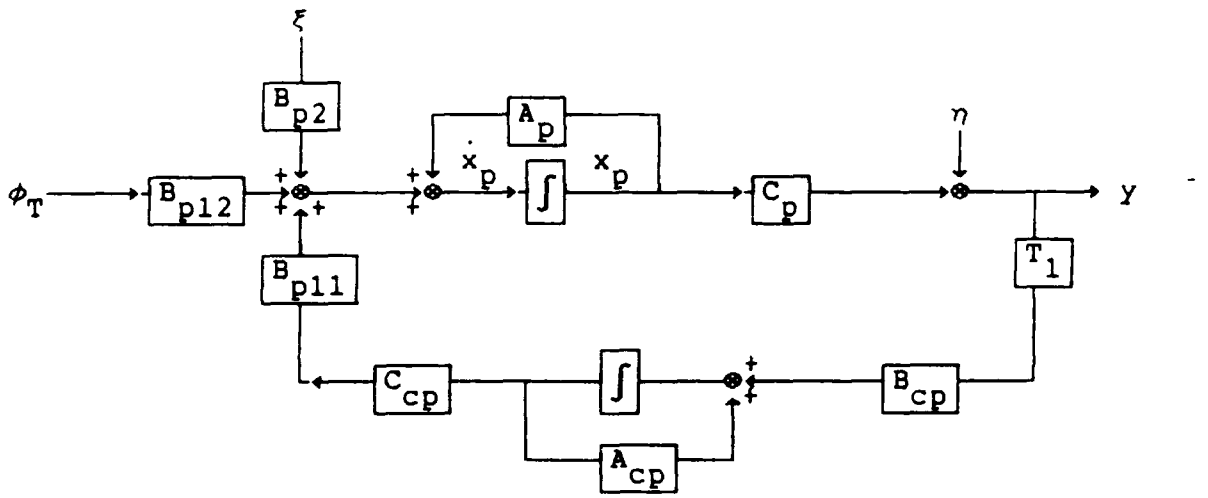

Figure 6.22. Closed Loop System Block Diagram

For this case, T_1 is given by

$$T_1 = \begin{bmatrix} -.7+.0025*\dot{R}_T & 0.150 & 0 & .0025*\dot{R}_T & 0 \\ 0 & -1 & 0 & 0 & 0 \\ 0 & 0 & -1 & 0 & 0 \\ 0 & 0 & 0 & -1 & 0 \\ 0 & 0.1 & 0.25 & 0 & 0 \end{bmatrix} \qquad (6.77)$$

Since δ and ω are generated internally, the above system may be

represented as

$$\dot{x}_{c1} = A_{c1}\, x_{c1} + B_{c1}\, u_{c1} \tag{6.78}$$

$$y_{c1} = C_{c1}\, x_{c1} + D_{c1}\, u_{c1} \tag{6.79}$$

where

$$x_{c1} = \begin{bmatrix} x_p \\ x_{cp} \end{bmatrix} \tag{6.80}$$

$$u_{c1} = \begin{bmatrix} \phi_T \\ \xi \\ \eta \end{bmatrix} \tag{6.81}$$

$$y_{c1} = y \tag{6.82}$$

$$A_{c1} = \begin{bmatrix} A_p & B_{p11}C_{cp} \\ B_{cp}T_1C_p & A_{cp}+B_{cp}T_1D_{p11}B_{p11}C_{cp} \end{bmatrix} \tag{6.83}$$

$$B_{c1} = \begin{bmatrix} B_{p12} & B_{p2} & 0 \\ B_{cp}T_1D_{p12} & B_{cp}T_1D_{p2} & B_{cp}T_1 \end{bmatrix} \tag{6.84}$$

$$C_{c1} = \begin{bmatrix} C_p & D_{p11}B_{p11}C_{cp} \end{bmatrix} \tag{6.85}$$

$$D_{c1} = \begin{bmatrix} D_{p2} & D_{p12} & I \end{bmatrix} \tag{6.86}$$

Thus, the closed loop system is derived directly from the open loop description and the designed compensator.

Compensator Order Reduction

Due to the nature of the Riccati equations (6.16 & 6.17), the compensator obtained in the above procedure is of the same order as the augmented plant; 23 states. When added to the plant, the resulting closed-loop system has a total of 30

states. This system is far too large to simulate in any efficient manner in PC-MATLAB. Due to array size limitations and time step requirements, it was desired to reduce the compensator to no more than thirteen states.

The first attempt at reduction was to perform a minimal realization of the system, to eliminate any pole-zero cancellations. This was accomplished via the PC-MATLAB function MINREAL, which allows the user to specify a tolerance for pole-zero cancellations. For a tolerance of 0.01, two states were removed. For a tolerance of 0.1, three states were removed, but a detrimental effect on system accuracy was observed. Accuracy was evaluated by feeding a random signal, a step command, and a ramp command to both the full order compensator and the reduced order compensator, then examining the output control signals. At this point, it became obvious that the minimal realization would not accomplish sufficient order reduction without serious loss of accuracy, so model order reduction via Hankel singular value elimination [10] was attempted.

Using this method, the compensator was reduced to 11 states without seriously compromising efficiency. This was sufficient to make simulation possible. Both the full order compensator and the reduced order compensator are described in Appendix C.

VII. H_∞ Controller Synthesis

The H_∞ design objective is to find the feedback compensator K(s) such that the ∞-norm of the closed loop transfer function matrix z(s)/w(s) is minimized, where w(s) and z(s) are as described in Chapter VI. The methodology for solving this problem is a relatively new development, so a more complete treatment will be given than in Chapter VI. For a complete treatment, see Doyle, et. al. [3].

Theory for State Space Solution of the H_∞ Design Problem

The development presented in this section was taken from [3]. The standard block diagram representation of the small gain problem is shown in Figure 7.1. Notice that the same basic setup is used as for the H_2 theory.

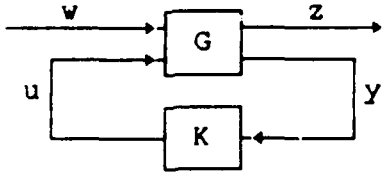

Figure 7.1. Standard Block Diagram

As in Chapter VI, w is the vector containing all system inputs, z is a vector of error signals to be controlled, u is the control input vector, and y is the vector of measured system errors. The resultant closed-loop matrix of transfer functions from w to z is denoted T_{zw}.

∞-norm Definition. The objective of H_∞ design is to find K such that T_{zw} is internally stabilized and the ∞-norm of

T_{zw}, denoted $\|T_{zw}\|_\infty$, is minimized. The ∞-norm of T_{zw} is defined as

$$\|T_{zw}\|_\infty := \sup_\omega \sigma_{max}\left[T_{zw}(j\omega)\right] \qquad (7.1)$$

where

$$\sigma_{max} := \text{maximum singular value} \qquad (7.2)$$

The above is read, "the ∞-norm of T_{zw} is defined as the supremum over all frequencies of the maximum singular value of T_{zw}." This concept can again be visualized easily in the SISO case, where the ∞-norm is equal to the maximum value of the Bode plot of the closed-loop transfer function. In the MIMO case, substitute "maximum singular value plot" for "Bode plot" in the above. Thus, the ∞-norm is a measure of the worst case amplification (in the frequency domain) of the output z in response to the input w, in contrast to the 2-norm being a measure of average amplification over the entire frequency spectrum. For this reason, controller designs based on optimizing the ∞-norm return controllers which make $T_{zw}(j\omega)$ have a maximum singular value plot which is flat, i.e. all frequencies are amplified at the same level.

Like the H_2 design method, solution of the H_∞ problem rests on solving two uncoupled Riccati equations. Unlike the H_2 methodology however, the H_∞ optimization problem yields a set of Riccati equations whose solution is stabilizing only if $\|T_{zw}\|_\infty \leq 1$. The reasons for this characteristic are very complex, and outside the scope of this paper. For a detailed explanation of this fact, see Doyle, et. al. [3]. This

limitation can be circumvented, however, by introducing a scaling factor γ.

The γ Iteration. The level to which the ∞-norm can be reduced is limited. In other words, it cannot be reduced to any arbitrary size desired. Therefore, there exists some optimal ∞-norm obtainable for any given system, no matter what controller is used. Since the Riccati equations are designed to return a compensator which reduces $\|T_{zw}\|_\infty$ to 1, it makes sense that this would not be possible if the optimal value of $\|T_{zw}\|_\infty$ is greater than 1. In this case, the set of Riccati equations has no stabilizing solution. Additionally, it is equally possible that the optimal value of $\|T_{zw}\|_\infty$ is less than 1, in which case the compensator obtained via the Riccati equations is not the optimal. Thus, a scaling factor γ is introduced. By a basic property of any norm, in particular the ∞-norm,

$$\| \gamma T_{zw} \|_\infty = \gamma \|T_{zw}\|_\infty \tag{7.3}$$

where γ is an arbitrary constant. Thus, to obtain a compensator which achieves the optimal $\|T_{zw}\|_\infty$, it is necessary to divide the input or the output or a combination of the two by a factor equal to the optimal $\|T_{zw}\|_\infty$. The optimal value of $\|T_{zw}\|_\infty$, however, is not known beforehand. For this reason, it is necessary to use an iterative approach.

To search for the optimal compensator, an artificial scaling factor γ must be added, producing a scaled input $\tilde{w}$ and scaled output $\tilde{z}$, such that

$$\tilde{w} = \sqrt{\gamma}\, w \qquad (7.4)$$

$$z = \sqrt{\gamma}\, \tilde{z} \qquad (7.5)$$

The block diagram of the resultant system is shown in Figure 7.2. Note that the problem has not really been changed, only the way in which it is perceived.

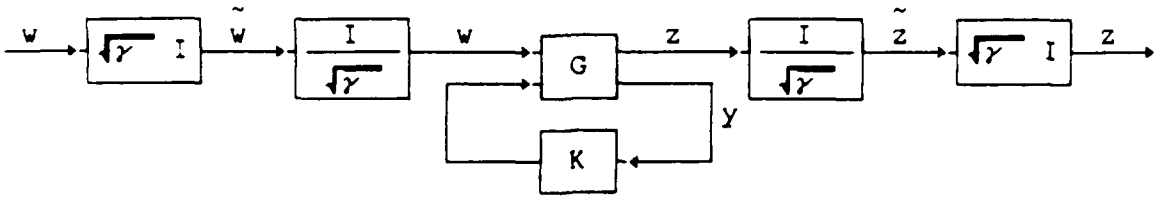

Figre 7.2. System with Scaled Inputs and Outputs

Now solving the Riccati equations for the system with $\tilde{w}$ as the input and $\tilde{z}$ as the output will produce a compensator such that $\|T_{\tilde{z}\tilde{w}}\|_\infty$ is equal to 1. The iteration comes about from the fact that if γ is picked too large, a less than optimal solution will be obtained, and if γ is too small, no stabilizing solution will be obtained. Thus, it is possible to determine upper and lower bounds on the optimal $\|T_{zw}\|_\infty$ which may be narrowed as much as desired, but the optimal may never be reached exactly.

In addition to the necessity to perform this iteration on γ, there are other problem requirements and scalings needed before the theory can be applied.

<u>Problem Requirements and Scaling</u>. To solve the H_∞ problem the following conditions must be satisfied;

$$1)\ D_{11} = 0 \qquad (7.6)$$

$$2)\ D_{22} = 0 \qquad (7.7)$$

3) a) $D_{12}^T D_{12} = I$ (7.8)

b) $D_{21} D_{21}^T = I$ (7.9)

4) (A,B_1) controllable & (C_1,A) observable

5) (A,B_2) stabilizable & (C_2,A) detectable

Note that these conditions are very similar to the conditions for the H_2 case, with the exception of Condition 4, which is a stronger requirement than in the H_2 problem. Also, both Conditions 1 and 2 may be removed when necessary [5] & [11]. Removing Condition 1, however, complicates the problem, and Condition 2 is trivially satisfied for the problem studied here. As described in Chapter VI, the modified system used is controllable and observable, so no additional modifications are necessary to meet this requirement. Condition 1 is satisfied in Chapter VI by introducing weights on the inputs and outputs. Exactly the same weights as used in Chapter VI are used here, so no further comment on these weightings is warranted.

As in the H_2 problem, Conditions 3a and 3b require that the input u and the output y be scaled. This scaling is accomplished exactly as before, via a Cholesky decomposition, which yields unique upper triangular matrices that satisfy

$$S_u^T S_u = \frac{1}{\gamma} D_{12}^T D_{12} \tag{7.10}$$

$$S_y^{-1} S_y^{-T} = \frac{1}{\gamma} D_{21} D_{21}^T \tag{7.11}$$

The scaling is appended to the original plant G as before,

which together with the γ scaling, results in a plant which looks as shown in Figure 7.3.

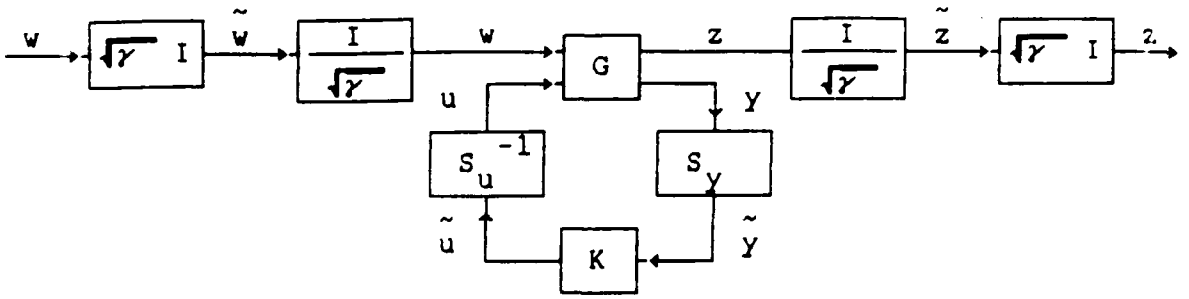

Figure 7.3. System with Scaled Inputs and Outputs

With these scalings all in place, the new system becomes

$$\dot{x} = A\,x + \tilde{B}1\,\tilde{w} + \tilde{B}2\,\tilde{u} \tag{7.12}$$

$$\tilde{z} = \tilde{C}1\,x + \tilde{D}12\,\tilde{u} \tag{7.13}$$

$$\tilde{y} = \tilde{C}2\,x + \tilde{D}21\,\tilde{w} \tag{7.14}$$

where

$$\tilde{B}_1 = \frac{1}{\sqrt{\gamma}}\,B_1 \tag{7.15}$$

$$\tilde{C}_1 = \frac{1}{\sqrt{\gamma}}\,C_1 \tag{7.16}$$

$$\tilde{B}_2 = B_2\,S_u^{-1} \tag{7.17}$$

$$\tilde{C}_2 = S_y\,C_2 \tag{7.18}$$

$$\tilde{D}_{12} = \frac{1}{\sqrt{\gamma}}\,D_{12}\,S_u \tag{7.19}$$

$$\tilde{D}_{21} = \frac{1}{\sqrt{\gamma}}\,S_y\,D_{21} \tag{7.20}$$

Note that D11 and D22 have been excluded, as they are identically zero to meet Conditions 1 and 2 above. The problem is now in the form required for application of the

method described by Doyle et. al. [3].

Solution. This method requires obtaining the real, unique, symmetric solutions X_∞ and Y_∞ to two uncoupled Riccati equations

$$F_1^T X_\infty + X_\infty F_1 - X_\infty G_1 X_\infty + H_1 = 0 \tag{7.21}$$

$$F_2^T Y_\infty + Y_\infty F_2 - Y_\infty G_2 Y_\infty + H_2 = 0 \tag{7.22}$$

where

$$F_1 = A - \tilde{B}_2 \tilde{D}_{12}^T \tilde{C}_1 \tag{7.23}$$

$$G_1 = \tilde{B}_2 \tilde{B}_2^T - \tilde{B}_1 \tilde{B}_1^T \tag{7.24}$$

$$H_1 = \hat{C}_1^T \hat{C}_1 \tag{7.25}$$

$$\hat{C}_1 = (I - \tilde{D}_{12} \tilde{D}_{12}^T) \tilde{C}_1 \tag{7.26}$$

$$F_2 = A - \tilde{B}_1 \tilde{D}_{21}^T \tilde{C}_2 \tag{7.27}$$

$$G_2 = \tilde{C}_2^T \tilde{C}_2 - \tilde{C}_1^T \tilde{C}_1 \tag{7.28}$$

$$H_2 = \hat{B}_1 \hat{B}_1^T \tag{7.29}$$

$$\hat{B}_1 = \tilde{B}_1 (I - \tilde{D}_{21}^T \tilde{D}_{21}) \tag{7.30}$$

Note that the above Riccati equations are not the same as in the H_2 problem. In addition to the extra scaling on B_1 and C_1, the quadratic terms G (with appropriate subscripts) have an extra term in them. This extra term is the limiting factor which makes the H_∞ problem inherently more difficult than the H_2 problem. For more detail, see [3] and [4].

The optimal controller for the H_∞ problem is then given by

$$A_{cp} = A - K_f \tilde{C}_2 - \tilde{B}_2 K_c + Y_\infty \tilde{C}_1^T (\tilde{C}_1 - \tilde{D}_{12} K_c) \tag{7.31}$$

$$B_{cp} = K_f \tag{7.32}$$

$$C_{cp} = -K_c \tag{7.33}$$

$$D_{cp} = 0 \tag{7.34}$$

where

$$K_c = (\tilde{B}_2^T X_\infty + \tilde{D}_{12}^T \tilde{C}_1) (I - Y_\infty X_\infty)^{-1} \tag{7.35}$$

$$K_f = Y_\infty \tilde{C}_2^T + \tilde{B}_1 \tilde{D}_{21}^T \tag{7.36}$$

There are three additional conditions which must be met for the solutions to the above Riccati equations to be stabilizing controllers for the system:

1) $X_\infty \geq 0$ (7.37)

2) $Y_\infty \geq 0$ (7.38)

3) $\bar{\rho}(X_\infty Y_\infty) \leq 1$ (7.39)

where ρ denotes the spectral radius, defined as

$$\bar{\rho}(X_\infty Y_\infty) := \max \left[\text{abs} \left[\lambda^{1/2} (X_\infty Y_\infty) \right] \right] \tag{7.40}$$

where λ denotes eigenvalue. Equation 7.39 guarantees that the inverse of $(I - X_\infty Y_\infty)$ exists, as required for equation (7.35) above.

Problem Set-up

As mentioned previously, the identical problem set-up used for the H_2 problem will be used for the H_∞ problem.

Procedure

The H_∞ solution was obtained by taking the problem set-up as described in Chapter VI and iterating values of γ until an acceptable solution was obtained. γ was reduced to a value of 500 which yielded solutions X_∞ and Y_∞ which satisfied the

conditions above. The spectral radius of the solution obtained is 0.9254. Although somewhat less than the optimal value of 1, this solution is very close to optimal, since testing γ = 499 yields a spectral radius greater than 1 (the spectral radius increases exponentially as the optimal γ is approached) and the solution obtained for γ = 501 differed only slightly from the solution for γ = 500 (the 1-norm of the difference in the compensators obtained was less than 10).

Although the same problem set-up was used for the H_2 and H_∞ solutions presented here, one problem was encountered during the design process which must be mentioned. The author originally sought to use bandpass filters on the disturbances inputs to more accurately reflect the expected noises. This worked well for the H_2 problem, but caused difficulty for the H_∞ problem. When attempting to obtain solutions to equations (7.21) and (7.22), an error message was generated which indicated that the system presented was uncontrollable when γ was reduced below values which yielded spectral radii of approximately 0.3. This (uncontrollability) was known not to be the case from prior analysis, so it was suspected that the problem was arising from some ill-conditioned terms in the problem posed. In order to implement bandpass filters and still satisfy the conditions reflected in equations (7.8) and (7.9), it was necessary to place zeros in the filter which were widely spaced in frequency. This is demonstrated in Figure 7.5, which displays the Bode plot for one of the original filters. Examination of this figure reveals that in

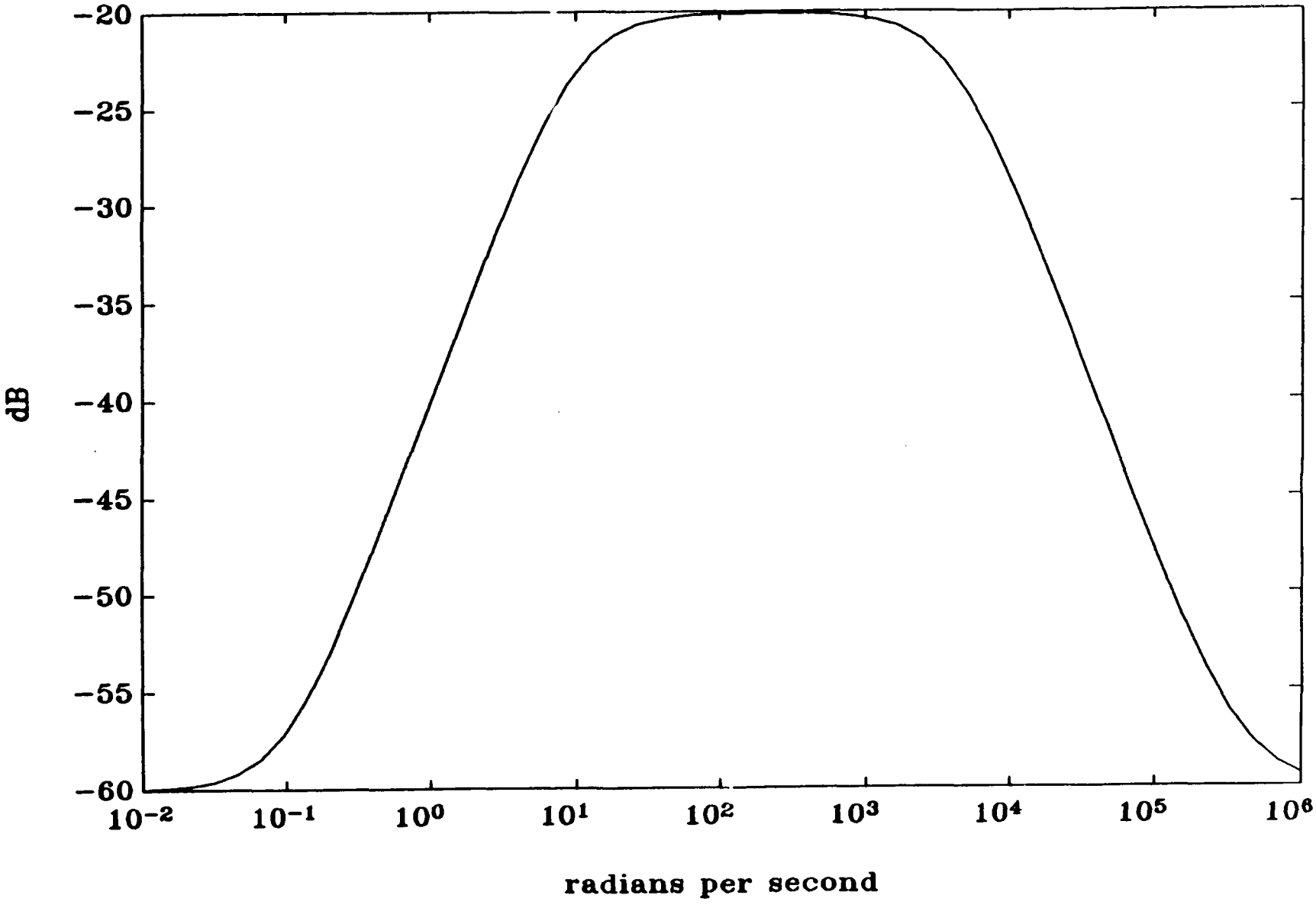

Figure 7.5. Bandpass Filter

order to maintain a 'floor' which is 40 dB below the peak and obtain a two decade passband, it is necessary to place two zeros six decades apart, for a difference in magnitude of 10^6. This large separation of zeros was suspected to be the cause of the numerical problems, and when the bandpass filters were converted to high-pass filters, the problem completely disappeared. For consistency between solutions, the highpass filters were also used for the H_2 problem, even though the bandpass filters caused no problem there.

Order Reduction of the Compensator

As in the H_2 case, the H_∞ solution yields a compensator which is of the same order as the modified plant presented to the Riccati equations, so model order reduction was required for the compensator obtained for this case as well. This was accomplished in a manner identical to that presented in Chapter VI. A full description of both the full and the reduced order compensators is contained in Appendix C.

Closed-Loop System Representation.

The closed-loop representation for the H_∞ problem is obtained the same manner as described in Chapter VI.

VIII. Performance Comparisons

Missile Flyout Simulation

To evaluate the performance of the different controllers developed herein, it was necessary to develop a digital simulation of the missile, simulating the control system, the changing environment, the noise inputs, and the target and missile geometry calculations. A PC-MATLAB script file was created to carry out the simulation.

The simulation computes target position as a function of time, calls a subroutine which generates disturbances as functions of time, computes the parameter variations, computes the closed-loop representation of the system with compensator, computes the new guidance inputs, and increments the states and bearing to target for each time increment. After end-game conditions are indicated, the simulation calculates the point of closest approach and stores the state, output, missile position, and target position time histories and the miss distance. The simulation uses a 0.02 second time step, and uses the PC-MATLAB function c2d to convert the state-space representation to a discrete iteration model.

Flyout Results

Each controller was evaluated over 112 flyouts, composed of 16 scenarios each of which was run 7 times under different conditions. The 7 conditions were: one flyout in the nominal

environment (1), two flyouts with parameter variations but no disturbance inputs (2,3), three flyouts with both parameter variations and disturbance inputs (4,5,6), and one flyout in which the target position data is lost for two 0.5 second intervals (7). The 16 engagement scenarios are described in Table 8.1.

Table 8.1. Engagement Scenarios

Scenario	Velocity	Trajectory
1	200 m/s	90° offset
2	400 m/s	90° offset
3	600 m/s	90° offset
4	800 m/s	90° offset
5	200 m/s	45° offset
6	400 m/s	45° offset
7	600 m/s	45° offset
8	800 m/s	45° offset
9	200 m/s	6g pull-in
10	400 m/s	6g pull-in
11	600 m/s	6g pull-in
12	800 m/s	6g pull-in
13	200 m/s	6g pull-out
14	400 m/s	6g pull-out
15	600 m/s	6g pull-out
16	800 m/s	6g pull-out

Examples of scenarios 4, 8, 12, and 16 are shown in Figures 8.1-8.4, respectively. The resultant miss distances (to the nearest meter) are tabulated in Tables 8.2-8.4, for the Classical, H_2, and H_∞ controllers, respectively.

Table 8.2. Classical Controller Miss Distances (m)

	Environment/System Condition						
Scenario	1	2	3	4	5	6	7
1	56	36	17	11	27	33	48
2	32	61	61	65	70	7	84
3	6	62	51	66	70	60	81
4	41	33	27	34	34	80	46
5	70	22	10	29	7	35	98
6	140	45	21	32	27	400	124
7	355	169	127	131	153	146	170
8	82	32	49	17	85	114	160
9	66	81	65	53	60	66	133
10	14	45	41	55	50	41	12
11	3	14	14	6	41	55	42
12	17	16	2	8	12	49	51
13	90	26	10	14	14	38	153
14	118	31	15	36	13	82	312
15	102	7	31	2	14	54	8
16	57	20	17	24	24	3	3
Mean	78	44	35	37	43	79	96

Examination of the miss distance results reveals several

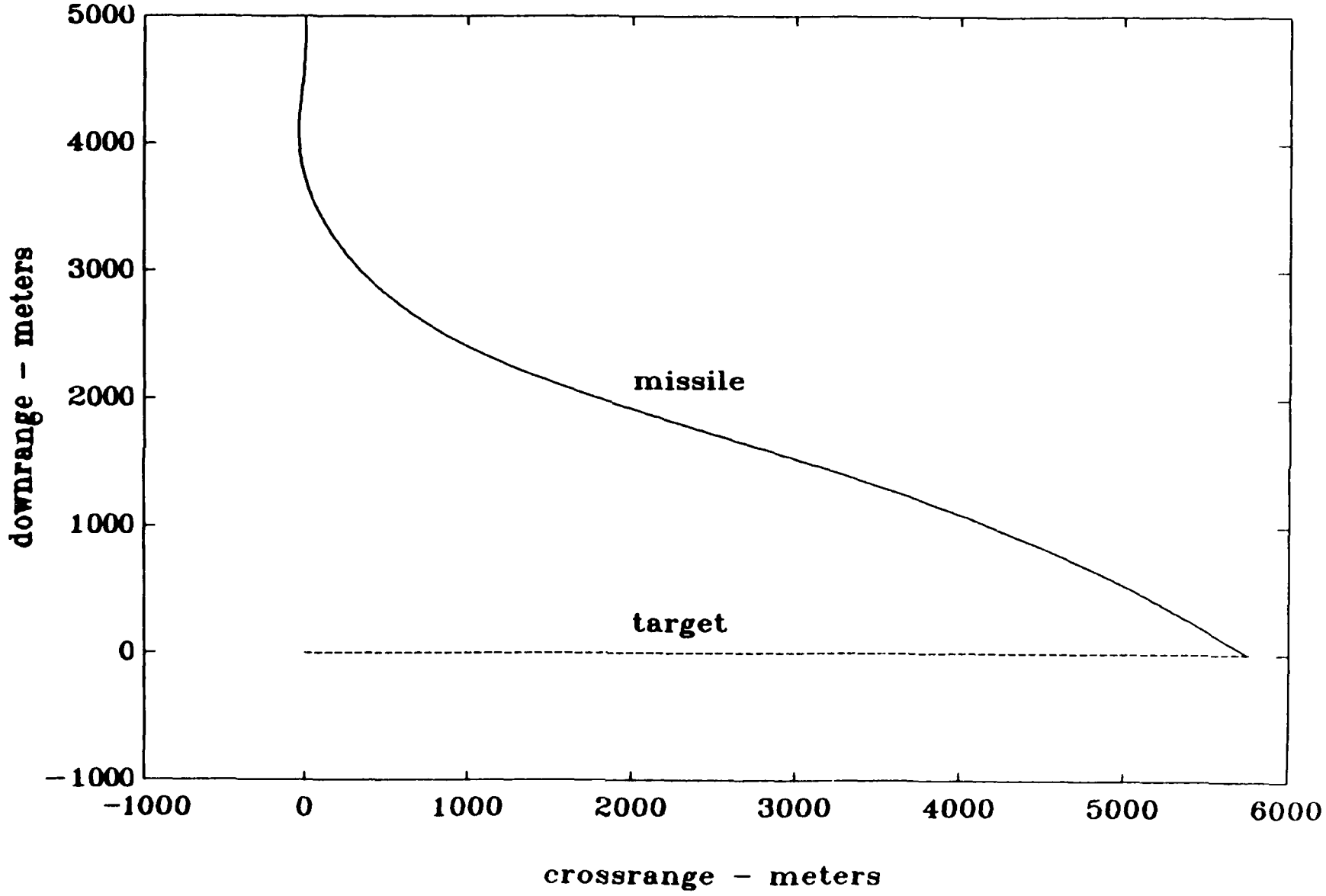

Figure 8.1. Scenario 4 Engagement

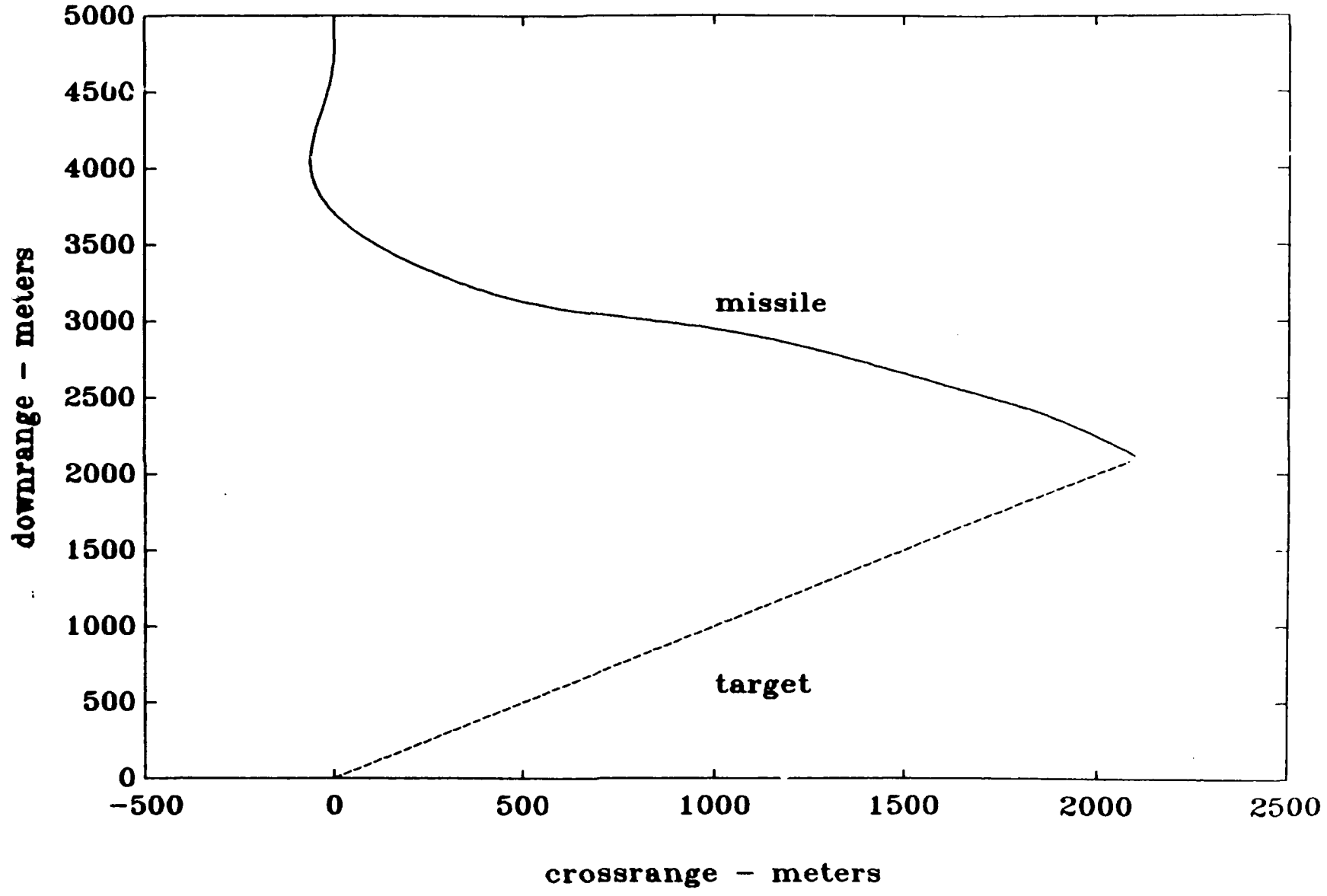

Figure 8.2. Scenario 8 Engagement

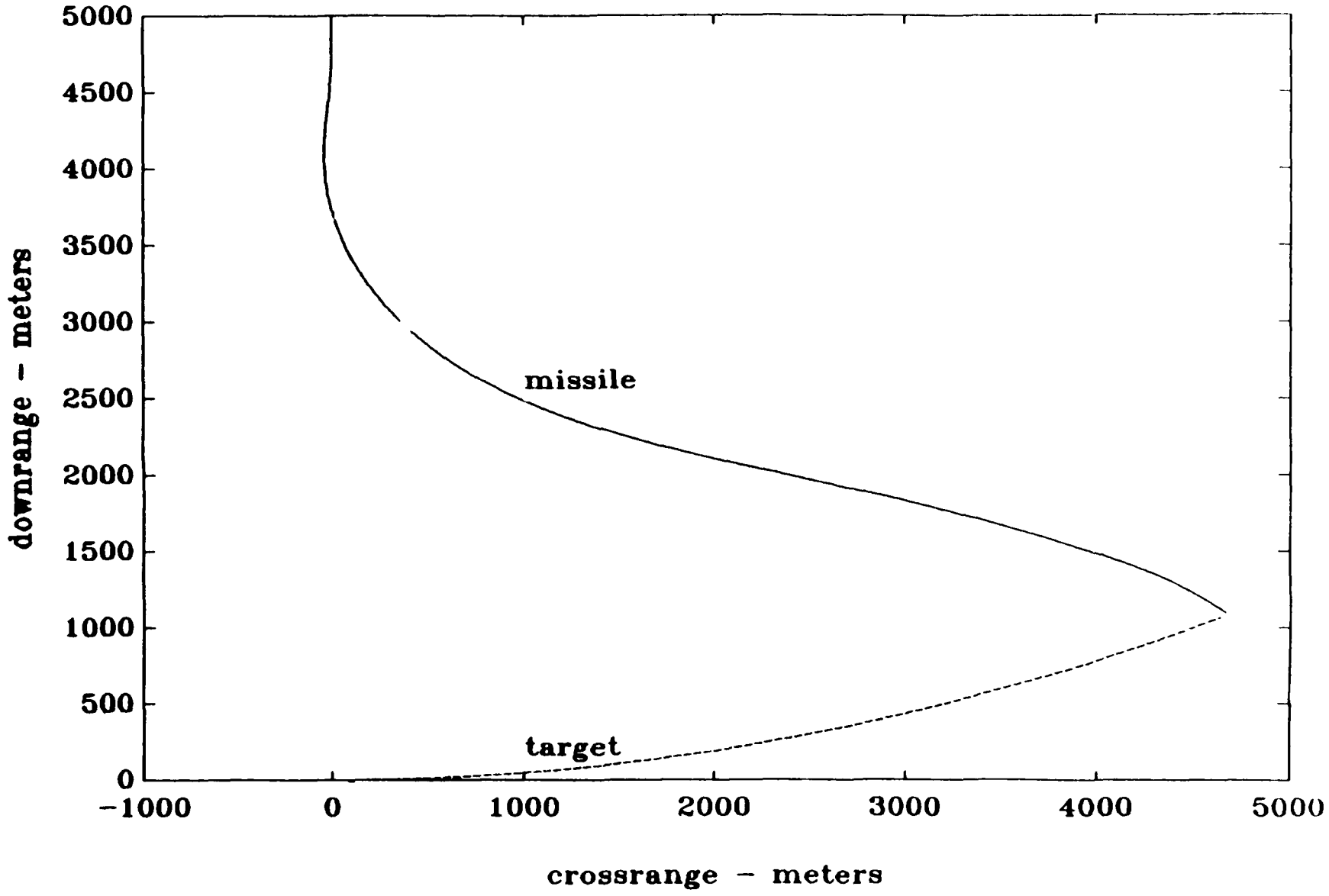

Figure 8.3. Scenario'12 Engagement

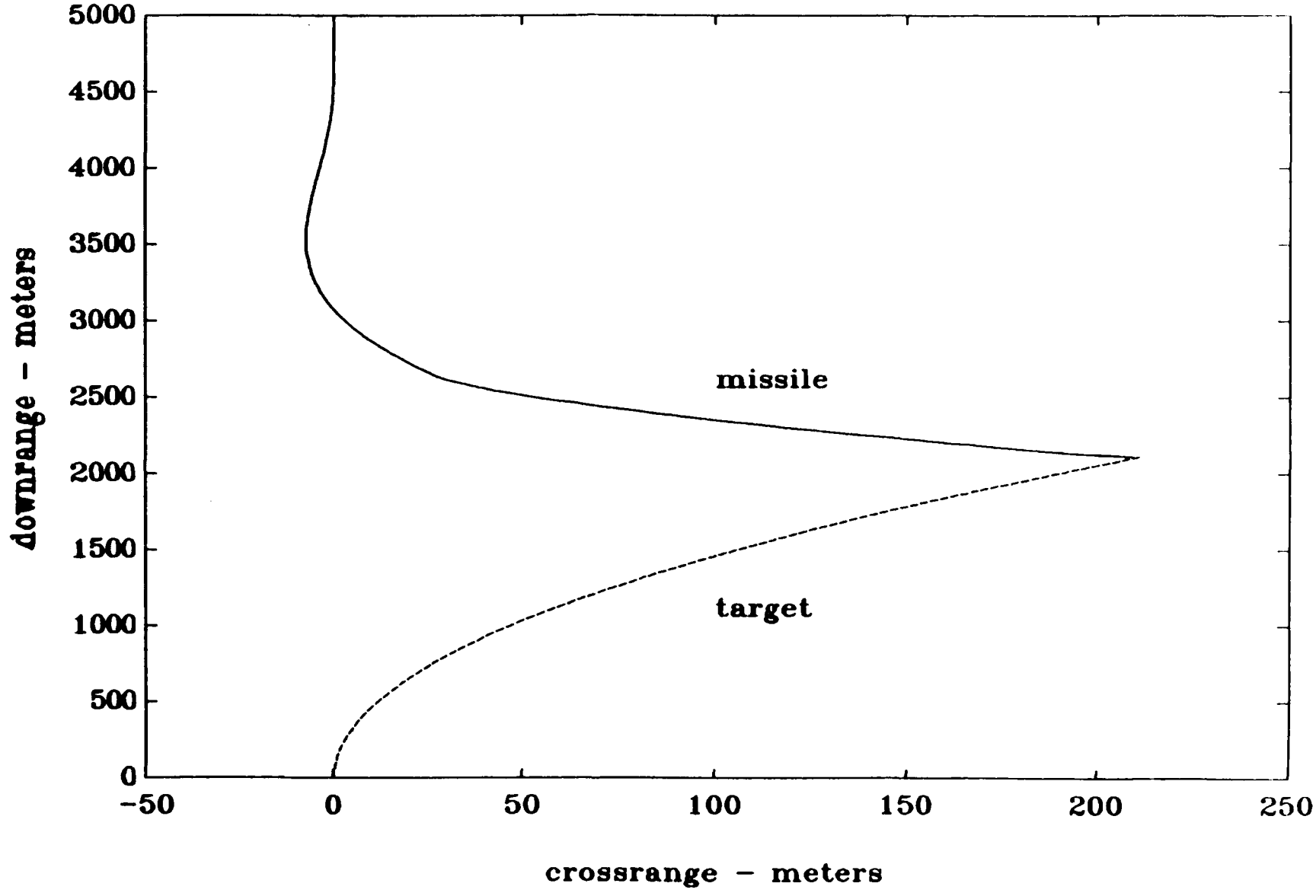

Figure 8.4. Scenario 16 Engagement

Table 8.3. H_2 Controller Miss Distances (m)

	Environment/System Condition						
Scenario	1	2	3	4	5	6	7
1	54	8	21	5	2	26	59
2	31	40	68	34	35	24	24
3	2	40	42	42	42	22	67
4	16	9	11	13	9	38	5
5	62	23	30	12	3	50	123
6	134	95	78	116	8	12	137
7	355	234	325	128	111	16	145
8	365	347	112	114	143	91	156
9	52	67	42	67	45	56	51
10	13	8	4	15	15	74	17
11	24	12	12	24	11	48	75
12	48	34	52	38	63	21	92
13	85	7	14	8	38	83	151
14	104	20	19	18	10	97	168
15	80	28	10	13	16	61	16
16	22	18	16	16	17	2	29
Mean	91	62	54	42	35	64	82

surprising trends. The first is that adding the parameter variations to the simulation (Conditions 2 and 3) had a very beneficial effect on miss distance as compared to the nominal case (Condition 1). Analysis of the time history and equations for the parameter variations reveals that this was

Table 8.4. H_∞ Controller Miss Distances (m)

	Environment/System Condition						
Scenario	1	2	3	4	5	6	7
1	95	32	37	20	26	81	63
2	90	4	7	13	25	14	11
3	75	32	21	37	34	14	36
4	1	19	27	21	21	13	21
5	86	54	43	154	60	19	108
6	183	132	92	131	97	1	221
7	394	315	335	283	320	80	320
8	62	8	119	176	83	122	23
9	30	48	45	61	63	53	68
10	59	4	4	7	1	5	50
11	63	30	19	40	41	110	110
12	82	75	65	63	42	98	109
13	132	90	80	49	64	63	181
14	320	70	61	63	77	49	320
15	255	38	36	23	26	19	116
16	65	11	7	8	12	18	18
Mean	125	65	63	66	62	48	111

caused by the fact that the missile begins its flight in a stable configuration when the parameter variations are present. The early trajectory for this condition exhibits less oscillatory behavior, and thus achieves the required heading correction earlier and with less oscillation than in

the nominal case. This favorable effect of parameter variations was not anticipated, and complicates evaluation of the robustness of the designs.

Another surprising trend evident in the tables is the tendency for miss distance to not be dramatically affected by noise inputs. Figures 8.5 and 8.6 display the time responses for the H_2 controller in Scenario 2, for both the nominal run and the run with noise added, respectively. The effect of the power plant noise is clearly evident in the plot, but miss distance remains virtually unchanged. This would seem to indicate that the controllers are more robust than is practically possible, i.e. the more disturbances and parameter variations that are added, the better the system performs. It is the author's opinion that the parameter variations resulting from the flight conditions specified and tested above happen to fall, by coincidence, in a region advantageous to missile performance. This was unfortunate in this case since the purpose of the study was to examine the detrimental effects of these parameter variations. A more statistically significant sample of parameter variations would have to be run in order to truly get some measure of system robustness to parameter variations and disturbances. Also, the time step size (0.02 seconds) was initially set based on the nominal runs, where it was maximized in order to decrease run time.

In retrospect, it is the author's opinion that this time step size does not allow the full effects of the noise inputs

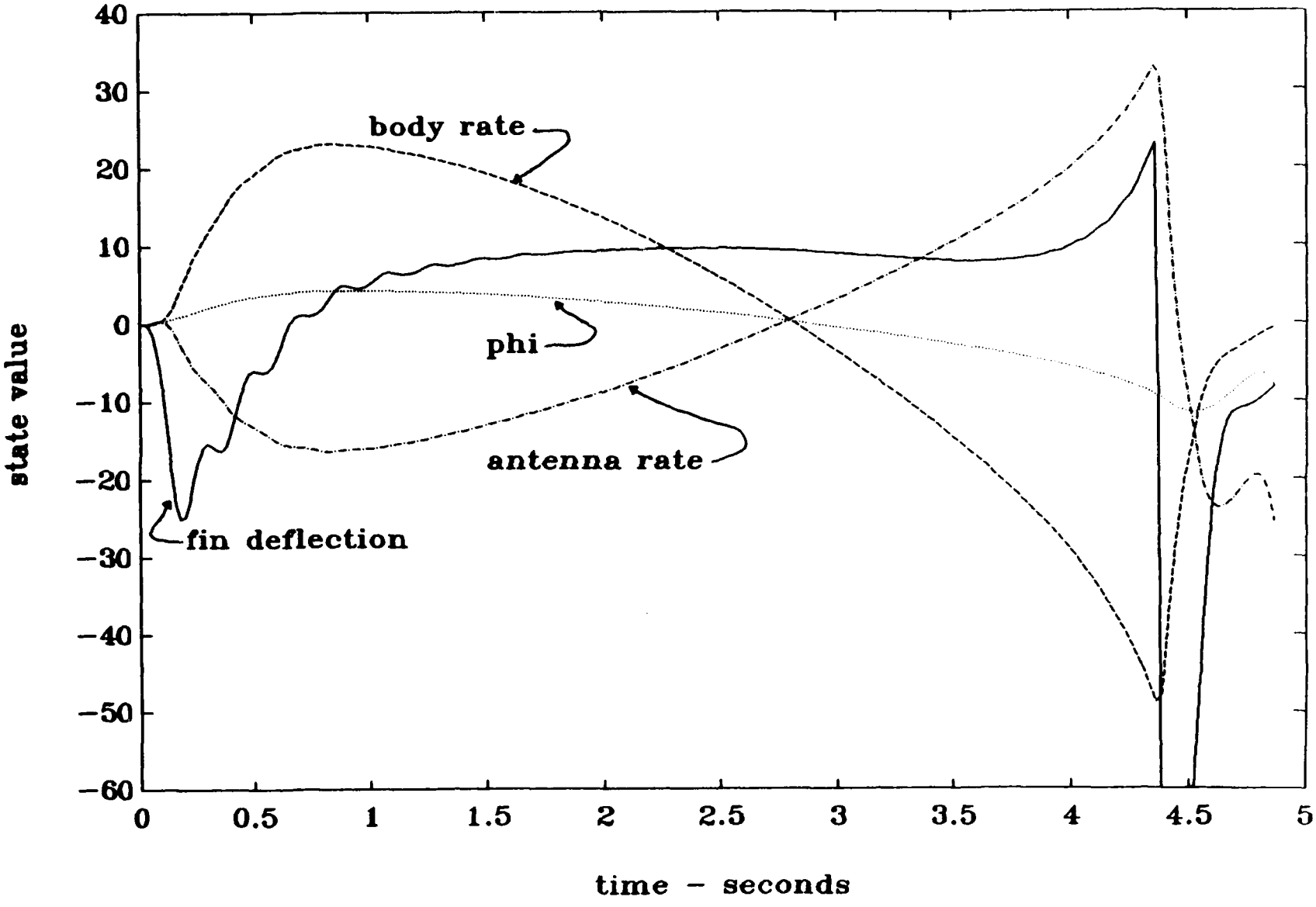

Figure 8.5. H_2 Controller System Response, Nominal Environment

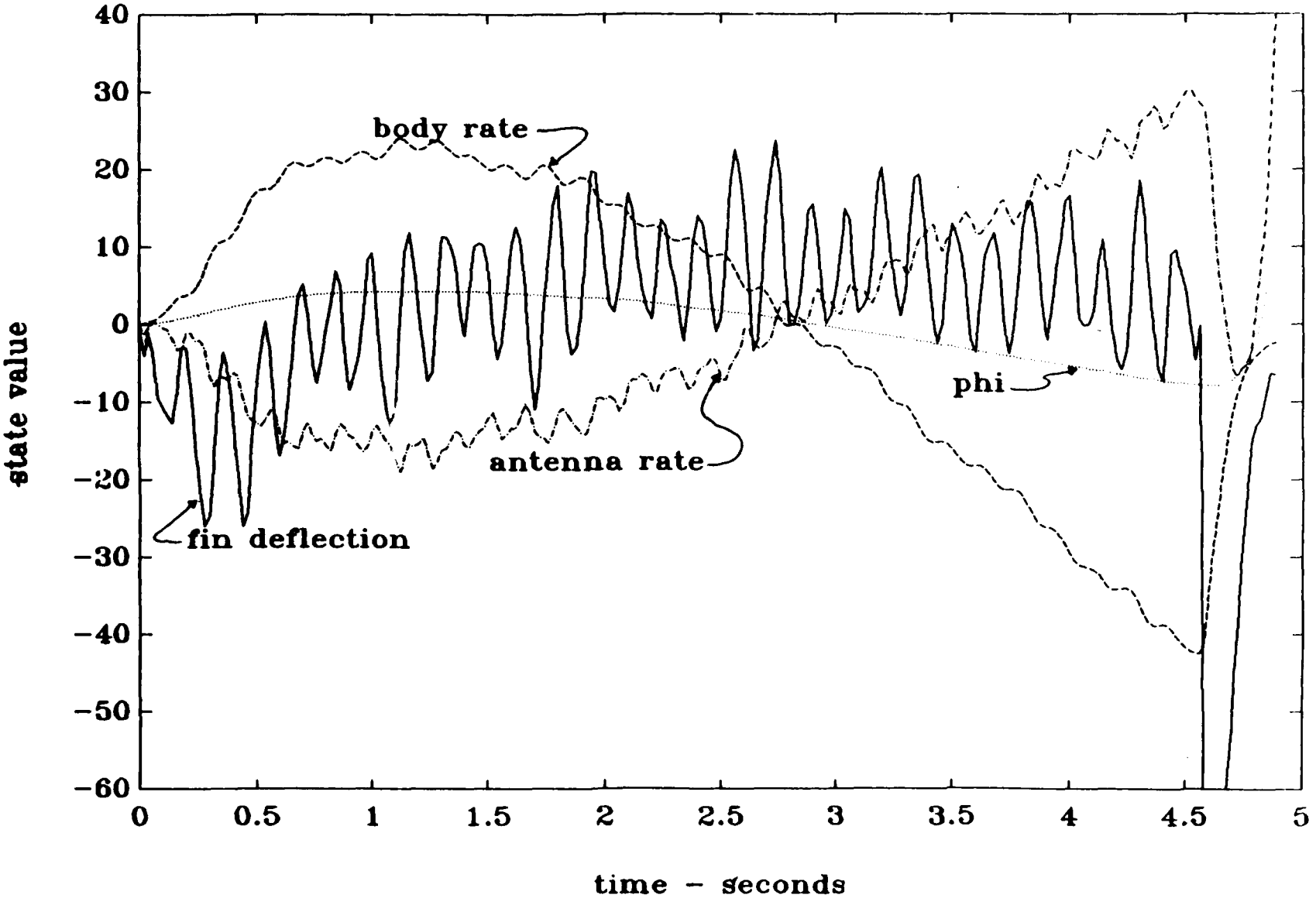

Figure 8.6. H_2 Controller System Response, Noisy Environment

to be felt, since the PC-MATLAB function c2d implements a zero-order hold over the time step.

Much the same can be said for the loss of target runs, in which it was hoped the H_∞ would prove to be robust to deterministic disturbances. Examination of the miss distance data does not reveal any significant advantages for the H_∞ controller. Examination of the state time histories, however, does reveal some encouraging trends. The H_∞ controller does indeed seem to be handling the disturbance better, as the transients are less pronounced. Figure 8.7 shows the state time histories for scenario 1 using the classical controller, and Figure 8.8 shows the state time histories for the same scenario using the H_∞ controller. Notice that both the body rate and the antenna rate display less severe transients for the system with the H_∞ controller.

While these results do not quite exemplify the advantages of designing controllers using the H_2 and H_∞ methodologies, sufficient data is available to reach some qualitative conclusions and point the way to future investigations. These will be discussed in Chapter IX.

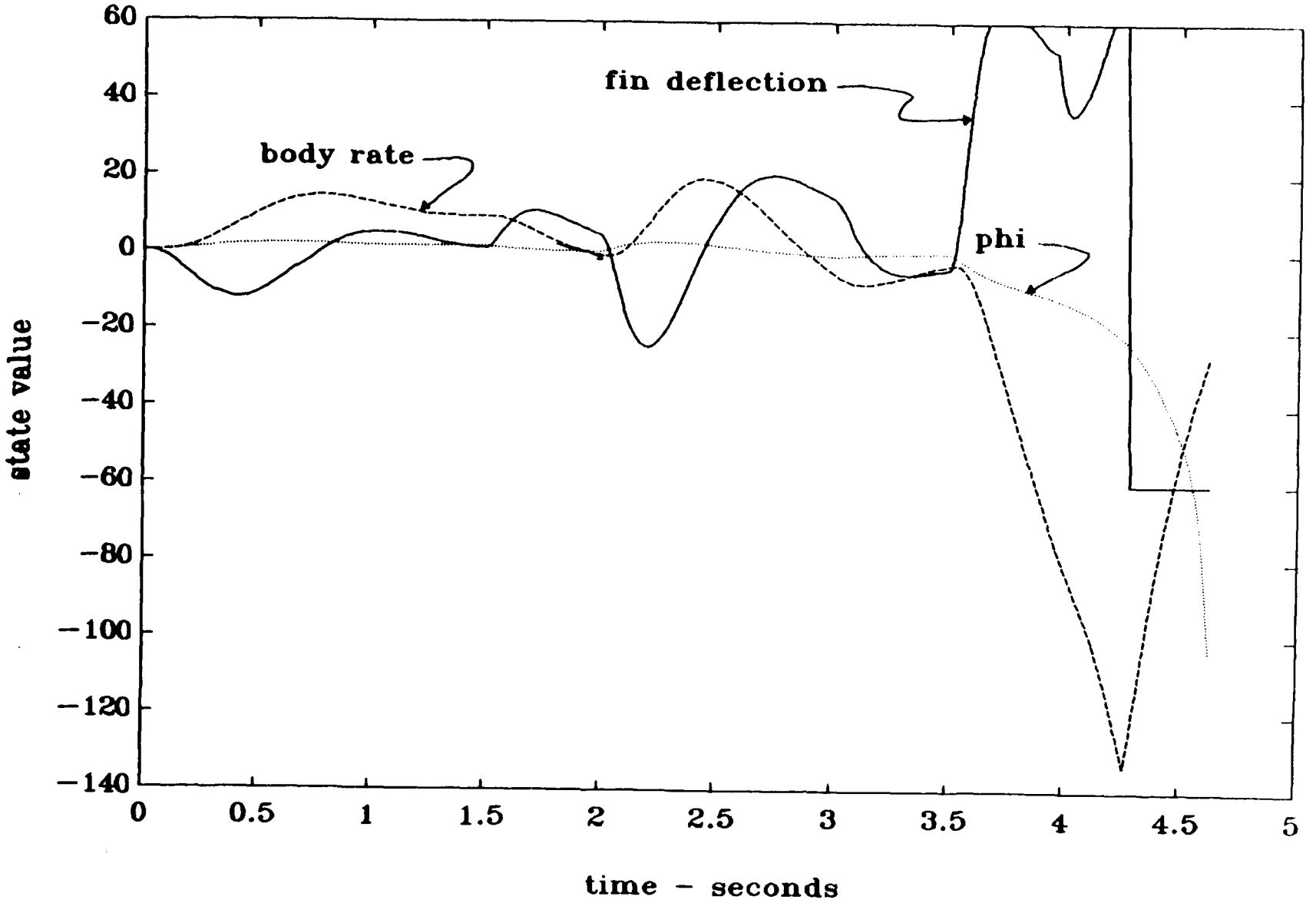

Figure 8.7. Classical Controller System Response, Loss of Target

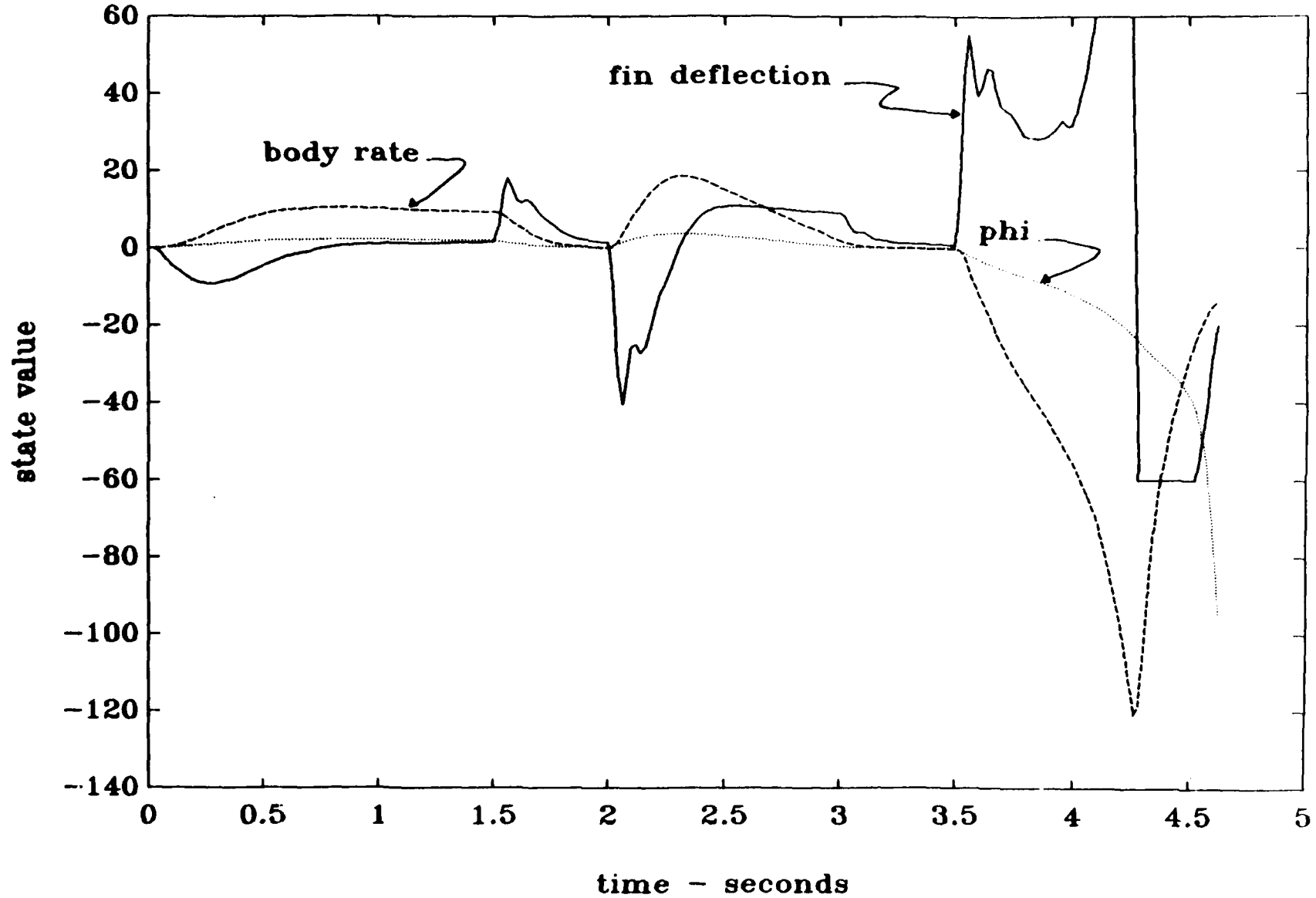

Figure 8.8. H_∞ Controller System Response, Loss of Target

IX. Results and Conclusions

The design study failed to reach the goal of providing quantitative data which exemplify the robustness of controllers designed using the H_2 and H_∞ design techniques. However, the data obtained and the design process itself allow several observations to be made. In addition, several lessons were learned which will be of use in any follow-on effort and which will be of interest to anyone working with these methodologies.

Robustness of H_2 and H_∞ Controllers

The H_2 optimal control theory does indeed produce controllers which can handle parameter variations well, and the H_∞ theory produces controllers which perform well also. Though the quantitative results obtained were inconclusive, the qualitative results described in Chapter VIII do display some encouraging trends. Neither the H_2 nor the H_∞ controller were found to have any shortcomings in the scenarios simulated. In fact, both performed quite well. This is indicative of a sound approach, and a more refined simulation and a broader spectrum of scenarios would probably yield more meaningful results. It is the author's opinion that the parameter variation results are realistic, but the simulation requires a shorter iteration time step to fully realize the effects of noise on the system. This refinement is suggested

as an area of further study.

Problem Complexity

The complexity in setting up the problem and executing the design effort for the H_2 and H_∞ designs creates a considerable work load for the designer, even on a problem as simple as this one. It is hoped that the methodology developed herein for executing this process will prove to be one of the most beneficial results of this study. In addition, the reader may benefit from some of the lessons learned during this design effort.

Lessons Learned

During execution of the H_∞ design process, a problem was encountered concerning the weighting of the disturbance inputs. This problem proved to be very difficult to isolate, and was finally traced to the use of bandpass filters to shape these inputs. The problem was finally isolated by repeating the entire H_2 design process, using the H_∞ design algorithm. By doing this, the author was able to isolate the problem as occurring when the bandpass filters were introduced. A bandpass filter with a one decade passband and two decade rolloffs at both the low- and high-frequency ends requires zeros which differ by five orders of magnitude. Apparently, this magnitude difference causes ill-conditioning of the state-space matrices, which results in a system which looks uncontrollable and unobservable to the computer algorithms

which solve the Riccati equations. Converting these filters to high-pass solved the problem. The designer is therefore cautioned to guard against this occurrence.

Another lesson was learned concerning 'overmodifying' the filters. In one instance, the author was able to get perfectly acceptable performance from the system by suppressing the gain on the body rate input command to a level of -60 dB at low frequency and placing a pole at 0.000001 rad/sec. This configuration was extremely fragile with respect to varying the other filter weights, however, as system performance degraded rapidly when other weights were modified to 'tune' the performance. The bottom line on this lesson is not to pursue modifications that look strange, even if they seem at first to yield good results.

Finally, a lesson was learned concerning converting the system to the form required for implementation of the existing theory. During the initial design effort, the original system was modified to meet the necessary conditions by using the boresight error as an input, rather than a state. This modification was required because only body rate, normal acceleration, antenna rate, and antenna position were being interpreted as commanded values, so missile heading had to be excluded from the state vector to preserve observability. This resulted in omission of the boresight error resolver dynamics, and exclusion of the natural loop closure provided by the resolver. The exclusion of this loop resulted quite

naturally in the stability problems caused by any loop closure, so that it was possible to obtain compensators which proved to be unstable when the complete system dynamics were simulated. This problem was overcome by introducing a fictitious boresight error command to the problem. By adding this fictitious command, the full system dynamics could be included, and the stability problem disappeared. Thus, the designer should always attempt to add components to the system representation rather than omit any of the system dynamics just to satisfy the conditions.

Areas of Further Study

There are many options available for carrying out further study of this design effort. The most promising of these is refinement of the simulation. It is suggested that the system simulation be converted to a Fortran routine, so that the limitations of PC-MATLAB be circumvented. Such a simulation could implement a much smaller time step, and thus bring out the full effects of noisy disturbance inputs. Also, such a simulation could be extended to five degrees of freedom, so that motion in both the pitch and yaw planes as well as the effects of gravity and drag could be fully effected.

Another area of further study related to the above is the simulation of a broader spectrum of flyout scenarios. The limited class of flyouts depicted herein could easily be extended to a more representative sample of possible target encounters. This task would also require conversion to a

faster Fortran format for the simulation, as each flyout in the PC-MATLAB subroutine takes in excess of 20 minutes, due to memory-crunching and array size requirements.

Another area of further study is high-frequency unmodelled dynamics. The H_∞ controller design methodology is thought to be robust to unmodelled dynamics, and an investigation of this would yield insight into the accuracy of this conjecture.

Lastly, there are some techniques which allow the designer to tailor the design to specific parameter variations expected. Use of these algorithms should improve robustness to parameter variations, as the resultant design should be less conservative.

Appendix A. Weighting Filters

The weighting filters derived for the optimal controller formulations are listed below. The filters are given in state-space form and as Bode magnitude plots.

State Space Representation

Using the nomenclature of Chapter VI, the weighting functions W_1, W_2, W_3, and $\tilde{W}_z$ can be expressed in state space form as follows, where the A, B, C, and D subscripts match the respective subcripts on W.

$$A_1 = \begin{bmatrix} -0.1 & 0 \\ 0 & -0.01 \end{bmatrix} \qquad \text{(A.1)}$$

$$B_1 = \begin{bmatrix} 0.1 & 0 & 0 & 0 & 0 \\ 0 & 0 & 0 & 0 & 0.01 \end{bmatrix} \qquad \text{(A.2)}$$

$$C_1 = \begin{bmatrix} 10 & 0 \\ 0 & 0 \\ 0 & 0 \\ 0 & 0 \\ 0 & 800 \end{bmatrix} \qquad \text{(A.3)}$$

$$D_1 = \begin{bmatrix} 0 & 0 & 0 & 0 & 0 \\ 0 & 1 & 0 & 0 & 0 \\ 0 & 0 & 1 & 0 & 0 \\ 0 & 0 & 0 & 1 & 0 \\ 0 & 0 & 0 & 0 & 0 \end{bmatrix} \qquad \text{(A.4)}$$

$$A_2 = \begin{bmatrix} -10 & 0 & 0 & 0 \\ 0 & -40 & 0 & 0 \\ 0 & 0 & -10 & 0 \\ 0 & 0 & 0 & -20 \end{bmatrix} \quad \text{(A.5)}$$

$$B_2 = \begin{bmatrix} -9.9 & 0 & 0 & 0 \\ 0 & -39.6 & 0 & 0 \\ 0 & 0 & -9.9 & 0 \\ 0 & 0 & 0 & -19.8 \end{bmatrix} \quad \text{(A.6)}$$

$$C_2 = \begin{bmatrix} 1 & 0 & 0 & 0 \\ 0 & 1 & 0 & 0 \\ 0 & 0 & 0 & 0 \\ 0 & 0 & 1 & 0 \\ 0 & 0 & 0 & 1 \end{bmatrix} \quad \text{(A.7)}$$

$$D_2 = \begin{bmatrix} 1 & 0 & 0 & 0 \\ 0 & 1 & 0 & 0 \\ 0 & 0 & 0 & 0 \\ 0 & 0 & 1 & 0 \\ 0 & 0 & 0 & 1 \end{bmatrix} \quad \text{(A.8)}$$

$$A_3 = \begin{bmatrix} -5 & 0 & 0 & 0 \\ 0 & -1 & 0 & 0 \\ 0 & 0 & -50 & 0 \\ 0 & 0 & 0 & -200 \end{bmatrix} \quad \text{(A.9)}$$

$$B_3 = \begin{bmatrix} 5 & 0 & 0 & 0 \\ 0 & -0.99 & 0 & 0 \\ 0 & 0 & -49.5 & 0 \\ 0 & 0 & 0 & -198 \end{bmatrix} \quad \text{(A.10)}$$

$$C_3 = \begin{bmatrix} 1 & 0 & 0 & 0 \\ 0 & 1 & 0 & 0 \\ 0 & 0 & 1 & 0 \\ 0 & 0 & 0 & 1 \end{bmatrix} \qquad \text{(A.11)}$$

$$D_3 = \begin{bmatrix} 0.01 & 0 & 0 & 0 \\ 0 & 1 & 0 & 0 \\ 0 & 0 & 1 & 0 \\ 0 & 0 & 0 & 1 \end{bmatrix} \qquad \text{(A.12)}$$

$$A_z = \begin{bmatrix} -1 & 0 & 0 & 0 & 0 & 0 & 0 \\ 0 & 0 & 1 & 0 & 0 & 0 & 0 \\ 0 & -3000 & -130 & 0 & 0 & 0 & 0 \\ 0 & 0 & 0 & -0.01 & 0 & 0 & 0 \\ 0 & 0 & 0 & 0 & 0 & 1 & 0 \\ 0 & 0 & 0 & 0 & -2000 & -210 & 0 \\ 0 & 0 & 0 & 0 & 0 & 0 & -40 \end{bmatrix} \qquad \text{(A.13)}$$

$$B_z = \begin{bmatrix} 1 & 0 & 0 & 0 & 0 \\ 0 & 0 & 0 & 0 & 0 \\ 0 & -100 & 0 & 0 & 0 \\ 0 & 0 & 0.01 & 0 & 0 \\ 0 & 0 & 0 & 0 & 0 \\ 0 & 0 & 0 & -300 & 0 \\ 0 & 0 & 0 & 0 & 40 \end{bmatrix} \qquad \text{(A.14)}$$

$$C_z = \begin{bmatrix} 1 & 0 & 0 & 0 & 0 & 0 & 0 \\ 0 & 0.001 & 1 & 0 & 0 & 0 & 0 \\ 0 & 0 & 0 & 1 & 0 & 0 & 0 \\ 0 & 0 & 0 & 0 & 0.1 & 1 & 0 \\ 0 & 0 & 0 & 0 & 0 & 0 & 1 \end{bmatrix} \qquad \text{(A.15)}$$

$$D_z = \begin{bmatrix} 0 & 0 & 0 & 0 & 0 \\ 0 & 0 & 0 & 0 & 0 \\ 0 & 0 & 0 & 0 & 0 \\ 0 & 0 & 0 & 0 & 0 \\ 0 & 0 & 0 & 0 & 0 \end{bmatrix} \qquad \text{(A.16)}$$

Bode Magnitude Plots

To provide the reader with a graphical interpretation of the above filter representations, Figures A.1 and A.2 show the Bode magnitude plots for the filtering of inputs 1 and 5 ($\dot{\theta}_{m_{com}}$ and $\theta_{s_{com}}$) in W_1 (signals 2 thru 4 are equally weighted across the entire spectrum, so no graphical representation is deemed necessary). Similarly, Figures A.3-A.6 provide the Bode magnitude plots for filter W_2; Figures A.7-A.10 Bode magnitude plots for filter W_3; and A.11-A.15 Bode magnitude plots for $\tilde{W}_z$. Each of these plots is titled in reference to the respective input, disturbance, or error filtered.

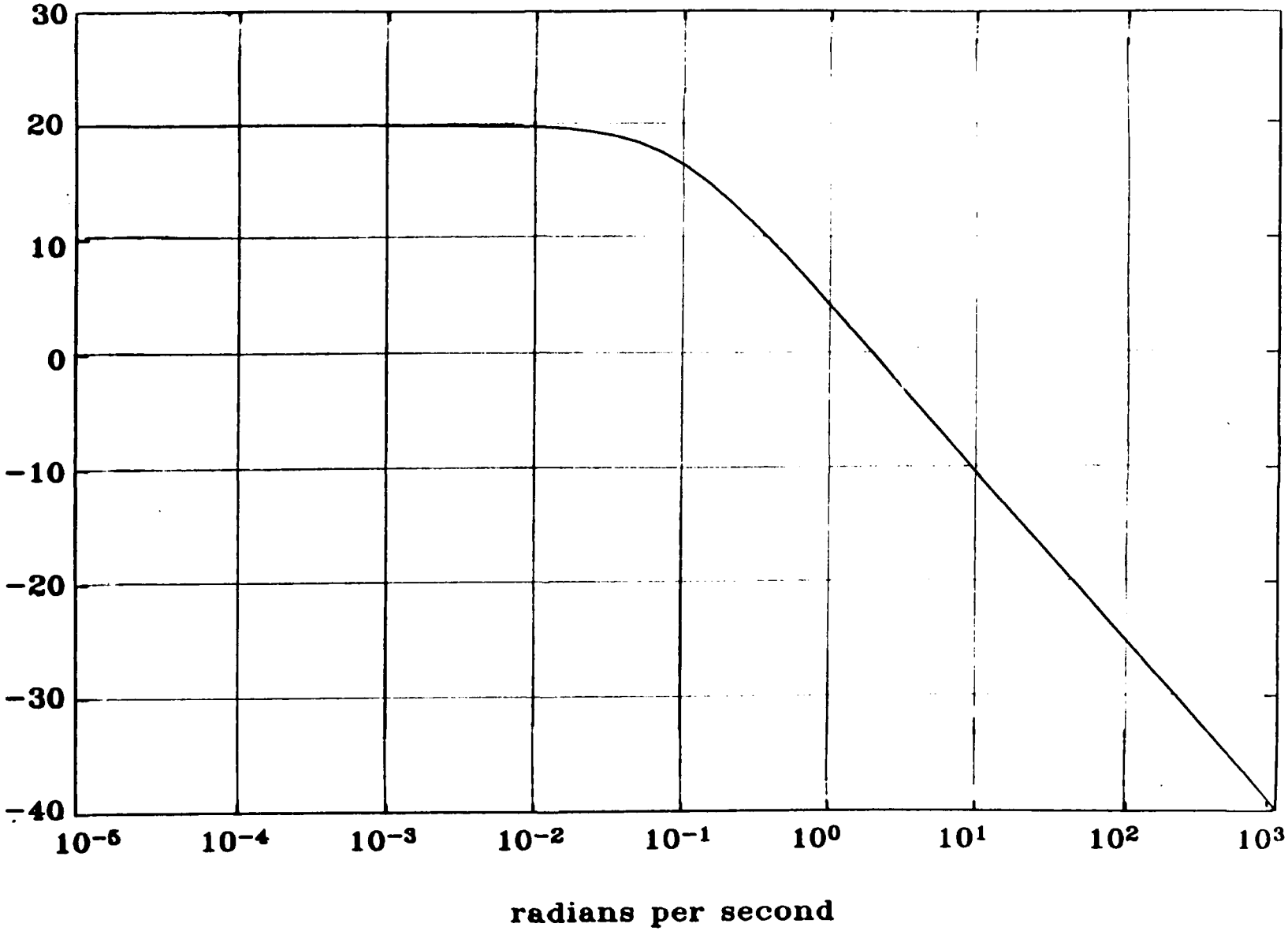

Figure A.1. Body Rate Command Input Filter

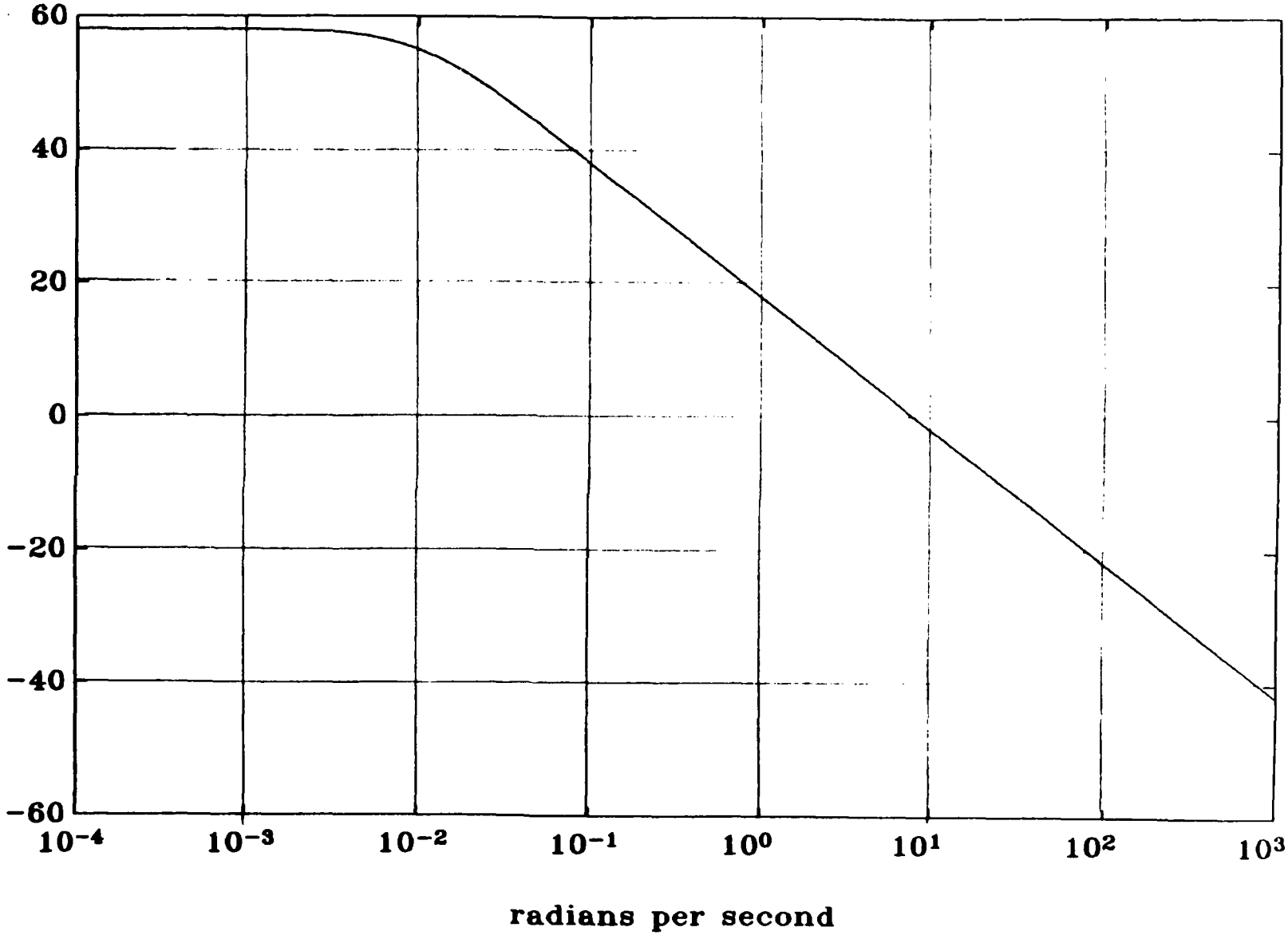

Figure A.2. Tracker Rate Command Input Filter

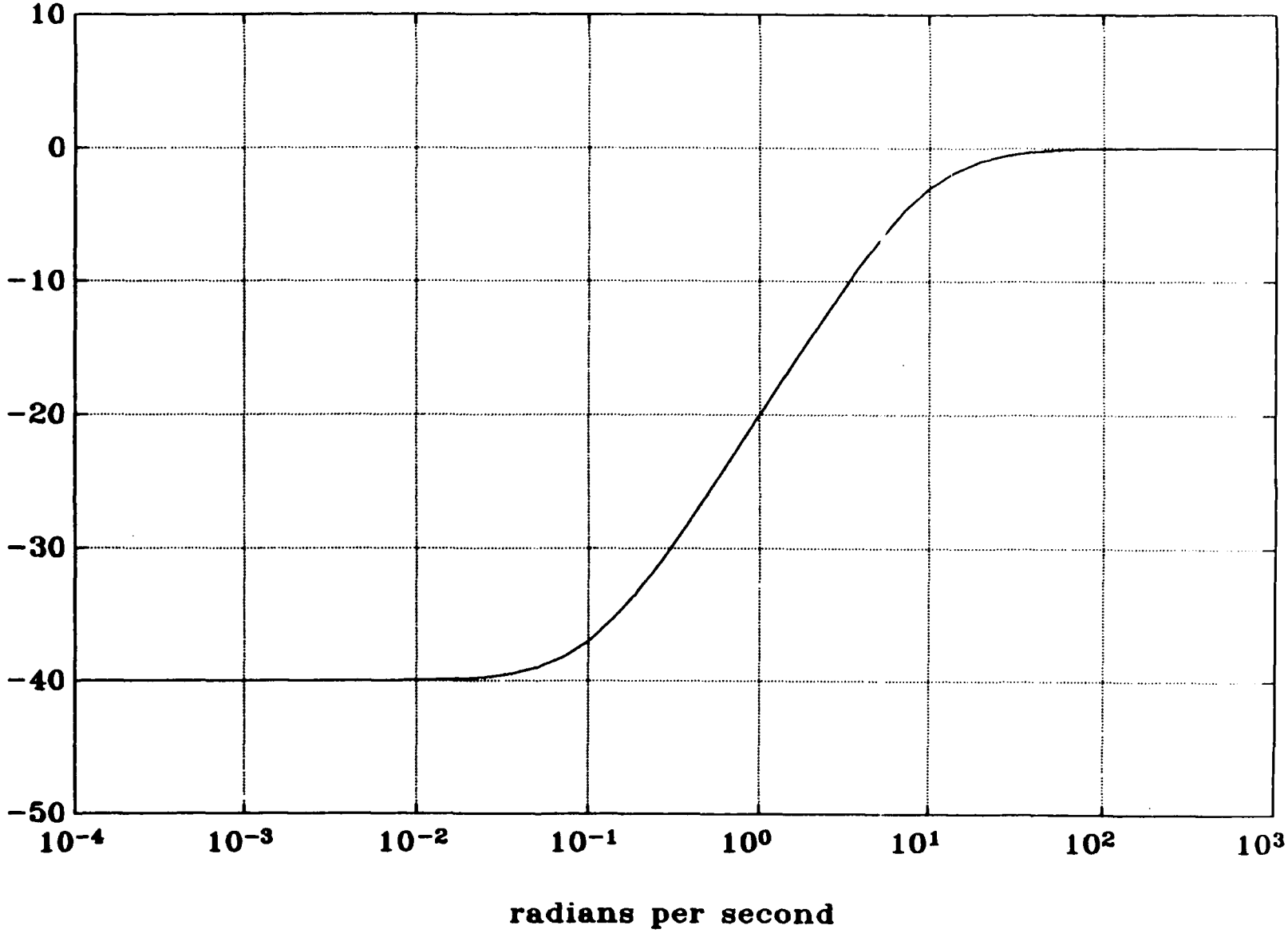

Figure A.3. Accelerometer Noise Input Filter

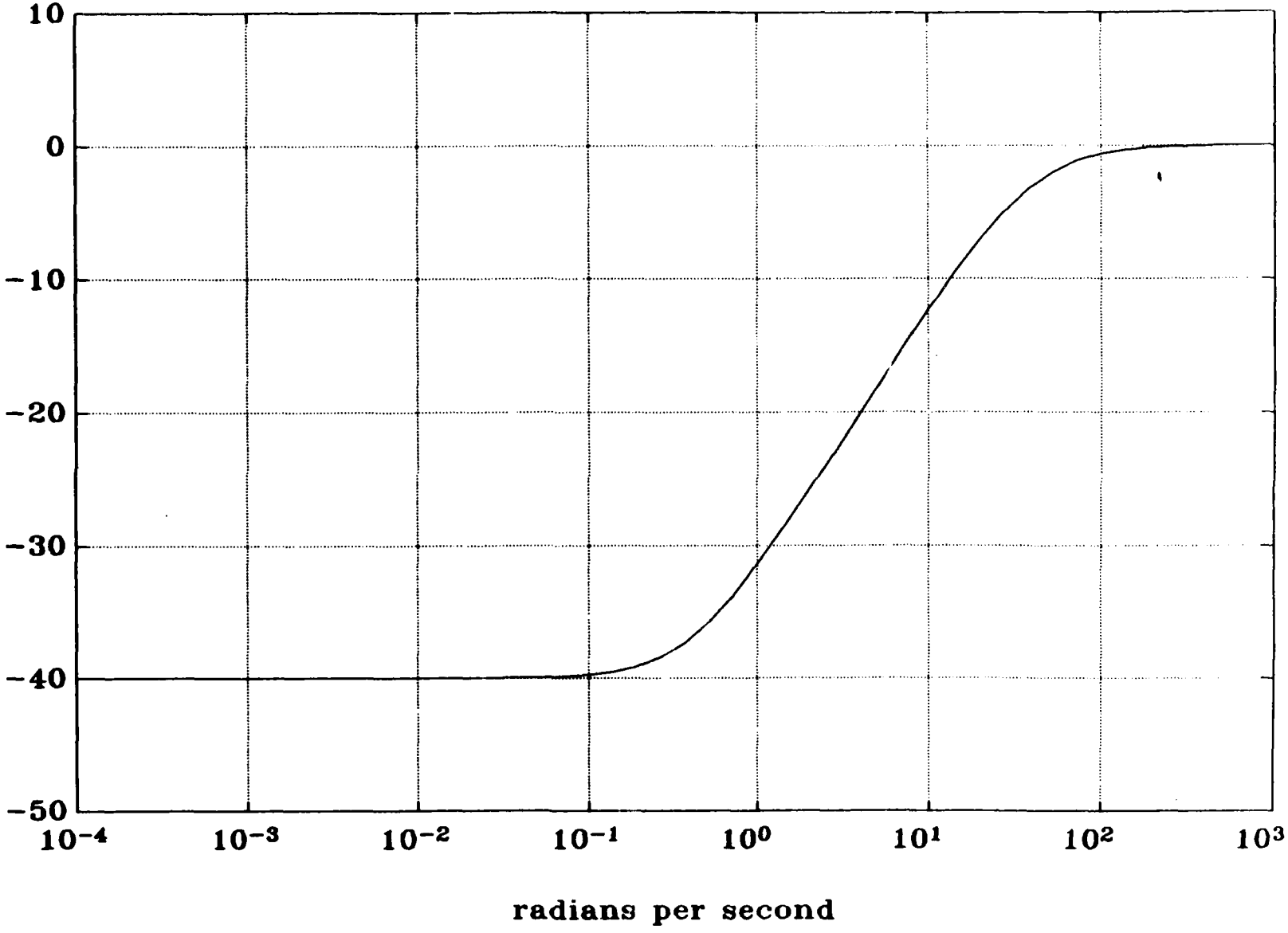

Figure A.4. Body Rate Gyro Noise Input Filter

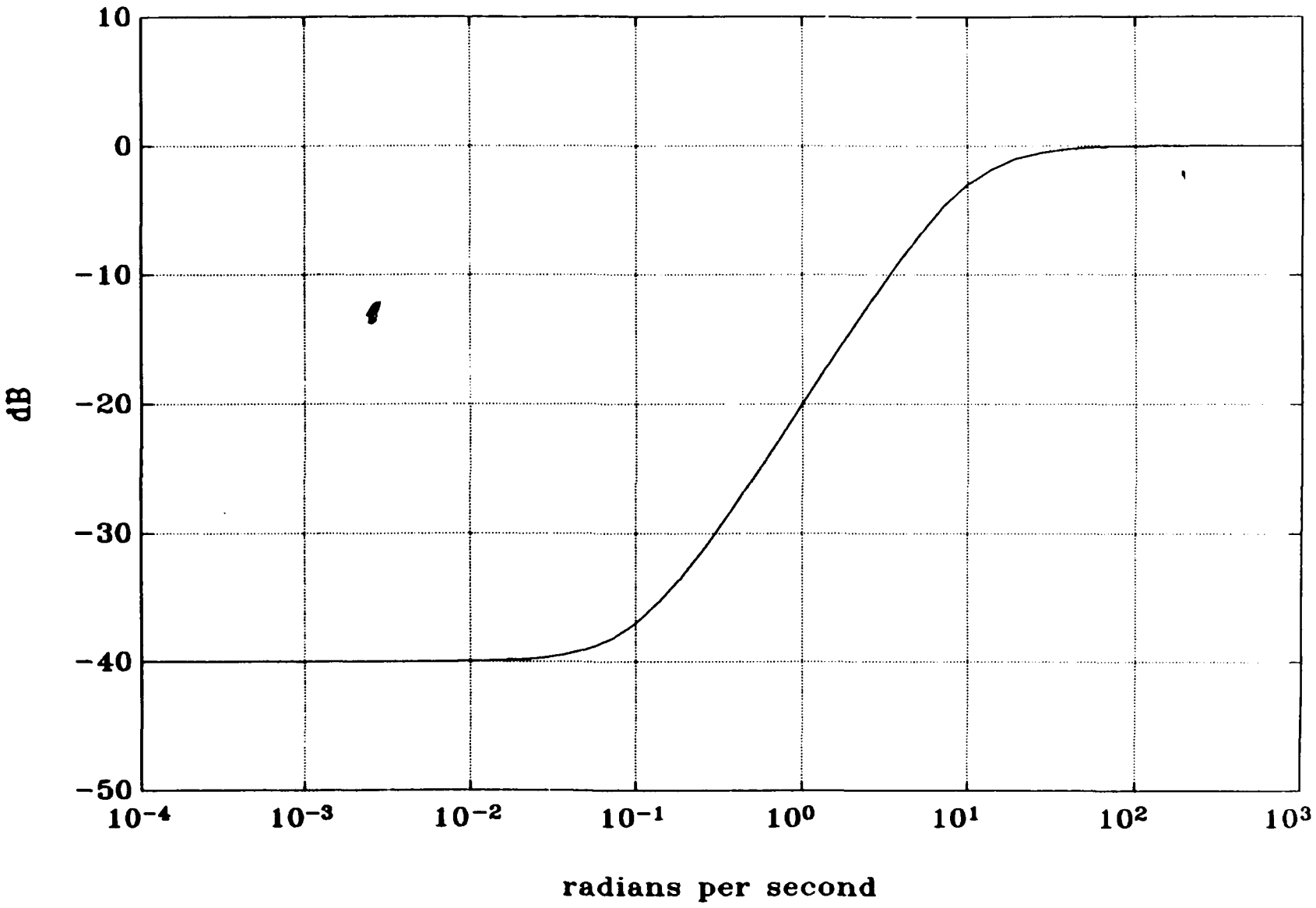

Figure A.5. Antenna Rate Gyro Noise Input Filter

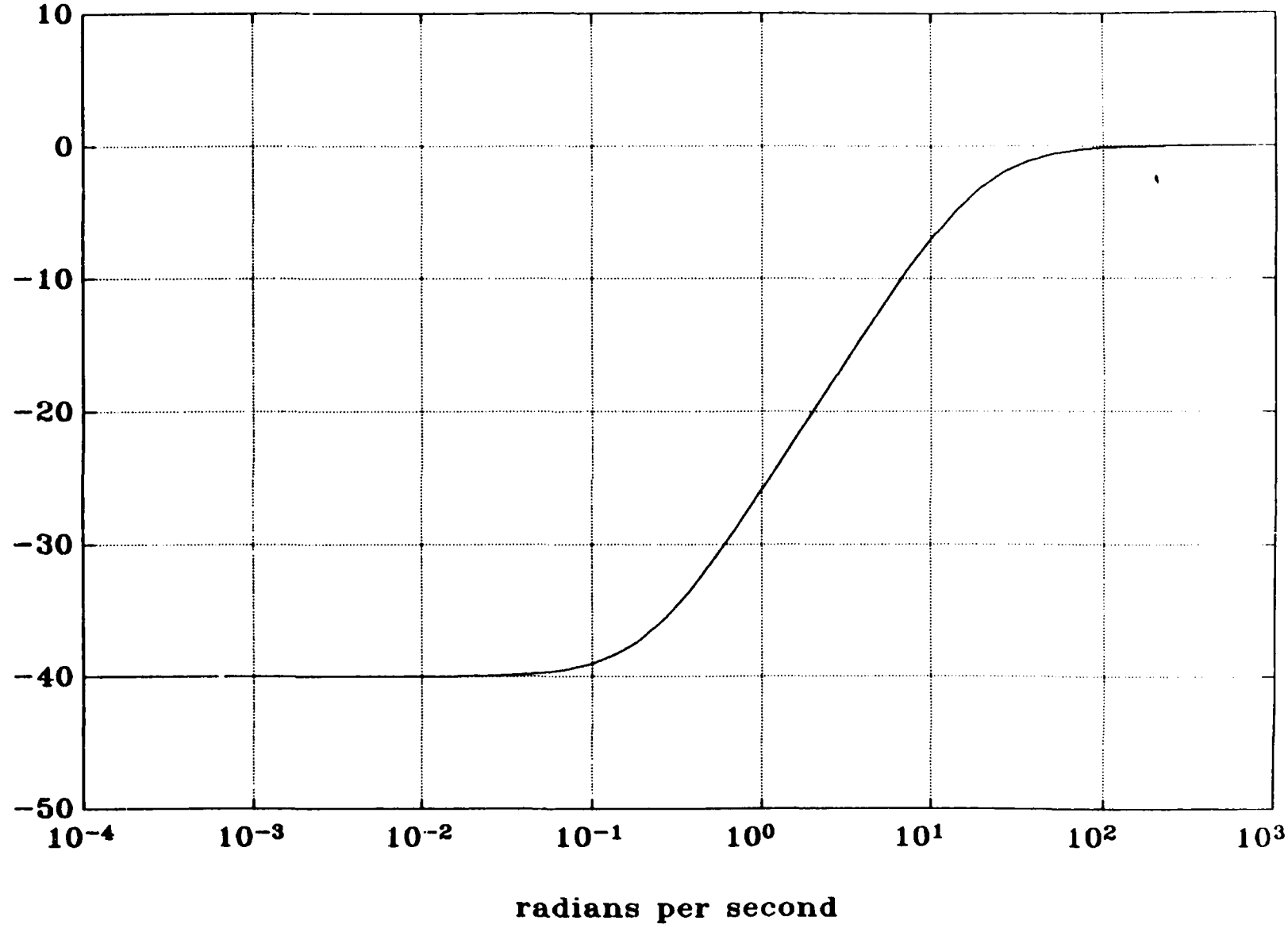

Figure A.6. Antenna Position Potentiometer Input Filter

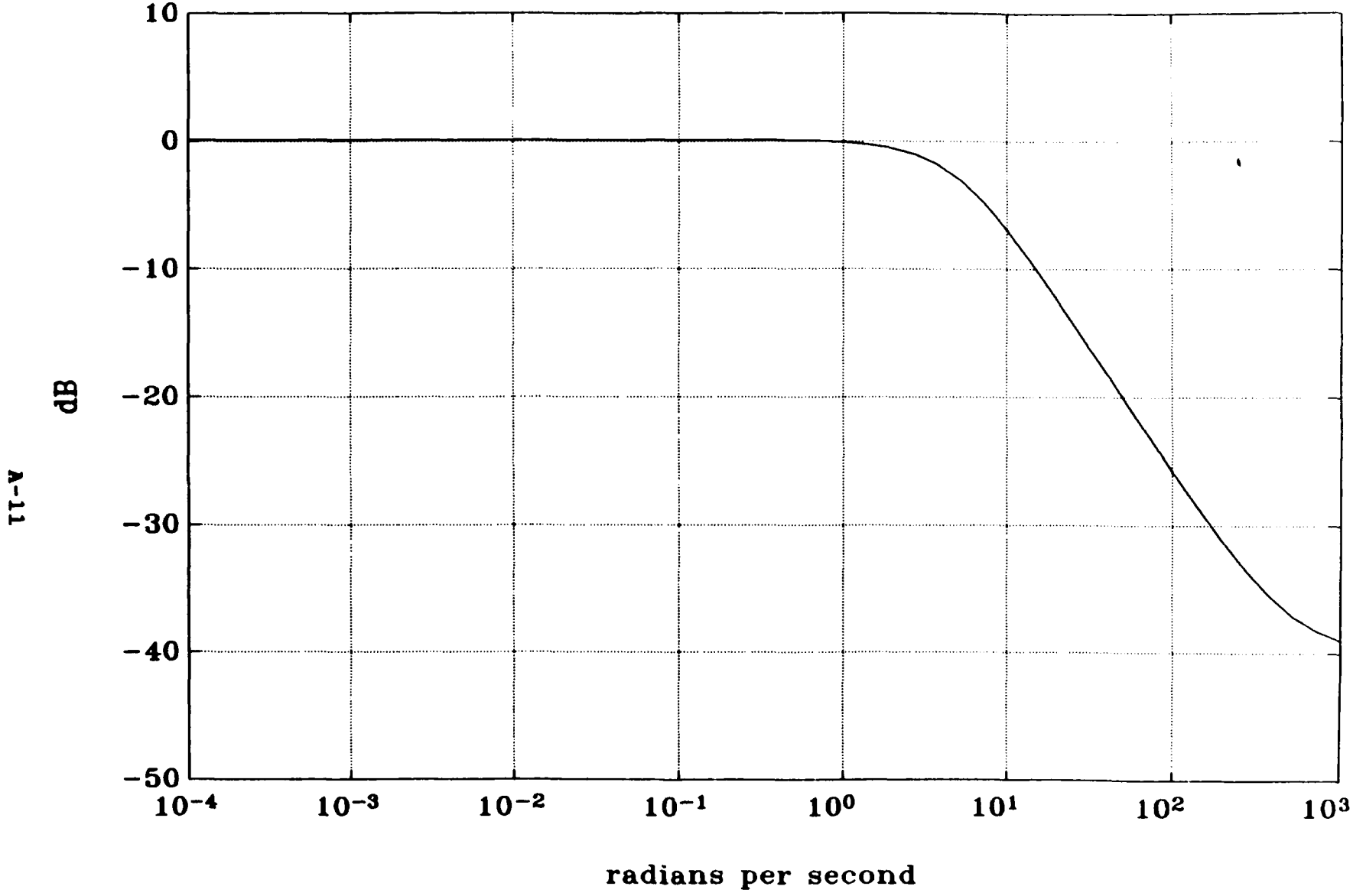

Figure A.7. Target Position Input Filter

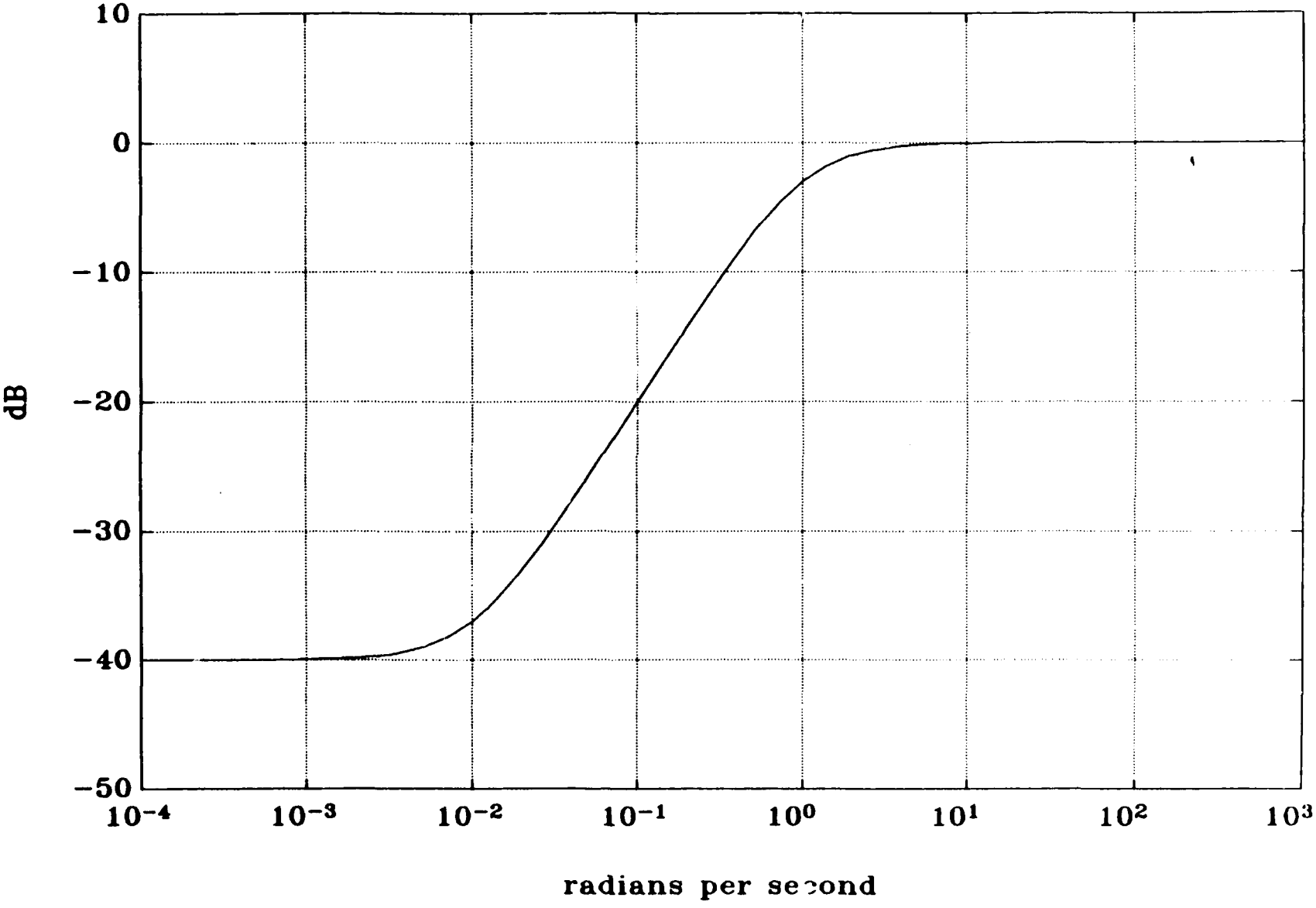

Figure A.8. Turbulence Input Filter

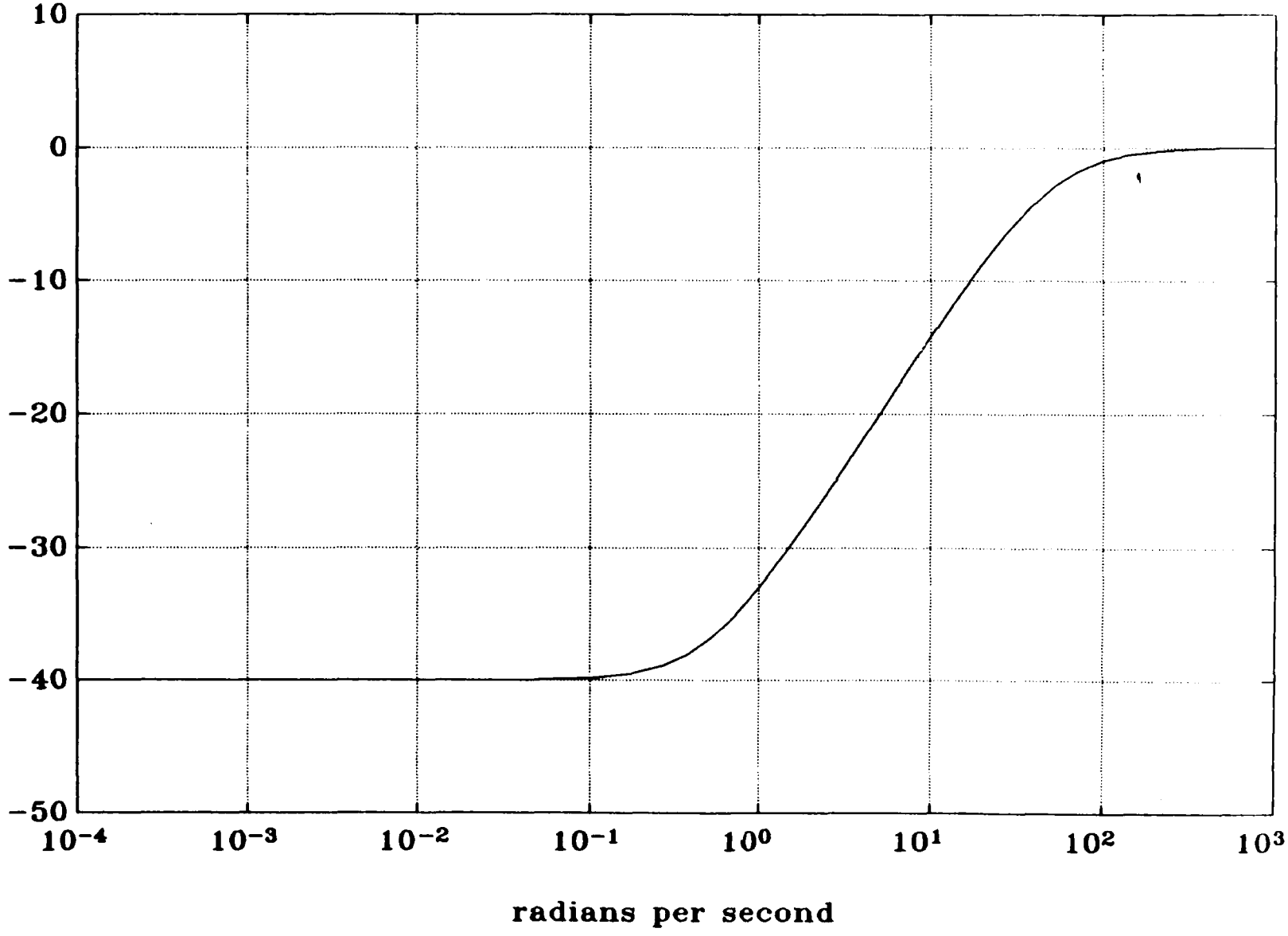

Figure A.9. Glint Input Filter

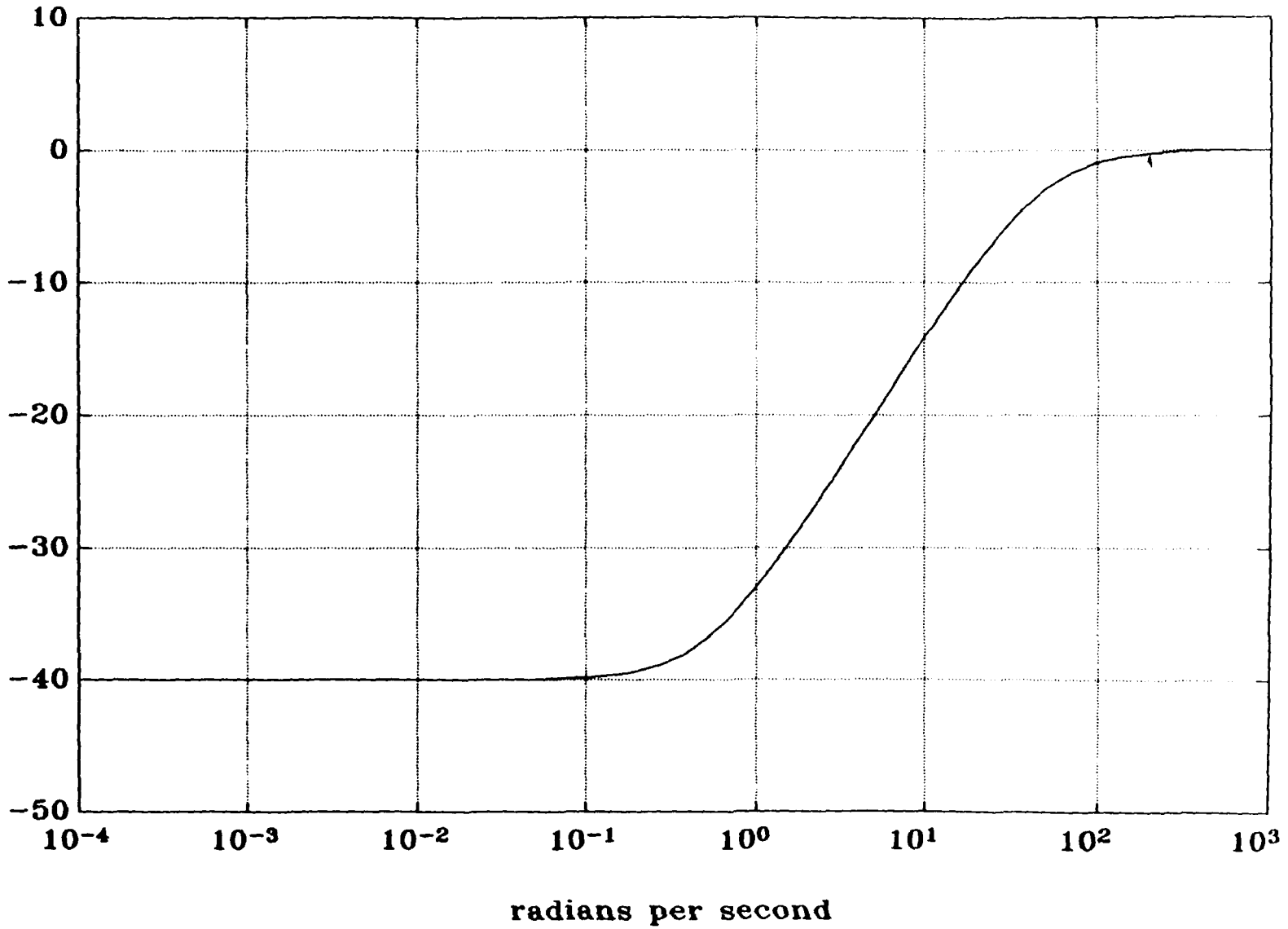

Figure A.10. Power Supply Noise Input Filter

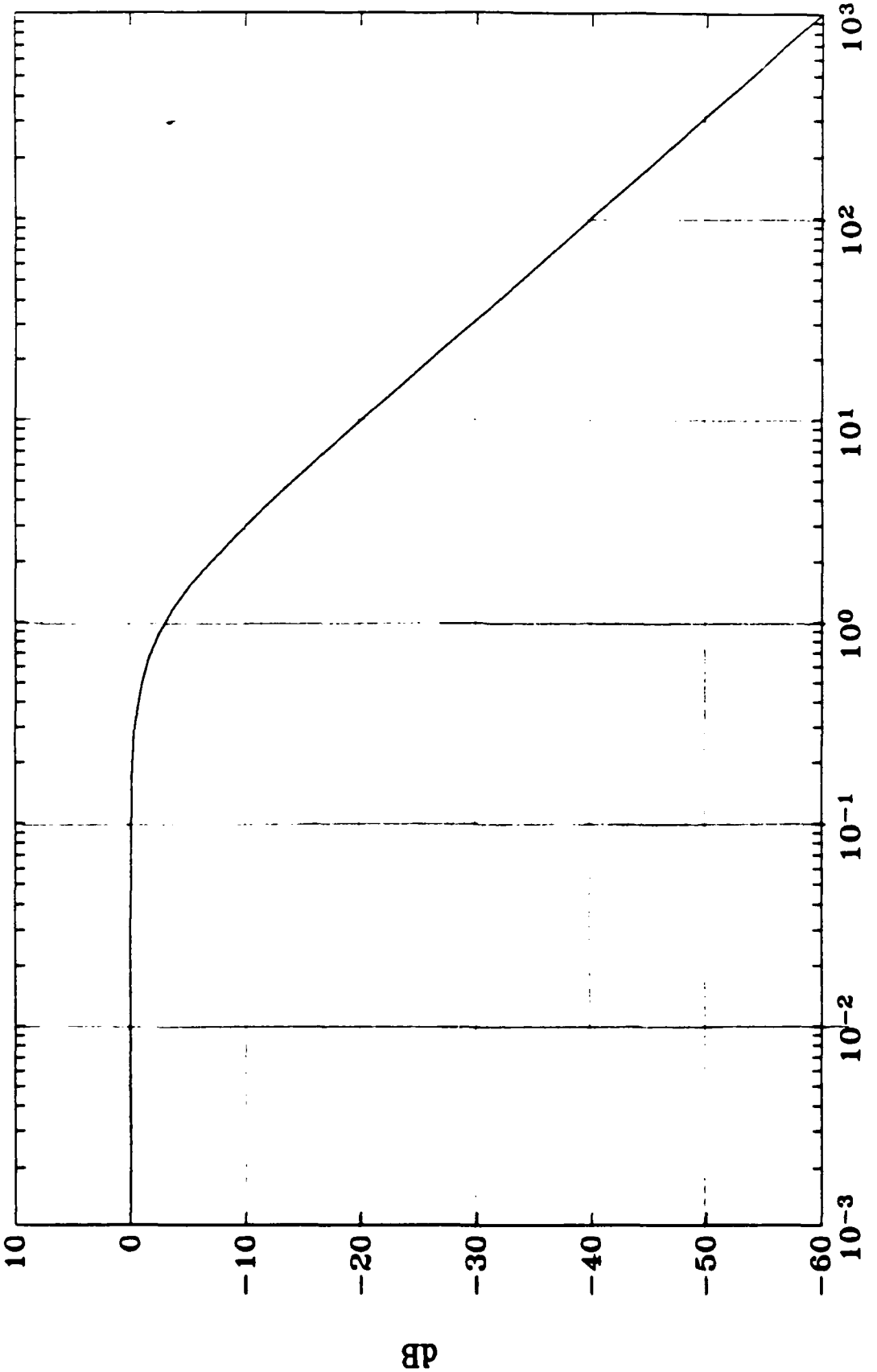

Figure A.11. Body Rate Error Filter

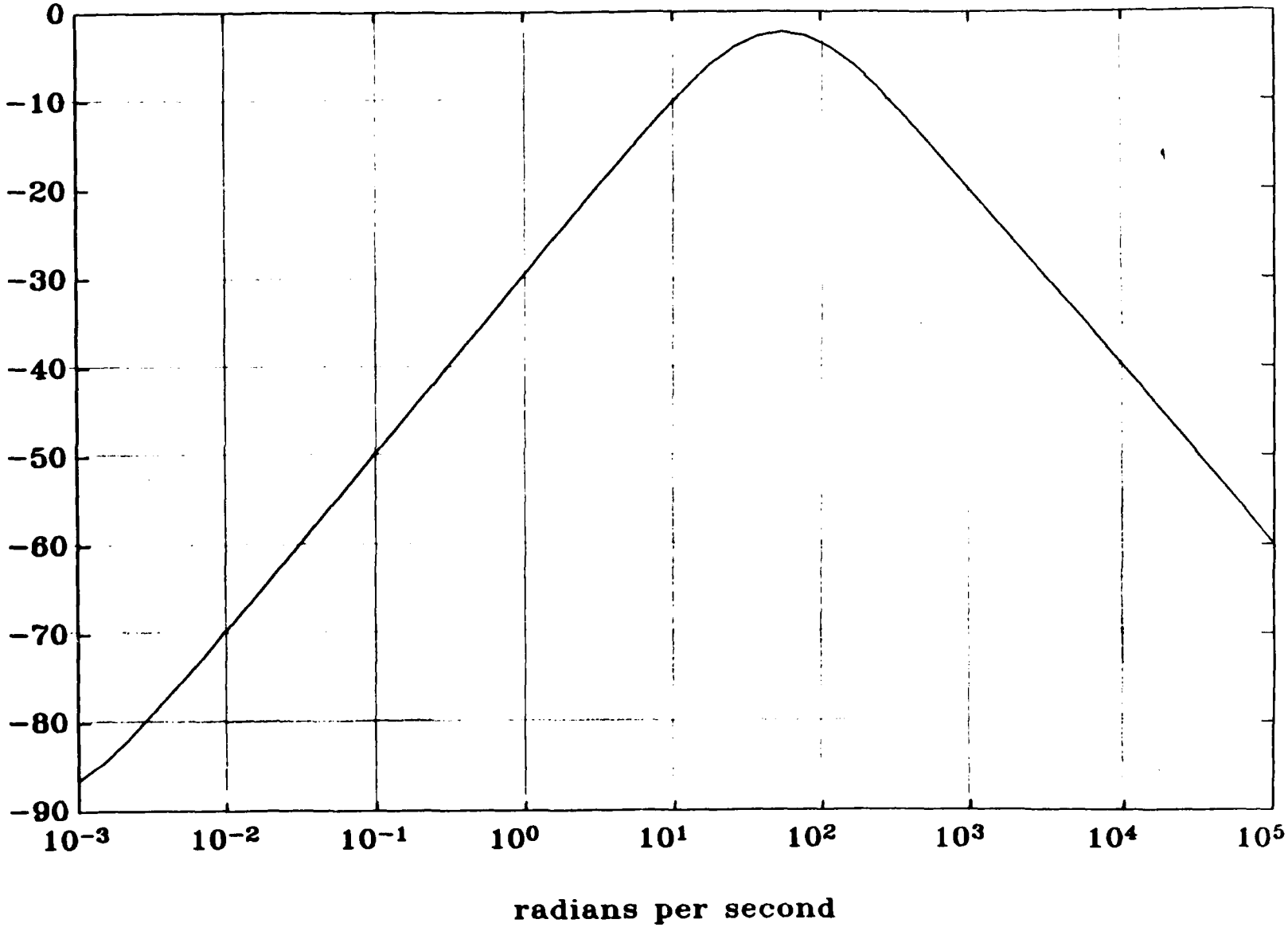

Figure A.12. Normal Acceleration Error Filter

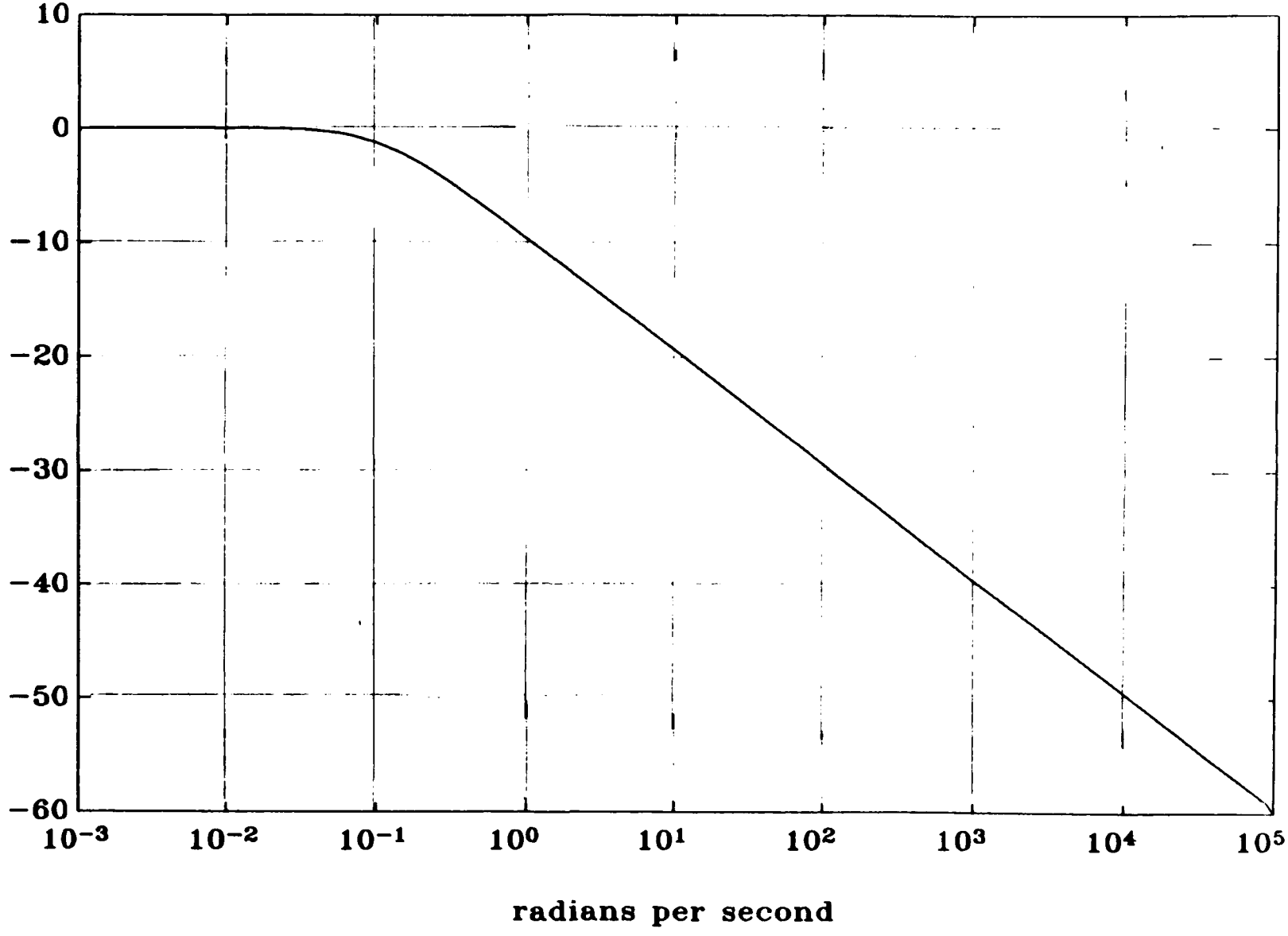

Figure A.13. Phi Error Filter

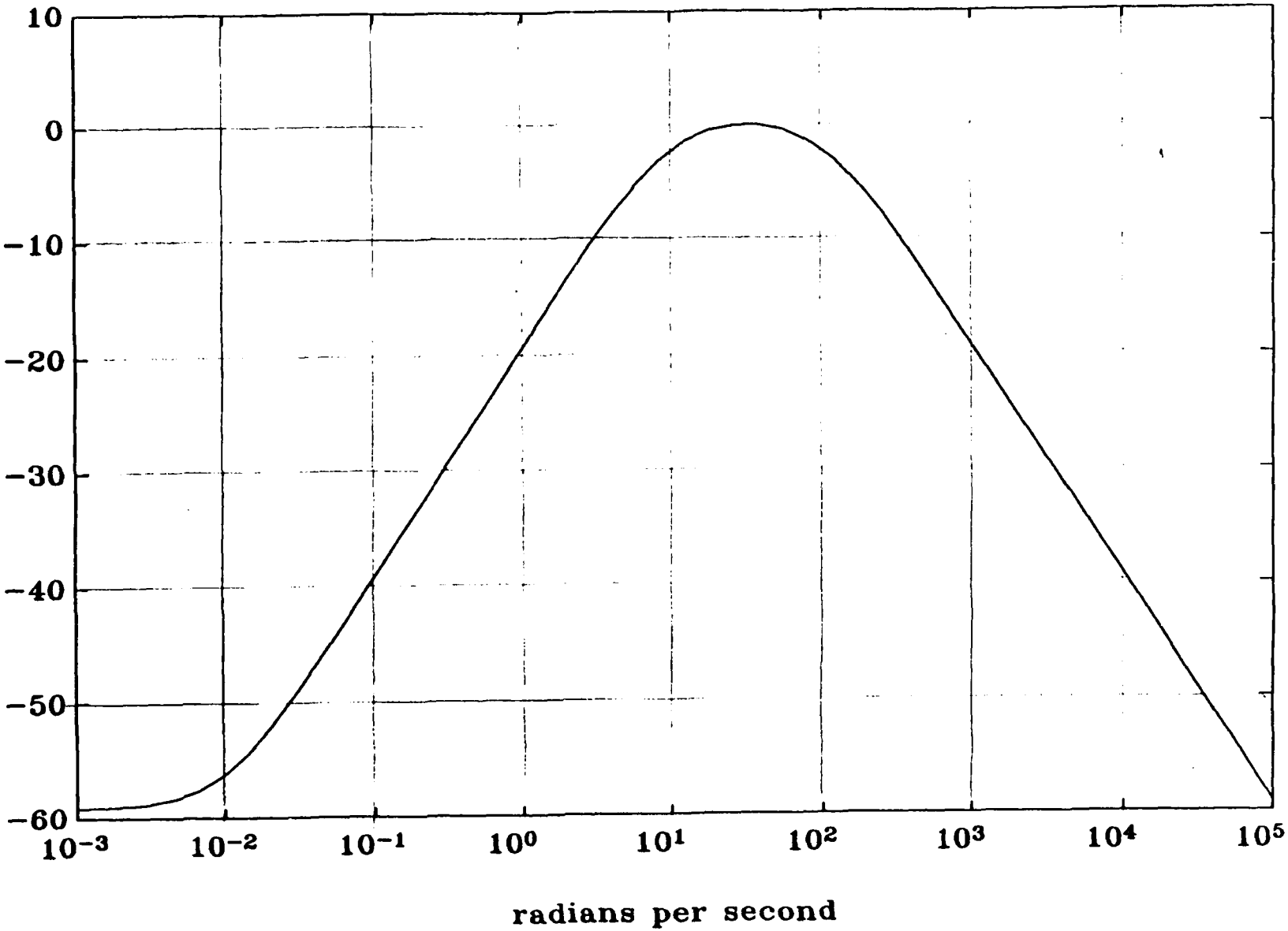

Figure A.14. Antenna Rate Error Filter

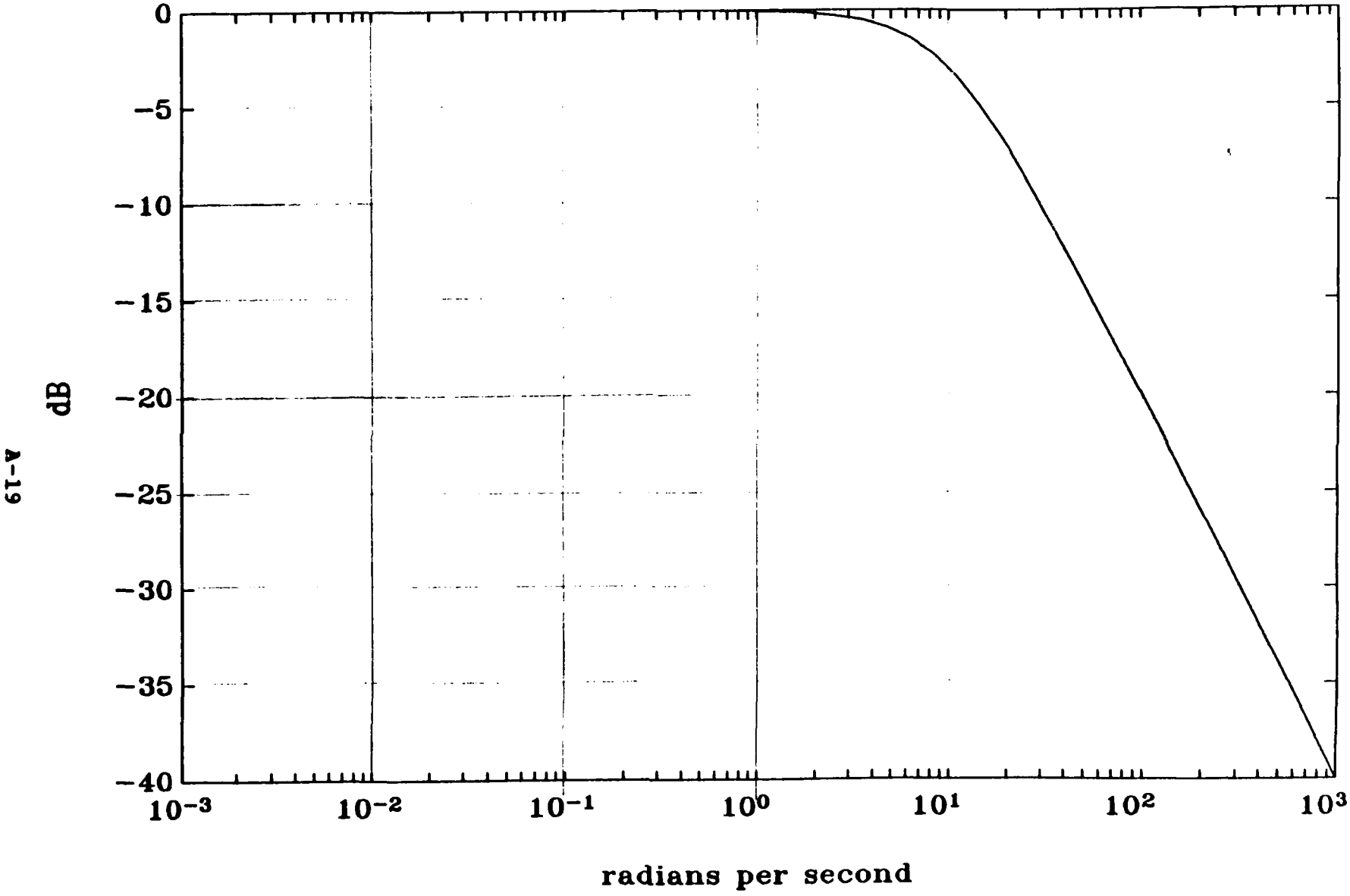

Figure A.15. Antenna Position Error Filter

Appendix B. Simulation Flyout Time Histories

In this appendix, a representative sample of the flyout time histories is given in the form of missile and target trajectories and state history diagrams. The large number of flyout runs precludes inclusion of all the flyout histories, but this representative sample should give the reader sufficient insight into actual flyout conditions.

Missile and Target Trajectories

Figure B.1 shows a typical missile and target trajectory plot for scenario 4 (see Chapter VIII) in which the missile is initially approaching the target broadside and the target is traveling at 800 m/s.

Figure B.2 shows the trajectory plots for scenario 8, in which the missile is initially approaching the target at a 45 degree offset from head-on, and the target is traveling at 800 m/s.

Figure B.3 shows the trajectory plots for scenario 12, where the missile is initially approaching the target head-on, and the target executes a 6-g pull-out away from the missile. The target is travelling at 800 m/s.

Figure B.4 shows the trajectory plot for scenario 16, where the missile is initially approaching the target broadside, and the target executes a 6-g pull-in toward the missile. The target is travelling at 800 m/s.

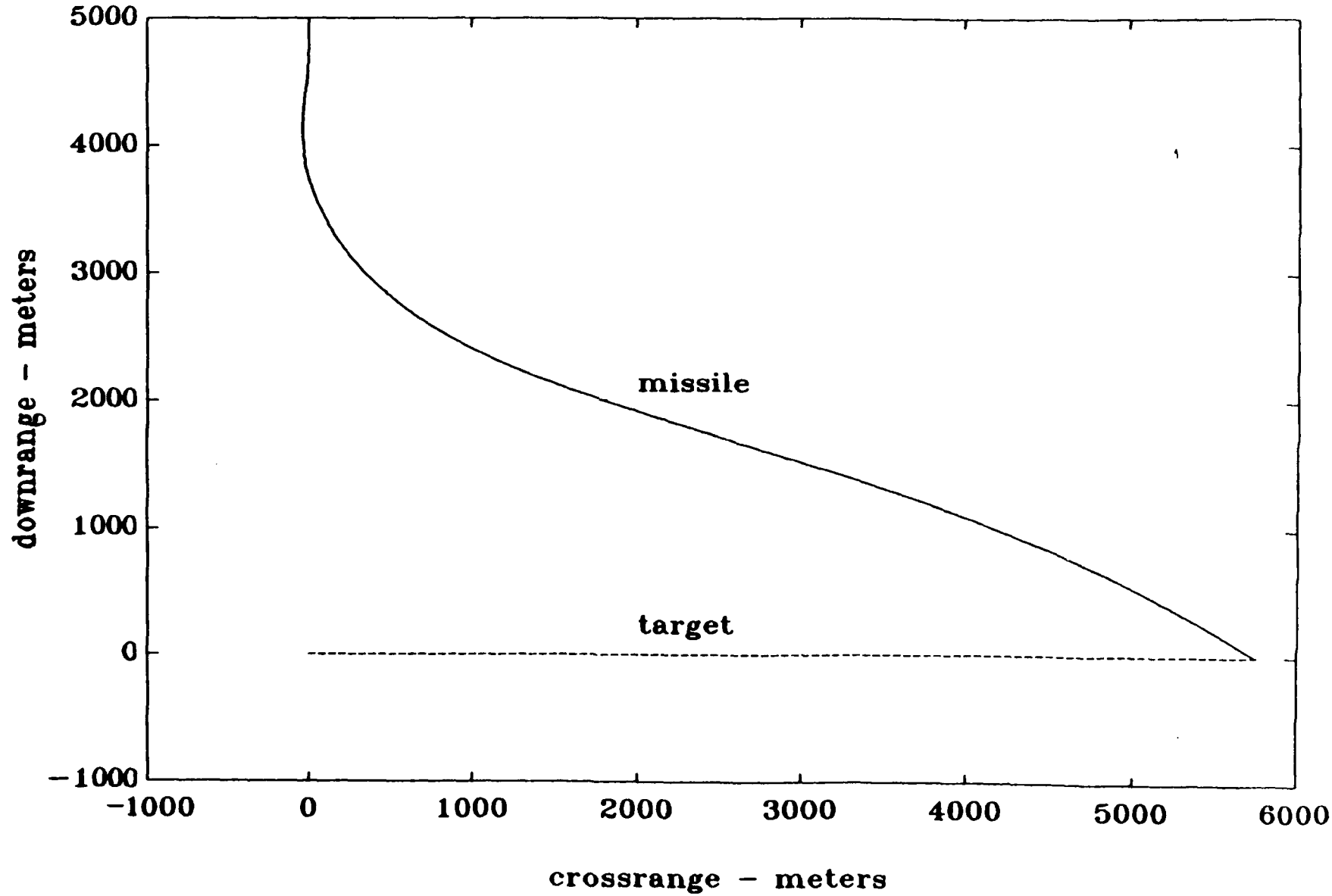

Figure B.1. Scenario 4 Missile and Target Trajectories

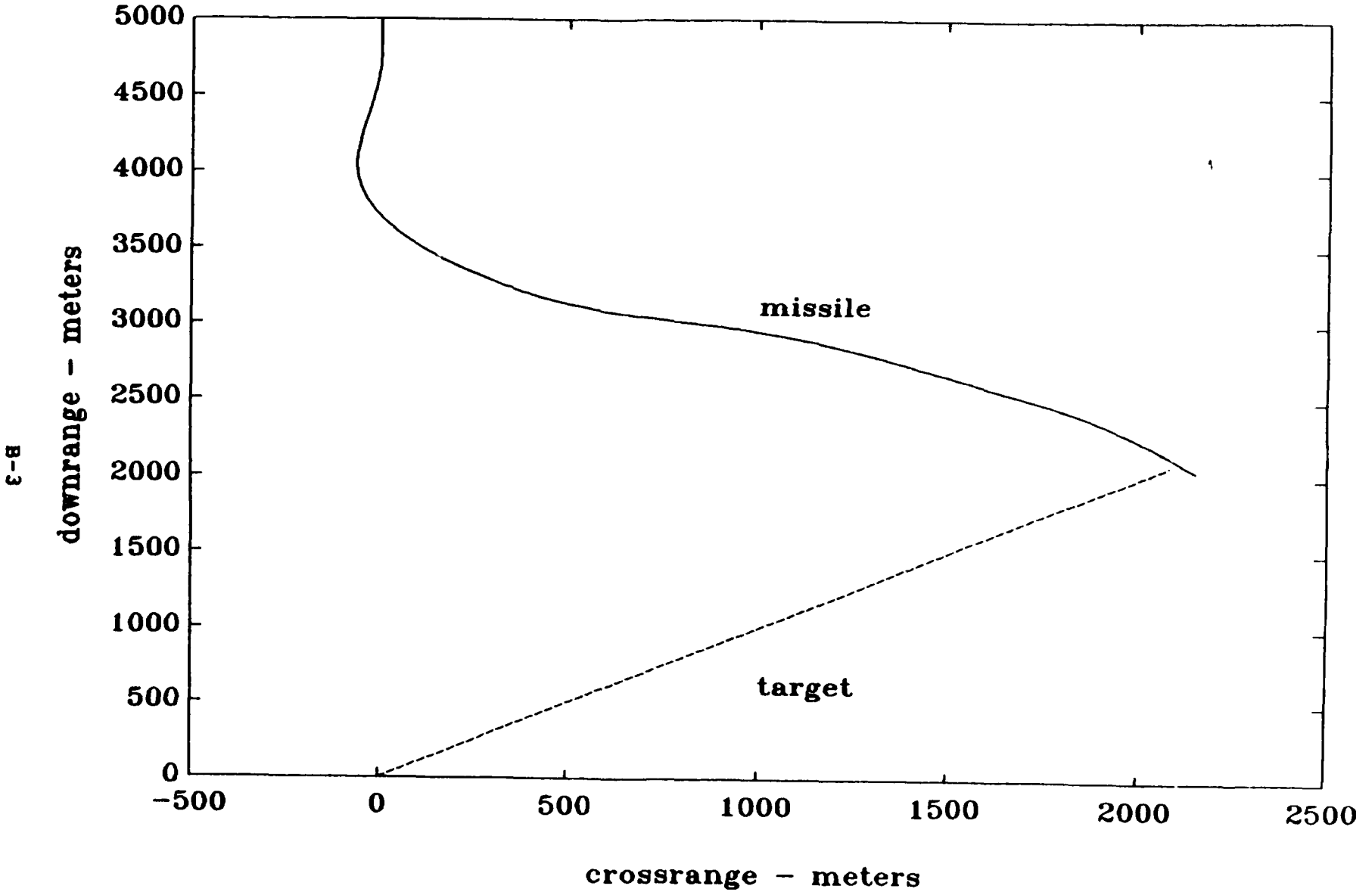

Figure B.2. Scenario 8 Missile and Target Trajectories

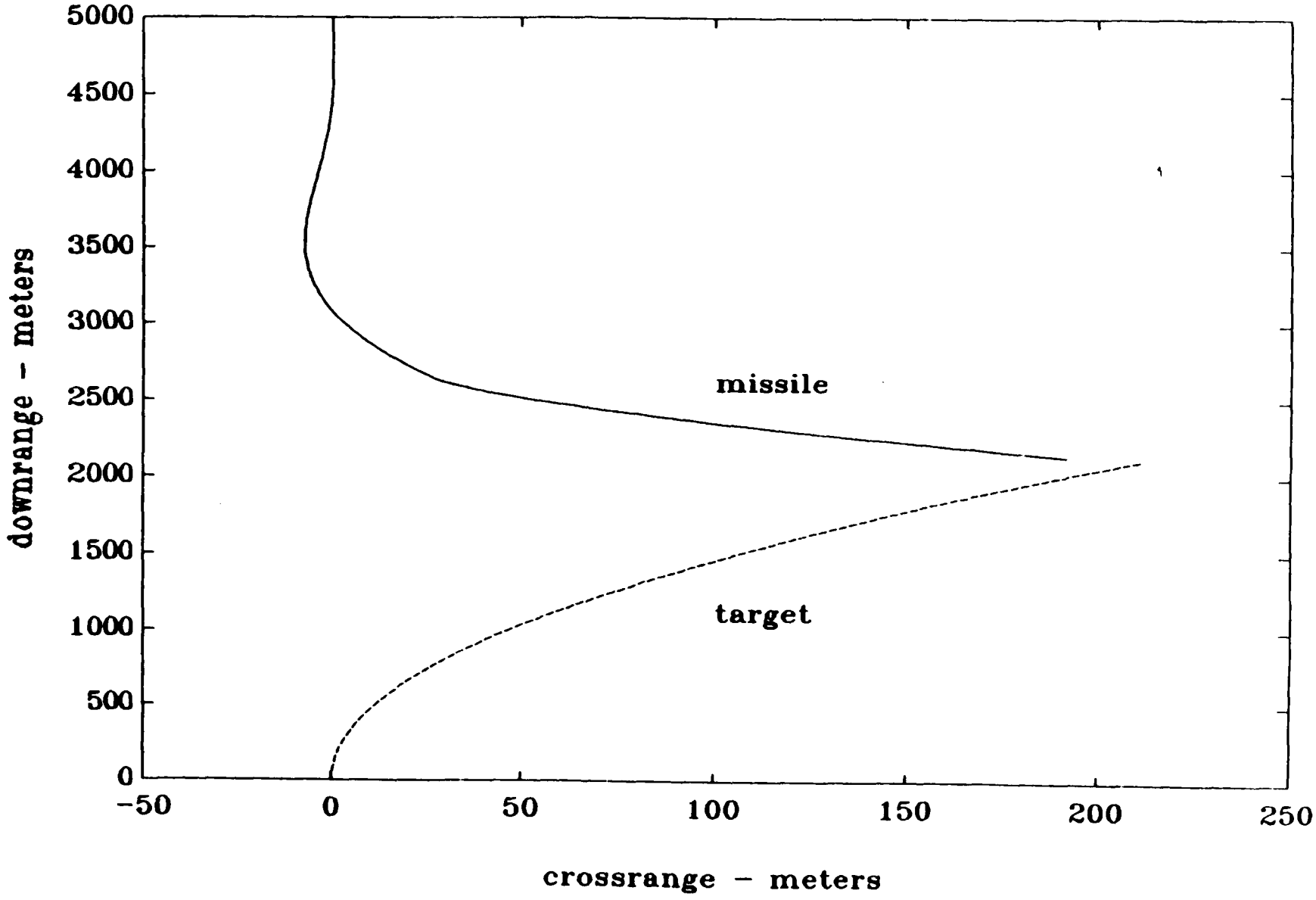

Figure B.3. Scenario 12 Missile and Target Trajectories

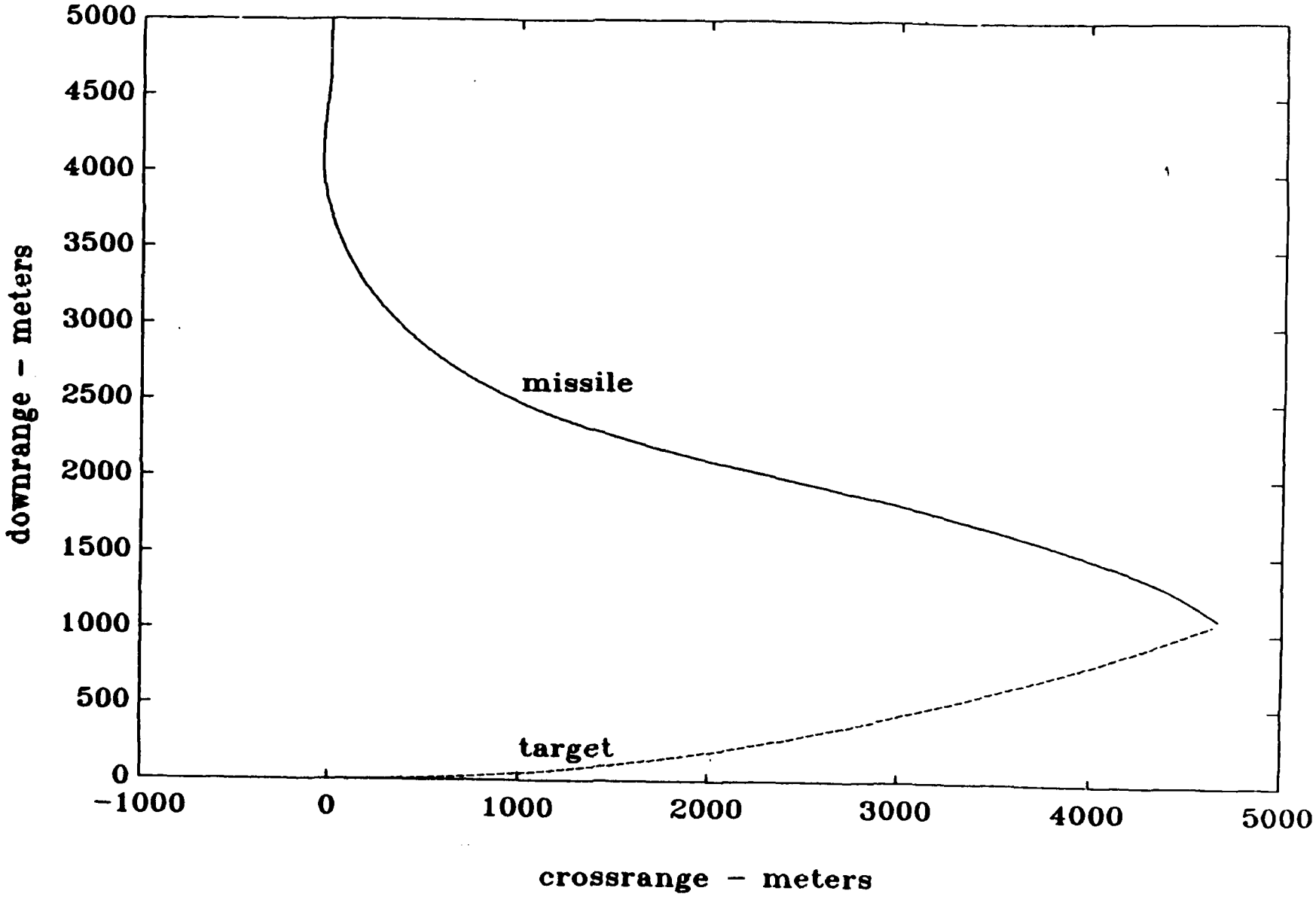

Figure B.4. Scenario 16 Missile and Target Trajectories

State Time Histories

In this section, a representative sample of the missile system state time histories will be given. All the state time histories given herein are for simulation runs using the classical controller. The state time histories for the H_2 and H_∞ controller simulation runs display similar characteristics, and are nearly indistinguishable to the unaided eye, with the obvious exception of the additional states of the respective controllers. Therefore, only state time histories for the classical controller will be shown.

Figures B.5 and B.6 show the state time histories for scenario 4, as described above. Similarly, Figures B.7-B.12 show the state time histories for scenarios 8, 12, and 16, as labelled.

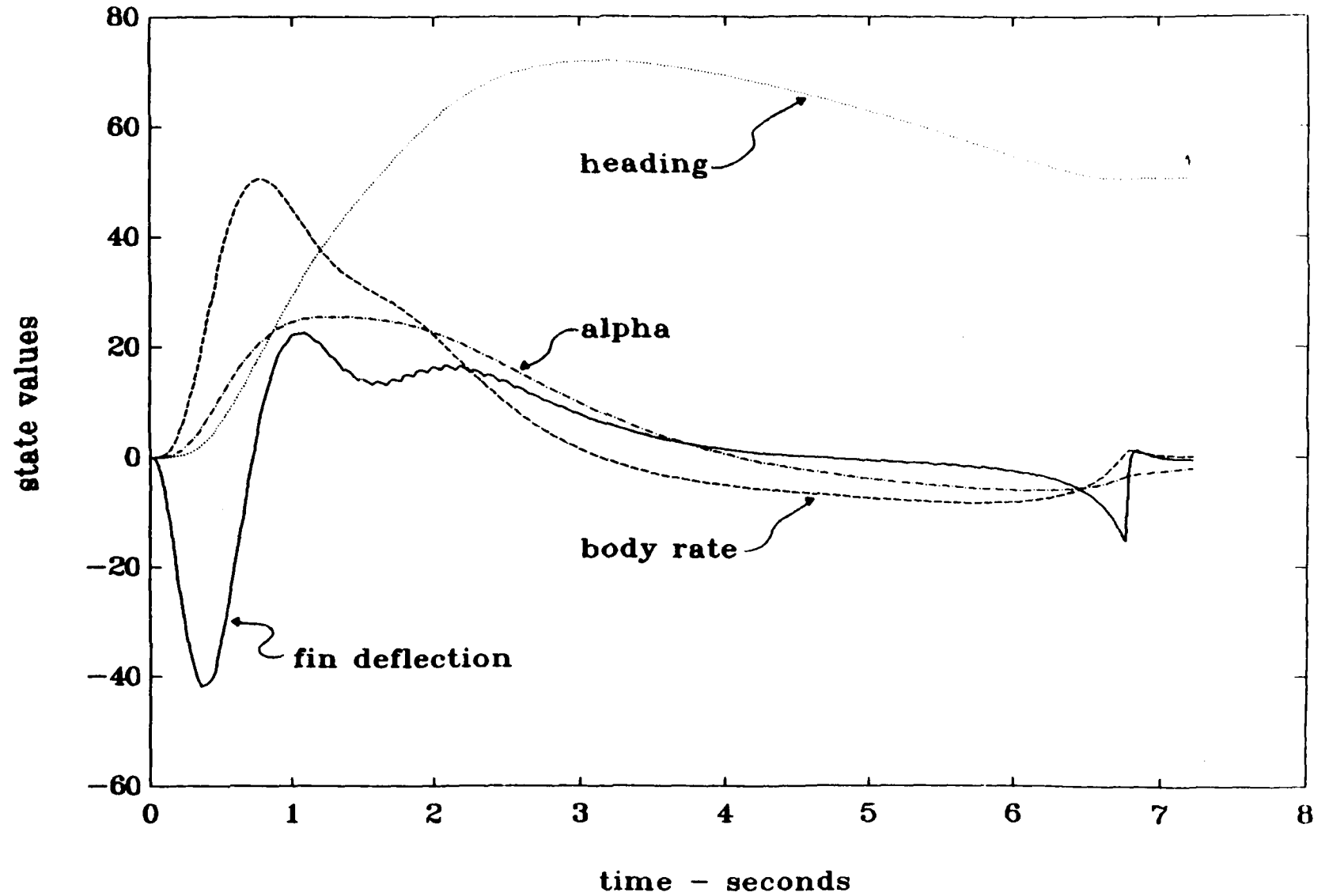

Figure B.5. Airframe State Time History, Scenario 4

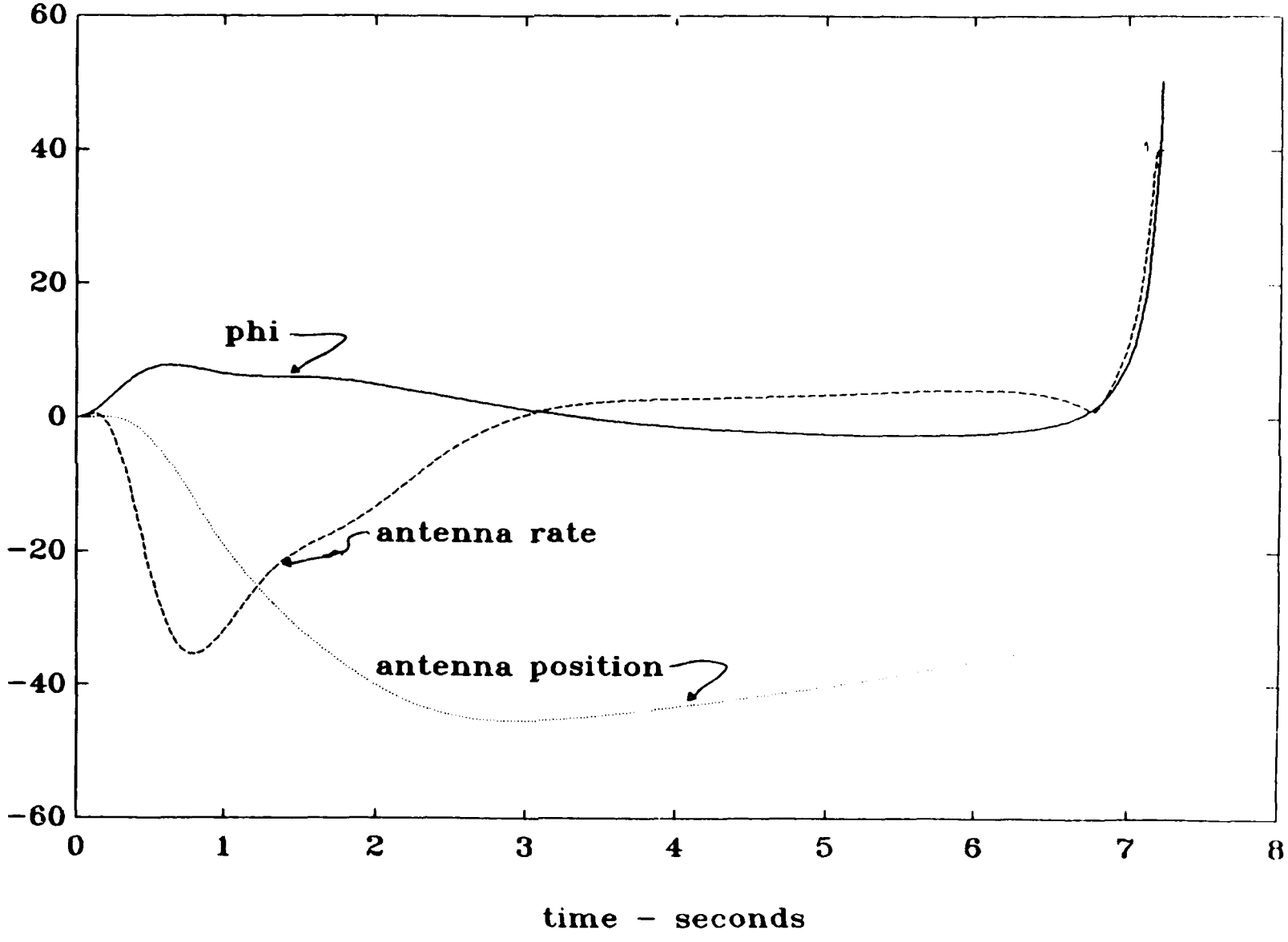

Figure B.6. Target Tracker Time History, Scenario 4

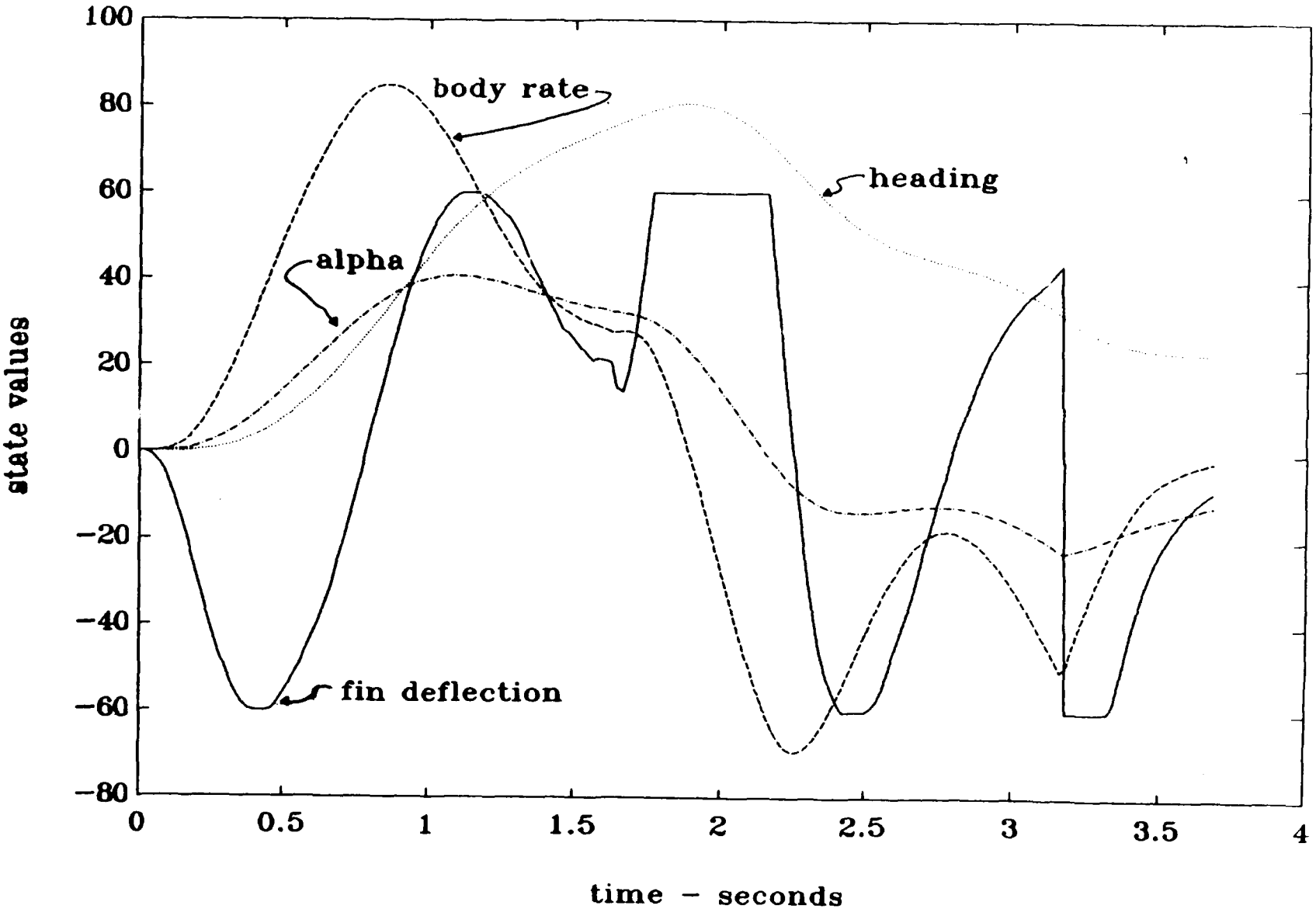

Figure B.7. Airframe State Time History, Scenario 8

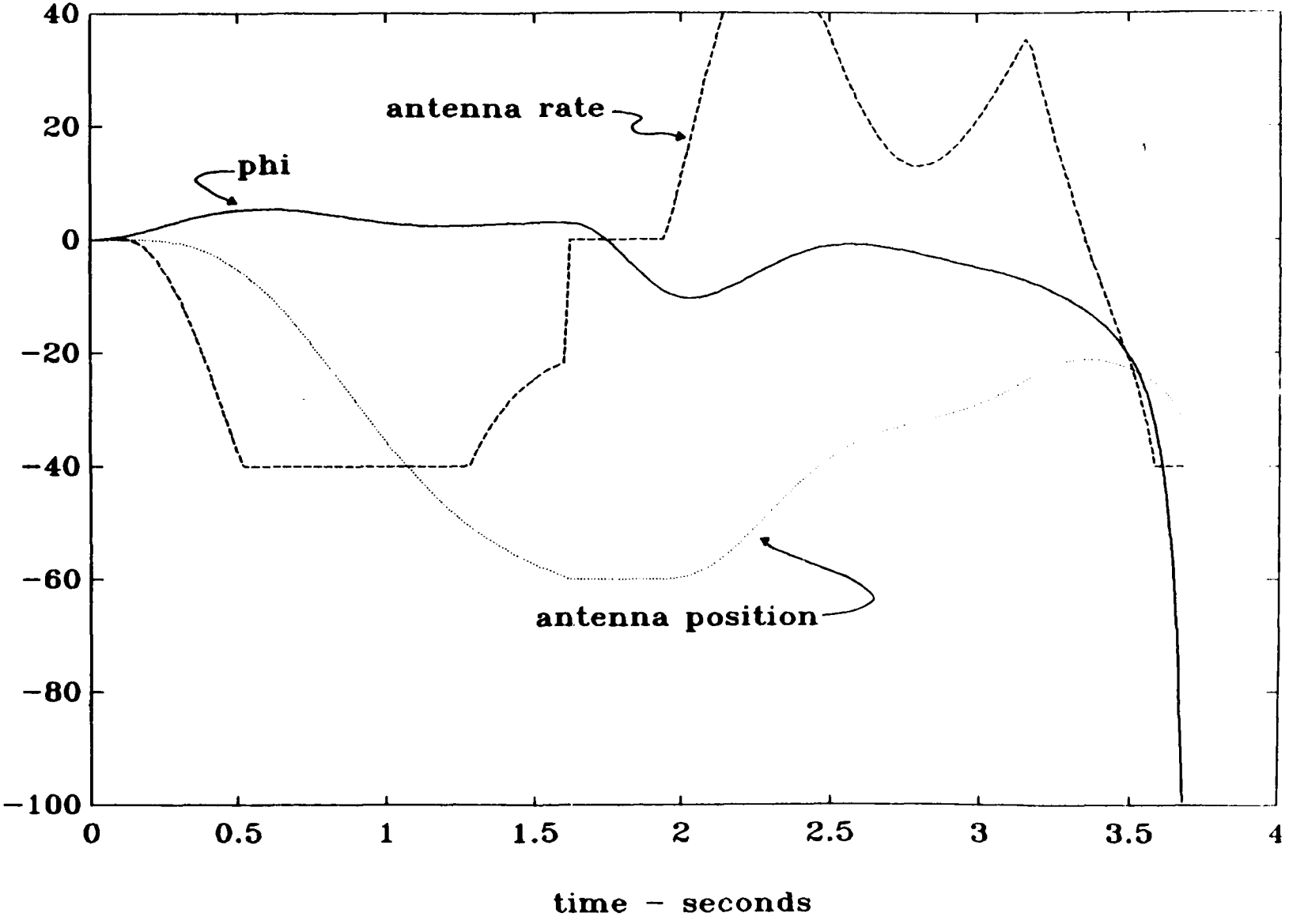

Figure B.8. Target Tracker Time History, Scenario 8

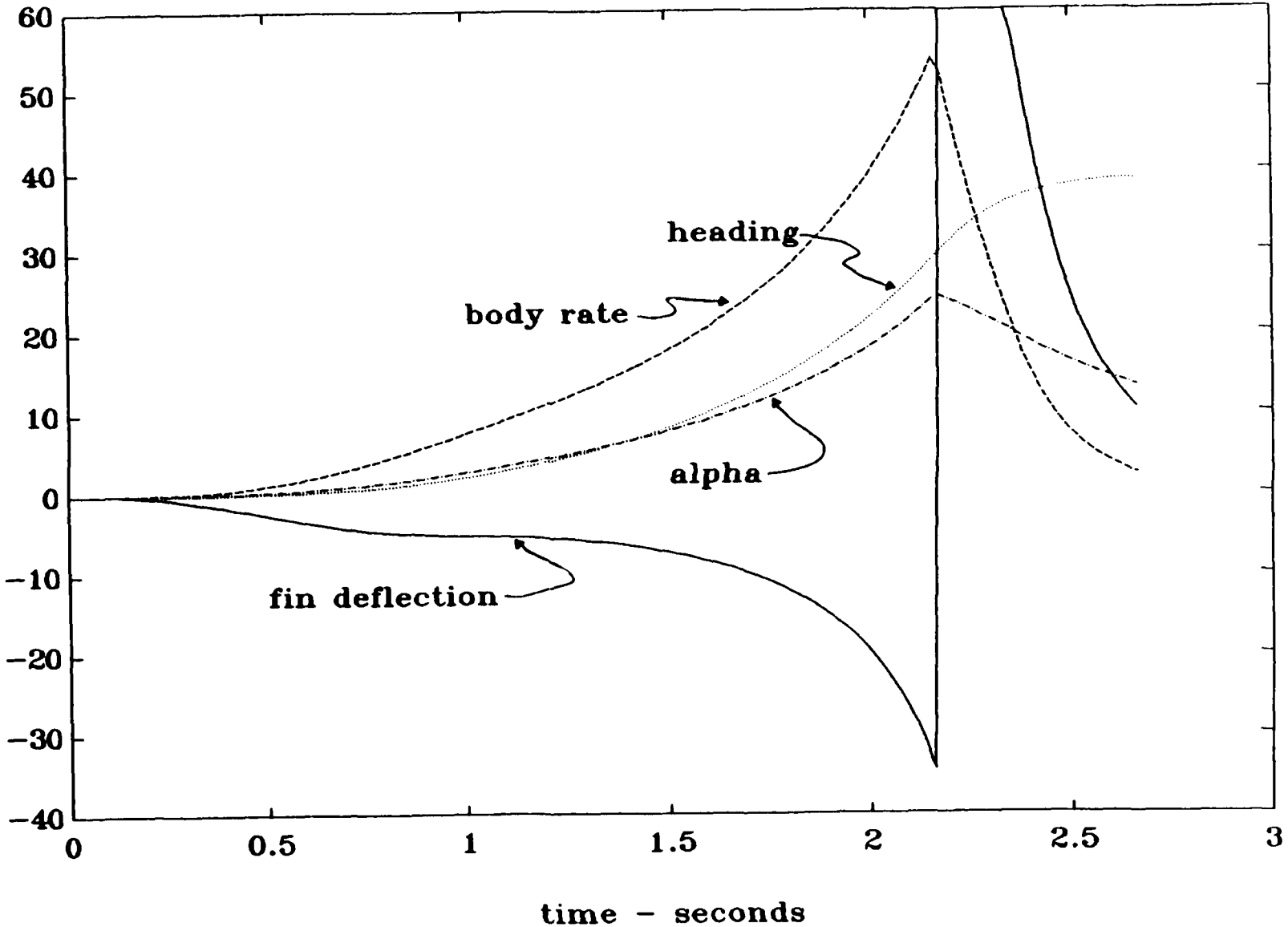

Figure B.9. Airframe State Time History, Scenario 12

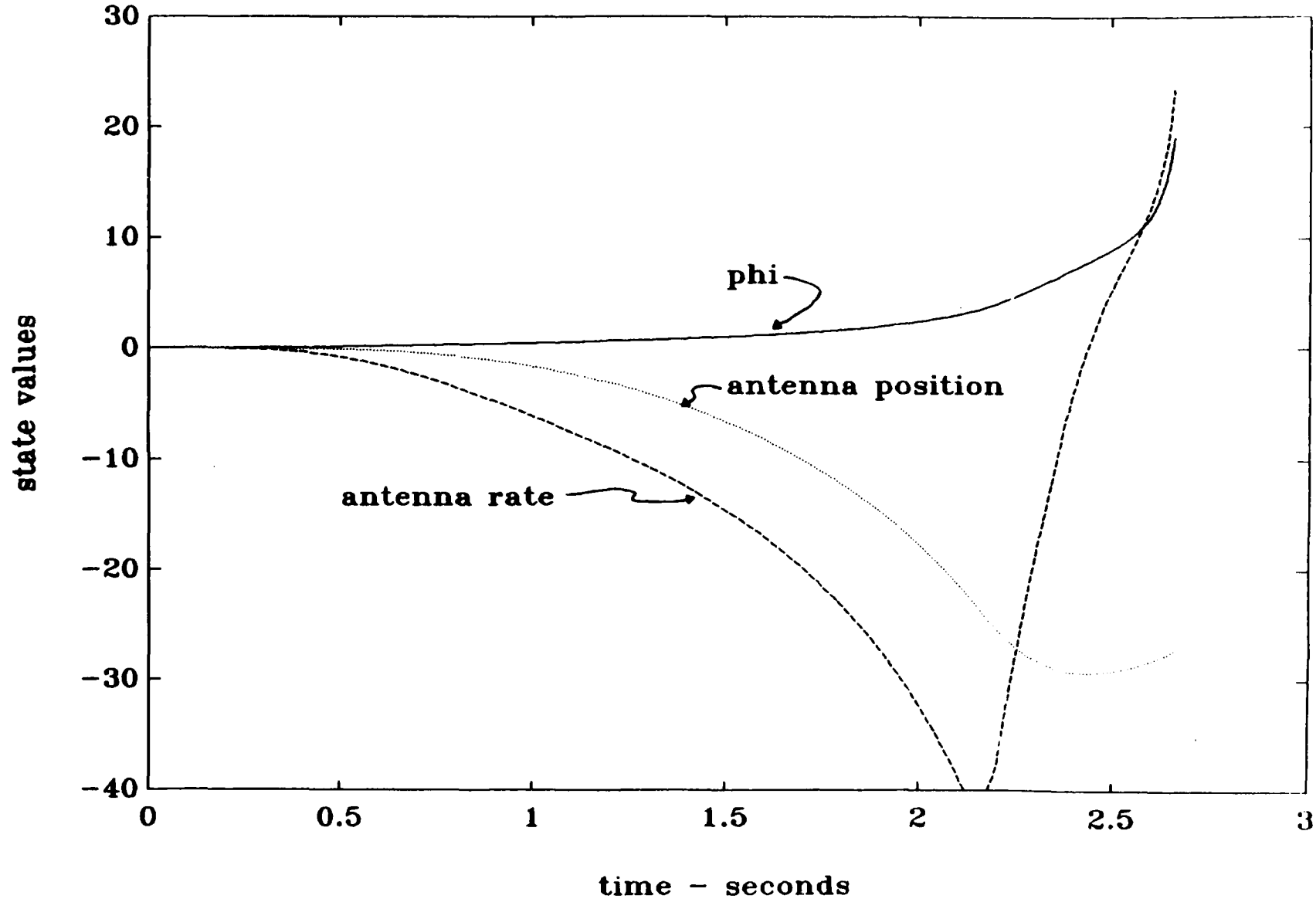

Figure B.10. Target Tracker Time History, Scenario 12

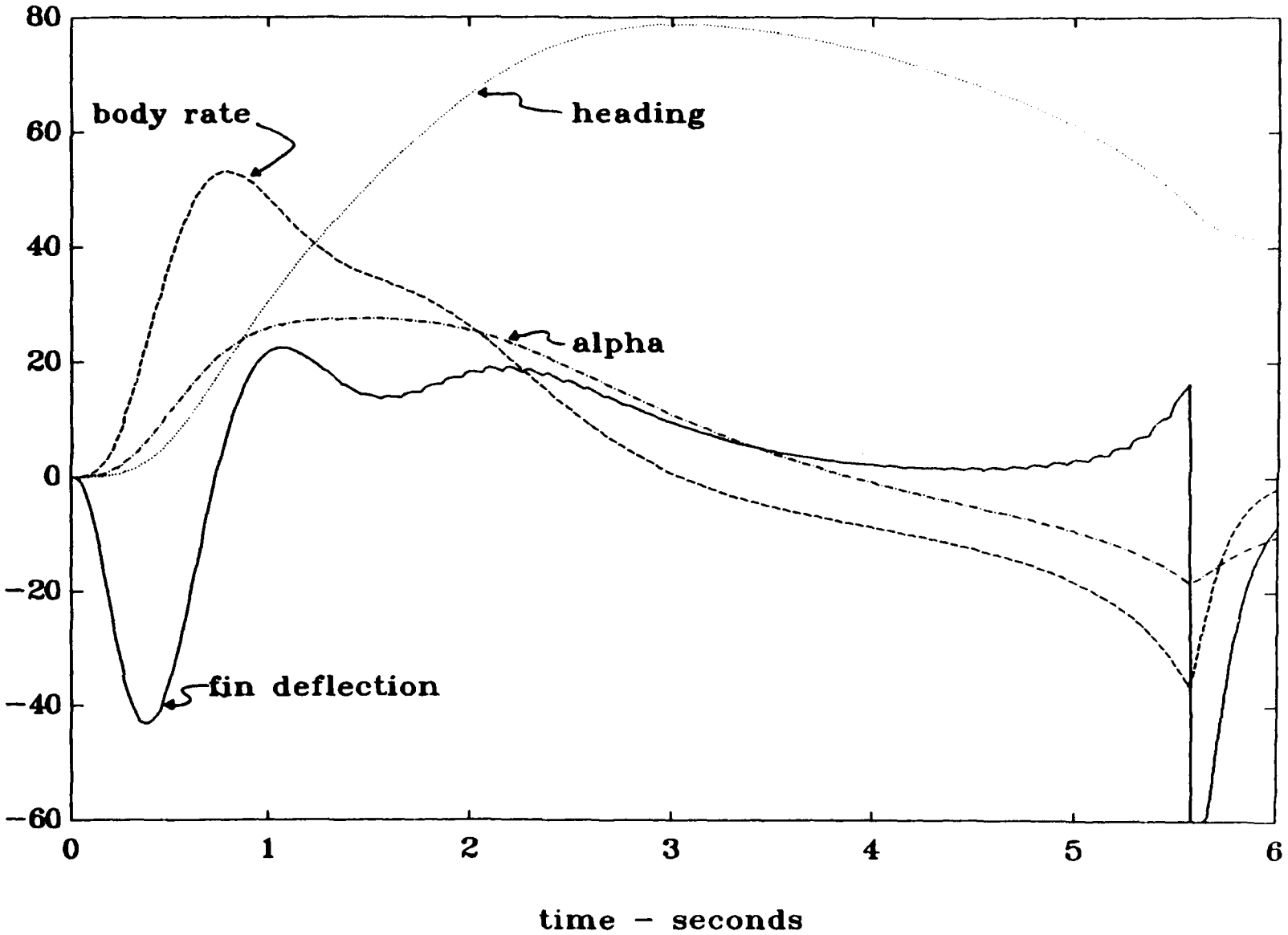

Figure B.11. Airframe State Time History, Scenario 16

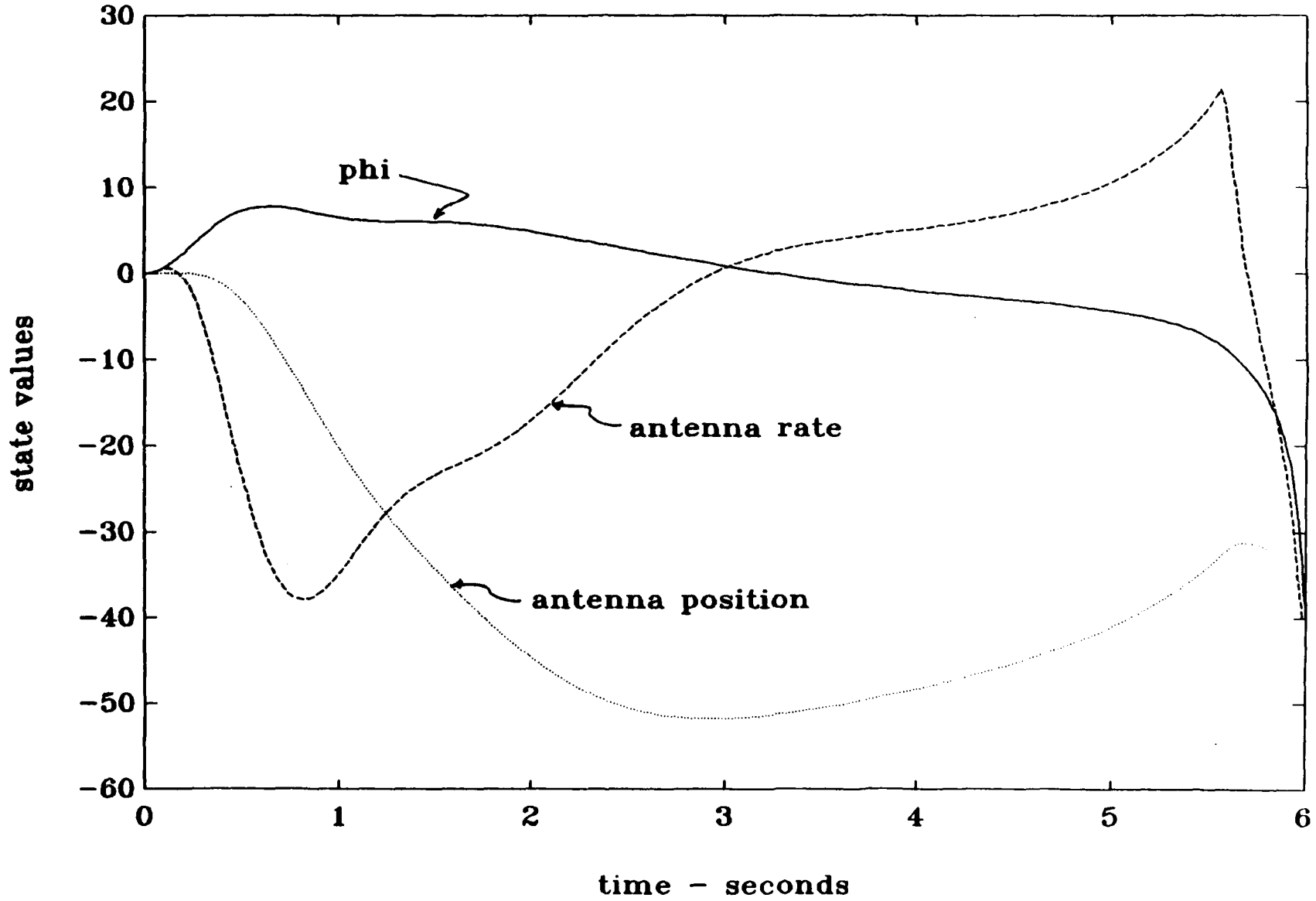

Figure B.12. Target Tracker Time History, Scenario 16

Appendix C. Full- and Reduced-Order Compensators

H_2 Full-Order Compensator

The state matrices for the full-order H_2 compensator are given below. The A matrices for the compensators listed herein are very large, due to the large number of states present, and so must be represented as partitioned matrices. Also, scientific notation had to be used due to the many large and small magnitudes of the numbers contained. This makes the matrices difficult to comprehend at a glance, but no other representation is possible. The full order H_2 compensator can be represented by the state-space description

$$\dot{x}_{cp2f} = A_{cp2f}\, x_{cp2f} + B_{cp2f}\, y_p \qquad (C.1)$$

$$u_p = C_{cp2f}\, x_{cp2f} + D_{cp2f}\, y_p \qquad (C.2)$$

where y_p and u_p correspond to the plant error vector and control input vector, respectively, as described in Chapter 6, and the other terms are given by

x_{cp2f} = compensator states

$$A_{cp2f} = [A1_{cp2f} | A2_{cp2f} | A3_{cp2f} | A4_{cp2f} | A5_{cp2f}] \qquad (C.3)$$

$$B_{cp2f} = [\ B1_{cp2f}\ ] \qquad (C.4)$$

$$C_{cp2f} = [C1_{cp2f} | C2_{cp2f} | C3_{cp2f} | C4_{cp2f} | C5_{cp2f}] \qquad (C.5)$$

$$D_{cp2f} = [\ D1_{cp2f}\ ] \qquad (C.6)$$

where the above are given by

$$A1_{cp2f} = \begin{bmatrix}
-1.30e+02 & 1.69e+03 & 2.21e+02 & 5.06e+01 & -4.11e-02 \\
-3.32e+00 & -5.46e-01 & 0 & -2.69e-01 & 4.07e-01 \\
-3.55e-01 & 8.02e-01 & 0 & -7.10e-01 & 7.26e-01 \\
-9.61e-01 & 5.49e-01 & 0 & -1.92e+00 & 2.50e-01 \\
3.51e-01 & 1.97e-01 & -2.07e+01 & 7.02e-01 & -1.20e+01 \\
-8.61e-04 & -6.61e-05 & -3.90e-02 & -1.72e-03 & -1.70e-03 \\
1.00e-06 & 1.88e-06 & 0 & 2.01e-06 & -6.05e-06 \\
-2.85e-02 & 7.78e-02 & 0 & -5.70e-02 & 3.29e-02 \\
2.73e-09 & 2.03e-09 & 0 & 5.47e-09 & 1.35e-09 \\
-3.21e-01 & 6.07e+00 & 0 & -6.42e-01 & 1.20e-01 \\
1.13e+01 & -3.50e-01 & 0 & 2.27e+01 & 2.03e-01 \\
-3.21e-06 & 7.94e-07 & 0 & -6.43e-06 & -1.98e-05 \\
2.68e-07 & 4.18e-08 & 0 & 5.37e-07 & 3.41e-07 \\
-1.33e-01 & -6.15e-02 & 0 & -2.65e-01 & -2.14e+00 \\
3.50e-01 & 4.02e-01 & 0 & 7.01e-01 & 1.05e-02 \\
-7.49e-06 & -4.00e-06 & 0 & -1.49e-05 & -1.06e-03 \\
1.88e-01 & -5.77e-03 & 0 & 3.76e-01 & 4.71e-01 \\
0 & 0 & 0 & 0 & 0 \\
6.62e-15 & 1.41e-14 & 0 & 1.32e-14 & -5.11e-15 \\
-1.27e-13 & -2.89e-13 & 0 & -2.55e-13 & 1.28e-13 \\
0 & 0 & 0 & 0 & 0 \\
2.11e-17 & 1.22e-15 & 0 & 4.23e-17 & -7.94e-17 \\
-4.05e-15 & -2.45e-13 & 0 & -8.11e-15 & 1.60e-14 \\
0 & 0 & 0 & 0 & 0
\end{bmatrix} \tag{C.7}$$

$$A2_{cp2f} = \begin{bmatrix}
-8.58e-04 & -1.20e-03 & 4.42e+03 & 6.46e+04 & 1.24e+03 \\
-6.86e-08 & 2.54e-07 & 5.46e+00 & -2.03e-04 & -5.46e-01 \\
1.61e-06 & 1.35e-04 & 1.97e+00 & -1.08e-01 & -1.97e-01 \\
2.11e-07 & 5.37e-08 & 4.50e+00 & -4.30e-05 & -4.50e-01 \\
-8.78e-04 & -2.07e+01 & -1.97e+00 & 5.43e-03 & 1.97e-01 \\
-2.22e+03 & -5.56e+05 & -3.29e+00 & 4.45e+08 & 3.83e-03 \\
1.00e+00 & -1.36e-04 & -1.88e-05 & 1.09e-01 & 1.88e-06 \\
5.70e-08 & -3.20e-09 & -8.78e-01 & 2.56e-06 & 7.78e-02 \\
3.29e-09 & 9.99e-03 & -2.03e-08 & -8.00e+00 & 2.03e-09 \\
-6.47e-07 & 1.15e-08 & -6.07e+01 & -9.23e-06 & -3.92e+00 \\
-7.10e-06 & -8.51e-07 & 3.50e+00 & 6.80e-04 & -3.50e-01 \\
2.92e+00 & -1.94e-06 & -7.94e-06 & 1.55e-03 & 7.94e-07 \\
1.58e-06 & 8.40e+00 & -4.18e-07 & -6.72e+03 & 4.18e-08 \\
-4.90e-06 & 4.12e-07 & 6.15e-01 & -3.29e-04 & -6.15e-02 \\
1.64e-07 & -3.89e-08 & -4.02e+00 & 3.11e-05 & 4.02e-01 \\
8.53e-02 & 3.12e-03 & 4.00e-05 & -2.49e+00 & -4.00e-06 \\
1.66e-01 & 1.64e-03 & 5.77e-02 & -1.31e+00 & -5.77e-03 \\
0 & 0 & 0 & 0 & 0 \\
1.08e-14 & 6.08e-14 & -1.41e-13 & -4.86e-11 & 1.41e-14 \\
-1.06e-12 & -5.01e-13 & 2.89e-12 & 4.01e-10 & -2.89e-13 \\
0 & 0 & 0 & 0 & 0 \\
1.17e-16 & 9.16e-16 & -1.22e-14 & -7.33e-13 & 1.22e-15 \\
-5.68e-14 & -2.04e-13 & 2.45e-12 & 1.63e-10 & -2.45e-13 \\
0 & 0 & 0 & 0 & 0
\end{bmatrix} \tag{C.8}$$

$$A3_{cp2f} = \begin{bmatrix}
-4.33e+00 & -8.58e-04 & -4.16e-02 & -1.62e-01 & 4.90e+01 \\
-5.89e-01 & -6.86e-08 & 2.54e-07 & 0 & 1.00e+00 \\
-3.55e-01 & 1.61e-06 & 1.35e-04 & 0 & 0 \\
-4.51e-01 & 2.11e-07 & 5.37e-08 & 0 & 1.00e+00 \\
3.51e-01 & -8.78e-04 & -6.79e-06 & 2.07e+01 & 0 \\
-8.62e-04 & 7.65e+03 & -3.81e+05 & 1.34e-04 & -5.15e-07 \\
1.00e-06 & -8.62e-07 & -1.36e-04 & 0 & 0 \\
-2.85e-02 & 5.70e-08 & -3.20e-09 & 0 & 0 \\
2.73e-09 & 3.29e-09 & 9.99e-03 & 0 & 0 \\
-3.21e-01 & -6.47e-07 & 1.15e-08 & 0 & 0 \\
-2.86e+01 & -7.10e-06 & -8.51e-07 & 0 & 0 \\
-3.21e-06 & -7.07e+00 & -1.94e-06 & 0 & 0 \\
2.68e-07 & 1.58e-06 & -1.15e+01 & 0 & 0 \\
-1.33e-01 & -4.90e-06 & 4.12e-07 & -5.00e+00 & 0 \\
3.50e-01 & 1.64e-07 & -3.89e-08 & 0 & -1.00e+00 \\
-7.49e-06 & 8.53e-02 & 3.12e-03 & 0 & 0 \\
1.88e-01 & 1.66e-01 & 1.64e-03 & 0 & 0 \\
0 & 0 & 0 & 0 & 0 \\
6.62e-15 & 1.08e-14 & 6.08e-14 & 0 & 0 \\
-1.27e-13 & -1.06e-12 & -5.01e-13 & 0 & 0 \\
0 & 0 & 0 & 0 & 0 \\
2.11e-17 & 1.17e-16 & 9.16e-16 & 0 & 0 \\
-4.05e-15 & -5.68e-14 & -2.04e-13 & 0 & 0 \\
0 & 0 & 0 & 0 & 0
\end{bmatrix} \quad \text{(C.9)}$$

$$A4_{cp2f} = \begin{bmatrix}
-1.94e-11 & 7.72e-01 & -2.88e+04 & 1.04e+02 & 8.85e+00 \\
0 & 0 & 0 & 0 & 0 \\
0 & 0 & 0 & 0 & 0 \\
0 & 0 & 0 & 0 & 0 \\
0 & 1.00e+00 & 0 & 0 & 0 \\
6.31e-03 & 2.94e-02 & -3.68e-02 & -5.56e-06 & 4.48e-08 \\
0 & 0 & 0 & 0 & 0 \\
0 & 0 & 0 & 0 & 0 \\
0 & 0 & 0 & 0 & 0 \\
0 & 0 & 0 & 0 & 0 \\
0 & 0 & 0 & 0 & 0 \\
0 & 0 & 0 & 0 & 0 \\
0 & 0 & 0 & 0 & 0 \\
0 & 0 & 0 & 0 & 0 \\
0 & 0 & 0 & 0 & 0 \\
-5.00e+01 & 0 & 0 & 0 & 0 \\
0 & -2.00e+02 & 0 & 0 & 0 \\
0 & 0 & -1.00e+00 & 0 & 0 \\
0 & 0 & 0 & 0 & 1.00e+00 \\
0 & 0 & 0 & -3.00e+03 & -1.30e+02 \\
0 & 0 & 0 & 0 & 0 \\
0 & 0 & 0 & 0 & 0 \\
0 & 0 & 0 & 0 & 0 \\
0 & 0 & 0 & 0 & 0
\end{bmatrix} \quad \text{(C.10)}$$

$$A5_{cp2f} = \begin{bmatrix} 2.05e+01 & 9.54e-06 & 3.86e-06 & 1.47e-02 \\ 0 & 0 & 0 & 0 \\ 0 & 0 & 0 & 0 \\ 0 & 0 & 0 & 0 \\ 0 & 0 & 0 & 0 \\ -1.71e-02 & -5.75e+04 & -6.40e+03 & 3.83e+05 \\ 0 & 0 & 0 & 0 \\ 0 & 0 & 0 & 0 \\ 0 & 0 & 0 & 0 \\ 0 & 0 & 0 & 0 \\ 0 & 0 & 0 & 0 \\ 0 & 0 & 0 & 0 \\ 0 & 0 & 0 & 0 \\ 0 & 0 & 0 & 0 \\ 0 & 0 & 0 & 0 \\ 0 & 0 & 0 & 0 \\ 0 & 0 & 0 & 0 \\ 0 & 0 & 0 & 0 \\ 0 & 0 & 0 & 0 \\ -1.00e-02 & 0 & 0 & 0 \\ 0 & 0 & 1.00e+00 & 0 \\ 0 & -2.00e+03 & -2.10e+02 & 0 \\ 0 & 0 & 0 & -4.00e+01 \end{bmatrix} \quad (C.11)$$

$$B1_{cp2f} = \begin{bmatrix} -5.89e-07 & -9.14e-04 & -1.89e-03 & -8.58e-04 & -1.07e-06 \\ -5.46e-01 & -5.89e-01 & 4.07e-01 & -6.86e-08 & 2.54e-07 \\ -1.97e-01 & -3.55e-01 & 7.26e-01 & 1.61e-06 & 1.35e-04 \\ -4.50e-01 & -4.51e-01 & 2.50e-01 & 2.11e-07 & 5.37e-08 \\ 1.97e-01 & 3.51e-01 & -6.83e+00 & -8.78e-04 & -6.79e-06 \\ -3.36e-06 & -8.62e-04 & -1.73e-03 & -2.45e-03 & -1.89e-06 \\ 1.88e-06 & 1.00e-06 & -6.05e-06 & -8.62e-07 & -1.36e-04 \\ 7.78e-02 & -2.85e-02 & 3.29e-02 & 5.70e-08 & -3.20e-09 \\ 2.03e-09 & 2.73e-09 & 1.35e-09 & 3.29e-09 & 9.99e-03 \\ 6.07e+00 & -3.21e-01 & 1.20e-01 & -6.47e-07 & 1.15e-08 \\ -3.50e-01 & 1.13e+01 & 2.03e-01 & -7.10e-06 & -8.51e-07 \\ 7.94e-07 & -3.21e-06 & -1.98e-05 & 2.92e+00 & -1.94e-06 \\ 4.18e-08 & 2.68e-07 & 3.41e-07 & 1.58e-06 & 8.40e+00 \\ -6.15e-02 & -1.33e-01 & -2.14e+00 & -4.90e-06 & 4.12e-07 \\ 4.02e-01 & 3.50e-01 & 1.05e-02 & 1.64e-07 & -3.89e-08 \\ -4.00e-06 & -7.49e-06 & -1.06e-03 & 8.53e-02 & 3.12e-03 \\ -5.77e-03 & 1.88e-01 & 4.71e-01 & 1.66e-01 & 1.64e-03 \\ 1.00e+00 & 0 & 0 & 0 & 0 \\ 1.41e-14 & 6.62e-15 & -5.11e-15 & 1.08e-14 & 6.08e-14 \\ -2.89e-13 & 1.00e+02 & 1.28e-13 & -1.06e-12 & -5.01e-13 \\ 0 & 0 & 1.00e-02 & 0 & 0 \\ 1.22e-15 & 2.11e-17 & -7.94e-17 & 1.17e-16 & 9.16e-16 \\ -2.45e-13 & -4.05e-15 & 1.60e-14 & -3.00e+02 & -2.04e-13 \\ 0 & 0 & 0 & 0 & 4.00e+01 \end{bmatrix} \quad (C.12)$$

$$C1_{cp2f} = \begin{bmatrix} -6.94e-01 & 2.13e+01 & 2.88e+00 & 6.57e-01 & -5.09e-04 \\ 1.36e-08 & -6.67e-07 & -4.14e-04 & -9.85e-09 & 3.46e-07 \end{bmatrix} \quad (C.13)$$

$$C2_{cp2f} = \begin{bmatrix} -3.74e-10 & -1.55e-05 & 5.75e+01 & 8.39e+02 & 1.61e+01 \\ -2.26e+01 & -5.92e+03 & -3.50e-02 & 4.73e+06 & 4.08e-05 \end{bmatrix} \quad (C.14)$$

$$C3_{cp2f} = \begin{bmatrix} -5.63e-02 & 8.48e-09 & -5.40e-04 & -2.11e-03 & 6.37e-01 \\ -2.67e-09 & 8.14e+01 & -4.06e+03 & 1.43e-06 & -5.48e-09 \end{bmatrix} \quad (C.15)$$

$$C4_{cp2f} = \begin{bmatrix} -2.52e-13 & -2.95e-03 & -3.75e+02 & 1.35e+00 & 1.14e-01 \\ -1.05e-02 & -1.03e-02 & -3.91e-04 & -5.92e-08 & 4.76e-10 \end{bmatrix} \quad (C.16)$$

$$C5_{cp2f} = \begin{bmatrix} 2.67e-01 & 1.23e-07 & 5.01e-08 & 1.91e-04 \\ -1.82e-04 & -6.12e+02 & -6.81e+01 & 4.07e+03 \end{bmatrix} \quad (C.17)$$

$$D1_{cp2f} = \begin{bmatrix} 0 & 0 & 0 & 0 & 0 \\ 0 & 0 & 0 & 0 & 0 \end{bmatrix} \quad (C.18)$$

H_2 Reduced Order Compensator

The above compensator can be reduced in size by use of the Hankel singular value elimination technique described in Chapter VI. The Hankel singular values for the H_2 compensator are given in Table C.1. The last 13 Hankel singular values were eliminated to produce the reduced order compensator, as indicated by the dashed line in Table C.1. The resultant reduced order compensator, composed of 11 states, can be represented by

$$\dot{x}_{cp2r} = A_{cp2r}\, x_{cp2r} + B_{cp2r}\, y_p \quad (C.19)$$

$$u_p = C_{cp2r}\, x_{cp2r} + D_{cp2r}\, y_p \quad (C.20)$$

Table C.1. H_2 Compensator Hankel Singular Values

4.02e+01
3.15e+01
9.00e+00
3.08e+00
2.69e+00
2.06e+00
1.98e+00
5.56e-01
4.56e-01
3.54e-01
1.25e-01
8.76e-02
4.27e-02
2.58e=02
1.25e-02
7.30e-03
2.26e-03
9.07e-04
3.43e-04
1.69e-04
7.03e-06
3.71e-06
3.41e-07
1.88e-08

where

$$x_{cp2r} = \text{compensator states}$$

$$A_{cp2r} = [A1_{cp2r} | A2_{cp2r}] \qquad (C.21)$$

$$B_{cp2r} = \begin{bmatrix} B1_{cp2r} \end{bmatrix} \qquad (C.22)$$

$$C_{cp2r} = [C1_{cp2r} | C2_{cp2r}] \qquad (C.23)$$

$$D_{cp2r} = \begin{bmatrix} D1_{cp2r} \end{bmatrix} \qquad (C.24)$$

and

$$A1_{cp2r} = \begin{bmatrix} -7.19e+04 & 2.61e+05 & 1.14e+05 & -1.03e+04 \\ -4.19e+04 & 1.52e+05 & 6.69e+04 & -6.01e+03 \\ 6.07e+02 & -2.20e+03 & -9.70e+02 & 8.94e+01 \\ -1.42e+04 & 5.18e+04 & 2.27e+04 & -2.04e+03 \\ 8.69e+02 & -3.16e+03 & -1.38e+03 & 1.20e+02 \\ -3.06e+03 & 1.11e+04 & 4.87e+03 & -4.22e+02 \\ 6.64e+03 & -2.41e+04 & -1.05e+04 & 9.42e+02 \\ -2.24e+03 & 8.15e+03 & 3.57e+03 & -3.21e+02 \\ 8.66e+02 & -3.14e+03 & -1.37e+03 & 1.24e+02 \\ -2.37e+02 & 8.63e+02 & 3.75e+02 & -3.13e+01 \\ 1.02e+03 & -3.70e+03 & -1.62e+03 & 1.46e+02 \end{bmatrix} \quad (C.25)$$

$$A2_{cp2r} = \begin{bmatrix} 1.15e+05 & -1.16e+05 & -1.44e+05 & 3.19e+03 \\ 6.73e+04 & -6.79e+04 & -8.41e+04 & 1.86e+03 \\ -9.84e+02 & 9.66e+02 & 1.23e+03 & -2.68e+01 \\ 2.29e+04 & -2.31e+04 & -2.86e+04 & 6.34e+02 \\ -1.38e+03 & 1.44e+03 & 1.72e+03 & -3.83e+01 \\ 4.85e+03 & -5.08e+03 & -6.03e+03 & 1.35e+02 \\ -1.06e+04 & 1.07e+04 & 1.32e+04 & -2.95e+02 \\ 3.59e+03 & -3.63e+03 & -4.50e+03 & -9.96e+01 \\ -1.38e+03 & 1.39e+03 & 1.73e+03 & -3.77e+01 \\ 3.73e+02 & -4.02e+02 & -4.57e+02 & 1.05e+01 \\ -1.63e+03 & 1.65e+03 & 2.04e+03 & -4.57e+01 \end{bmatrix} \quad (C.26)$$

$$A3_{cp2r} = \begin{bmatrix} 5.71e+04 & 8.94e+03 & 6.07e+06 \\ 3.33e+04 & 5.21e+03 & 3.54e+06 \\ -5.18e+02 & 1.82e+01 & -5.13e+04 \\ 1.13e+04 & 1.71e+03 & 1.20e+06 \\ -6.31e+02 & -2.66e+02 & -7.35e+04 \\ 2.17e+03 & 9.53e+02 & 2.58e+05 \\ -5.15e+03 & -1.08e+03 & -5.59e+05 \\ 1.78e+03 & 2.78e+02 & 1.89e+05 \\ -7.07e+02 & -6.49e+01 & -7.28e+04 \\ 1.43e+02 & 1.01e+02 & 2.00e+04 \\ -8.13e+02 & -1.21e+02 & -8.61e+04 \end{bmatrix} \quad (C.27)$$

$$B1_{cp2r} = \begin{bmatrix} -4.75e-03 & -1.39e-01 & -4.40e-02 & 9.43e+00 & 2.01e+01 \\ 7.37e-02 & -1.02e-01 & -2.78e-02 & 5.24e+00 & -3.53e+01 \\ -1.52e+00 & 9.14e-01 & 3.40e-02 & -1.16e-02 & -2.48e+00 \\ -9.95e-02 & -1.19e+00 & -1.20e-01 & 1.74e+00 & -5.03e-01 \\ 4.73e+00 & -3.56e+00 & 4.78e-03 & -1.59e-02 & 6.89e-01 \\ 1.55e+00 & 9.12e+00 & 8.65e-01 & 2.97e-01 & -1.13e+00 \\ 1.54e+00 & -5.07e+00 & -3.00e-01 & -1.16e+00 & -6.27e+00 \\ 1.26e-02 & -2.72e-02 & 9.44e-04 & -9.23e+01 & -2.92e-01 \\ 4.02e+00 & -5.21e-01 & 3.15e-01 & 2.50e-01 & -1.72e+00 \\ -5.46e+00 & 1.34e+00 & 7.08e-01 & 6.79e-02 & 1.45e-01 \\ -2.77e-02 & 1.08e-01 & 5.18e-03 & -3.13e-01 & -2.97e-01 \end{bmatrix} \quad (C.28)$$

$$C1_{cp2r} = \begin{bmatrix} 3.81e\text{-}02 & -4.68e\text{-}02 & -7.45e\text{-}01 & 9.04e\text{-}01 \\ 1.07e{+}03 & -3.91e{+}03 & -1.71e{+}03 & 1.54e{+}02 \end{bmatrix} \quad (C.29)$$

$$C2_{cp2r} = \begin{bmatrix} -3.71e{+}00 & -6.01e{+}00 & 5.58e{+}00 & -2.78e\text{-}02 \\ -1.72e{+}03 & 1.74e{+}03 & 2.16e{+}03 & -4.78e{+}01 \end{bmatrix} \quad (C.30)$$

$$C3_{cp2r} = \begin{bmatrix} -1.47e{+}01 & 3.88e{+}01 & -1.58e{+}01 \\ -8.56e{+}02 & -1.34e{+}02 & -9.09e{+}04 \end{bmatrix} \quad (C.31)$$

$$D1_{cp2r} = \begin{bmatrix} 0 & 0 & 0 & 0 & 0 \\ 0 & 0 & 0 & 0 & 0 \end{bmatrix} \quad (C.32)$$

H_∞ Full Order Compensator

The full order compensator developed for the H_∞ design can be represented in state-space form as

$$\dot{x}_{cpif} = A_{cpif}\, x_{cpif} + B_{cpif}\, y_p \quad (C.33)$$

$$u_p = C_{cpif}\, x_{cpif} + D_{cpif}\, y_p \quad (C.34)$$

where y_p and u_p correspond to the plant error vector and control input vector as before, and the other terms are given by

x_{cpif} = compensator states

$$A_{cpif} = [A1_{cpif} | A2_{cpif} | A3_{cpif} | A4_{cpif} | A5_{cpif}] \quad (C.35)$$

$$B_{cpif} = [\, B1_{cpif} \,] \quad (C.36)$$

$$C_{cpif} = [C1_{cpif} | C2_{cpif} | C3_{cpif} | C4_{cpif} | C5_{cpif}] \quad (C.37)$$

$$D_{cpif} = [\, D1_{cpif} \,] \quad (C.38)$$

where

$$A1_{cpif} = \begin{bmatrix}
-1.30e+02 & 1.69e+03 & 4.01e+02 & 5.06e+01 & -4.84e-02 \\
-3.32e+00 & -5.46e-01 & 0 & -2.69e-01 & 4.07e-01 \\
-3.55e-01 & 8.02e-01 & 0 & -7.10e-01 & 7.26e-01 \\
-9.61e-01 & 5.49e-01 & 0 & -1.92e+00 & 2.50e-01 \\
3.51e-01 & 1.97e-01 & -2.07e+01 & 7.02e-01 & -1.20e+01 \\
-3.92e-02 & 1.87e+00 & 1.17e+03 & 2.58e-02 & -3.44e-01 \\
1.00e-06 & 1.88e-06 & 0 & 2.01e-06 & -6.05e-06 \\
-2.85e-02 & 7.78e-02 & 0 & -5.70e-02 & 3.29e-02 \\
2.73e-09 & 2.03e-09 & 0 & 5.47e-09 & 1.35e-09 \\
-3.21e-01 & 6.07e+00 & 0 & -6.42e-01 & 1.20e-01 \\
1.13e+01 & -3.50e-01 & 0 & 2.27e+01 & 2.03e-01 \\
-3.21e-06 & 7.94e-07 & 0 & -6.43e-06 & -1.98e-05 \\
2.68e-07 & 4.18e-08 & 0 & 5.37e-07 & 3.41e-07 \\
-1.33e-01 & -6.15e-02 & 0 & -2.65e-01 & -2.14e+00 \\
3.50e-01 & 4.02e-01 & 0 & 7.01e-01 & 1.05e-02 \\
-7.49e-06 & -4.00e-06 & 0 & -1.49e-05 & -1.06e-03 \\
1.88e-01 & -5.77e-03 & 0 & 3.76e-01 & 4.71e-01 \\
0 & 0 & 0 & 0 & 0 \\
8.24e-13 & -3.12e-11 & 0 & 1.64e-12 & -2.05e-12 \\
-1.61e-11 & 7.39e-10 & 0 & -3.22e-11 & 3.85e-11 \\
0 & 0 & 0 & 0 & 0 \\
8.60e-16 & -2.34e-14 & 0 & 1.72e-15 & 1.36e-14 \\
-1.54e-13 & 4.60e-12 & 0 & -3.09e-13 & -2.77e-12 \\
0 & 0 & 0 & 0 & 0
\end{bmatrix} \quad \text{(C.39)}$$

$$A2_{cpif} = \begin{bmatrix}
-2.60e-02 & -2.91e+02 & 2.22e+04 & 3.21e+05 & 1.22e+03 \\
-6.86e-08 & 2.54e-07 & 5.46e+00 & -2.03e-04 & -5.46e-01 \\
1.61e-06 & 1.35e-04 & 1.97e+00 & -1.08e-01 & -1.97e-01 \\
2.11e-07 & 5.37e-08 & 4.50e+00 & -4.30e-05 & -4.50e-01 \\
-8.78e-04 & -2.07e+01 & -1.97e+00 & 5.43e-03 & 1.97e-01 \\
-2.75e+03 & -6.67e+06 & -1.10e+05 & 5.34e+09 & -1.16e+02 \\
1.00e+00 & -1.36e-04 & -1.88e-05 & 1.09e-01 & 1.88e-06 \\
5.70e-08 & -3.20e-09 & -8.78e-01 & 2.56e-06 & 7.78e-02 \\
3.29e-09 & 9.99e-03 & -2.03e-08 & -8.00e+00 & 2.03e-09 \\
-6.47e-07 & 1.15e-08 & -6.07e+01 & -9.23e-06 & -3.92e+00 \\
-7.10e-06 & -8.51e-07 & 3.50e+00 & 6.80e-04 & -3.50e-01 \\
2.92e+00 & -1.94e-06 & -7.94e-06 & 1.55e-03 & 7.94e-07 \\
1.58e-06 & 8.40e+00 & -4.18e-07 & -6.72e+03 & 4.18e-08 \\
-4.90e-06 & 4.12e-07 & 6.15e-01 & -3.29e-04 & -6.15e-02 \\
1.64e-07 & -3.89e-08 & -4.02e+00 & 3.11e-05 & 4.02e-01 \\
8.53e-02 & 3.12e-03 & 4.00e-05 & -2.49e+00 & -4.00e-06 \\
1.66e-01 & 1.64e-03 & 5.77e-02 & -1.31e+00 & -5.77e-03 \\
0 & 0 & 0 & 0 & 0 \\
-4.85e-14 & 8.08e-13 & -3.12e-10 & -6.46e-10 & -3.12e-11 \\
-5.25e-12 & -4.10e-11 & -7.39e-09 & 3.28e-08 & -7.39e-10 \\
0 & 0 & 0 & 0 & 0 \\
2.04e-16 & -4.65e-15 & -2.34e-13 & -3.72e-12 & -2.34e-14 \\
-5.68e-14 & -1.73e-12 & -4.60e-11 & 1.38e-09 & -4.60e-12 \\
0 & 0 & 0 & 0 & 0
\end{bmatrix} \quad \text{(C.40)}$$

$$A3_{cpif} = \begin{bmatrix}
-4.33e+00 & 1.25e+00 & -2.57e+02 & -1.93e-01 & 4.90e+01 \\
-5.89e-01 & -6.86e-08 & 2.54e-07 & 0 & 1.00e+00 \\
-3.55e-01 & 1.61e-06 & 1.35e-04 & 0 & 0 \\
-4.51e-01 & 2.11e-07 & 5.37e-08 & 0 & 1.00e+00 \\
3.51e-01 & -8.78e-04 & -6.79e-06 & 2.07e+01 & 0 \\
-6.63e-03 & 2.73e+04 & -5.88e+06 & -1.42e+00 & -1.53e-02 \\
1.00e-06 & -8.62e-07 & -1.36e-04 & 0 & 0 \\
-2.85e-02 & 5.70e-08 & -3.20e-09 & 0 & 0 \\
2.73e-09 & 3.29e-09 & 9.99e-03 & 0 & 0 \\
-3.21e-01 & -6.47e-07 & 1.15e-08 & 0 & 0 \\
-2.86e+01 & -7.10e-06 & -8.51e-07 & 0 & 0 \\
-3.21e-06 & -7.07e+00 & -1.94e-06 & 0 & 0 \\
2.68e-07 & 1.58e-06 & -1.15e+01 & 0 & 0 \\
-1.33e-01 & -4.90e-06 & 4.12e-07 & -5.00e+00 & 0 \\
3.50e-01 & 1.64e-07 & -3.89e-08 & 0 & -1.00e+00 \\
-7.49e-06 & 8.53e-02 & 3.12e-03 & 0 & 0 \\
1.88e-01 & 1.66e-01 & 1.64e-03 & 0 & 0 \\
0 & 0 & 0 & 0 & 0 \\
8.24e-13 & -4.85e-14 & 8.08e-13 & 0 & 0 \\
-1.61e-11 & -5.25e-12 & -4.10e-11 & 0 & 0 \\
0 & 0 & 0 & 0 & 0 \\
8.60e-16 & 2.04e-16 & -4.65e-15 & 0 & 0 \\
-1.54e-13 & -5.68e-14 & -1.73e-12 & 0 & 0 \\
0 & 0 & 0 & 0 & 0
\end{bmatrix} \quad \text{(C.41)}$$

$$A4_{cpif} = \begin{bmatrix}
-1.20e-03 & 7.73e-01 & -2.87e+04 & 1.04e+02 & 8.85e+00 \\
0 & 0 & 0 & -9.28e-21 & -9.28e-18 \\
0 & 0 & 0 & 4.83e-22 & 4.83e-19 \\
0 & 0 & 0 & -2.22e-21 & -2.22e-18 \\
0 & 1.00e+00 & 0 & 7.64e-21 & 7.64e-18 \\
-5.13e-02 & -5.22e-02 & -1.11e+03 & -1.65e-01 & -1.33e-03 \\
0 & 0 & 0 & 2.56e-21 & 2.56e-18 \\
0 & 0 & 0 & -2.72e-22 & -2.72e-19 \\
0 & 0 & 0 & -3.48e-23 & -3.48e-20 \\
0 & 0 & 0 & 1.77e-21 & 1.77e-18 \\
0 & 0 & 0 & 7.00e-20 & 7.00e-17 \\
0 & 0 & 0 & 7.79e-21 & 7.79e-18 \\
0 & 0 & 0 & 7.63e-21 & 7.63e-18 \\
0 & 0 & 0 & -8.30e-21 & -8.30e-18 \\
0 & 0 & 0 & 8.50e-22 & 8.50e-19 \\
-5.00e+01 & 0 & 0 & 2.20e-20 & 2.20e-17 \\
0 & -2.00e+02 & 0 & -7.15e-20 & -7.15e-17 \\
0 & 0 & -1.00e+00 & 0 & 0 \\
0 & 0 & 0 & 2.55e-22 & 1.00e+00 \\
0 & 0 & 0 & -3.00e+03 & -1.30e+02 \\
0 & 0 & 0 & 0 & 0 \\
0 & 0 & 0 & 7.77e-25 & 7.77e-22 \\
0 & 0 & 0 & -1.55e-22 & -1.55e-19 \\
0 & 0 & 0 & 0 & 0
\end{bmatrix} \quad \text{(C.42)}$$

$$A5_{cpif} = \begin{bmatrix} 2.44e+01 & -3.43e+00 & 7.85e-01 & 2.70e+02 \\ 0 & -1.01e-15 & -1.01e-14 & 0 \\ 0 & -4.07e-16 & -4.07e-15 & 0 \\ 0 & 1.45e-16 & 1.45e-15 & 0 \\ 0 & 1.12e-14 & 1.12e-13 & 0 \\ 1.80e+02 & -6.94e+04 & 1.01e+04 & 6.25e+06 \\ 0 & 2.76e-17 & 2.76e-16 & 0 \\ 0 & -4.68e-16 & -4.68e-15 & 0 \\ 0 & -7.44e-18 & -7.44e-17 & 0 \\ 0 & 2.21e-15 & 2.21e-14 & 0 \\ 0 & 1.41e-14 & 1.41e-13 & 0 \\ 0 & 4.17e-16 & 4.17e-15 & 0 \\ 0 & 2.55e-15 & 2.55e-14 & 0 \\ 0 & -7.32e-16 & -7.32e-15 & 0 \\ 0 & 9.12e-16 & 9.12e-15 & 0 \\ 0 & 5.21e-15 & 5.21e-14 & 0 \\ 0 & 3.70e-14 & 3.70e-13 & 0 \\ 0 & 0 & 0 & 0 \\ 0 & -9.90e-17 & -9.90e-16 & 0 \\ 0 & -2.19e-16 & -2.19e-15 & 0 \\ 1.00e-02 & 0 & 0 & 0 \\ 0 & 5.31e-19 & 1.00e+00 & 0 \\ 0 & -2.00e+03 & -2.10e+02 & 0 \\ 0 & 0 & 0 & -4.00e+01 \end{bmatrix} \quad (C.43)$$

$$B1_{cpif} = \begin{bmatrix} -5.89e-07 & -9.14e-04 & -1.89e-03 & -8.58e-04 & -1.07e-06 \\ -5.46e-01 & -5.89e-01 & 4.07e-01 & -6.86e-08 & 2.54e-07 \\ -1.97e-01 & -3.55e-01 & 7.26e-01 & 1.61e-06 & 1.35e-04 \\ -4.50e-01 & -4.51e-01 & 2.50e-01 & 2.11e-07 & 5.37e-08 \\ 1.97e-01 & 3.51e-01 & -6.83e+00 & -8.78e-04 & -6.79e-06 \\ -3.36e-06 & -8.62e-04 & -1.73e-03 & -2.45e-03 & -1.89e-06 \\ 1.88e-06 & 1.00e-06 & -6.05e-06 & -8.62e-07 & -1.36e-04 \\ 7.78e-02 & -2.85e-02 & 3.29e-02 & 5.70e-08 & -3.20e-09 \\ 2.03e-09 & 2.73e-09 & 1.35e-09 & 3.29e-09 & 9.99e-03 \\ 6.07e+00 & -3.21e-01 & 1.20e-01 & -6.47e-07 & 1.15e-08 \\ -3.50e-01 & 1.13e+01 & 2.03e-01 & -7.10e-06 & -8.51e-07 \\ 7.94e-07 & -3.21e-06 & -1.98e-05 & 2.92e+00 & -1.94e-06 \\ 4.18e-08 & 2.68e-07 & 3.41e-07 & 1.58e-06 & 8.40e+00 \\ -6.15e-02 & -1.33e-01 & -2.14e+00 & -4.90e-06 & 4.12e-07 \\ 4.02e-01 & 3.50e-01 & 1.05e-02 & 1.64e-07 & -3.89e-08 \\ -4.00e-06 & -7.49e-06 & -1.06e-03 & 8.53e-02 & 3.12e-03 \\ -5.77e-03 & 1.88e-01 & 4.71e-01 & 1.66e-01 & 1.64e-03 \\ 1.00e+00 & 0 & 0 & 0 & 0 \\ -3.12e-11 & 8.24e-13 & -2.05e-12 & -4.85e-14 & 8.08e-13 \\ 7.39e-10 & 1.00e+02 & 3.85e-11 & 5.25e-12 & -4.10e-11 \\ 0 & 0 & 1.00e-02 & 0 & 0 \\ -2.34e-14 & 8.60e-16 & 1.36e-14 & 2.04e-16 & -4.65e-15 \\ 4.60e-12 & -1.54e-13 & -2.77e-12 & -3.00e+02 & -1.73e-12 \\ 0 & 0 & 0 & 0 & 4.00e+01 \end{bmatrix} \quad (C.44)$$

$$C1_{cpif} = \begin{bmatrix} -6.95e-01 & 2.20e+01 & 5.21e+00 & 6.57e-01 & -6.05e-04 \\ -4.08e-04 & 1.99e-02 & 1.25e+01 & 2.93e-04 & -3.64e-03 \end{bmatrix} \quad (C.45)$$

$$C2_{cpif} = \begin{bmatrix} -3.26e-04 & -3.78e+00 & 2.88e+02 & 4.17e+03 & 1.59e+01 \\ -2.81e+01 & -7.10e+04 & 1.17e+03 & 5.68e+07 & -1.23e+00 \end{bmatrix} \quad (C.46)$$

$$C3_{cpif} = \begin{bmatrix} -5.63e-02 & 1.63e-02 & -3.33e+00 & -2.50e-03 & 6.37e-01 \\ 7.97e-05 & 2.91e+02 & -6.26e+04 & -1.51e-02 & 1.63e-04 \end{bmatrix} \quad (C.47)$$

$$C4_{cpif} = \begin{bmatrix} -1.56e-05 & -2.94e-03 & -3.73e+02 & 1.35e+00 & 1.14e-01 \\ -1.11e-02 & -1.11e-02 & 1.18e+01 & 1.76e-03 & -1.42e-05 \end{bmatrix} \quad (C.48)$$

$$C5_{cpif} = \begin{bmatrix} 3.17e-01 & -4.46e-02 & 1.02e-02 & 3.51e+00 \\ 1.91e+00 & -7.39e+02 & -1.07e+02 & 6.65e+04 \end{bmatrix} \quad (C.49)$$

$$D1_{cpif} = \begin{bmatrix} 0 & 0 & 0 & 0 & 0 \\ 0 & 0 & 0 & 0 & 0 \end{bmatrix} \quad (C.50)$$

H_∞ Reduced Order Compensator

As in the H_2 case, the compensator obtained from the H_∞ design was reduced via Hankel singular value elimination. The Hankel singular values for the full-order H_∞ compensator are given in Table C.2. As in the H_2 case, the last 13 singular values were eliminated, as indicated by the dashed line in Table C.2. The resultant reduced order compensator, composed of 11 states, can be represented by

$$\dot{x}_{cpir} = A_{cpir}\, x_{cpir} + B_{cpir}\, y_p \quad (C.51)$$

$$u_p = C_{cpir}\, x_{cpir} + D_{cpir}\, y_p \quad (C.52)$$

Table C.2. H_∞ Compensator Hankel Singular Values

4.91e+02
4.78e+02
9.39e+00
7.04e+00
3.15e+00
2.20e+00
1.79e+00
6.29e-01
1.48e-01
1.29e-01
1.10e-01
7.41e-02
6.21e-02
1.73e=02
1.40e-02
6.10e-03
2.68e-03
1.37e-03
1.10e-03
2.21e-04
4.83e-05
6.67e-06
7.24e-07
7.23e-08

where

x_{cpir} = compensator states

$$A_{cpir} = [A1_{cpir} | A2_{cpir}] \quad (C.53)$$

$$B_{cpir} = [\ B1_{cpir}\ ] \quad (C.54)$$

$$C_{cpir} = [C1_{cpir} | C2_{cpir}] \quad (C.55)$$

$$D_{cpir} = [\ D1_{cpir}\ ] \quad (C.56)$$

and

$$A1_{cp2r} = \begin{bmatrix} -3.57e+05 & -4.72e+06 & -2.24e+06 & 9.96e+05 \\ 6.62e+04 & 8.73e+05 & 4.15e+05 & -1.84e+05 \\ -5.00e+04 & -6.61e+05 & -3.13e+05 & 1.39e+05 \\ -7.16e+04 & -9.45e+05 & -4.49e+05 & 1.99e+05 \\ -8.59e+03 & -1.13e+05 & -5.38e+04 & 2.39e+04 \\ 2.81e+04 & 3.72e+05 & 1.76e+05 & -7.85e+04 \\ -1.26e+04 & -1.66e+05 & -7.90e+04 & 3.51e+04 \\ 5.95e+03 & 7.85e+04 & 3.73e+04 & -1.65e+04 \\ -5.06e+03 & -6.68e+04 & -3.17e+04 & 1.41e+04 \\ 1.08e+03 & 1.42e+04 & 6.77e+03 & -3.01e+03 \\ -7.28e+02 & -9.61e+03 & -4.56e+03 & 2.02e+03 \end{bmatrix} \quad (C.57)$$

$$A2_{cp2r} = \begin{bmatrix} -6.15e+05 & 1.49e+06 & -1.40e+06 & 6.15e+05 \\ 1.13e+05 & -2.76e+05 & 2.60e+05 & -1.13e+05 \\ -8.61e+04 & 2.09e+05 & -1.97e+05 & 8.61e+04 \\ -1.23e+05 & 2.99e+05 & -2.82e+05 & 1.23e+05 \\ -1.47e+04 & 3.59e+04 & -3.38e+04 & 1.47e+04 \\ 4.85e+04 & -1.18e+05 & 1.11e+05 & -4.84e+04 \\ -2.16e+04 & 5.28e+04 & -4.96e+04 & 2.16e+04 \\ 1.02e+04 & -2.48e+04 & 2.34e+04 & -1.04e+04 \\ -8.69e+03 & 2.11e+04 & -1.99e+04 & 8.71e+03 \\ 1.86e+03 & -4.52e+03 & 4.26e+03 & -1.85e+03 \\ -1.25e+03 & 3.04e+03 & -2.86e+03 & 1.25e+03 \end{bmatrix} \quad (C.58)$$

$$A3_{cp2r} = \begin{bmatrix} 6.23e+05 & 4.87e+06 & -1.01e+08 \\ -1.15e+05 & -9.01e+05 & 1.87e+07 \\ -8.72e+04 & 6.81e+05 & -1.41e+07 \\ 1.24e+05 & 9.75e+05 & -2.02e+07 \\ -1.49e+04 & -1.16e+05 & -2.43e+06 \\ -4.90e+04 & -3.82e+05 & 7.97e+06 \\ -2.19e+04 & -1.71e+05 & -3.56e+06 \\ -1.03e+04 & -8.11e+04 & 1.68e+06 \\ -8.81e+03 & -6.92e+04 & -1.43e+06 \\ -1.88e+03 & -1.46e+04 & 3.05e+05 \\ -1.26e+03 & -9.94e+03 & -2.06e+05 \end{bmatrix} \quad (C.59)$$

$$B1_{cp2r} = \begin{bmatrix} -1.37e-01 & 1.12e+00 & 4.00e-01 & 9.99e+00 & -5.32e+00 \\ 1.14e-01 & -1.70e-01 & -5.26e-02 & -1.48e+00 & -3.83e+01 \\ -3.30e-01 & 1.00e-01 & 2.43e-02 & 1.41e+00 & -1.29e+01 \\ 1.43e-01 & -1.27e+00 & 1.76e-02 & 1.83e+00 & 2.81e-01 \\ 8.35e-01 & -6.33e-01 & 4.22e-02 & -8.14e-02 & 2.80e+00 \\ 1.30e+00 & 9.03e+00 & 5.48e-01 & 1.96e+00 & -1.22e+00 \\ 2.25e+00 & -8.31e+00 & -2.54e-01 & -4.97e+00 & -3.78e+00 \\ 8.56e-02 & -1.37e+00 & 8.30e-02 & 9.33e+01 & -1.37e-01 \\ -4.10e+00 & 3.58e+00 & -5.17e-01 & 3.70e+00 & -4.33e-01 \\ -4.33e+00 & 1.89e-01 & 5.14e-01 & -1.33e+00 & -3.12e-01 \\ -2.46e-01 & 2.65e-01 & 3.40e-02 & 6.73e-01 & -2.47e-01 \end{bmatrix} \quad (C.60)$$

$$C1_{cp2r} = \begin{bmatrix} -3.29e-01 & -2.53e+00 & -2.83e+00 & 1.45e+00 \\ -4.07e+03 & -5.37e+04 & -2.55e+04 & 1.13e+04 \end{bmatrix} \quad (C.61)$$

$$C2_{cp2r} = \begin{bmatrix} 5.48e-01 & -4.63e+00 & -2.82e+00 & 1.21e+00 \\ -7.00e+03 & 1.70e+04 & -1.60e+04 & 7.00e+03 \end{bmatrix} \quad (C.62)$$

$$C3_{cp2r} = \begin{bmatrix} 3.98e+00 & 6.01e+01 & -8.21e+01 \\ 7.09e+03 & -5.54e+04 & -1.15e+06 \end{bmatrix} \quad (C.63)$$

$$D1_{cp2r} = \begin{bmatrix} 0 & 0 & 0 & 0 & 0 \\ 0 & 0 & 0 & 0 & 0 \end{bmatrix} \quad (C.64)$$

Comparison of Full- and Reduced-Order Compensators

To gain some insight into the effect of using the reduced order compensators above, it is necessary to compare the singular value plots of the respective compensators. Figure C.1 shows the singular value plot for the full-order H_2 compensator, and Figure C.2 is the singular value plot for the reduced-order compensator. Figure C.3 shows these two plots superimposed. As can be seen from the plots, the only major difference occurs at very low frequency, where there are some directions of the input vector which are magnified more for the reduced-order compensator than for the full-order one. This difference would generate some steady-state error if the simulation were run for a very long time. The short period of the simulation (eight seconds maximum), makes this effect inconsequential, so the reduced order compensator can be used.

Likewise, the singular value plots for the full- and reduced-order H_∞ compensators, shown in Figures C.4 and C.5, respectively, display a similar trend when superimposed, as seen in Figure C.6. As in the H_2 case, this difference is

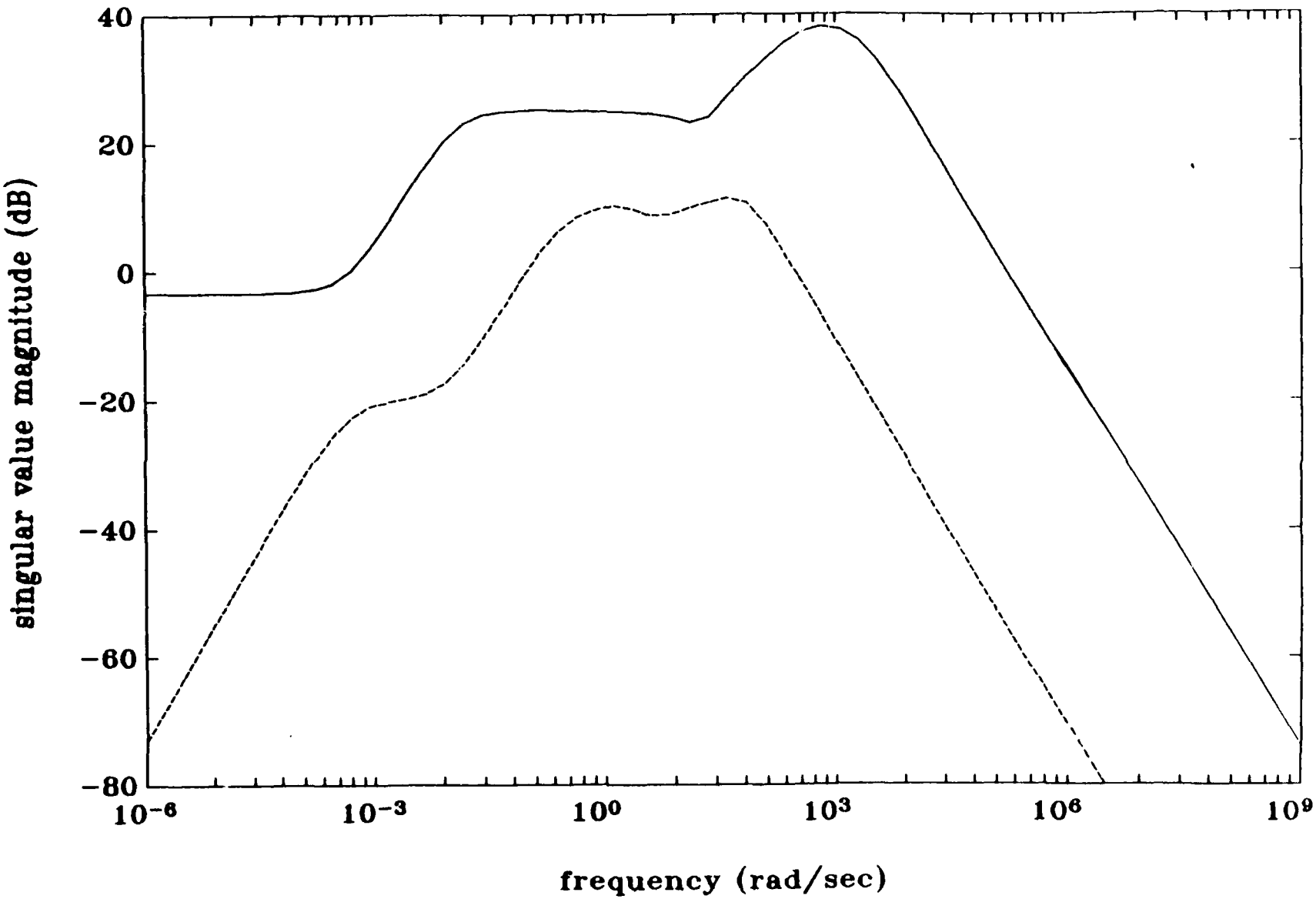

Figure C.1. Full-Order H_2 Compensator Singular Value Plot

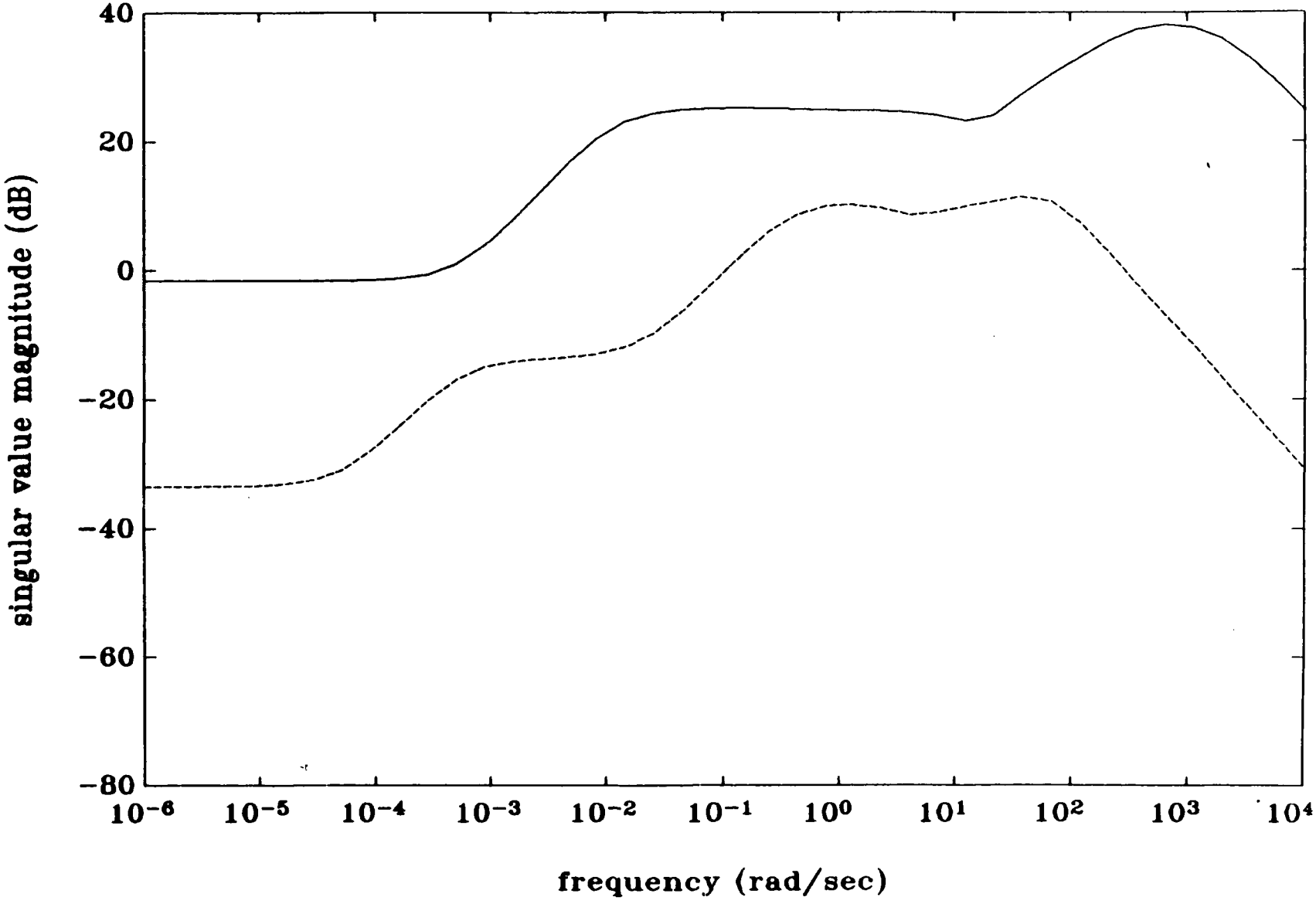

Figure C.2. Reduced-Order H_2 Compensator Singular Value Plot

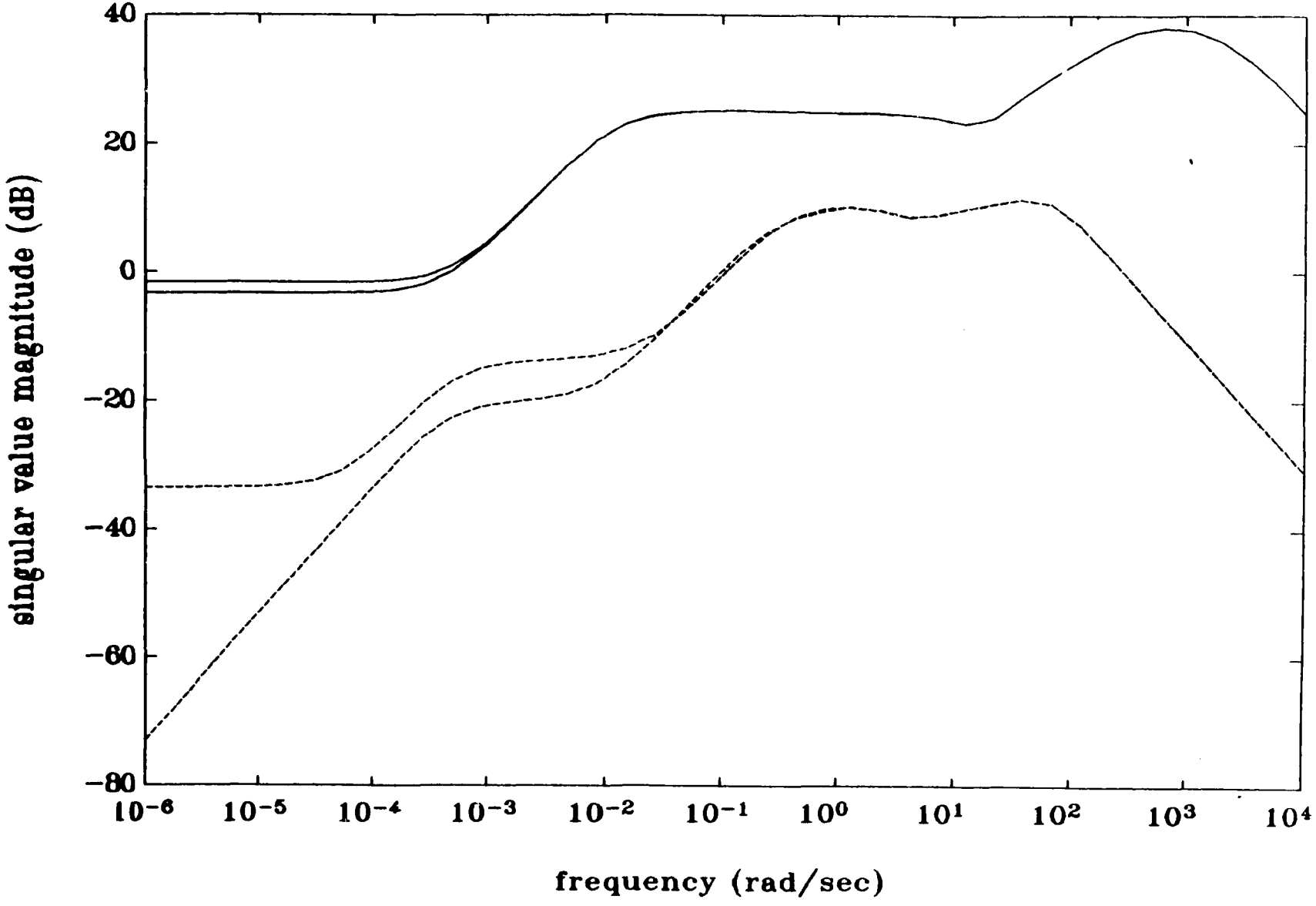

Figure C.3. Full- and Reduced-Order H_2 Compensators Singular Value Plots

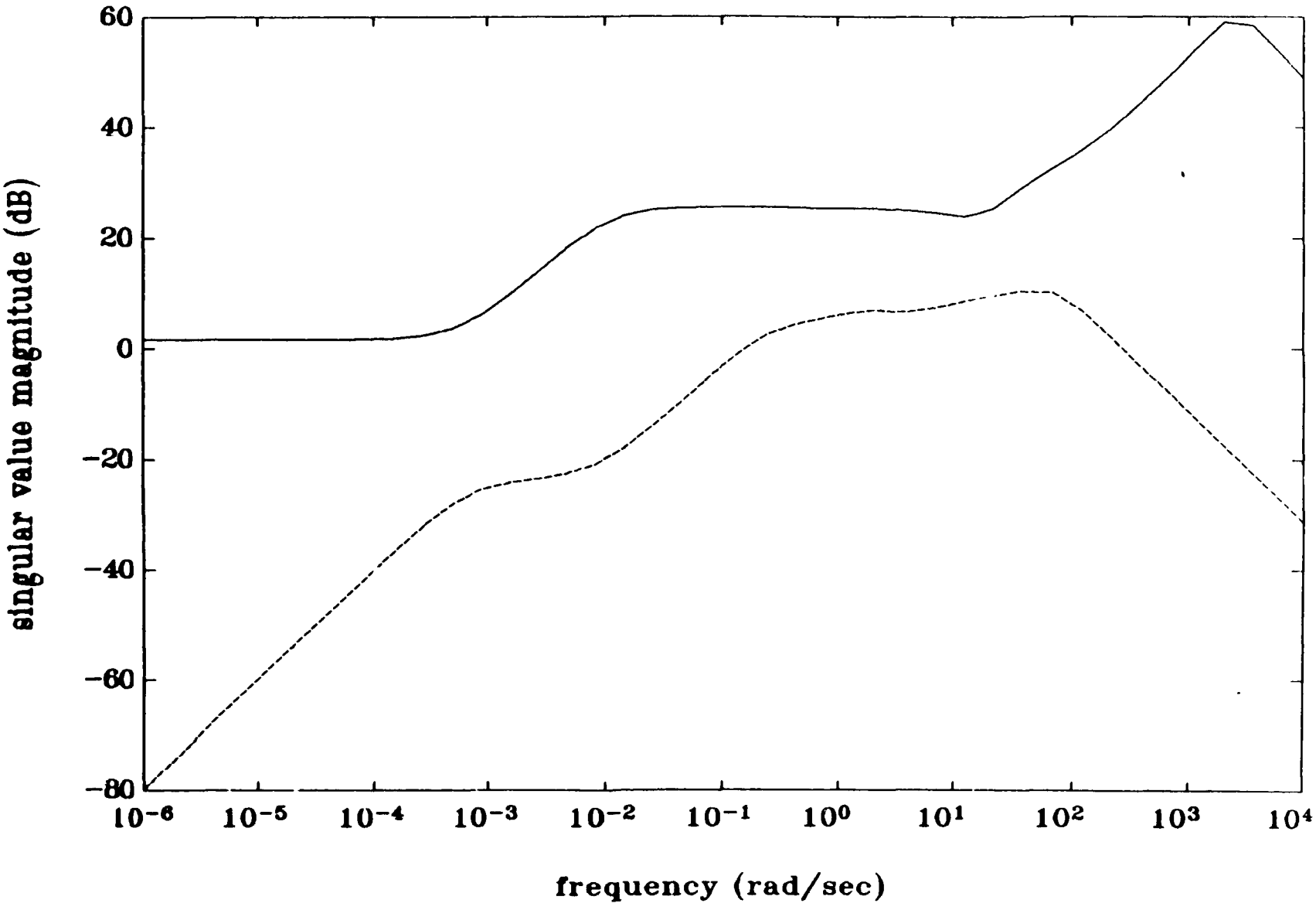

Figure C.4. Full-Order H_∞ Compensator Singular Value Plot

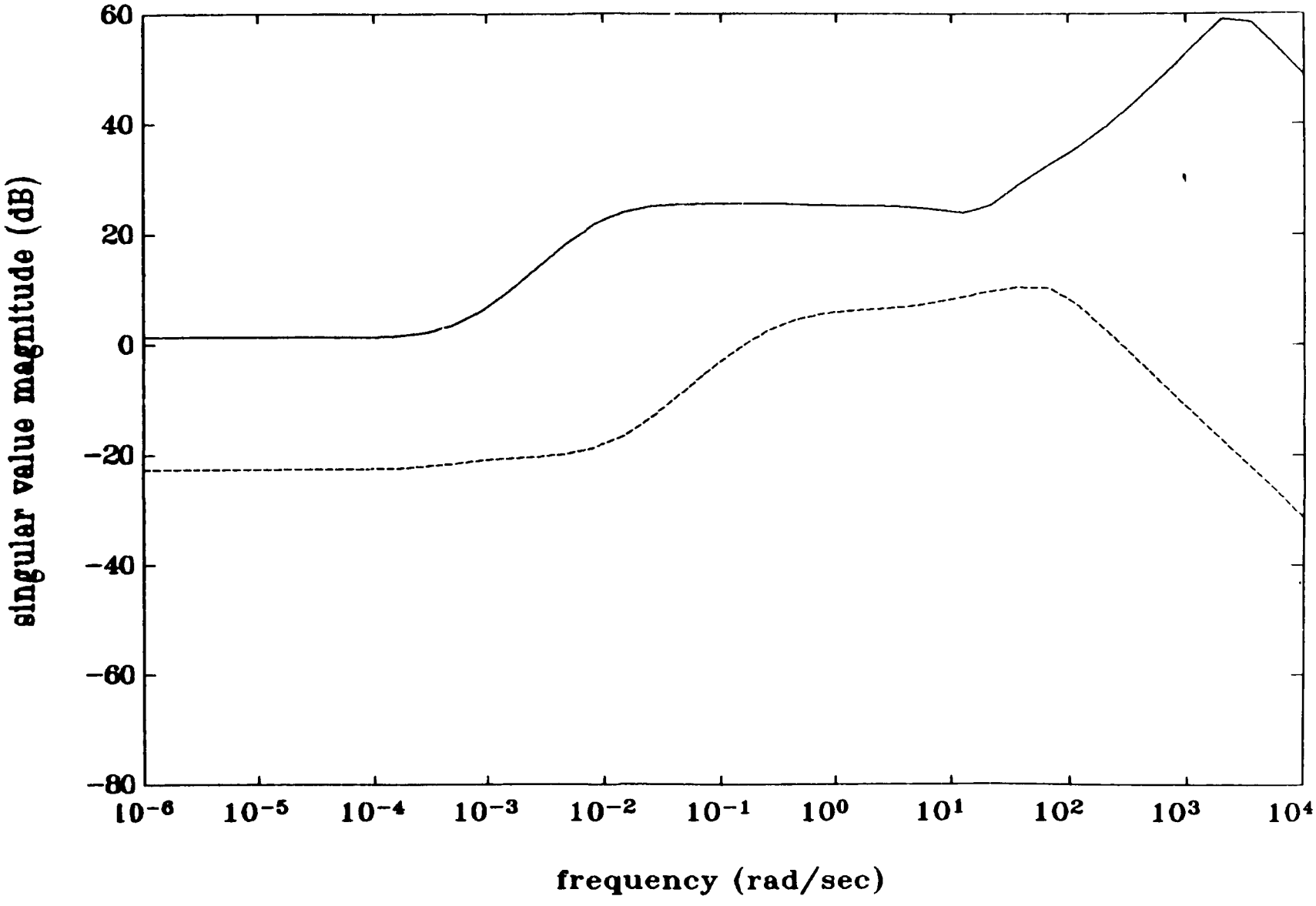

Figure C.5. Reduced-Order H_∞ Compensator Singular Value Plot

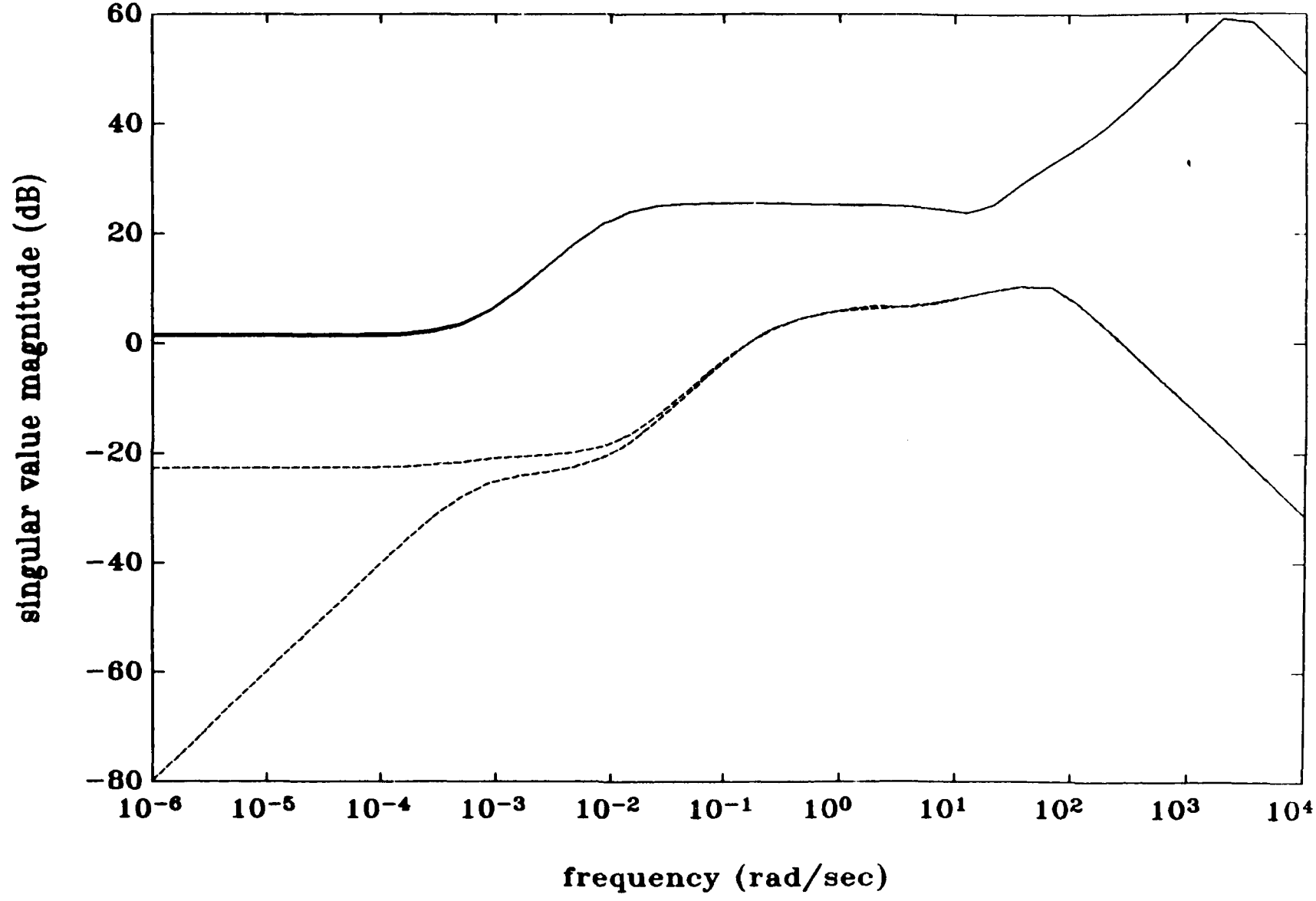

Figure C.6. Full- and Reduced-Order H_∞ Compensators Singular Value Plots

judged inconsequential for the short period of simulation herein used, and the reduced-order compensator can be used.

Bibliography

1. Aeronautical Vestpocket handbook. PWA Part No. 79500. Pratt & Whitney Aircraft of Canada, Ltd. August 1981.

2. Class Notes for a Short Course in Homing Guided Missiles. FAAC Report FR203U/2534. Michigan; First Ann Arbor Corporation, 1975.

3. Doyle, John; Glover, K.; Khargonekar, P.; and Francis, B. "State-space Solution to Standard H_2 and H_∞ Control Problems." IEEE Trans. Auto. Control. New York, IEEE Press, 1989.

4. Francis, Bruce. "A course in H_∞ Control Theory." Lecture Notes in Control and Information Sciences. Edited by M. Thoma and A. Wyner. Springer-Verlog, Toronto, May 1986.

5. Glover, K. and Doyle, J. "State-Space formulae for all stabilizing controllers that satisfy an H_∞-norm bound and relations to risk sensitivity." Systems and Control Letters 11 167-172. North-Holland, 1988.

6. Kwakernaak, H.; and Sivan,R. Linear Optimal Control Systems. New York; John Wiley & Sons, 1972.

7. Ogata, K. Modern Control Engineering. New Jersey; Prentice-Hall, Inc., 1970.

8. Ridgely, D.B. and Banda, S. Introduction to Robust Multivariable Control. AFWAL-TR-85-3102. February, 1986.

9. Roskam, Jan. Airplane Flight Dynamics and Automatic Flight Controls. (Second Edition) Kansas; Roskam Aviation and Engineering Corporation, 1979 (1982).

10. Safonov, M. and Chiang, R. "Schur Balanced Model Reduction." IEEE Trans. Auto. Contr. New York; IEEE Press, 1988.

11. Safonov, M. and Limebeer, R. "Simplifying the H∞ Theory Via Loop Shifting." Proc. of the 27th Conf. on Dec. and Cont., Dec 1988. New York; IEEE press, 1988.

12. Sverdrup Technology, Inc. Missile Six-Degree-of-Freedom Digital Simulation MS6DOF. Unpublished working papers. May 1989.

Vita

Captain Randall L. (Randy) Riddle [redacted] he graduated from high school in Pilot Mtn., North Carolina, in 1980 and attended North Carolina State University, from which he received the degree of Bachelor of Science in Aerospace Engineering in May 1984. Upon graduation, he received a commission in the USAF through the ROTC program. He entered active duty in October 1984 at the Foreign Technology Division, Wright Patterson AFB, Ohio, until entering the School of Engineering, Air Force Institute of Technology, in May 1988.

[redacted]

UNCLASSIFIED
SECURITY CLASSIFICATION OF THIS PAGE

REPORT DOCUMENTATION PAGE

Form Approved
OMB No 0704-0188

1a. REPORT SECURITY CLASSIFICATION
UNCLASSIFIED

1b. RESTRICTIVE MARKINGS

2a. SECURITY CLASSIFICATION AUTHORITY

2b. DECLASSIFICATION / DOWNGRADING SCHEDULE

3. DISTRIBUTION / AVAILABILITY OF REPORT
Approved for public release;
distribution unlimited

4. PERFORMING ORGANIZATION REPORT NUMBER(S)
AFIT/GAE/ENY/89D-29

5. MONITORING ORGANIZATION REPORT NUMBER(S)

6a. NAME OF PERFORMING ORGANIZATION
School of Engineering

6b. OFFICE SYMBOL (If applicable)
AFIT/ENY

7a. NAME OF MONITORING ORGANIZATION

6c. ADDRESS (City, State, and ZIP Code)
Air Force Institute of Technology (AU)
Wright-Patterson AFB, Ohio 45433-6583

7b. ADDRESS (City, State, and ZIP Code)

8a. NAME OF FUNDING / SPONSORING ORGANIZATION

8b. OFFICE SYMBOL (If applicable)

9. PROCUREMENT INSTRUMENT IDENTIFICATION NUMBER

8c. ADDRESS (City, State, and ZIP Code)

10. SOURCE OF FUNDING NUMBERS

PROGRAM ELEMENT NO.	PROJECT NO.	TASK NO	WORK UNIT ACCESSION NO.

11. TITLE (Include Security Classification)
DESIGN OF A ROBUST CONTROLLER FOR AN UNSTABLE NONMINIMUM PHASE GUIDED MISSILE

12. PERSONAL AUTHOR(S)
Randall L. Riddle, Captain, USAF

13a. TYPE OF REPORT	13b. TIME COVERED	14. DATE OF REPORT (Year, Month, Day)	15. PAGE COUNT
MS Thesis	FROM _____ TO _____	1989 December	195

16. SUPPLEMENTARY NOTATION

17. COSATI CODES			18. SUBJECT TERMS (Continue on reverse if necessary and identify by block number)
FIELD	GROUP	SUB-GROUP	Robust Control; H_∞ Control Theory; H_2 Control Theory; Multivariable Control
01	04		
17	07	03	

19. ABSTRACT (Continue on reverse if necessary and identify by block number)

D. Brett Ridgely, Capt, USAF

20. DISTRIBUTION / AVAILABILITY OF ABSTRACT
☒ UNCLASSIFIED/UNLIMITED ☐ SAME AS RPT. ☐ DTIC USERS

21. ABSTRACT SECURITY CLASSIFICATION
UNCLASSIFIED

22a. NAME OF RESPONSIBLE INDIVIDUAL	22b. TELEPHONE (Include Area Code)	22c. OFFICE SYMBOL
D. Brett Ridgely, PhD	(513) 785-5691	AFIT/ENY

DD Form 1473, JUN 86 *Previous editions are obsolete.* SECURITY CLASSIFICATION OF THIS PAGE

H_2 and H_∞ design techniques are applied to a state space representation of a surface-to-air- missile system with unstable nonminimum phase airframe response characteristics. A method for converting the tracking and command following problems to the "standard problem" is given. Artificial frequency-dependent filtering of external inputs is required for proper closed loop system performance, and a method for deriving the filters is developed. Areas requiring further study are identified.